Pecten maximus, archive multi-proxy haute-résolution de la production primaire en rade de Brest

Valentin Siebert

COLLEGE SCIENCES DOCTORAL DE LA MER BRETAGNE ET DU LITTORAL

Université de Bretagne Occidentale

THÈSE DE DOCTORAT DE

L'UNIVERSITE
DE BRETAGNE OCCIDENTALE

ECOLE DOCTORALE N° 598
Sciences de la Mer et du Littoral
Spécialité : *Biologie Marine*

Par
Valentin SIEBERT

Pecten maximus, archive multi-proxy haute-résolution de la production primaire en rade de Brest

Thèse présentée et soutenue à Plouzané, le 02 Juin 2023
Unité de recherche : Laboratoire des Sciences de l'Environnement marin (LEMAR – UMR 6539)

Rapporteurs avant soutenance :

Melita PEHARDA	Senior scientist – Institute of Oceanography and Fisheries, Split, Croatie
Uta PASSOW	Senior scientist – Memorial University of Newfoundland, St-John's, Canada

Composition du Jury :

Président :	Yves-Marie PAULET	Professeur – Université de Bretagne Occidentale
Examinateurs :	Nicolas SAVOYE	Physicien CNAP – Université de Bordeaux
	Melita PEHARDA	Senior scientist – Institute of Oceanography and Fisheries
	Uta PASSOW	Senior scientist – Memorial University of Newfoundland
Dir. de thèse :	Julien THÉBAULT	Maître de conférences – Université de Bretagne Occidentale
Co-dir. de thèse :	Brivaëla MORICEAU	Directrice de recherche – CNRS

Invité(s)
Yvan PAILLER — Ingénieur de Recherche - Université de Bretagne Occidentale

REMERCIEMENTS

Plus de trois ans et demi viennent de s'écouler, et avant d'entamer la lecture de ce manuscrit, je tiens à remercier toutes les personnes qui ont rendu ce projet de thèse possible, et qui ont participé à son bon déroulement. Et comment ne pas commencer par mes deux directeurs de thèse : Julien Thébault et Bivaëla Moriceau.

Julien, cela fait maintenant 7 ou 8 ans que je t'ai vu pour la première fois enseigner la biologie à la fac des sciences, alors que je n'étais qu'un petit étudiant de Licence 2 qui assistait à ton cours. Je n'aurais alors jamais imaginé pouvoir avoir la chance de travailler un jour à tes côtés. Et puis j'ai pu réaliser deux stages de master dans lesquels tu étais impliqué, et qui m'ont ouvert les portes de ce projet de thèse. Je te remercie alors pour ta gentillesse, ton humanité, ta bienveillance et ta compréhension durant ces trois ans, surtout durant les moments compliqués qui ont précédé le rendu de ce manuscrit. Mais je te remercie également pour tout le savoir que tu m'as apporté au cours de toutes ces années d'étude. Je te suis très reconnaissant que tu m'aies fait confiance pour une telle mission.

Briva, je t'ai rencontré qu'au début de ce doctorat, il y a un peu plus de trois et demi, et je voulais également te remercier pour ta bonne humeur et ta gentillesse. Bien que je n'étais pas totalement familier avec la biogéochimie ainsi que l'étude des agrégats, je te remercie d'avoir pris le temps de m'expliquer les principes liés à ce domaine et de m'avoir aidé à mettre en place des expérimentations afin de répondre aux différents objectifs que l'on s'était fixé. Et encore félicitations pour ton nouveau poste de directeur de recherche !

Je tenais vraiment à vous dire à quel point j'avais été ravi de travailler sous votre supervision, vous formez une super équipe et je ne pouvais pas rêver mieux comme encadrement. Je garde de très bons souvenirs de tous ces moments que nous avons partagés, en lien ou non avec le travail. Un très très grand MERCI à tous les deux. Surtout ne changez rien !

Je souhaiterais également remercier Bernd Schöne, le co-porteur de projet HIPPO. Je tenais à te remercier pour ton accueil lors de mes différents voyages à Mainz, pour les discussions que nous avons pu avoir ensemble, ainsi que pour tous les conseils que tu m'as donnés, notamment au moment

de l'écriture des articles scientifiques.

En termes de personne rencontrée durant cette thèse, je ne peux pas oublier Lukas Fröhlich, mon homologue allemand et un scientifique incroyable. Lukas, je tiens à te remercier pour tous les échanges que nous avons eus, que ce soit concernant le travail ou non (et surtout ceux qui ne le concernaient pas). Aujourd'hui, et depuis quelque temps maintenant, je vois en toi plus seulement un collègue, mais un ami, et j'espère sincèrement que nous resterons en contact et que nous continuerons à partager des bons moments ensemble (au Baron peut-être). Et si tu veux revivre une sortie bateau comme celle que tu as vécue au début du mois de mars 2020, n'hésite pas à me le dire et on essayera de se réorganiser ça. Quoi qu'il en soit, je te souhaite le meilleur pour le début de ta carrière, qui, j'en suis sûr au vu de ce que tu es capable de produire, sera prolifique et teintée de réussite.

Pour avoir accepté de m'accueillir au sein du laboratoire LEMAR, j'adresse des remerciements chaleureux à Luis Tito de Morais, ainsi qu'à son successeur, Géraldine Sarthou. Je remercie également l'agence nationale pour la recherche (ANR) ainsi que la région Bretagne d'avoir financé cette thèse.

Je remercie ensuite Melita Peharda, Uta Passow, Nicolas Savoye et Yves-Marie Paulet d'avoir accepté de faire partie de mon jury de thèse. Je suis honoré que vous ayez accepté d'évaluer ce travail. J'espère de tout cœur que vous l'apprécierez.

Enfin, pour leurs encouragements et leurs précieux conseils durant les trois comités de suivi individuel qui ont lieu durant ces années de doctorat, j'adresse des remerciements à Claire Labry et Matthieu Carré.

Le moment phare du projet HIPPO et de ce projet de thèse a été le suivi environnemental, qui s'est déroulé durant 8 mois à Lanvéoc. Je dois avouer avoir été impressionné par l'ampleur de la tâche au début, moi qui n'y connaissais pas grand-chose en analyses chimiques. C'est pourquoi je tiens à remercier toutes les personnes qui m'ont aidé à mettre en place ce suivi et qui ont grandement participé à son bon déroulement :

Un grand merci à toute l'équipe de la plateforme PACHIDERM, à savoir Morgane Gallinari, Manon Le Goff, Émilie Grossteffan, Kévin Bihannic, Isabelle Bihannic et Jérémy Devesa, pour l'aide que vous m'avez apportée au moment de mettre en place les protocoles d'analyse (car je partais de presque zéro), ainsi que durant les nombreuses commandes de matériels qui ont suivies.

Je tiens également à remercier Erwan Amice, Thierry Le Bec, Isabelle Bihannic ainsi qu'Émilie Grossteffan pour m'avoir accompagné durant la quarantaine de plongée qui a été réalisée dans le cadre de ce suivi. Sans vous, jamais ce suivi n'aurait pu avoir lieu. J'en profite également pour remercier Pierre Chauvaud et Maria Lopez qui ont plongé de manière plus ponctuelle avec moi et qui m'ont aidé dans mon échantillonnage. Et encore merci à toi Julien de m'avoir accompagné sur quelques sorties également. C'était un plaisir de plonger avec vous tous et je garde beaucoup de bons souvenirs de ces moments. Julien, je te remercie (une nouvelle fois) de m'avoir offert l'opportunité de passer mon classe 1B ainsi que mon permis bateau !

J'adresse également un immense merci à Gaspard Delebecq pour sa disponibilité et son expertise sur les analyses des communautés phytoplanctoniques. Tu as répondu à un grand nombre de questions et tu m'as aidé sur énormément de choses que je ne pourrais pas tout citer ici. Tu as toujours fait preuve de bienveillance envers mes demandes et je te suis très reconnaissant de cela. Ne change rien et je te souhaite le meilleur pour la suite.

Merci à Peggy Rimmelin-Maury pour ton aide concernant la préparation et la récupération des données recueillies par les différentes sondes qui ont été déployées dans le cadre de ce suivi. Je n'aurais jamais pu tout gérer sans toi.

Merci également à Marc Picheral et à toute l'équipe du laboratoire d'Océanographie de Villefranche-sur-mer d'avoir accepté de nous prêter leur nouvel UVP, qui a produit des résultats extrêmement importants pour ce travail de thèse. J'espère que les données produites vous sont également utiles pour le développement de votre instrument.

Au début du suivi, plus de 3000 coquilles ont été déposées sur le sédiment à Lanvéoc. Pour cela, je remercie Florian Breton, directeur de l'écloserie du Tinduff, ainsi que toute son équipe, de nous avoir fourni ces coquilles, ainsi que de nous avoir prêté une cage dans laquelle nous avons pu les semer pour répondre à certaines problématiques. J'en profite également pour te remercier pour tous les précieux conseils que tu m'as apportés concernant le maintien des coquilles St-Jacques en aquarium,

au moment de mettre en place ces expérimentations.

Toujours concernant ces coquilles, je tiens à dire merci à Caroline Chauvet qui a travaillé dessus durant son stage de master 1, le premier que j'ai eu la chance d'encadrer. Un grand merci à toi pour l'intérêt que tu portais pour notre projet, et pour ton aide sur les quelques mois où tu étais là, notamment sur la dissection des coquilles et l'étude de leur croissance. Tu as fait un super travail.

Pour les analyses en éléments traces de l'eau de mer, qui reste un point sur lequel je n'avais aucune expérience, je tiens à adresser un immense merci à Matthieu Waeles. Merci de m'avoir transmis les protocoles d'analyse et de m'avoir aidé à préparer les échantillons. Pour les analyses ICP-MS qui ont suivi, je remercie Marie-Laure Rouget, Yoan Germain et Céline Liorzou du Pôle Spéctrométrie Océan (PSO).

Pour terminer sur le suivi HIPPO, je remercie les membres d'équipage de l'Albert Lucas, Franck et Robin, de nous avoir accompagné sur la plupart des sorties et qui nous ont aidé sur le pont quand il y en avait besoin, tout en participant de manière non-négligeable à la bonne ambiance du bateau. Encore une fois, je garde de très bons souvenirs de tous ces moments passés en mer.

J'espère de tout cœur avoir cité tout le monde et n'avoir oublié personne. Si jamais votre nom n'apparaît pas au-dessus et que vous estimez y avoir votre place, je tiens en vous présenter mes plus plates excuses et je vous remercie bien évidemment pour tout ce que vous avez apporté à ce suivi, qui que vous soyez.

La seconde phase de cette thèse concernait l'étude des agrégats en laboratoire. Dans un premier temps, et pour tout ce qu'il a fait sur ces expérimentations, je remercie Tom RAINBOW, qui a accepté d'effectuer un stage avec Brivaëla et moi et qui, malgré un travail parfois compliqué, ne s'est jamais plaint et n'a jamais rechigné à la tâche. Je te remercie pour le travail que tu as effectué et pour ton aide sur ces expérimentations (même si c'est plutôt moi qui t'aidais).

Ces expérimentations ont nécessité la construction de nouveaux rolling tanks. Pour leur élaboration et leur construction, je tiens à remercier les équipes de Synoxis, pour la qualité du travail effectué ainsi que pour leur réactivité.

Enfin, je tiens à remercier Philippe Miner, Moussa Diagne ainsi que Matthias Hubert pour nous avoir fourni les différentes souches de micro-algue lorsque nous en avions besoin.

Enfin, il est venu temps de remercier toutes les personnes qui sont intervenues sur le dernier chapitre de thèse, à savoir toutes les équipes archéologiques de l'IUEM et du centre archéologique du Faou, pour nous avoir aidé à retrouver, avec succès, les légendaires coquilles St-Jacques archéologiques.

Pour cela, j'adresse un immense merci à Yvan Pailler, dans un premier temps pour m'avoir invité à l'archéologie sur l'île de Béniguet durant la session de fouille annuel que tu organises, mais également pour toutes les connaissances que tu m'as apportées sur ce domaine. J'ai découvert un domaine et un jargon qui a été très déstabilisant au début, je dois l'avouer, mais que je trouvais tout de même, et que je trouve encore, fascinant.

Merci également à Clément Violet et Caroline Vandenberghe pour les bons moments passés sur l'île de Béniguet et pour m'avoir initié un néophyte au travail rigoureux de l'archéologie. Même si le jour où j'étais présent sur Béniguet, cela s'est traduit par un grand nombre d'aller-retour à transporter du sable dans une brouette. Je garde quand même un super souvenir de cette journée. Un grand merci à vous pour cela.

Enfin, je remercie chaleureusement Élodie Guezennec et Ronan Pérennec, du centre archéologique du Finistère, sans qui nous n'aurions pas pu disposer de coquilles archéologiques, afin de les analyser. Merci pour vos recherches et pour toutes les informations que vous nous avez fournies concernant les échantillons que nous vous avons empruntés.

Pour clore cette section, je tiens enfin à remercier Brigitte Stoll de l'institut Max Planck de Mainz, pour les analyses de ces coquilles archéologiques au LA-ICP-MS (ainsi que pour toutes les coquilles qui ont été analysées durant le projet HIPPO).

Je pense avoir fait le tour de toutes les personnes qui sont intervenues dans le bon déroulement de ce doctorat. Cependant, j'ai également un bon nombre de personnes à remercier pour tous les bons moments passés en dehors (cela reste mine de rien important).

Dans un premier temps, je remercie tous les membres du bureau A107 avec qui j'ai pu passer des grands moments de rigolades. Je pense bien évidemment à Manon, Laura, Maéva, Mallorie, Clémentine, Léna, Clément et José. Sans vous, l'ambiance aurait été bien terne dans le bureau. Et merci pour

votre soutien dans les moments de doutes. Vous êtes géniaux !

Je remercie également tous mes collègues doctorants avec lesquels j'ai pu partager de bonnes tranches de rigolade tout au long de ces années de doctorat. C'est toujours bénéfique de pouvoir échanger avec des personnes qui vivent les mêmes choses que nous. Je ne pourrais pas citer tous les noms sans en oublier, car vous être trop nombreux, mais je suis certain que vous vous reconnaîtrez.

Parmi mes collègues doctorants, j'adresse un remerciement tout particulier à Clémence Blais, qui m'a traîné (comme un boulet) au moment où j'avais besoin d'acquérir des connaissances sur les cultures phytoplanctoniques, leur maintien, le repiquage, la réalisation de milieu de culture, les analyses au cytomètre, au PAM, etc. Merci à toi de m'avoir tant aidé durant plusieurs mois. Je n'ai malheureusement pas eu l'occasion de te rendre la pareille. Surtout ne change rien ! Tu as été incroyablement patiente et profondément gentille, et je te souhaite le meilleur pour la suite et fin de ton doctorat, je suis certain que tu vas tout déchirer ! !

Enfin, je tiens à remercier les personnes les plus importantes pour moi : ma famille. Voilà maintenant presque 9 ans que je vis à l'autre bout de la France, et, bien que je manque un certain nombre de moments de vie à vos côtés, je pense à vous très souvent. Je pense bien évidemment à mes parents, à mon grand frère et sa petite famille (Cath' et mes deux beaux neveux), ainsi que mes grands-parents. Une spéciale dédicace à mon grand-père qui collectionne depuis longtemps les coquillages et qui à travers sa passion, ses histoires et ses voyages, a peut-être influencé mes choix de vie. Merci pour votre soutien durant toutes ces années, et pour votre aide tout au long de mes études.

Merci également à mon petit cercle d'amis rencontrés, depuis la licence ou le collège, qui m'ont fait oublier à travers nos soirées les petits déboires du quotidien. Pour tout ça, merci à David, Noéline, Yacine, Floriane, Quentin et Jean-Charles. Vous êtes incroyables et on va pouvoir continuer à se perdre sereinement dans des labyrinthes !

Et enfin, la dernière personne que je souhaite remercier est celle qui partage ma vie depuis quasiment 8 ans. Merci à toi, Sophie, pour ton soutien et la patience dont tu as fait preuve durant toutes ces années. Même si c'est moi la personne la plus simple à vivre entre nous deux (haha), je ne sais pas comment ce serait passé cette phase de ma vie si jamais tu n'avais pas été là. J'ai hâte d'entamer de nouveaux projets avec toi et j'espère qu'on ira loin ensemble.

Bon, j'ai le sentiment d'avoir le tour de toutes les personnes qui sont intervenues de près ou de loin dans ce projet. Du coup, je vous le redis une dernière fois, et en majuscule cette fois : UN GRAND MERCI ! À VOUS TOUS !

Ah, j'allais oublier ! ! Merci à mes deux amis à grandes oreilles, Prout et Rillette, pour les câlins réconfortants.

AVANT-PROPOS

Cette thèse a été réalisée au Laboratoire des Sciences de l'Environnement Marin (UMR 6539 - LEMAR) entre le 01 septembre 2019 et le 30 avril 2023, sous l'encadrement de Julien Thébault (Maître de conférences, Université de Bretagne Occidentale - UBO) et Brivaëla Moriceau (Directrice de recherche, Centre National de la Recherche Scientifique - CNRS). Elle a été financée à 50% par l'Agence Nationale de la Recherche (ANR) et à 50% par la région Bretagne dans le cadre de l'Allocation de Recherche Doctorale (ARED) et fait partie intégrante du projet HIPPO (HIgh-resolution Primary Production multi-prOxy archives). Ce projet, dont les financements proviennent d'une part de l'ANR et d'autre part de la DFG, est le fruit d'une collaboration Franco-Allemande et est coordonnée du côté français par Julien Thébault et du côté allemand par Bernd R. Schöne (Professeur, Johannes Gutenberg Universität - JGU).

Ce manuscrit a été écrit en partie en Français et en Anglais.

TABLE DES MATIÈRES

TABLE DES FIGURES

LISTE DES TABLEAUX

INTRODUCTION GÉNÉRALE

1 LA PRODUCTION PRIMAIRE

Les producteurs primaires sont des organismes autotrophes qui ont la capacité de convertir des composés inorganiques en matière organique. Cette production de matière organique est la première source d'alimentation pour les autres organismes de l'écosystème, ce qui place les producteurs primaires à la base des réseaux trophiques. Ce processus de production de matière organique est réalisé par un mécanisme de réduction du carbone inorganique (dioxyde de carbone - CO_2), qui nécessite un apport d'énergie. Plusieurs mécanismes peuvent être utilisés, mais le plus commun est la photosynthèse. Les producteurs primaires utilisent la lumière comme source d'énergie pour réduire le carbone et produire de la matière organique. Simultanément, ces organismes photosynthétiques produisent un gaz, un déchet de cette réaction, qui sera disponible pour les autres organismes de l'écosystème : le dioxygène. Cette réaction est catalysée par des pigments présents dans les cellules des producteurs primaires, dont la Chlorophylle a (Chl) est la plus ubiquitaire. En résumé, la photosynthèse se fait selon l'équation suivante (Falkowski et Raven, 2013) :

$$12\,H_2O + 6\,CO_2 + \text{Lumière} \xrightarrow{chl} C_6H_{12}O_6 + 6\,H_2O + 6\,O_2 \tag{1}$$

1.1 L'émergence du phytoplancton

La photosynthèse est l'un des premiers processus biologiques à avoir émergé sur Terre. Bien que les débats persistent quant à la période exacte de son apparition, les scientifiques estiment que les premières traces de production primaire remontent à environ 2,7 à 3,5 milliards d'années (Buick, 1992 ; Blankenship, 1992). À cette époque, les eaux de la planète atteignaient des températures de l'ordre de 70-100°C et son atmosphère était principalement composée de vapeur d'eau (H_2O), de dioxyde de carbone (CO_2) et de diazote (N_2). Ces conditions extrêmes rendaient l'émergence et la survie de la vie impossible. Cependant, les premières formes de vie unicellulaires procaryotes ont pu apparaître dans ces eaux chaudes. Pour se développer, ces cyanobactéries utilisaient la lumière solaire, le CO_2 et l'eau pour produire de la matière organique. Cette réaction s'accompagnait également de la libération de O_2, qui était primordiale pour le développement de nouvelles formes de vie. Ce processus correspondait alors à la photosynthèse. Les scientifiques s'accordent en revanche sur le fait que la photosynthèse pratiquée dans le passé était presque identique à celle des plantes supérieures actuelles (Blankenship, 1992), utilisant les mêmes systèmes photosynthétiques (Cardona, 2018 ; Cardona et al., 2019).

Par ce relargage d'O_2, ces cyanobactéries ont alors initié une oxygénation globale de l'atmosphère et de l'hydrosphère à travers deux périodes distinctes : la Grande Période d'Oxygénation ("Great Oxidation Event" - GOE) il y a 2,45 milliards d'années (Bekker et al., 2004 ; Lyons et al., 2014) et

l'Évènement d'Oxygénation Néoprotérozoïque ("Neoproterozoic Oxygenation Event" - NOE) il y a 800-600 millions d'années (Och et Shields-Zhou, 2012). Ces deux périodes ont augmenté les concentrations en O_2 dans l'atmosphère jusqu'aux niveaux actuels (Figure 1). L'oxygénation de l'atmosphère a entraîné une diminution progressive des températures à la surface de la planète, ainsi que l'apparition de formes de vie animale qui se basent sur la respiration pour se développer. De plus, la NOE a également permis l'émergence d'un groupe primordial pour le maintien du bon fonctionnement de la planète et de la vie qu'elle abrite : le phytoplancton (Falkowski et al., 2004 ; Brocks et al., 2017).

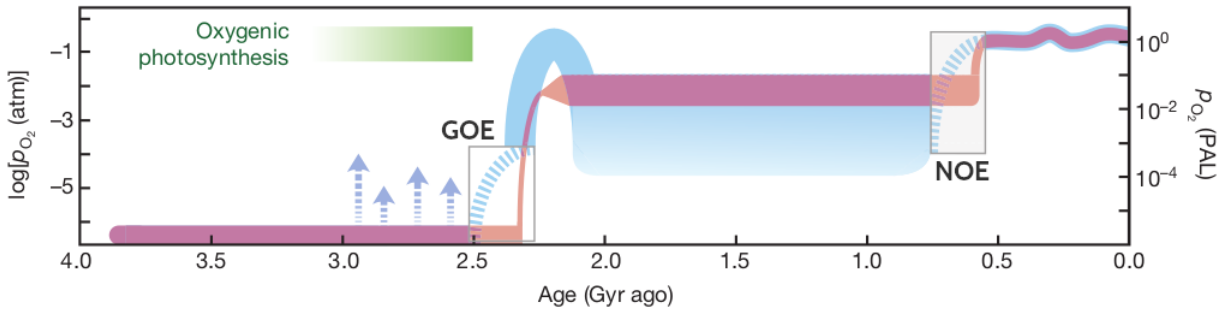

FIGURE 1 – Évolution des concentrations en O_2 atmosphérique (courbe violette) montrant les deux grandes périodes d'oxygénation (de Lyons et al., 2014).

1.2 Le phytoplancton et son rôle dans les écosystèmes marins

Le phytoplancton est un ensemble d'algues planctoniques, qui dérivent avec les courants et ne sont pas capables de lutter contre. Ce terme vient du grec "phyton" qui signifie "plante" et "planktos" qui signifie "errant". Le phytoplancton se caractérise par une grande diversité, avec plus de 20 000 espèces réparties dans huit embranchements phylogénétiques. Les groupes des diatomées et des dinoflagellés sont les plus représentatifs, représentant chacun 40% du nombre total d'espèces de phytoplancton. Les 20% restants se répartissent entre différents groupes tels que les Haptophytes et les Cryptophytes. Les organismes du phytoplancton ne représentent qu'une partie des producteurs primaires dans les écosystèmes aquatiques, car ils sont accompagnés par des organismes procaryotes tels que certains protistes, des cyanobactéries, mais également des macroalgues ou encore des phanérogames marines. Au vu de leur rôle important dans l'apparition et le maintien de la vie sur Terre, les organismes du phytoplancton sont des composants primordiaux des écosystèmes de la biosphère et de l'hydrosphère. Grâce à leur activité photosynthétique, les producteurs primaires capturent le carbone dissous dans l'eau, sous forme de CO_2, et produisent de la matière organique et de l'oxygène. Ainsi, le phytoplancton réduit les niveaux de CO_2 dans l'océan et l'atmosphère, ce qui a un impact sur la pompe biologique de carbone, régulant ainsi le climat et limitant l'acidification des océans.

Aujourd'hui, il est généralement admis que le phytoplancton, bien que sa biomasse soit faible à l'échelle de la biosphère, fixe entre 45 et 50 Gt de carbone par an (Field et al., 1998 ; Uitz et al., 2010),

soit 45% de la production primaire nette de la planète. Cette production place ces organismes à la base des réseaux trophiques océaniques, ce qui permet de contrôler les stocks des maillons trophiques supérieurs (Siegel et Franz, 2010). En effet, il a été prouvé que la quantité de producteurs primaires présents dans un écosystème influence les stocks de pêche (Chassot et al., 2010). Toutefois, cette productivité n'est pas uniforme à travers le monde (Figure 2). Les écosystèmes côtiers ainsi que les zones d'upwelling (par exemple, la côte ouest africaine ou sud-américaine) sont les plus productifs, contrairement aux grands bassins océaniques (Field et al., 1998 ; Uitz et al., 2010). Cela est favorisé par les apports de nutriments en provenance du fond de l'océan (dans le cas des zones d'upwelling) ou par les côtes, ce qui favorise le développement du phytoplancton. Actuellement, entre un quart et un tiers de la production primaire nette mondiale se produit dans les écosystèmes côtiers (Pauly et Christensen, 1995 ; Boyce et al., 2010). Par exemple, la rade de Brest, notre site d'étude tout au long de ce manuscrit que nous présenterons plus en détail dans les prochains chapitres, est une région où la production primaire annuelle réalisée par le phytoplancton a été estimée à 148 $gC.m^{-2}.an^{-1}$ (Del Amo et al., 1997 ; Cloern et al., 2014), ce qui est plus élevé que ce qui est enregistré dans le bassin nord Atlantique (Uitz et al., 2010). Toutefois, bien que ces écosystèmes côtiers soient extrêmement productifs, ils font également partie des régions du globe les plus touchées par les activités anthropiques et sont donc soumis à des modifications importantes qui ont des conséquences sur leurs biocénoses.

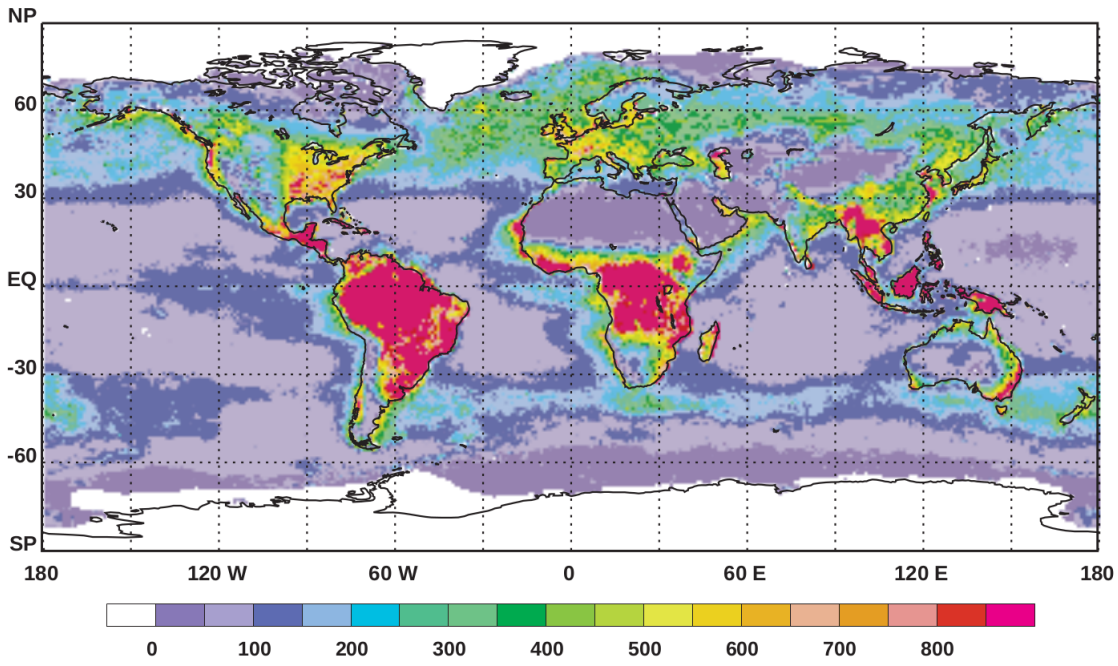

FIGURE 2 – Prodution primaire nette globale à l'échelle de la biosphère. Les valeurs sont en gramme de carbone par mètre carré et par an ($gC.m^{-2}.an^{-1}$)(de Field et al., 1998).

2 LES ÉCOSYSTÈMES CÔTIERS

Les écosystèmes côtiers subissent diverses pressions dues à leur proximité avec les zones côtières et aux impacts humains. Les littoraux sont des régions où la population humaine est concentrée, avec 60 % de la population mondiale vivant à moins de 100 km des côtes (Vitousek et al., 1997). De plus, 14 des 17 plus grandes villes du monde étant des villes côtières (Creel, 2003). La proximité de l'océan facilite l'accès aux ressources et favorise l'installation des êtres humains dans ces régions. Des scientifiques ont mis en évidence l'importance économique de ces régions et ont même estimé que le littoral contribuerait à un total de 12 600 milliards de dollars par an au bien-être humain, soit environ 60 % de la valeur de l'océan mondial (Costanza, 1999). Cependant, l'intérêt des êtres humains pour les littoraux a des conséquences sur l'environnement et l'intensification de leurs activités entraîne une pollution et des modifications chimiques, biologiques et physiques qui affectent ces écosystèmes (Boehm et al., 2017). Cette pollution comprend (i) la contamination microbienne pouvant être liée aux traitements des eaux usées et à leur évacuation, pouvant provoquer des cas de maladies digestives ou respiratoires chez les organismes marins (e.g., Shuval, 2003), (ii) le rejet de débris et de déchets plastiques (e.g., Jambeck et al., 2015), (iii) la surpêche pouvant créer des déséquilibres dans les chaînes trophiques (e.g., Jackson et al., 2001), (iv) la pollution sonore liée au transport maritime ou aux travaux d'aménagement (e.g., Slabbekoorn et al., 2010), (v) l'urbanisation, (vi) le changement climatique et toutes les conséquences qui y sont liées. Cependant, l'un des impacts les plus importants est le déséquilibre nutritif causé par l'apport artificiel de nutriments dans l'environnement. Ces apports peuvent avoir plusieurs origines, comme l'utilisation d'engrais azoté en agriculture, le rejet de composés phosphorés (par exemple les lessives) ou encore la construction de barrages mais ils peuvent également être introduits par des phénomènes naturels tels que le lessivage des roches. Ce phénomène est déjà connu et est appelé eutrophisation (Cloern, 2001 ; Pinay et al., 2018). L'apport artificiel de composés azotés et/ou phosphorés affecte directement les communautés phytoplanctoniques, dont les dynamiques temporelles se voient alors modifiées. De manière conceptuelle, Pinay et al. (2018) donne une indication des modifications des assemblages phytoplanctoniques en fonction du degré d'eutrophisation (Figure 3). Ces changements importants dans les espèces présentes ont un impact sur les écosystèmes et la vie qu'ils abritent, avec notamment une perte de la biodiversité et une diminution des concentrations en oxygène. De plus, ces changements peuvent mener à l'émergence et au sur-développement d'espèces de micro-algues toxiques (connu en anglais sous le terme de "Harmful Algae Bloom" - HAB) qui vont fortement modifier et créer des dysfonctionnements importants pour l'écosystème (contamination et maladie sur les maillons trophiques supérieurs par exemple).

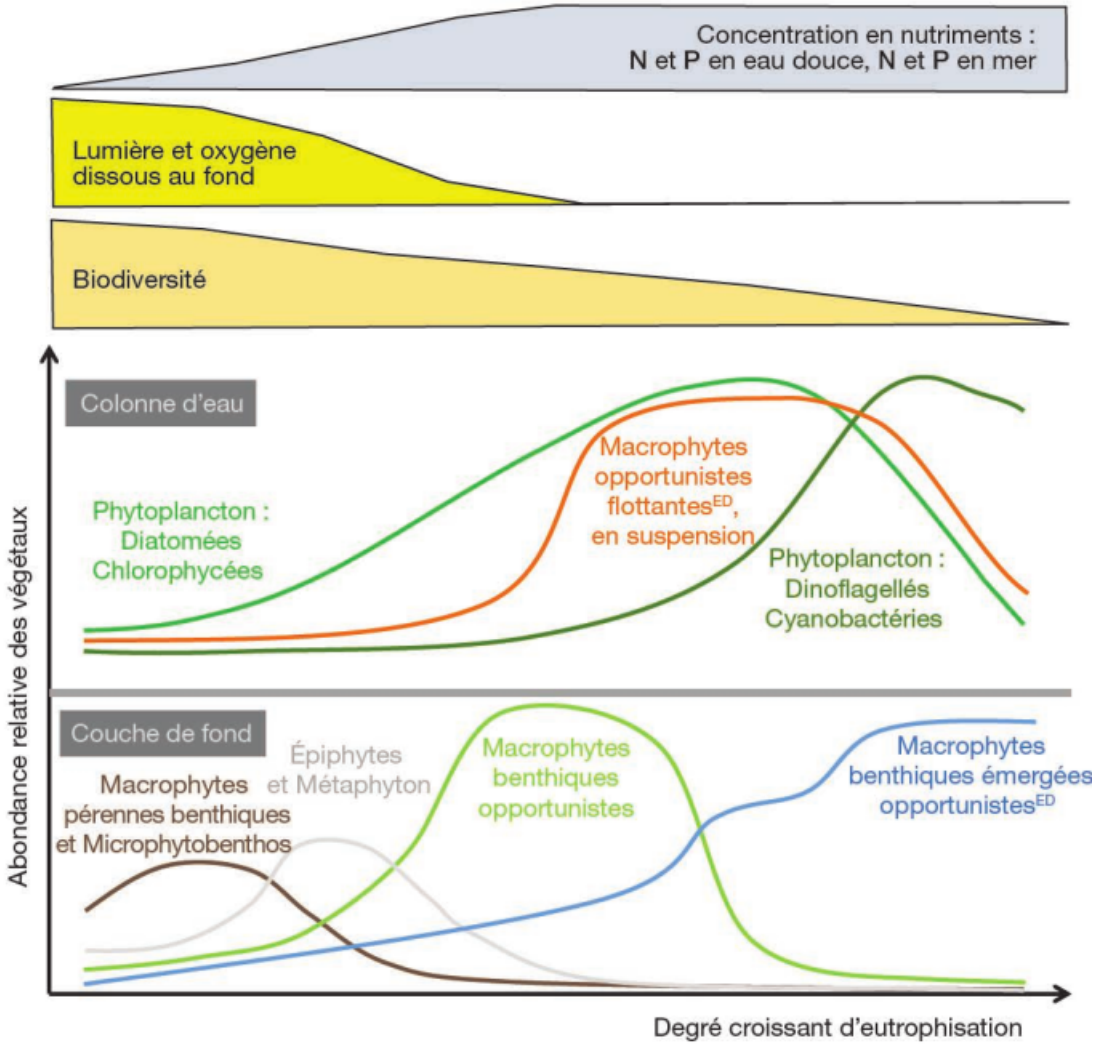

FIGURE 3 – Changement des communautés phytoplanctoniques en fonction du degré d'eutrophisation (Pinay et al., 2018).

3 LES DYNAMIQUES DE PRODUCTEURS PRIMAIRES DANS L'OCÉAN

3.1 Mesurer les dynamiques phytoplanctoniques dans l'océan

En raison de l'importance du phytoplancton pour les écosystèmes, plusieurs études ont tenté de dresser des séries temporelles des dynamiques passées de la production primaire. L'objectif est d'observer des tendances générales concernant les quantités de producteurs primaires, à petite ou grande échelle, afin d'acquérir des informations et de pouvoir établir des plans de gestion si des zones se trouvent menacées. Plusieurs méthodes existent pour cela. La première méthode consiste simplement à réaliser des suivis *in-situ* et à mesurer directement les quantités de phytoplanctons présents. Ces programmes servent de sentinelles pour identifier les changements futurs dans les écosystèmes marins (Hays et al., 2005). Cette méthode a été utilisée de nombreuses fois dans toutes les régions du globe (e.g., Hallegraeff et Jeffrey, 1984 ; Smayda, 1998 ; Edwards, 2004a ; Edwards et al., 2006b ;

Martin et al., 2009 ; Hinder et al., 2012 ; Davies et al., 2016 ; Rombouts et al., 2019 ; Lundsør et al., 2022). Cependant, l'inconvénient principal de cette méthode est qu'elle est très chronophage et nécessite une implication humaine ainsi que des coûts importants, limitant ainsi l'obtention de données à grande échelle temporelle et/ou spatiale. De plus, l'évolution des méthodes ne permet pas toujours la comparaison entre les données obtenues.

La deuxième méthode, qui s'est avérée très efficace, consiste à utiliser des satellites pour mesurer la couleur de l'océan. Cette couleur est directement liée aux concentrations de chlorophylle, et donc aux quantités de phytoplancton. Cette technique est appelée télédétection. Les premiers satellites ont été lancés à la fin des années 1970, mais une alliance internationale permettant la couverture de toute la surface de l'océan impliquant les satellites de plusieurs pays n'a vu le jour qu'en 2002 (Martin, 2014). De nombreuses études ont utilisé cette technique pour dresser, à l'échelle mondiale, des cartes de distribution du phytoplancton et son évolution au fil du temps (e.g., Gregg et al., 2005 ; McClain, 2009 ; Demarcq et al., 2011 ; Rousseaux et Gregg, 2015 ; Gregg et Rousseaux, 2019). Ils ont ainsi pu observer des tendances générales, dont nous discuterons dans la prochaine section. Cependant, bien que l'avantage majeur de cette technique soit la couverture quasi-totale de la planète, elle présente des défauts. En effet, la couverture nuageuse et les aérosols peuvent empêcher ces mesures, ce qui peut être extrêmement problématique. De plus, l'obscurité des hautes latitudes ainsi que le reflet des rayons solaires aux basses et moyennes latitudes sont également des problèmes (Gregg et Rousseaux, 2019). Enfin, bien que cette technique puisse être efficace au niveau de l'océan ouvert, mesurer la couleur de l'eau dans les écosystèmes côtiers présente un nouvel obstacle dû à de nombreux facteurs (réflectance du fond, concentrations en particules organiques et inorganiques plus élevées que dans l'océan ouvert, etc.) (Richardson et LeDrew, 2006).

3.2 Les modifications observées dans les dynamiques du phytoplancton

Les études scientifiques se sont multipliées dans toutes les régions du globe afin de mieux comprendre les dynamiques des producteurs primaires. Au cours des dernières décennies, les quantités de producteurs primaires marins ont présenté des tendances générales, mais l'ampleur et la direction de ces changements sont encore débattues par la communauté scientifique (Boyce et al., 2010 ; McQuatters-Gollop et al., 2011 ; Rykaczewski et Dunne, 2011). Les raisons réelles de ces tendances observées restent encore méconnues étant donné qu'il n'existe pas de donnée disponible avant l'intensification des activités anthropiques. Ces raisons peuvent en effet être liées à l'activité humaine ou encore faire partie d'un cycle naturel à long terme. Cependant, une diminution globale des quantités de phytoplancton à l'échelle du globe a été observée, et dans 74% des cas, cela se passe dans des régions où la température de surface de l'océan (Sea Surface Temperature - SST) augmentait (Behrenfeld et al., 2006). Cette diminution globale des quantités de phytoplancton a déjà été rapportée par Boyce et al. (2010), mais cela fait encore débat (McQuatters-Gollop et al., 2011 ; Rykaczewski et

Dunne, 2011). En effet, Gregg et al. (2005) ont par exemple enregistré une augmentation globale de 4% de la production primaire mondiale entre 1998 et 2003 à l'aide de mesures satellites.

À des échelles spatiales plus petites, Hinder et al. (2012) ont montré que les concentrations de dinoflagellés, toxiques ou non, ont fortement diminué depuis 2006 en mer du Nord, ce qui n'est pas le cas des diatomées. D'autres scientifiques s'intéressant à d'autres régions du globe ont également observé ce genre de tendances ou des tendances inverses (e.g., Hallegraeff, 2010 ; Edwards et al., 2006a). Cela montre alors la difficulté de caractériser au mieux l'évolution du phytoplancton dans les océans, étant donné que chaque région du globe et chaque écosystème, de par sa complexité et ses caractéristiques, possède une tendance générale qui lui est propre (Rousseaux et Gregg, 2015).

Cependant, même à des échelles temporelles plus petites, c'est-à-dire sur une seule année, des modifications importantes ont été observées en réponse aux pressions que subissent les producteurs primaires actuellement. En effet, on peut observer un important élargissement des fenêtres d'efflorescences phytoplanctoniques (ou bloom), en lien avec une augmentation des températures de l'eau (Moore et al., 2008). Cela peut alors induire une modification de la phénologie des blooms d'une année à l'autre, ce qui a déjà été observé par Edwards (2004a). Ces auteurs ont en effet signalé que les blooms de certaines espèces s'intensifiaient en mer du Nord et qu'ils apparaissaient quatre à six semaines plus tôt que les années précédentes. De plus, cela peut également induire un plus grand nombre de blooms durant une année ainsi qu'une augmentation de leur durée (Edwards et Richardson, 2004b), ce qui peut causer des problèmes pour les écosystèmes (e.g., perte de luminosité, hypoxie, etc.). L'intensification de ces blooms peut alors poser de graves problèmes écologiques, en particulier si cela favorise l'émergence et le développement d'espèces toxiques.

La problématique soulignée ici est que les techniques précédemment évoquées ne permettent pas d'obtenir de mesures fiables avant le déploiement des différents outils ou nécessitent la présence directe des scientifiques. En outre, elles ne permettent pas la construction de séries temporelles relativement longues pour observer des tendances significatives à long terme. En effet, selon Henson et al. (2010, 2016), une série temporelle climatique à long terme doit durer au moins 30 à 40 ans pour être suffisamment robuste. Bien que certaines séries temporelles dépassent ce seuil, cela ne concerne que très peu d'études et toujours à une faible échelle spatiale. Tout cela alimente le débat et soulève la question de l'évolution du phytoplancton au fil du temps, montrant la complexité de la problématique. Bien que l'augmentation de l'activité anthropique soit l'hypothèse la plus avancée pour expliquer toutes ces modifications, le manque de données à long terme, c'est-à-dire avant l'augmentation de ces activités au milieu du XIX^{ème} siècle pendant la révolution industrielle, ne permet pas de quantifier réellement l'impact des humains sur la dynamique spatio-temporelle des producteurs primaires, qui reste mal caractérisée. Il est donc primordial de trouver un moyen d'accéder à de telles données. C'est ainsi qu'un nouveau champ scientifique capable de répondre à cette problématique a vu le jour : la sclérochronologie.

4 LA SCLÉROCHRONOLOGIE

4.1 Présentation des principes

Le terme "sclérochronologie", formé des mots grecs "sklêros", "khronos" et "logos", a été utilisé pour la première fois dans une publication scientifique au milieu des années 1970 (Hudson et al., 1976). Il est défini comme l'étude des variations physiques et chimiques des tissus durs accrétionnaires des organismes, ainsi que du contexte temporel dans lequel ils ont été formés. Ce domaine repose sur le fait qu'au cours de leur vie, des organismes marins possédant une structure calcaire vont enregistrer au sein de celle-ci les variations des paramètres physico-chimiques de leur environnement. Dérivé directement de la dendrochronologie, alors déjà bien implantée dans le paysage scientifique, la sclérochronologie bénéficie des outils déjà existants et couramment utilisés pour l'étude des cernes d'arbres, permettant une démocratisation relativement rapide de la discipline. Le nombre de publications a en effet augmenté au fil des années, passant de moins de cinq articles par an dans les années 1990 à une quarantaine de publications par an à partir de 2017 (Gillikin et al., 2019 ; Peharda et al., 2021). L'objectif principal de ces études est alors de reconstruire les environnements et les climats passés à des échelles temporelles petites ou grandes, afin de combler le manque de données environnementales passées qui, soit n'existent pas, soit sont inaccessibles au-delà d'une certaine époque. Cela permet en partie d'allonger les séries temporelles existantes, d'alimenter les modèles climatiques pour les tester et les affiner, ou encore de comparer les paléoenvironnements avec l'environnement actuel. Cependant, pour entreprendre des études sclérochronologiques, il est nécessaire de remplir un certain nombre de conditions.

Pour utiliser un organisme comme archive environnementale, il est tout d'abord crucial que celui-ci produise et possède une structure rigide (coquille, squelette, os, etc.) qui reste inerte et ne se dégrade pas avec le temps. De plus, il est nécessaire que cet organisme présente des marques de croissance qui apparaissent de manière périodique sur cette structure et que leur fréquence d'apparition soit connue (annuelle, mensuelle, bi-mensuelle, quotidienne, etc.). Obtenir cette information est primordial pour donner un contexte temporel à chaque incrément [1] formé, et donc aux résultats extraits, qu'ils soient de nature structurale (croissance et largeur d'incrément) ou chimique (composition élémentaire ou isotopique de l'incrément). En effet, il est aujourd'hui établi que la composition chimique des coquilles de mollusques est liée à différents paramètres environnementaux (e.g., Klein et al., 1996 ; Vander Putten et al., 2000 ; Gillikin et al., 2006 ; Gillikin et al., 2008 ; Markulin et al., 2019 ; Doré et al., 2020 ; Thébault et al., 2022). Ces éléments chimiques sont appelés traceurs environnementaux, ou proxies, et leur mesure dans les structures calcaires permet d'accéder à des informations sur les environnements dans lesquels l'organisme s'est développé et a formé cette structure. Par exemple, la

1. Un incrément correspond à la portion de carbonate (de coquille par exemple) qui se trouve entre deux lignes de croissance

mesure des rapports isotopiques de l'oxygène (notée $\delta^{18}O$) dans les tissus durs accrétionnaires est l'un des indicateurs paléoclimatiques les plus anciens et les plus largement utilisés. Ce proxy dépend de la température, et également du $\delta^{18}O$ de l'eau, et a permis de reconstruire les températures (e.g., Schöne et al., 2004), ainsi que les précipitations (e.g., Azzoug et al., 2012) des paléoenvironnements.

Au cours des dernières décennies, le nombre d'organismes servant d'archives sclérochronologiques n'a cessé d'augmenter, permettant ainsi d'élargir le spectre des réponses possibles aux différents questionnements de la communauté scientifique. Chaque archive possède en effet ses avantages en fonction des problématiques posées. Les plus couramment utilisées sont les coquilles de mollusques, les squelettes de coraux, les otolithes [2] de poissons ou encore les algues coralligènes (Peharda et al., 2021). À titre d'exemple, l'un des modèles les plus connus et les plus utilisés pour les études sclérochronologiques et sclérochimiques est la palourde arctique, *Arctica islandica*, un mollusque bivalve que l'on retrouve dans l'Atlantique nord. Avec l'apparition de marques de croissance annuelles, une large répartition à l'échelle du bassin Nord-Atlantique, et sa longévité extraordinaire (507 ans au maximum - Butler et al., 2013), elle est un modèle de choix afin de dresser des séries temporelles reconstruisant plusieurs paramètres de la colonne d'eau sur plusieurs siècles (e.g., Witbaard, 1996 ; Schöne et al., 2005 ; Schöne, 2013 ; Butler et al., 2013 ; Poitevin et al., 2019 ; Doré et al., 2020 ; Brosset et al., 2022 ; Höche et al., 2022). Cependant, ce type de modèle n'est pas efficace pour reconstruire les paramètres physico-chimiques de la colonne d'eau avec une grande résolution temporelle, i.e., à l'échelle sub-annuelle ou journalière, ce qui est nécessaire pour étudier les variations hautes fréquences des structures de communautés phytoplanctoniques, dont les modifications dans l'environnement interviennent à de petites échelles spatiales et temporelles. Dans ce cas, l'utilisation d'une archive biogénique présentant des marques de croissance journalières est alors nécessaire, et l'un des meilleurs candidats répondant à ces exigences est la coquille St-Jacques, *Pecten maximus*.

4.2 La sclérochronologie de la coquille St-Jacques, *Pecten maximus*

La coquille St-Jacques, un mollusque bivalve de la famille des Pectinidés, est une espèce emblématique des côtes ouest de l'Europe et particulièrement de la région Bretagne. Il s'agit d'un organisme microphage suspensivore, c'est-à-dire qu'il se nourrit de phytoplancton en filtrant l'eau et en retenant les particules avec ses branchies, qui seront ensuite ingérées et digérées. Les spécimens de *P. maximus* ont une période de croissance annuelle allant du mois de février/mars au mois d'octobre/novembre et arrêtent leur croissance pendant l'hiver, ce qui forme un anneau concentrique sur la surface de la coquille, appelé strie hivernale (Figure 4A). En plus de ces marques de croissance annuelles, l'intérêt de la communauté scientifique pour cette espèce a grandi suite à la découverte de stries de croissance qui se déposent quotidiennement sur la surface de la coquille (Antoine, 1978 ; Chauvaud et al., 1998)

2. Structure osseuse se trouvant au niveau de l'oreille interne des poissons

(Figure 4B). Grâce à l'analyse structurelle et chimique de ces incréments journaliers, il est possible de retracer, au jour près, les paramètres physico-chimiques de son environnement. Pour ce faire, les signaux chimiques sont analysés dans chaque incrément suivant l'axe de croissance (de la charnière vers la marge ventrale - flèche blanche sur la figure 4A) afin d'obtenir des mesures quotidiennes.

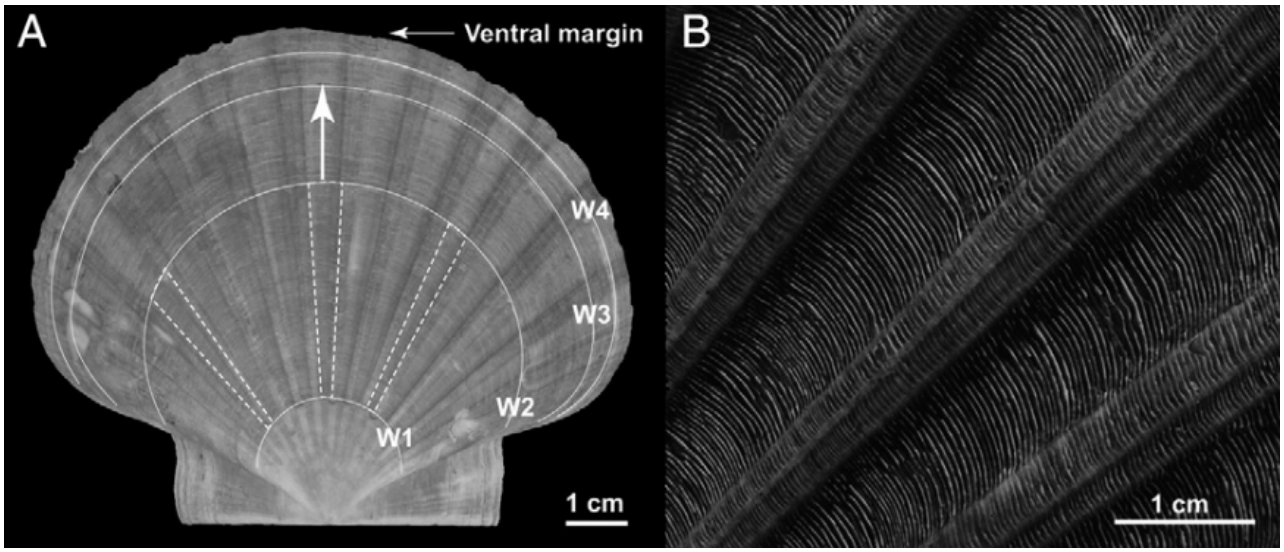

FIGURE 4 – Surface de la couche externe d'une valve gauche de coquille St-Jacques présentant les marques de croissance hivernales (A) ainsi que les stries de croissance journalière (B) (de Thébault et Chauvaud, 2013).

Jusqu'à présent, plusieurs traceurs incorporés dans la coquille sont utilisés pour estimer les quantités de phytoplancton dans l'environnement. Le premier de ces traceurs est structurel et concerne les variations des taux de croissance journaliers de la coquille. Habituellement, la croissance de la coquille se caractérise par une augmentation des taux de croissance journaliers entre la fin de l'hiver et l'été, suivie d'une diminution jusqu'au début de l'hiver suivant, au moment où l'organisme stoppe sa croissance. Cependant, une diminution importante des taux de croissance journaliers peut également se produire au printemps, en raison de la formation d'un bloom de phytoplancton, qui pourrait obstruer les branchies en raison de la sédimentation d'une quantité de cellules très importante, de la formation d'agrégats phytoplanctoniques ou encore de l'apparition d'espèces toxiques (Chauvaud et al., 1998 ; Lorrain et al., 2000 ; Fröhlich et al., 2022a). Cependant, de nombreux autres paramètres peuvent impacter la croissance de *P. maximus*, tels que la température, la nourriture ou l'hydrodynamisme, ce qui rend ce traceur peu précis pour reconstruire les dynamiques phytoplanctoniques. Pour ce faire, les indicateurs les plus précis et les plus couramment utilisés sont basés sur la composition chimique de la coquille.

Dans les coquilles de bivalves, le proxy le plus utilisé dans le but de retracer les dynamiques de production primaire passées est le rapport baryum-calcium (Ba:Ca). La présence de pics de Ba:Ca nets et erratiques dans la coquille est une caractéristique frappante observée dans différentes espèces de bivalves (e.g., Stecher et al., 1996 ; Vander Putten et al., 2000 ; Lazareth et al., 2003 ; Gillikin et al.,

2006 ; Thébault et al., 2009), dont *P. maximus* (e.g., Gillikin et al., 2008 ; Barats et al., 2009 ; Fröhlich et al., 2022b). Étant donné que ces pics se produisent de manière synchrone chez les spécimens contemporains d'une même population, il est fort probable que l'incorporation de cet élément dans la coquille soit dû à un forçage environnemental. La plupart des études ci-dessus ont trouvé une forte corrélation entre ces pics de Ba:Ca et les blooms de phytoplancton, généralement des diatomées. L'hypothèse serait que le baryum est absorbé par des oxyhydroxydes de fer qui sont précipités à la surface des frustules [3] de diatomées (Sternberg et al., 2005). Ces diatomées se retrouveraient alors ingérées et digérées par les organismes et le baryum accumulé sur les cellules se retrouverait incorporé dans leur coquille.

Tout comme les signaux de Ba:Ca, le rapport lithium-calcium (Li:Ca) mesuré dans les valves de la Coquille St-Jacques s'est révélé être un proxy efficace des dynamiques des diatomées présentes dans la colonne d'eau (Thébault et Chauvaud, 2013 ; Thébault et al., 2022). Les hypothèses sous-jacentes sont similaires à celles pour le baryum : le lithium serait adsorbé à la surface des diatomées, puis transporté lors de leur sédimentation à la fin d'un bloom vers le fond, où il serait incorporé dans la coquille de *P. maximus* suite à l'ingestion de ces cellules. De plus, la reminéralisation de la silice biogénique au niveau de l'interface eau sédiment permettait d'expliquer le délai observé de quelques semaines entre le bloom de diatomées observé, et le pic de Li:Ca observé dans la coquille de *P. maximus* (Thébault et al., 2022).

Enfin, le rapport molybdène-calcium (Mo:Ca) présente un profil similaire à celui du ratio Ba:Ca dans la coquille. Il est caractérisé par une ligne de base interrompue par des pics nets et importants, et a déjà permis d'expliquer les dynamiques des producteurs primaires (e.g., Fröhlich et al., 2022a ; Thébault et al., 2022). Les hypothèses sous-jacentes à ce traceur concernent l'ingestion d'agrégats phytoplanctoniques chargés en molybdène. À la fin d'un bloom et dans des conditions stressantes, les cellules du phytoplancton sont connues pour produire des composés collants qui conduisent à la formation d'agglomérats de cellules ainsi que d'autres particules organiques (fèces) ou inorganiques (particules minérales) (e.g., Alldredge et al., 1993 ; Passow et Alldredge, 1994 ; Myklestad, 1995 ; Dam et Drapeau, 1995 ; Engel, 2000). Ces agrégats constituent ce qu'on appelle plus communément la "neige marine" et sont connus pour former de véritables microenvironnements avec des conditions physico-chimiques différentes de l'eau environnante. En raison de ces caractéristiques, des études ont rapporté que ces agrégats pouvaient adsorber de manière significative le molybdène et le transporter vers le fond (Dellwig et al., 2007 ; Mori et al., 2021). L'ingestion de ces agrégats enrichis en Mo pourrait alors expliquer en partie l'apparition des pics de Mo:Ca enregistrés dans la coquille (Thébault et al., 2022).

Il existe donc un certain nombre de traceurs environnementaux disponibles afin de retracer les dynamiques phytoplanctoniques de l'environnement.

3. Le frustule correspond à l'enveloppe siliceuse qui recouvre et protège les cellules de diatomées

5 PROBLÉMATIQUES, OBJECTIFS ET PLAN DU MANUSCRIT

Malgré l'utilisation de ces traceurs par une partie de la communauté scientifique, il reste des zones d'ombre à éclaircir et des connaissances à affiner. En effet, des questions subsistent quant aux mécanismes et aux voies empruntées par ces éléments avant leur incorporation dans la coquille. De plus, la plupart des études citées ci-dessus relient les signaux mesurés dans la coquille aux quantités de chlorophylle *a* mesurées dans l'environnement, un paramètre plus accessible que les quantités réelles de phytoplancton. Cependant, ces deux paramètres ne sont pas nécessairement corrélés. Des études récentes ont par exemple montré que les signaux de Ba:Ca mesurés dans les coquilles de *P. maximus* pourraient être liés à l'apparition de blooms d'espèces phytoplanctoniques particulières plutôt qu'au groupe des diatomées en général, ces espèces ayant une teneur en baryum naturellement plus élevée que d'autres (Fröhlich et al., 2022b). Cela met alors en évidence une autre limitation et soulève une autre question majeure : dans quelles mesures les dynamiques phytoplanctoniques à petite échelle temporelle (variations dans les structures des communautés, apparition de blooms, formation d'agrégats) affectent les propriétés chimiques et la biodisponibilité du baryum, du lithium et du molybdène pour les consommateurs primaires ? Apporter des réponses à cette question est crucial afin de mieux comprendre les mécanismes d'incorporation de ces éléments dans les valves de *P. maximus*. Les hypothèses avancées jusqu'à présent se verraient alors infirmées ou confirmées, et d'autres pourraient voir le jour. Il deviendrait alors possible d'appliquer ces nouvelles connaissances à des coquilles anciennes afin de retracer les dynamiques phytoplanctoniques à petite échelle temporelle dans les écosystèmes côtiers il y a plusieurs siècles ou millénaires. Jusqu'à présent, de telles études n'existent toujours pas, mais elles pourraient représenter une avancée majeure pour la communauté scientifique, car elles permettraient de comparer un environnement passé, exempt d'activités humaines, avec l'environnement actuel et ainsi de quantifier l'impact de l'Homme sur les écosystèmes côtiers. Ces différentes problématiques appellent donc plusieurs objectifs :

— **Objectif 1 :** Le premier objectif de ce travail de thèse consiste à mieux comprendre les relations qui existent entre les variations hautes fréquences des structures des communautés phytoplanctoniques et les variations des concentrations en éléments traces dans la colonne d'eau. Cela permettra alors de mieux comprendre comment le phytoplancton, de par sa dynamique et la formation d'agrégats, peut accumuler certains éléments et donc influencer leur transport vers l'interface eau-sédiment.

— **Objectif 2 :** Le deuxième objectif consiste à appliquer les hypothèses émises en réponse au premier afin d'expliquer les profiles en éléments traces incorporés dans les valves de coquilles St-Jacques. Il s'agira alors de vérifier si les variations dans les rapports Li:Ca, Mo:Ca et Ba:Ca

suivent les variations hautes fréquences des structures des communautés de micro-algues, et ainsi calibrer ces différents traceurs dans le but de reconstruire les dynamiques phytoplanctoniques.

— **Objectif 3 :** En se basant sur les connaissances acquises précédemment, le dernier objectif de ce travail de thèse est de réaliser les premières reconstructions des dynamiques phytoplanctoniques des environnements passés, en analysant la composition chimique de valves de *P. maximus* archéologiques. À partir des signaux obtenus, nous tenterons d'observer des différences ou des similitudes entre la phénologie des blooms ainsi que la structure des communautés de phytoplancton des paléoenvironnements, dépourvus de tout impact anthropique, et celles de l'environnement actuel. Il deviendrait alors possible de quantifier l'impact des activités humaines sur les écosystèmes côtiers.

Dans le but de répondre à ces trois objectifs, ce manuscrit de thèse sera divisé en cinq chapitres rédigés en anglais. Afin de répondre aux deux premiers objectifs, un suivi environnemental a été réalisé en rade de Brest durant lequel un grand nombre de paramètres physiques, chimiques et biologiques, ont été mesurés. Le **chapitre 1** de ce manuscrit présente ce suivi ainsi que tous ces paramètres, et consiste en un article scientifique qui a été soumis dans le journal *Earth System Science Data*. Avec un échantillonnage à haute fréquence (une à deux fois par semaine) qui s'est étendu sur huit mois, nous avons pu traquer différents évènements inhérents aux dynamiques phytoplanctoniques (efflorescences, formation d'agrégats, etc.) que nous avons lié aux modifications observées dans les propriétés chimiques de la colonne d'eau (e.g., variations des concentrations en éléments traces dans la fraction dissoute et particulaire). Les résultats obtenus ont alors été discutés dans le cadre du **chapitre 2**, qui est une publication dernièrement soumise dans le journal *Estuarine, Coastal and Shelf Science* (actuellement en cours de révision).

Avant de vérifier si les hypothèses avancées au cours de ce dernier chapitre pouvaient expliquer les profils en éléments traces mesurées dans les coquilles de *P. maximus*, des expérimentations en laboratoire ont été menées. Le but de ces expériences était d'étudier l'accumulation des éléments traces dans les agrégats formés artificiellement à partir de différentes souches de phytoplancton, dans le but de dresser une liste d'éléments qui pourraient être considérés comme des traceurs des évènements d'agrégation. Les résultats seront présentés et discutés au cours du **chapitre 3** de ce manuscrit.

Une fois toutes ces hypothèses dressées, il était de temps de voir si les profils de Li:Ca, Mo:Ca et Ba:Ca mesurés dans les coquilles de *P. maximus* récoltées à la fin du suivi environnemental était en accord avec ces dernières. Cela a permis de calibrer ces différents proxies afin de retracer à petite échelle temporelle les dynamiques phytoplanctoniques de la colonne d'eau. Cette étude a donc permis de répondre au deuxième objectif de ce manuscrit et les résultats seront discutés dans le **chapitre 4**.

Ce chapitre a fait l'objet d'un article qui a récemment été soumis dans le journal *Limnology and Oceanography* (en cours de révision).

Enfin, le **chapitre 5** est un chapitre d'ouverture qui présente les toutes premières analyses sclérochimiques effectuées sur des coquilles archéologiques de *P. maximus*, provenant d'il y a 4500 ans et du XIII^{ème} siècle. Les premières reconstructions hautes fréquences des dynamiques phytoplanctoniques ont alors été effectuées et des comparaisons avec les dynamiques observées dans l'environnement actuel ont pu être faîtes, en réponse au troisième objectif.

CHAPTER 1

HIPPO ENVIRONMENTAL MONITORING

PREAMBLE/PRÉAMBULE

Based on the objectives given above, the first chapter of this manuscript provides an introduction to the HIPPO environmental monitoring, which was the cornerstone of this thesis as well as our research project. This monitoring was conducted between March and October 2021 in the Bay of Brest (Brittany - France), and generated a significant amount of chemical, biological and physical data. Due to the vast quantity of data obtained (which have been made publicly available at https://www.seanoe.org/data/00808/92043/ (Siebert et al., 2023)), an article was written to present the results. The publication, entitled "HIPPO environmental monitoring: Impact of phytoplankton dynamics on water column chemistry and the sclerochronology of the king scallop (*Pecten maximus*) as a biogenic archive for past primary production reconstructions", has been submitted to *Earth System Science Data* and is currently under review. The results and figures presented in this chapter provide a general overview of the dataset, and will not be discussed in detail. Nonetheless, the subsequent chapters of this manuscript will provide an in-depth discussion of the results.

En se basant sur les objectifs donnés ci-dessus, ce manuscrit de thèse s'ouvre sur un premier chapitre présentant le suivi environnemental HIPPO, qui constitue la pierre angulaire de notre projet de recherche. Ce suivi a eu lieu entre mars et octobre 2021 en rade de Brest (Bretagne - France), et a produit un jeu de données conséquent (ce jeu de données a été rendu publique et est consultable à cette adresse : https://www.seanoe.org/data/00808/92043/ (Siebert et al., 2023)). En raison de la quantité de données chimiques, biologiques et chimiques recueillies, nous avons décidé de rédiger un article présentant les résultats obtenus pour les différents paramètres. Cette publication, intitulée "HIPPO environmental monitoring: Impact of phytoplankton dynamics on water column chemistry and the sclerochronology of the king scallop (*Pecten maximus*) as a biogenic archive for past primary production reconstructions", a été soumis au journal *Earth System Science Data*. Les résultats et les figures présentés ici ne représentent qu'un aperçu des données obtenues et ne seront pas discutés en détail. Toutefois, cela sera fait dans les prochains chapitres de ce manuscrit.

HIPPO environmental monitoring: Impact of phytoplankton dynamics on water column chemistry and the sclerochronology of the king scallop (*Pecten maximus*) as a biogenic archive for past primary production reconstructions

Valentin Siebert[1], Brivaëla Moriceau[1], Lukas Fröhlich[2], Bernd R. Schöne[2], Erwan Amice[1], Beatriz Becker[3], Kevin Bihannic[1], Isabelle Bihannic[1], Gaspard Delebecq[1], Jérémy Devesa[1], Morgane Gallinari[1], Yoan Germain[4], Émilie Grossteffan[5], Klaus-Peter Jochum[6], Thierry Le Bec[5], Manon Le Goff[1], Céline Liorzou[7], Claudie Marec[5], Marc Picheral[8], Peggy Rimmelin-Maury[5], Marie-Laure Rouget[5], Matthieu Waeles[1], Julien Thébault[1]

[1]*Univ Brest, CNRS, IRD, Ifremer, LEMAR, F-29280 Plouzané, France*

[2]*Institute of Geosciences, University of Mainz, Johann-Joachim-Becher-Weg 21, 55128 Mainz, Germany*

[3]*Centre d'Océanologie de Marseille, rue de la Batterie des Lions, 13007 Marseille, France*

[4]*Department of Marine Geoscience, Institut Français de Recherche pour l'Exploitation de la Mer, Centre de Brest, 29280 Plouzané, France*

[5]*Institut Universitaire Européen de la Mer, IUEM, UAR 3113, Université de Bretagne Occidentale, CNRS, IRD , PLouzané, France*

[6]*Climate Geochemistry Department, Max Planck Institute for Chemistry, Mainz, Germany*

[7]*Université de Bretagne Occidentale, Laboratoire Geo-Ocean, CNRS-UBO-Ifremer-UBS, IUEM, Plouzané, France*

[8]*Sorbonne Université, Centre National de la Recherche Scientifique, Laboratoire d'Océanographie de Villefranche (LOV), Villefranche-sur-Mer, FranceUniv Brest, CNRS, IRD, Ifremer, LEMAR, F-29280 Plouzané, France*

ABSTRACT

As part of the HIPPO (HIgh-resolution Primary Production multi-prOxy archives) project, an environmental monitoring was carried out between March and October 2021 in the Bay of Brest. The aim of this survey was to better understand the processes which drive the incorporation of chemical elements into scallop shells and their links with phytoplankton dynamics. For this purpose, biological samples (scallops and phytoplankton) as well as water samples were collected in order to analyse various environmental parameters (element chemical properties, nutrients, chlorophyll, etc.). Here, some of the monitoring data are presented and discussed. The whole dataset is much larger and can potentially be very useful for other scientists performing sclerochronological investigations, studying

biogeochemical cycles or conducting various ecological research projects. The dataset is available at https://www.seanoe.org/data/00808/92043/ (Siebert et al., 2023).

1 INTRODUCTION

Primary producers form the foundation of marine food webs, control population sizes at higher trophic levels and influence fish stock recruitment (Chassot et al., 2010). Marine photoautotrophic organisms are responsible for nearly half of the global net primary production and fix substantial amounts of carbon (Field et al., 1998). Despite their key role in the functioning of marine ecosystems and the global climate, past primary production dynamics and mechanisms controlling them have not been well characterized (Boyce et al., 2010), especially for time intervals prior to the instrumental recording and significant anthropological disturbances of biogeochemical cycles. Available data sources on changes in marine primary production do not provide the necessary temporal resolution, are too short to determine long-term trends and do not cover the entirety of photoautotroph taxa. To compensate for this lack of past data, biogenic archives have been interrogated, such as bivalve shells, to track the past dynamics of primary production. It has already been shown that some bivalve species incorporate trace elements into their skeletal structures (e.g., calcite or aragonite) and that the observed trends follow the patterns of the dynamics of primary producers in the water column (e.g., Stecher et al., 1996; Barats et al., 2009; Thébault et al., 2009; Doré et al., 2020). In particular, the king scallop, *Pecten maximus* can record these signals on a daily scale, allowing high-resolution temporal reconstructions (Chauvaud et al., 1998; Thébault and Chauvaud, 2013; Fröhlich et al., 2022a). The research project HIPPO aims to better understand these environmental proxies and to develop new tracers and integrate them in a multi-proxy approach. For this purpose, environmental monitoring with a high temporal resolution was set up in 2021 in the Bay of Brest (France). Here, an overview of the physical, biological and chemical parameters of the seawater is presented along with geochemical data of king scallop shells. All data were obtained during the HIPPO survey.

2 STUDY SITE AND SAMPLING STRATEGY

The Bay of Brest is a semi-enclosed, macrotidal, marine ecosystem of 180 km^2 with a westward connection to the Iroise Sea via a deep (40 m max. depth) and narrow (2 km width) strait. Freshwater inputs are brought from the east via two main rivers, the Aulne in the south and the Elorn in the north of the bay (Figure 5). The study was carried out between early March and mid-October 2021, with a total of 38 cruises off Lanvéoc (48°17'39"N – 004°27'12"W), a site located in the southern part of the Bay of Brest (France, Figure 5A). This site was chosen for its status as a no-fishing and no-

hunting zone, allowing for undisturbed monitoring. Moreover, this site has already been the subject of scientific surveys in the past, conducted by the LEMAR-Laboratory and the observatory service of the European Institute for Marine Studies (IUEM). Lanvéoc is characterized by shallow waters (from approx. 8 m to 15 m depending on the tide, with a mean depth of approx. 11.5 m recorded at mid-tide) and a seafloor made up of sandy and silty sediment, with significant amounts of large-sized biogenic detritus (shells, maerl).

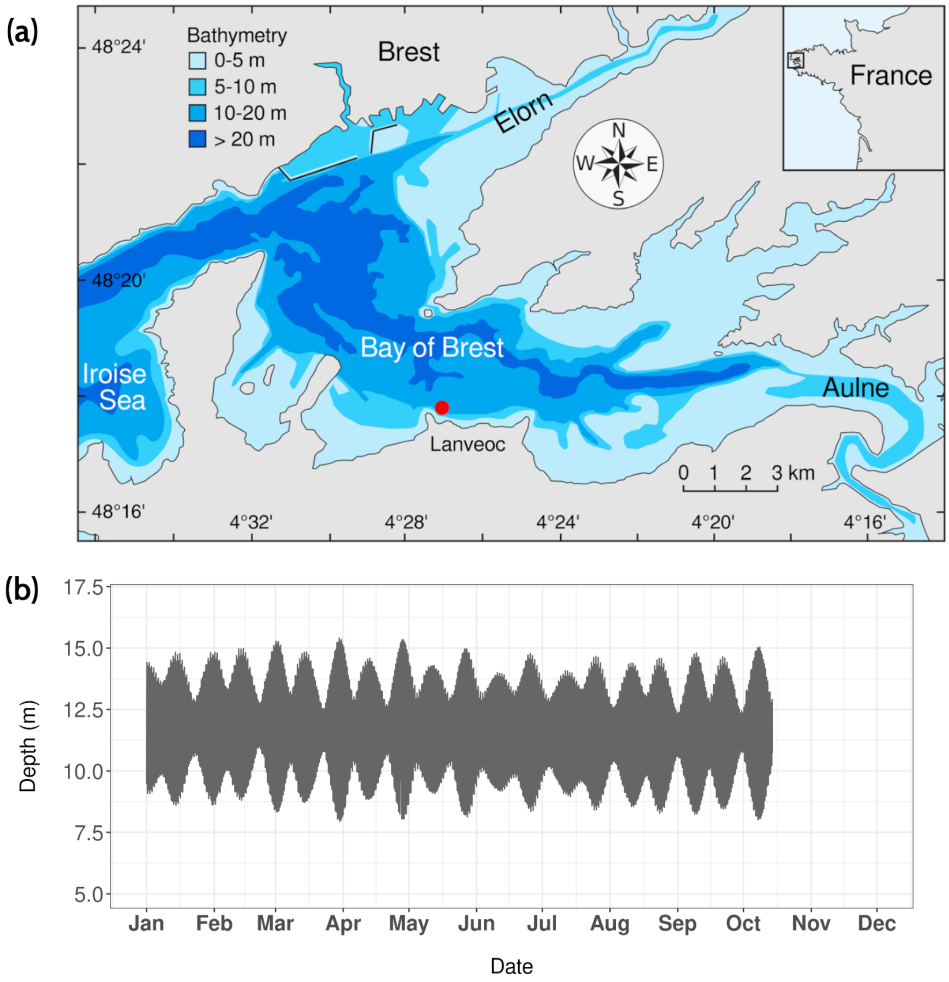

Figure 5 – (a) Sampling location of the HIPPO monitoring area: Lanvéoc (red dot) (adapted from Thébault et al., 2022). (b) Hourly depth variations recorded with NKE/Sambat probes deployed at the seafloor at Lanvéoc in 2021.

Water samples from the surface (1 m deep) and bottom (approx. 20 cm above the sediment) were collected twice a week between the 16 March and the end of June 2021, and once a week thereafter until mid-October 2021. No sampling was conducted during August, leading to a lack of data for this month. Several biological, chemicals or physical parameters were measured in these seawater samples: an exhaustive list is given in Table 1. For samples dedicated to trace element measurements, a 5 L Teflon-coated GoFlo sampling bottle was used. For the measurements of all other parameters, seawater was collected in a 5 L or a 8 L Niskin bottle. In addition to seawater sampling, two NKE/Sambat

probes were alternately deployed to track high frequency physical parameters (CTDO2FluoTurbpH – measurements every 20 minutes). For example, tidal dynamics were assessed in the Bay of Brest by recording the water depth at Lanvéoc (Figure 5B). The two major episodes of near-maximum tidal range occurred around 30 March (tidal range: 7.15 m) and 28 April (tidal range: 7.00 m). Two other instruments were deployed to track particle dynamics and chemistry: an imaging sensor, the Underwater Vision Profiler (UVP6), and a sediment trap. The settings used, specific to each instrument, will be described further below.

In addition to seawater sampling, 2,640 age-class I specimens of the king scallop, *Pecten maximus* (whose growth ceases only during the winter season - height = approx. 3 cm), were placed on the sediment surface on 21 February 2021, before the beginning of the HIPPO monitoring phase. These individuals come from the Tinduff hatchery (located in Plougastel-Daoulas, in the eastern part of the Bay of Brest) and are derived from a very limited number of spawners, and are thus genetically closely related. To assess the impact of the sediment on the incorporation of the different trace elements into their shells (calcite), 360 specimens were placed in a cage located 1 m above the seafloor, devoid of any sediment. During each cruise, five shells were collected directly on the sediment (when possible) and five others from the cage to analyze the soft tissues (gills, mantle, digestive glands and muscle) for element chemical composition. At the end of the monitoring interval (on 11 October 2021), a larger number of bivalves was collected to establish a growth and element chemical time-series for 2021.

3 DATA OVERVIEW

3.1 Physical data

To monitor some of the physical and chemical parameters in the water column, two NKE/Sambat probes were alternately deployed at the seafloor at Lanvéoc. Throughout the year, they recorded water depth (Figure 5B), temperature, salinity, pH, fluorescence and dissolved oxygen concentration (DO) every 20 minutes. Figure 6 shows the signals obtained for each parameter after removing outliers and data windows on which sensors showed malfunctions or recorded outliers, hence the lack of data for some variables for some time intervals. Water temperature increased from approx. 10 °C in March to 18 °C in August, remaining stable at this value until the end of September before decreasing slightly until the end of the monitoring. Simultaneously, salinity increased more rapidly from March (approx. 32 psu) to May (approx. 34.3 psu), caused by lower freshwater inflow from the Aulne due to a gradual decrease of its flow rate during spring (Aulne flow data are available on HydroFrance website: https://www.hydro.eaufrance.fr). Afterward, the salinity remained stable around a value of

34.5 psu until 14 October. While a gradual increase of DO (8.2 to 11.2 mg.L^{-1}) and pH (7.96 to 8.22) was detected between January and mid-April/early May, chlorophyll concentration (deducted from fluorescence) showed a more abrupt increase during the first two weeks of April from 2.5 to 9.44 µg.L^{-1}. This time interval coincides with the first increase in phytoplankton cell concentration (see Sect. 3.3.) and was followed by a significant decrease in the recorded values for DO, chlorophyll and pH, which ended in late May, just before the onset of the main diatom bloom of the year (see Sect. 3.3.). These decreases in DO and pH values were probably related to the end of the spring bloom, when the respiration activity in the water column intensified. The increased consumption of oxygen was accompanied by a release of CO_2, which contributed to a decrease in pH. For the rest of the year, DO and pH remained at a stable value that oscillated around 8.5 mg.L^{-1}and 8.05 respectively. However, fluorescence showed a flat background interrupted by sharp, narrow peaks, especially in June when the main diatom bloom was recorded, suggesting higher photosynthesis activity during this time of the year.

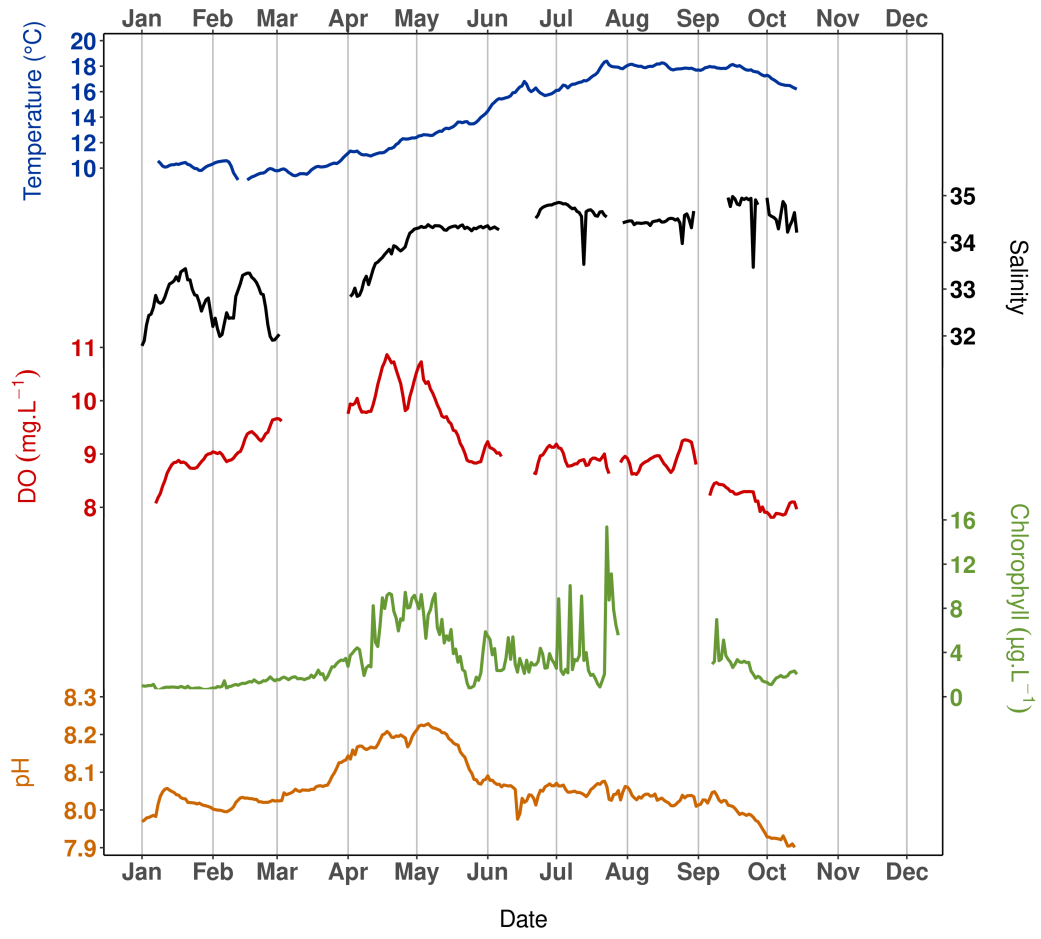

Figure 6 – Temperature, salinity, dissolved oxygen (DO), chlorophyll concentration computed from fluorescence and pH recorded with a NKE/Sambat probe deployed at the seafloor at Lanvéoc during 2021.

3.2 Nutrients

Concentrations of ammonium (NH_4^+), nitrate (NO_3^-), nitrite (NO_2^-), silicate ($Si(OH)_4$) and phosphate (PO_4^{3-}) were measured during the HIPPO monitoring scheme. For NH_4^+ concentration measurements, 100 mL glass vials were filled with seawater and immediately stored at -20 °C. To measure the other nutrients, 1 L of water was filtered through a 0.6 µm polycarbonate filter (Merck) within 3 h after sampling. The filtrate was recovered on 15 mL polypropylene tubes and stored at 4 °C for $Si(OH)_4$ measurements; the remainder was stored at -20 °C for NO_3^-, NO_2^- and PO_4^{3-} analyses. Then, the concentrations of all nutrients were measured with an AA3 HR SEAL-BRAN+LUEBBE auto-analyzer following the colorimetric (for NO_3^-, NO_2^-, $Si(OH)_4$ and PO_4^{3-}) or fluorimetric (for NH_4^+) methods of Aminot and Kérouel (2007). Concentrations of $Si(OH)_4$, PO_4^{3-}, and dissolved inorganic nitrogen (DIN) (measured as the sum of NH_4^+, NO_3^- and NO_2^-) reached their maximum on 07 February at sea surface (Figure 7). Times of low nutrient concentrations were detected based on the half-saturation constant for nutrient uptake (*Km*), since nutrient concentrations below this constant correspond to stressful conditions that limit phytoplankton development (Del Amo et al., 1997). In the Bay of Brest, these constants equal 2.0 µmol.L^{-1} for DIN and $Si(OH)_4$ as well as 0.2 µmol.L^{-1} for PO_4^{3-} (Del Amo et al., 1997).

Based on this method, PO_4^{3-} proved to be the first limiting nutrient, with concentrations that dropped below the *Km* as of 25 March, corresponding to the timing of the first increase in phytoplankton cells of the year (see Sect. 3.3.). $Si(OH)_4$ was the second limiting nutrient and had the shortest limitation interval (from 06 April to 21 June), which was interrupted by a slight enrichment in silicate at the end of May. Thereafter, silicate concentrations gradually increased until the end of the monitoring episode. DIN fell to limiting values three weeks after PO_4^{3-} values became limiting, lasting from mid-April until mid-September. At the end of September, DIN and PO_4^{3-}concentrations began to rise until the end of the experiment (Figure 7).

3.3 Phytoplankton and organic matter dynamics

Phytoplankton taxonomy and counting

For phytoplankton determination and counts, a 250 mL glass bottle was carefully filled with the surface water through a silicon tube to avoid turbulence and disintegration of phytoplankton cells. Phytoplankton cells were immediately fixed in 2 mL of acid Lugol's iodine solution and stored in a dark and cold (4 °C) place to avoid UV damage and evaporation. The identification of phytoplankton taxa as well as the calculation of the respective cell concentrations were performed within a month of sample collection using an aliquot of 50 mL of the water sample, used to fill a sedimentation column

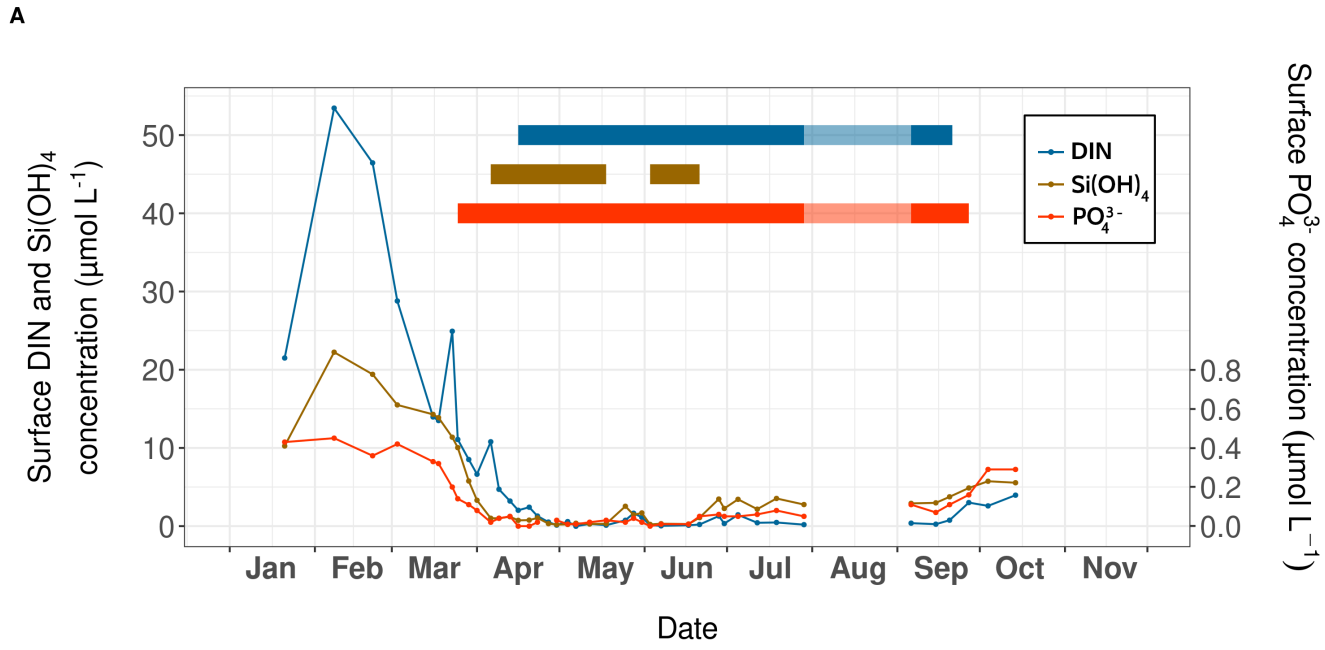

Figure 7 – Surface nutrient concentrations (DIN, silicates and phosphates) over time measured at Lanvéoc during 2021; their respective periods of limitation (thick solid lines) are indicated.

combined with a plate chamber (Hydrobios Kiel), according the the Utermöhl methods (Edler & Elbrächter, 2010). After 24h, the phytoplankton cells settled on a glass microscope slide and were identified and counted using an inverted microscope (Axio Observer.A1-ZEISS).

Phytoplankton communities at Lanvéoc were predominantly composed of diatom species, which represented 87% of the counted cells in the total phytoplankton samples from 2021 (Figure 8). Although the most dominant diatoms in the Bay of Brest are usually *Chaetoceros* spp. (e.g., Lorrain et al., 2000; Thébault et al., 2022), the two main blooms of 2021 mainly consisted of *Leptocylindrus danicus*, which occurred on 03 June (68% of total phytoplankton) and 15 September (95% of total phytoplankton). A smaller increase in the number of microalgal cells involving other species was also observed in mid-spring, caused by the presence of *Cerataulina pelagica* and *Guinardia* spp. cells (Figure 8A). This minor increase was particularly visible considering the biovolume of the species present, calculated with the equations provided in Smayda (1965) (Figure 8B). A succession of several diatom blooms was observed which were composed of different species, such as *Coscinodiscus waileisii*, *Cerataulina pelagica* and *Guinardia flaccida*, which reached maximum abundances on 23 March, 20 April and 18 May, respectively, while *L. danicus* remained the dominant diatom species (Figure 8B). Dinoflagellates were mainly represented by three species, i.e., *Gymnodinium* spp., which showed three blooms on 04 May, 17 July and 15 September, as well as *Protoperidinium bipes* and *Prorocentrum triestinum*, which bloomed on 02 June and on 15 September, respectively (Figure 8C). Potential causes for bloom decay will be given in Sect 3.3.

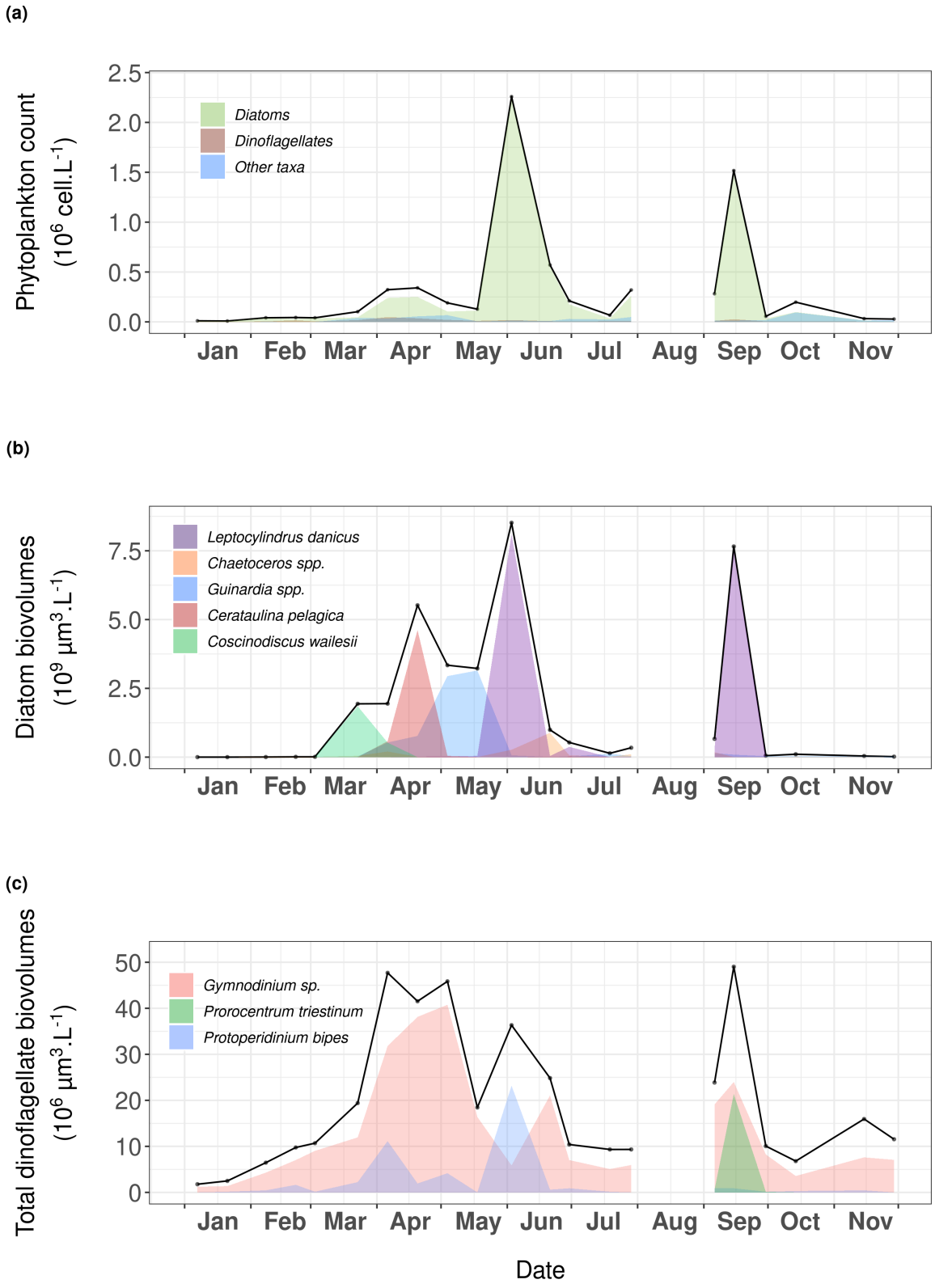

Figure 8 – (a) Phytoplankton dynamics recorded at Lanvéoc in 2021. Relative presence of the main (b) diatoms and (c) dinoflagellate species expressed as cell biovolumes.

Organic matter analyses

Seawater samples dedicated to chlorophyll a (Chl), pheophytin (Pheo), particulate organic carbon and nitrogen (POC and PON, respectively), and biogenic silica (BSi) analyses were collected from the surface and bottom waters using a 5 L or a 8 L Niskin bottle. Some samples for the bottom layer were collected using a syringe for a few dates (collecting strategy is specified in the dataset). Water samples were filtered through glass fiber filters (GF/F Whatman) pre-combusted for 4 h in a muffle furnace at 450 °C for Chl, Pheo, POC and PON measurements. BSi samples were analyzed after filtering seawater through 0.6 µm polycarbonate (Merck) filters. For each parameter, the filters were stored in an appropriate setting, i.e., POC/PON and BSi samples in dark and dry place, Chl and Pheo samples at -80 °C. POC and PON concentrations were measured with a CHN elemental analyzer using the combustion method (Thermo Fisher Flash 2000) (Aminot & Kérouel, 2004). In addition, the BSi content was determined using the protocols adapted from Ragueneau et al. (1994). Chl and Pheo were extracted in 6 ml of 90% acetone and kept in the dark at 4 °C for 12h. Samples were then centrifuged and fluorescence was measured with a Turner AU-10 fluorimeter using the equation provided in Lorenzen (1966).

The calculation of the Chl:Pheo ratio can be used to determine the freshness of the phytoplankton in the water column. According to Savoye (2001), a ratio below 1 indicates degraded organic matter, which can be considered as detrital if the value drops below 0.5, and a ratio greater than 2 describes fresh phytoplankton. At Lanvéoc in 2021, the physiological state of the phytoplankton was rather good because the ratio was always higher than 1 for the surface layer (Figure 9), with the exception of samples from 07 June and 27 September. In bottom waters, this value occasionally fell below 2, and even below 1, i.e., on 23 March (0.82), 06 April (0.76), 20 April (1.71), 04 May (1.67) and 18 May (1.07), contemporaneously with increases in phytoplankton cells (Figure 8). Moreover, during the main phytoplankton bloom of the year (03 June), a Chl:Pheo value below 2 was also recorded in bottom watters (1.16 on 06 June) and the minimum value was recorded a few days later (0.15), on 17 June. Between 19 July and 06 September, a time interval of low Chl:Pheo values was recorded in the bottom layer. These results indicate a degradation of phytoplankton cells that occurred after specific blooms or during summer. The reason behind this degradation may be the natural decay of cells due to a decrease in nutrient levels, having been consumed by the blooms (Figure 7), or due to intense grazing activities by zooplankton or heterotrophic dinoflagellates.

3.4 Trace element measurements

Seawater samples for trace element measurements were collected with 5 L Teflon-coated Go-Flo bottles (Teflon prevents element adsorption on the bottle walls) in surface and bottom waters.

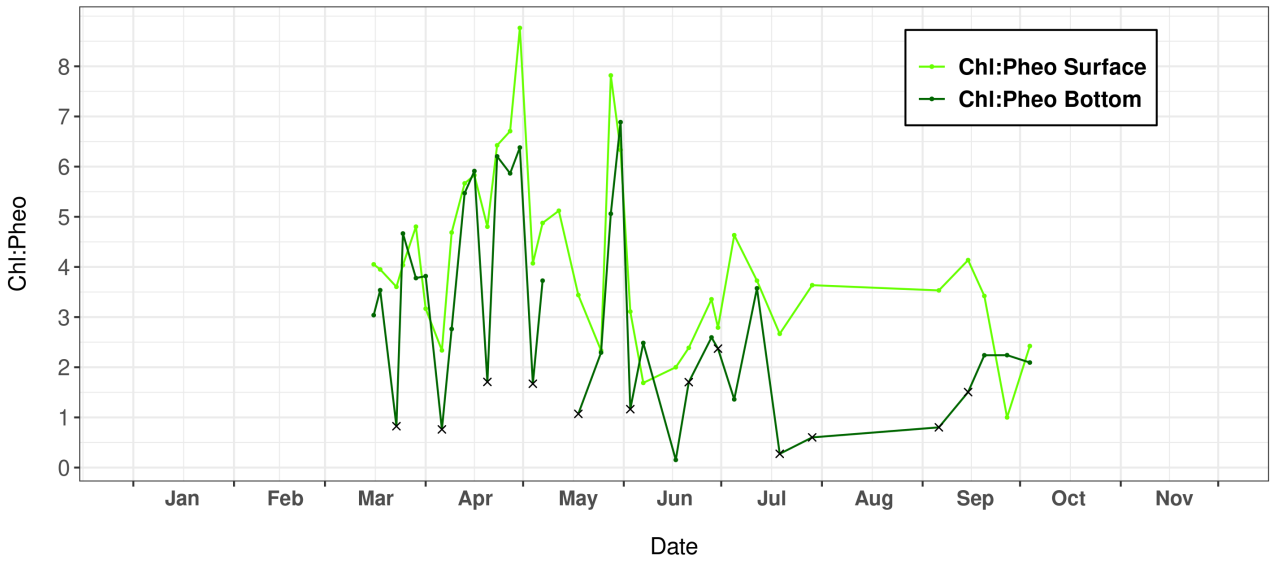

Figure 9 – Variations in the chlorophyll:pheophytin ratio (Chl:Pheo) measured in surface and bottom layers of the water column at Lanvéoc during 2021. Crosses indicate seawater sampled with a bottom syringe.

Approximately 1 L of water was filtered through 0.45 µm MF-Millipore™ mixed cellulose ester filters (Merck). The filters were then air-dried and stored in 30 mL PTFE vials (Savillex, Minnetonka, MN, USA) until analysis of particulate trace elements. The filtrates were recovered in 15 mL polypropylene (PP) tubes and stored at (4 °C) until analysis of the dissolved trace elements. Before use, filters and PP tubes were cleaned with HNO_3 solutions (pH 1) made from Suprapur HNO_3 65% (Merck, Darmstadt, Germany) and thoroughly rinsed with ultrapure water. PTFE vials were cleaned at 80 °C for 3 h with concentrated HNO_3 and H_2O_2 as for filter digestion (see next section) and then thoroughly rinsed with ultrapure water.

For trace element analysis of the particulate matter, filter digestions were carried out at 80 °C for 3h in closed 30 mL-PTFE screw-cap vials (Savillex, Minnetonka, MN, USA) by adding 2 mL of HNO_3 65% (Merck, Darmstadt, Germany) and 500 µL of suprapur 30% hydrogen peroxide (H_2O_2 – Merck, Darmstadt, Germany. The elemental analyses were then conducted on diluted mixtures (2.3% HNO_3) with a X-series II, quadrupole inductively coupled plasma mass spectrometer (Q-ICP-MS) (Thermo Scientific) and, for Ca, P, Zn and Al specifically, with an Horiba Jobin Yvon Ultima 2 ICP - optical emission spectrometry (ICP-OES) operating at the Pôle Spectrométrie Océan (Plouzané, France). Measurements of elemental concentration within the dissolved fraction were carried out with a sector field ICP-MS (Element XR, Thermo Scientific) operating at Ifremer (with the exception of Ca and Al again, which have been measured with a ICP-OES). Since the salt matrix of seawater samples can affect chemical measurements, samples were diluted 100 times with a 2% HNO_3 prior

to the measurement. All particulate and dissolved concentrations shown in the present study were above detection limits. The data obtained by ICP-MS or ICP-OES were also corrected for machine drift by inserting multi-element standard solutions every two samples. A certified reference materials was used: (NASS 6 seawater (National Research Council, Canada)), as well as a standard solution prepared from a multi-element solution (1 ppb - VWR chemicals - Prolabo), in order to assess the accuracy of measurements in the dissolved and the particulate phase respectively.

The network graphs show the Pearson correlations between all the trace elements measured in the particulate fraction of the surface and bottom water samples obtaining during the HIPPO monitoring (Figure 10A and 10B, respectively). The element dynamics in the water column were clearly different between the surface layer and bottom water, i.e., the measured elements appeared strongly correlated with each other in surface water but not in the bottom water. In surface water, only Mo and Cd were not correlated with any other element, unlike Ca, Mg, V, Li, Co, Mn, Fe, Sr and Al, which formed a strongly intercorrelated group. It is worth mentioning here that a cluster appear around particulate vanadium in both water layers. Vanadium, an essential element for phytoplankton cells (Moore et al., 1996), was significantly correlated with other elements also essentials for microalgae, such as Fe, Mn or Co which are involved in several enzyme systems (Whitfield, 2001). By contrast, Ba and Sr showed patterns that differed from the other elements, and both elements were only correlated to each other in bottom water.

The temporal changes in particulate and dissolved Ba (Figure 10C and 10D) showed interesting patterns. After the main bloom of *L. danicus* in early June 2021, the concentrations of Ba in the dissolved phase (DBa) drastically decreased, while the concentrations of particulate barium (PBa) strongly increased both in surface and in bottom waters. Ba is not known to have any physical function for diatoms, but may be adsorbed on their frustules (Dehairs et al., 1980; Fisher et al., 1991; Sternberg et al., 2005). Therefore, findings suggest a transition of Ba from the dissolved to the particulate phase during the bloom, associated with an adsorption of Ba onto diatom frustules. An alternative explanation includes the occurrence of Acantharea or Coccolithophoridae, known to adsorb Ba on their skeletons which are mainly composed of Sr or Ca respectively (Michaels, 1991; Bernstein et al., 1992; Langer et al., 2009). This affinity between these two elements is reflected in their significant correlation in the bottom layer only (see Figure 10B). However, no adequate method has been established to prove the presence of these organisms in 2021 in the Bay of Brest, although Coccolithophoridae cells have been observed in this region in the past, but mainly in bottom water.

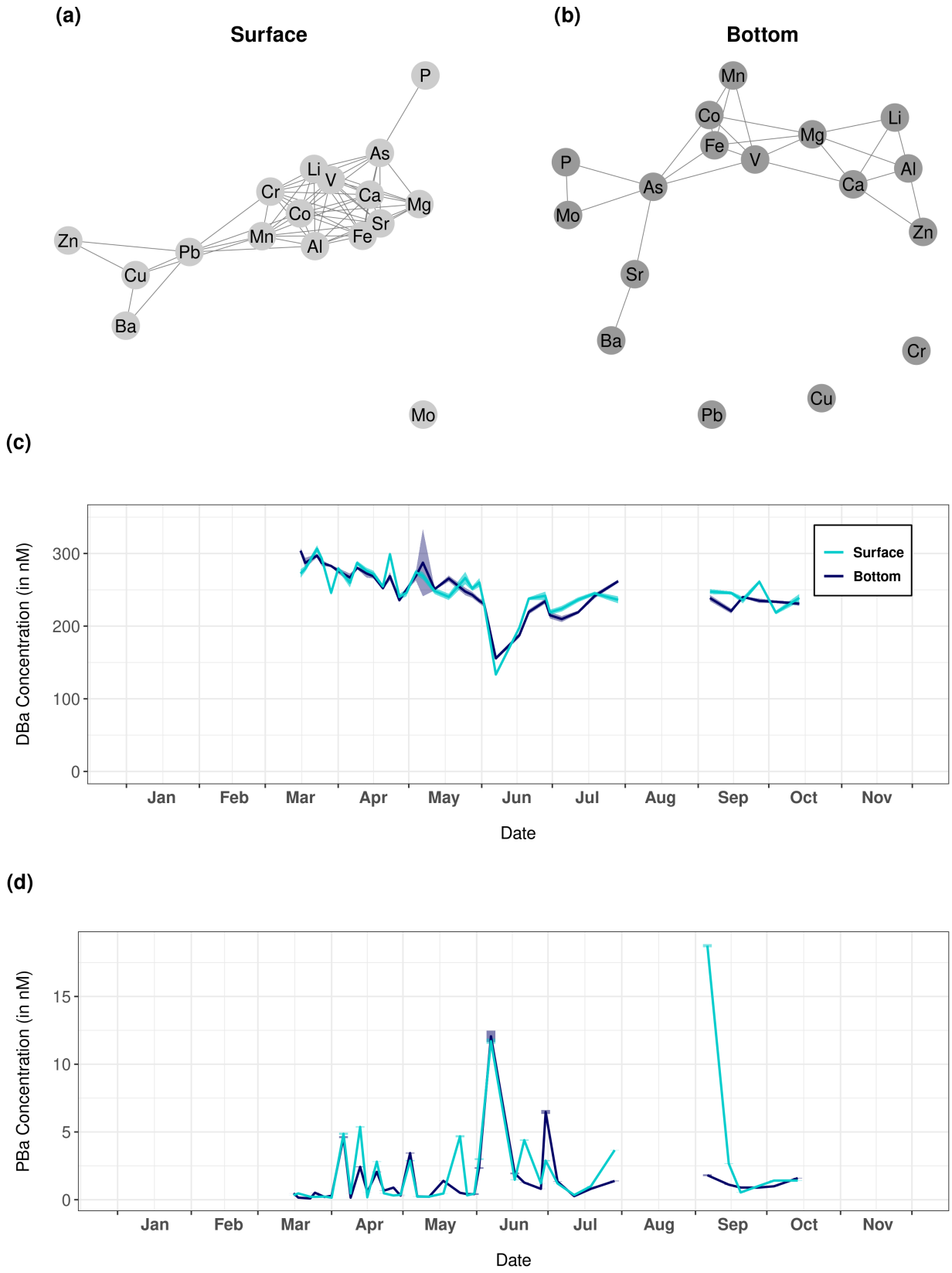

Figure 10 – Network graphs showing Pearson correlations between each measured trace element of the particulate fraction in (a) surface and (b) bottom waters. Only significant correlations with a coefficient greater than 0.62 are shown on these graphs. (c) Dissolved and (d) particulate barium (DBa and PBa, respectively) recorded at Lanvéoc during 2021 in surface and bottom waters; shadded areas and bars correspond to the relative standard deviation of measurements.

3.5 Particle dynamics and composition

Aggregation episodes

Under stress conditions, such as limitation in nutrients that had been entirely consumed during a bloom or changes in temperature, phytoplankton cells are known to excrete extracellular polymeric substances (EPS), which are precursors to transparent exopolymer particles (TEP) that favor the formation of aggregates (Alldredge et al., 1993; Passow, 2002). These aggregates often terminate the bloom and export the phytoplankton out of the euphotic layer to the deep oceanic layer in the open ocean, or toward the sediment (and benthic organisms) in coastal ecosystems. Particles were sized and counted using UVP6, a compact autonomous underwater imaging system (Picheral et al., 2021). This instrument has been designed for intermittent profile measurements in the water column, but here, the intention was to determine particle dynamics at the sediment-water interface as a continuous time-series. The design of the UVP6 was therefore modified to meet the needs of the present study. To minimize turbulence, particle resuspension and natural light variation, which can alter image quality and particle detection, the objective and the light source were integrated into an opaque cylinder. This cylinder is completely closed on the bottom to avoid taking pictures of resuspended particles rising from the sediment. To ensure constant hydrodynamics within the cylinder and attenuate horizontal fluxes, a 1x1 cm mesh was added covering the top of the cylinder. This device was deployed at the seafloor on 16 March 2021. Every hour, the UVP acquired two types of data. Firstly, a picture was taken every 20 seconds for 30 minutes to measure particle size and to calculate their concentration according to their size class (from 80.6 µmto 26 mm, divided into 25 size classes). The data are available from the ECOTAXA server (https://ecotaxa.obs-vlfr.fr) (https://ecotaxa.obs-vlfr.fr). Secondly, the UVP took full high-resolution images every 2 sec for 3 min to calculate particle trajectories and settling velocities. Due to the colossal size of these images, they are not available on SEANOE but are available upon request.

Figure 11 shows the temporal variation of small particles (daily sum of the mean concentration of particles ranging from 80.6 µm to 512 µm in size) and large particles (daily sum of the mean concentration of particles ranging from 512 µm to and 26 mm in size). Several aggregation periods were detected by isolating peaks in large particle concentrations whose amplitude were at least twice as large as the minimum values. Based on this method, four complete and one incomplete episodes of aggregation were identified from these time-series. The first episode took place on 30 March, the second on 26 April, the third on 12 May, the fourth incomplete episode was recorded between 26 and 28 May (incomplete due to the removal of the UVP to recover data and reload the battery) and, finally, the last episode on 05 June (Figure 11). Each of these episodes was preceded by a few days-long phytoplankton bloom characterized by different species (Figure 8B and 8C). The first

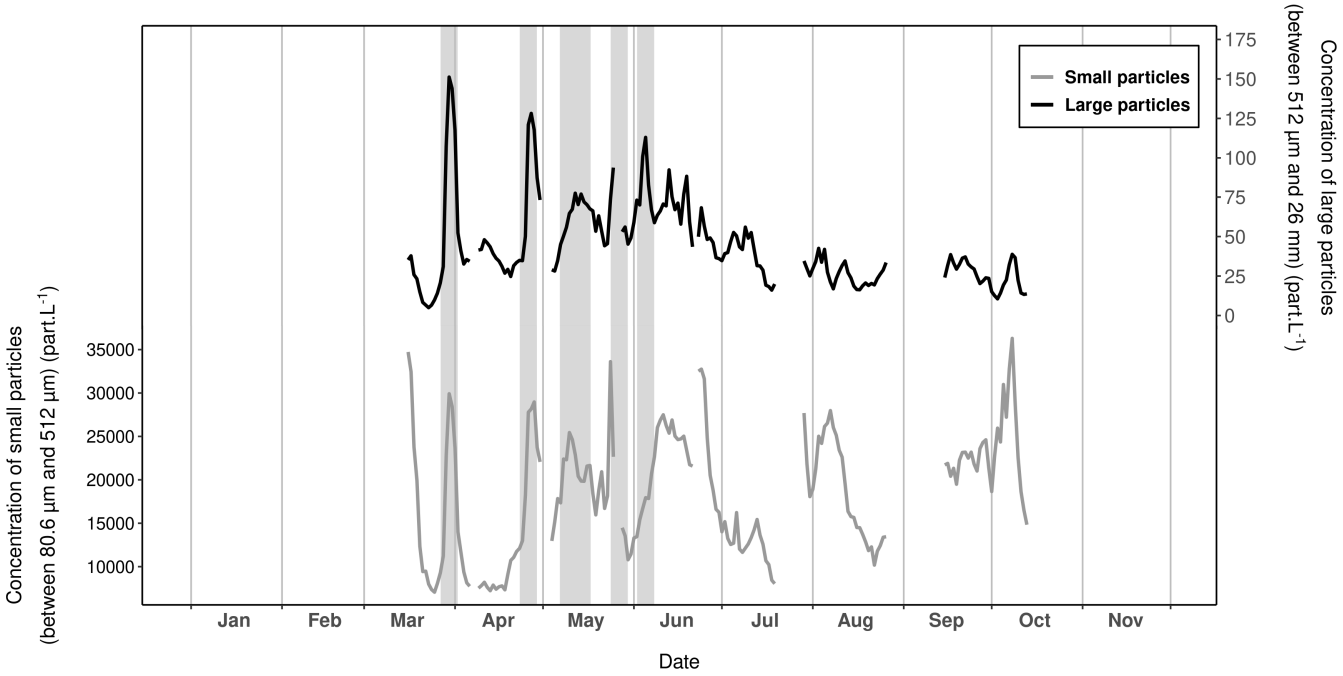

Figure 11 – Variations in the daily mean particle concentrations recorded with the UVP6 imaging sensor at Lanvéoc during 2021. The dark lines represent the concentration of large particles between 512 µm and 4.10 mm (equivalent spherical diameter, ESD) and the gray lines show the concentration of smaller particles, ranging from 50.8 to 512 µm (ESD). Grey-shaded areas denote aggregation events.

aggregation episode may have resulted from the collapse of the first bloom of *C. wailesii* due to the onset of PO_4^{3-} limitation (Figure 7). After this first aggregation event, N and P were almost constantly in growth-limiting concentrations. A second period of $Si(OH)_4$ limitations started in early June, corresponding to the last episode of aggregation recorded during the spring and summer. In contrast, the other aggregation events may have been triggered by other parameters. For instance, in their competition for resources, some mixotrophic dinoflagellate species such as *Gymnodinium spp.* or *Protoperidinium bipes*, which developed in late March, mid-May and early June (Figure 8C), are known to excrete compounds toxic to other microalgae, causing an allelopathic effect and therefore cell lysis and aggregation (e.g., Legrand et al., 2003; Band-Schmidt et al., 2020).

Sediment trap data

A HYDRO-BIOS Multi Sediment Trap with 12 collecting bottles (total volume: 290 mL) was deployed during the survey to analyze the chemical composition of the particles that sedimented at the seafloor. The catchment area of this model was 153.86 cm^2 with a rotation frequency every three days (between 02 March and 25 May) and every four days (between 26 May and 29 July). Before deployment, each bottle was poisoned to prevent biological activity and thus degradation of the organic matter. Sedimenting material was analyzed for the trace element composition, as well as

POC, PON, and biogenic silica (BSi). Protocols used for these measurements are described in Sect. 3.3. and 3.4. Before filtration, the samples were shaken (to break up the aggregates) and passed through a 1 mm mesh sieve to remove big particles and avoid clogging the filters.

In total, five complete episodes of high carbon flux were recorded at Lanvéoc during 28 - 31 March (5672.57 µmol.h^{-1}.m^{-2}), 26 - 29 April (3719.93 µmol.h^{-1}.m^{-2}), 26 - 28 May (4562.25 µmol.h^{-1}.m^{-2}), 10 - 12 June (1887.20 µmol.h^{-1}.m^{-2}) and 19 - 21 June (5031.75 µmol.h^{-1}.m^{-2}) (Figure 12). The average POC transport values outside these events oscillated around 700 µmol.h^{-1}.m^{-2}. During late March, late April and late May, POC transport peaks occurred at the same time as the aggregation episodes recorded with the UVP, but the two other transport peaks did not occur at the same time as the aggregation peaks (Figure 11). These results validate the signals obtained with the UVP and thus the deployment method of the present experiment. Furthermore, these findings highlight the role of aggregate dynamics in the transport of particulate carbon to the sediment-water interface. However, not all carbon transport events were caused by aggregation episodes, but sometimes simply by the development and the subsequent decay of phytoplankton cells. Through the calculation of the PBa:POC ratio, Figure 12 also shows the time intervals during which an enrichment in the particulate Ba flux was recorded. PBa:POC was relatively low during the year, with a baseline value between 0.01 and 1.76 nmol.µmol^{-1}. This baseline was interrupted by a large peak that occurred between 28 May and 16 June, reaching its maximum value (4.37 nmol.µmol^{-1}) on 6-9 June. During the same time, the largest diatom bloom of the year occurred (Figure 8), as well as the subsequent aggregation episode (Figure 11) and as the main phytoplankton degradation event (Figure 9). As stated in Sect. 3.4., Ba can be adsorbed onto diatom frustules, explaining the peak observed in the water column as well as the high Ba flux that occurs at cell decay after a bloom.

3.6 Shell data

As described in Sect. 2, a large number of shells was collected during this monitoring study. Here, only results are presented from shells collected at the end of the monitoring period, which were used to produce the growth and trace elements time-series for 2021.

Growth rate

The *P. maximus* specimens collected during this study were all treated in the same way, whether collected directly from the sediment surface or the cage. After collection, individuals were dissected and soft tissues (gills, mantles, digestive gland and muscle) were freeze-dried for further element chemical analyses. Left (flat) valves were gently cleaned with tap water using a nylon brush and rinsed ultrasonically for 3 min with deionized water. The outer surfaces of left valves were imaged

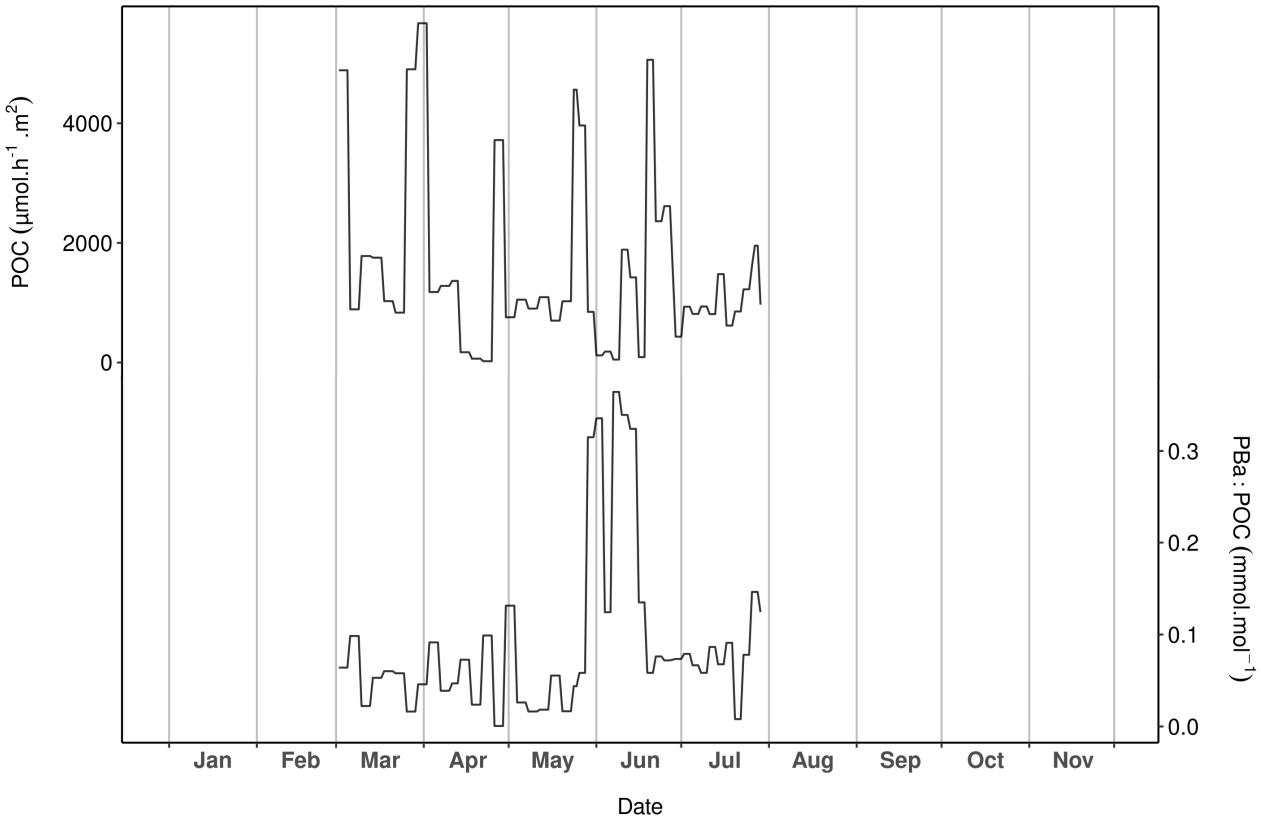

Figure 12 – Particulate organic carbon (POC) (upper curve) and the particulate barium-to-POC ratio (PBa:POC) (lower curve) measured in the sediment trap samples at Lanvéoc in 2021.

under reflected light using a Canon EOS 600 DSLR camera coupled with a Wild Heerbrugg binocular microscope equipped with a Schott VisiLED MC 1000 light source (sectoral dark field). Because the specimens were collected alive, the last growth line visible on the outer margin was formed immediately prior to the collection date. This allows to place each increment in an accurate temporal framework by counting the daily increments from the ventral margin toward the umbo, because scallop produces growth lines on a daily basis (Chauvaud et al., 1998).

The average growth rate calculated from six specimens collected from the sediment surface ranged from 69.8 to 220.6 µm.day^{-1} with an annual average value of 171.3 µm.day^{-1} (Figure 13). From the onset of the growth period, growth rate gradually increased and reached a maximum value in early June. However, this increasing trend was interrupted by a slow-growth episode between 26 April and 05 May. This decline in growth rate has already been observed in previous studies of scallops from Lanvéoc, but does not occur every year (e.g., Chauvaud et al., 1998; Fröhlich et al., 2022a; Fröhlich et al., 2022b). The slow-growth phase occurred after the main bloom of *Gymnodynium* spp., a dinoflagellate known to produce toxic blooms (Daranas et al., 2001) (Figure 8C), and after

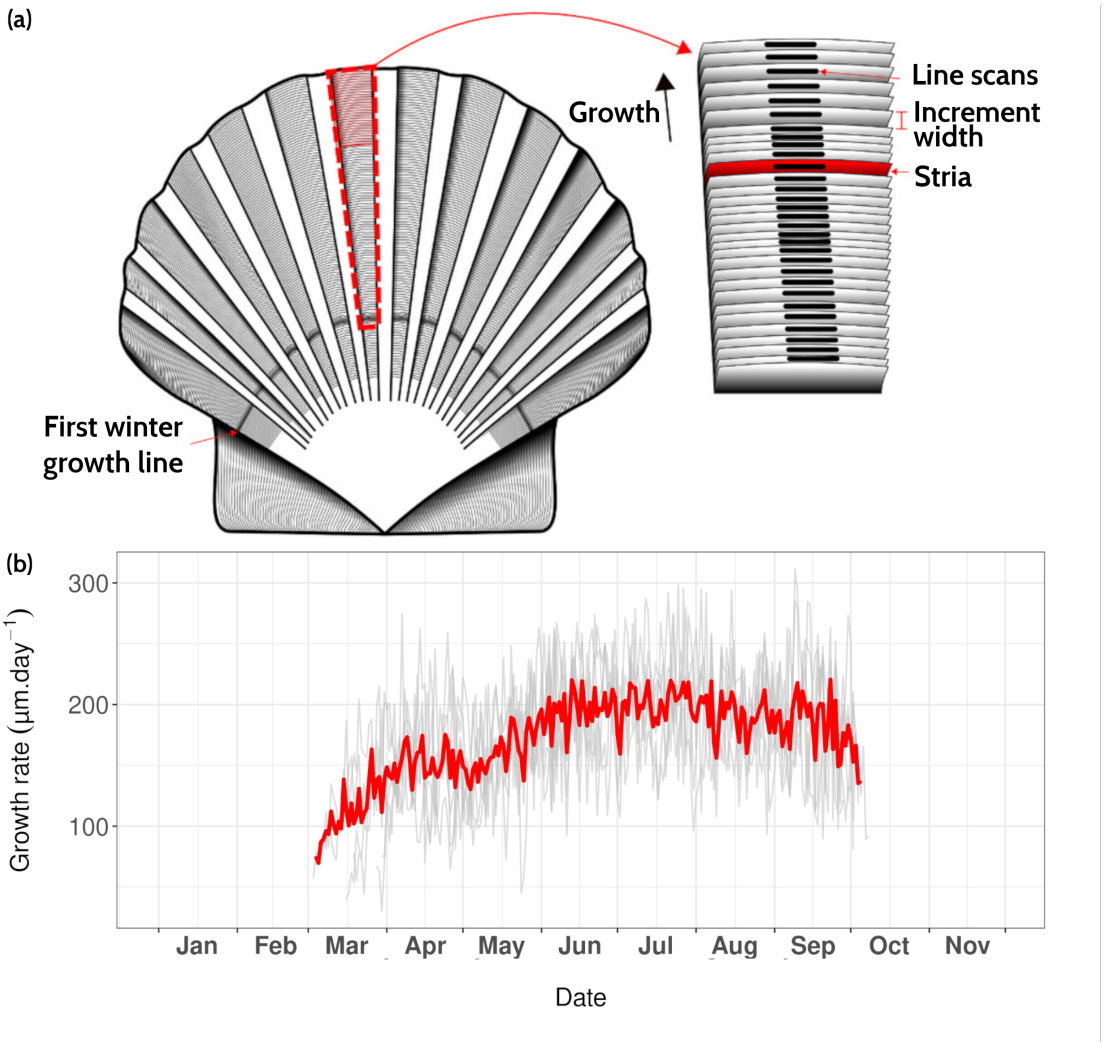

Figure 13 – (a) Surface of *Pecten maximus* shell (left valve), showing growth patterns (increments and lines, aka 'striae') as well as the sampling strategy for trace element measurements via LA-ICP-MS ("line scans") (from Fröhlich et al., 2022b). (b) Average daily growth rate (red curve) calculated from 6 specimens (grey curves) that were collected alive at Lanvéoc from the sediment surface.

an aggregation episode (Figure 11). These two phenomena combined may explain the drop in shell production rate, because scallops may decrease the filtration rate during stressful conditions.

Geochemical analyses

Geochemical analyses were performed according to protocols described in Fröhlich et al. (2022a, 2022b). The element chemical content of the shells was measured at the Max Planck Institute for Chemistry (Mainz, Germany) using a Laser Ablation (NewWave Research UP-213 Nd:YAG) - ICP-MS (Thermo Fisher Element 2) system. In total, slabe of six shells (three specimens from the sediment and three from the cage deployed 1 m above the sediment) were analyzed. Table 2 gives an exhaustive list of the elements that were measured in the present study. Laser scans were completed on every daily growth line (aka stria), by running the laser in line scan mode on the outer shell surface

perpendicular to the growth direction and parallel to the growth line (Figure 13A). Within each stria, measurements were completed using a laser spot diameter of 80 µm at a constant speed of 5 µm.s^{-1}. Prior to sample ablation and measurement, each sample was pre-ablated (100 µm spot size with a speed of 80 µm.s^{-1}) to remove potential contaminants. Results are expressed as molar element-to-calcium ratios because ^{43}Ca was used as an internal standard. Chemical data were place in accurate temporal context by means of growth pattern analysis.

Figure 14 presents the Ba/Ca data of shells collected directly on the sediment (sediment specimens) and 1 m above (cage specimens). The Ba/Ca profiles recorded in the shells are characterized by a baseline, whose values were different according to whether the shells came from the sediment (approx. 1 µmol.mol^{-1} in average) or from the cage (approx. 2 µmol.mol^{-1} in average). These baselines were interrupted by two major Ba/Ca peaks that occurred at approximately the same moment in all, although their amplitudes differed slightly. The first peak occurred around 07 or 08 June (sediment shells: 9.50 µmol.mol^{-1}, cage shells: 6.34 µmol.mol^{-1}), and the second around 02 July (4.91 µmol.mol^{-1} and 3.10 µmol.mol^{-1}, respectively). Furthermore, a third, smaller peak occurred on 30 July (2.72 µmol.mol^{-1}), exclusively in sediment shells. Ba content recorded in *P. maximus* shells followed more or less the same pattern as the PBa measured in bottom waters at Lanvéoc, where two major peaks were also observed at the beginning of June and July (Figure 10D). Moreover, the relative amplitudes of these peaks were also similar, since the first peak was approximately twice as high as the second one. Nonetheless, other smaller PBa peaks occurred in bottom waters throughout the monitoring phase, for instance, in April (Figure 10D), and did not coincide with any Ba/Ca increase in shells (Figure 14).

Previous studies have suggested that Ba/Ca of *P. maximus* shells can serve as a proxy for primary productivity (Barats et al., 2009) or species-specific blooms of phytoplankton (Fröhlich et al., 2022b). In the present study, the main Ba/Ca$_{shell}$ peak occurred during the main diatom peak, mainly represented by *L. danicus*, and during the main episode of Ba transport toward the sediment (Figure 12). The second Ba/Ca$_{shell}$ peak occurred a few days after a *Chaetoceros* spp. bloom. However, the third Ba peak recorded in sediment shells did not align with any diatom bloom. Fröhlich et al. (2022a) suggested an average time lag between diatom blooms and shell Ba peaks of 8 to 12 days, which corresponds more or less to the observations of the present study. However, the sampling frequency for phytoplankton determination was not sufficient to track the exact timing of the blooms.

4 CONCLUSION

In this article, only an overview of the results gathered during the HIPPO monitoring that was conducted at Lanvéoc during 2021 are presented. The dataset helps to better understand the links

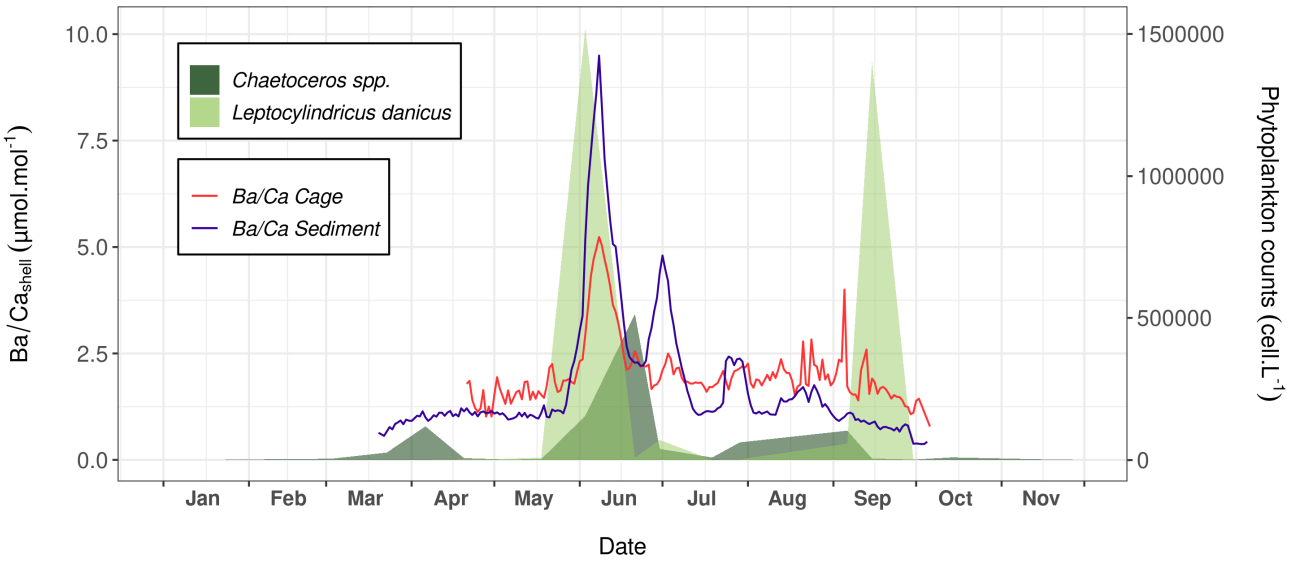

Figure 14 – Average Ba/Ca signals measured in shell of *P. maximus* that were collected from the sediment surface (n=3) and 1 m above the substrate (n =3). The abundances of *Chaetoceros spp.* (dark green areas) and *L. danicus* (light green areas) are also shown.

between phytoplankton dynamics, water column chemistry and the incorporation of trace elements into the shells of *P. maximus*. However, the dataset also contains information useful for other topics of interest. Table 1 and Table 2 compile all variables that have been made available for other scientists on the SEANOE platform (https://www.seanoe.org/data/00808/92043/ - Siebert et al., 2023). Moreover, the hypotheses and assumptions given in this paper as well as other topics that have not been mentioned will be in the focus of several articles that are currently in preparation.

Table 1 – List of the environmental parameters measured at Lanvéoc in 2021.

Date of first and last acquisition	Parameter	Sampling method	Water column layers	Frequency	Principals investigators	Processed
16.03.2021 - 14.10.2021	POC	Niskin bottle	Surface	Every 3 or 4 days	Jérémy Devesa	Available
16.03.2021 - 14.10.2021	POC	Niskin bottle	Bottom	Every 3 or 4 days	Jérémy Devesa	Available
02.03.2021 - 29.07.2021	POC	Sediment trap	Bottom	Every 3 or 4 days	Jérémy Devesa	Available
07.01.2021 - 13.12.2021	POC	Bottom Syringe	Bottom	Every 2 weeks	Jérémy Devesa	Available
16.03.2021 - 14.10.2021	PON	Niskin bottle	Surface	Every 3 or 4 days	Jérémy Devesa	Available
16.03.2021 - 14.10.2021	PON	Niskin bottle	Bottom	Every 3 or 4 days	Jérémy Devesa	Available
02.03.2021 - 29.07.2021	PON	Sediment trap	Bottom	Every 3 or 4 days	Jérémy Devesa	Available
07.01.2021 – 13.12.2021	PON	Bottom Syringe	Bottom	Every 2 weeks	Jérémy Devesa	Available
16.03.2021 - 14.10.2021	BSi	Niskin bottle	Surface	Every 3 or 4 days	Morgane Gallinari	Available
16.03.2021 - 14.10.2021	BSi	Niskin bottle	Bottom	Every 3 or 4 days	Morgane Gallinari	Available
02.03.2021 - 29.07.2021	BSi	Sediment trap	Bottom	Every 3 or 4 days	Morgane Gallinari	Available
16.03.2021 - 14.10.2021	NH_4^+	Niskin bottle	Surface	Every 3 or 4 days	Émilie Grossteffan	Available
16.03.2021 - 14.10.2021	NO_3^-	Niskin bottle	Surface	Every 3 or 4 days	Manon Le Goff	Available
16.03.2021 - 14.10.2021	NO_2^-	Niskin bottle	Surface	Every 3 or 4 days	Manon Le Goff	Available
16.03.2021 - 14.10.2021	$Si(OH)_4$	Niskin bottle	Surface	Every 3 or 4 days	Manon Le Goff	Available
16.03.2021 - 14.10.2021	PO_4^{3-}	Niskin bottle	Surface	Every 3 or 4 days	Manon Le Goff	Available
16.03.2021 - 14.10.2021	Chlorophylle	Niskin bottle	Surface	Every 3 or 4 days	Isabelle Bihannic	Available
16.03.2021 - 14.10.2021	Chlorophylle	Niskin bottle	Bottom	Every 3 or 4 days	Isabelle Bihannic	Available
07.01.2021 - 13.12.2021	Chlorophylle	Bottom Syringe	Bottom	Every 2 weeks	Isabelle Bihannic	Available
16.03.2021 - 14.10.2021	Pheophityne	Niskin bottle	Surface	Every 3 or 4 days	Isabelle Bihannic	Available
16.03.2021 - 14.10.2021	Pheophityne	Niskin bottle	Bottom	Every 3 or 4 days	Isabelle Bihannic	Available
07.01.2021 - 13.12.2021	Pheophityne	Bottom Syringe	Bottom	Every 2 weeks	Isabelle Bihannic	Available
01.01.2021 - 31.12.2021	Phytoplankton (taxonomy and counting)	Niskin bottle	Surface	Every 2 weeks	Gaspard Delebecq	Only available on request
01.01.2021 - 31.12.2021	Temperature	Sambat probes	Bottom	Every 20 minutes	Peggy Rimmelin-Maury	Available
01.01.2021 - 31.12.2021	Salinity	Sambat probes	Bottom	Every 20 minutes	Peggy Rimmelin-Maury	Available

01.01.2021 - 31.12.2021	Oxygen	Sambat probes	Bottom	Every 20 minutes	Peggy Rimmelin-Maury	Available
01.01.2021 - 31.12.2021	pH	Sambat probes	Bottom	Every 20 minutes	Peggy Rimmelin-Maury	Available
16.03.2021 - 14.10.2021	Fluorescence	Sambat probes	Bottom	Every 20 minutes	Peggy Rimmelin-Maury	Available
01.01.2021 - 31.12.2021	Depth	Sambat probes		Every 20 minutes	Peggy Rimmelin-Maury	Available
16.03.2021 - 14.10.2021	Particles concentration	UVP6	Bottom	Every 30 minutes	Marc Picheral	Available
16.03.2021 - 14.10.2021	Particles size distribution	UVP6	Bottom	Every 30 minutes	Marc Picheral	Available
16.03.2021 - 14.10.2021	Particles identification and character-isation	UVP6	Bottom	Every 30 minutes	Marc Picheral	Available
16.03.2021 - 14.10.2021	Particulate ^{7}Lithium	GoFlo Bottle	Surface	Every 3 or 4 days	Valentin Siebert - Marie Laure Rouget	Available
16.03.2021 - 14.10.2021	Particulate ^{7}Lithium	GoFlo Bottle	Bottom	Every 3 or 4 days	Valentin Siebert - Marie Laure Rouget	Available
02.03.2021 - 29.07.2021	Particulate ^{7}Lithium	Sediment trap		Every 3 or 4 days	Valentin Siebert - Marie Laure Rouget	Available
16.03.2021 - 14.10.2021	Particulate ^{25}Magnesium	GoFlo Bottle	Surface	Every 3 or 4 days	Valentin Siebert - Marie Laure Rouget	Available
16.03.2021 - 14.10.2021	Particulate ^{25}Magnesium	GoFlo Bottle	Bottom	Every 3 or 4 days	Valentin Siebert - Marie Laure Rouget	Available
02.03.2021 - 29.07.2021	Particulate ^{25}Magnesium	Sediment trap		Every 3 or 4 days	Valentin Siebert - Marie Laure Rouget	Available
16.03.2021 - 14.10.2021	Particulate ^{31}Phosphorus	GoFlo Bottle	Surface	Every 3 or 4 days	Valentin Siebert - Marie Laure Rouget	Available
16.03.2021 - 14.10.2021	Particulate ^{31}Phosphorus	GoFlo Bottle	Bottom	Every 3 or 4 days	Valentin Siebert - Marie Laure Rouget	Available
02.03.2021 - 29.07.2021	Particulate ^{31}Phosphorus	Sediment trap		Every 3 or 4 days	Valentin Siebert - Marie Laure Rouget	Available
16.03.2021 - 14.10.2021	Particulate ^{51}Vanadium	GoFlo Bottle	Surface	Every 3 or 4 days	Valentin Siebert - Marie Laure Rouget	Available
16.03.2021 - 14.10.2021	Particulate ^{51}Vanadium	GoFlo Bottle	Bottom	Every 3 or 4 days	Valentin Siebert - Marie Laure Rouget	Available
02.03.2021 - 29.07.2021	Particulate ^{51}Vanadium	Sediment trap		Every 3 or 4 days	Valentin Siebert - Marie Laure Rouget	Available
16.03.2021 - 14.10.2021	Particulate ^{52}Chromium	GoFlo Bottle	Surface	Every 3 or 4 days	Valentin Siebert - Marie Laure Rouget	Available
16.03.2021 - 14.10.2021	Particulate ^{52}Chromium	GoFlo Bottle	Bottom	Every 3 or 4 days	Valentin Siebert - Marie Laure Rouget	Available
02.03.2021 - 29.07.2021	Particulate ^{52}Chromium	Sediment trap		Every 3 or 4 days	Valentin Siebert - Marie Laure Rouget	Available

16.03.2021 - 14.10.2021	Particulate ^{55}Manganese	GoFlo Bottle	Surface	Every 3 or 4 days	Valentin Siebert - Marie Laure Rouget	Available
16.03.2021 - 14.10.2021	Particulate ^{55}Manganese	GoFlo Bottle	Bottom	Every 3 or 4 days	Valentin Siebert - Marie Laure Rouget	Available
02.03.2021 - 29.07.2021	Particulate ^{55}Manganese	Sediment trap		Every 3 or 4 days	Valentin Siebert - Marie Laure Rouget	Available
16.03.2021 - 14.10.2021	Particulate ^{56}Iron	GoFlo Bottle	Surface	Every 3 or 4 days	Valentin Siebert - Marie Laure Rouget	Available
16.03.2021 - 14.10.2021	Particulate ^{56}Iron	GoFlo Bottle	Bottom	Every 3 or 4 days	Valentin Siebert - Marie Laure Rouget	Available
02.03.2021 - 29.07.2021	Particulate ^{56}Iron	Sediment trap		Every 3 or 4 days	Valentin Siebert - Marie Laure Rouget	Available
16.03.2021 - 14.10.2021	Particulate ^{59}Cobalt	GoFlo Bottle	Surface	Every 3 or 4 days	Valentin Siebert - Marie Laure Rouget	Available
16.03.2021 - 14.10.2021	Particulate ^{59}Cobalt	GoFlo Bottle	Bottom	Every 3 or 4 days	Valentin Siebert - Marie Laure Rouget	Available
02.03.2021 - 29.07.2021	Particulate ^{59}Cobalt	Sediment trap		Every 3 or 4 days	Valentin Siebert - Marie Laure Rouget	Available
16.03.2021 - 14.10.2021	Particulate ^{63}Copper	GoFlo Bottle	Surface	Every 3 or 4 days	Valentin Siebert - Marie Laure Rouget	Available
16.03.2021 - 14.10.2021	Particulate ^{63}Copper	GoFlo Bottle	Bottom	Every 3 or 4 days	Valentin Siebert - Marie Laure Rouget	Available
02.03.2021 - 29.07.2021	Particulate ^{63}Copper	Sediment trap		Every 3 or 4 days	Valentin Siebert - Marie Laure Rouget	Available
16.03.2021 - 14.10.2021	Particulate ^{66}Zinc	GoFlo Bottle	Surface	Every 3 or 4 days	Valentin Siebert - Marie Laure Rouget	Available
16.03.2021 - 14.10.2021	Particulate ^{66}Zinc	GoFlo Bottle	Bottom	Every 3 or 4 days	Valentin Siebert - Marie Laure Rouget	Available
02.03.2021 - 29.07.2021	Particulate ^{66}Zinc	Sediment trap		Every 3 or 4 days	Valentin Siebert - Marie Laure Rouget	Available
16.03.2021 - 14.10.2021	Particulate ^{75}Arsenic	GoFlo Bottle	Surface	Every 3 or 4 days	Valentin Siebert - Marie Laure Rouget	Available
16.03.2021 - 14.10.2021	Particulate ^{75}Arsenic	GoFlo Bottle	Bottom	Every 3 or 4 days	Valentin Siebert - Marie Laure Rouget	Available
02.03.2021 - 29.07.2021	Particulate ^{75}Arsenic	Sediment trap		Every 3 or 4 days	Valentin Siebert - Marie Laure Rouget	Available
16.03.2021 - 14.10.2021	Particulate ^{88}Strontium	GoFlo Bottle	Surface	Every 3 or 4 days	Valentin Siebert - Marie Laure Rouget	Available
16.03.2021 - 14.10.2021	Particulate ^{88}Strontium	GoFlo Bottle	Bottom	Every 3 or 4 days	Valentin Siebert - Marie Laure Rouget	Available

02.03.2021 - 29.07.2021	Particulate ^{88}Strontium	Sediment trap		Every 3 or 4 days	Valentin Siebert - Marie Laure Rouget	Available
16.03.2021 - 14.10.2021	Particulate ^{95}Molybdenum	GoFlo Bottle	Surface	Every 3 or 4 days	Valentin Siebert - Marie Laure Rouget	Available
16.03.2021 - 14.10.2021	Particulate ^{95}Molybdenum	GoFlo Bottle	Bottom	Every 3 or 4 days	Valentin Siebert - Marie Laure Rouget	Available
02.03.2021 - 29.07.2021	Particulate ^{95}Molybdenum	Sediment trap		Every 3 or 4 days	Valentin Siebert - Marie Laure Rouget	Available
16.03.2021 - 14.10.2021	Particulate ^{137}Barium	GoFlo Bottle	Surface	Every 3 or 4 days	Valentin Siebert - Marie Laure Rouget	Available
16.03.2021 - 14.10.2021	Particulate ^{137}Barium	GoFlo Bottle	Bottom	Every 3 or 4 days	Valentin Siebert - Marie Laure Rouget	Available
02.03.2021 - 29.07.2021	Particulate ^{137}Barium	Sediment trap		Every 3 or 4 days	Valentin Siebert - Marie Laure Rouget	Available
16.03.2021 - 14.10.2021	Particulate ^{138}Barium	GoFlo Bottle	Surface	Every 3 or 4 days	Valentin Siebert - Marie Laure Rouget	Available
16.03.2021 - 14.10.2021	Particulate ^{138}Barium	GoFlo Bottle	Bottom	Every 3 or 4 days	Valentin Siebert - Marie Laure Rouget	Available
02.03.2021 - 29.07.2021	Particulate ^{138}Barium	Sediment trap		Every 3 or 4 days	Valentin Siebert - Marie Laure Rouget	Available
16.03.2021 - 14.10.2021	Particulate ^{206}Lead	GoFlo Bottle	Surface	Every 3 or 4 days	Valentin Siebert - Marie Laure Rouget	Available
16.03.2021 - 14.10.2021	Particulate ^{206}Lead	GoFlo Bottle	Bottom	Every 3 or 4 days	Valentin Siebert - Marie Laure Rouget	Available
02.03.2021 - 29.07.2021	Particulate ^{206}Lead	Sediment trap		Every 3 or 4 days	Valentin Siebert - Marie Laure Rouget	Available
16.03.2021 - 14.10.2021	Particulate ^{207}Lead	GoFlo Bottle	Surface	Every 3 or 4 days	Valentin Siebert - Marie Laure Rouget	Available
16.03.2021 - 14.10.2021	Particulate ^{207}Lead	GoFlo Bottle	Bottom	Every 3 or 4 days	Valentin Siebert - Marie Laure Rouget	Available
02.03.2021 - 29.07.2021	Particulate ^{207}Lead	Sediment trap		Every 3 or 4 days	Valentin Siebert - Marie Laure Rouget	Available
16.03.2021 - 14.10.2021	Particulate ^{208}Lead	GoFlo Bottle	Surface	Every 3 or 4 days	Valentin Siebert - Marie Laure Rouget	Available
16.03.2021 - 14.10.2021	Particulate ^{208}Lead	GoFlo Bottle	Bottom	Every 3 or 4 days	Valentin Siebert - Marie Laure Rouget	Available
02.03.2021 - 29.07.2021	Particulate ^{208}Lead	Sediment trap		Every 3 or 4 days	Valentin Siebert - Marie Laure Rouget	Available
16.03.2021 - 14.10.2021	Dissolved ^{7}Lithium	GoFlo Bottle	Surface	Every 3 or 4 days	Valentin Siebert - Yoan Germain	Available
16.03.2021 - 14.10.2021	Dissolved ^{7}Lithium	GoFlo Bottle	Bottom	Every 3 or 4 days	Valentin Siebert - Yoan Germain	Available

16.03.2021 - 14.10.2021	Dissolved ^{25}Magnesium	GoFlo Bottle	Surface	Every 3 or 4 days	Valentin Siebert - Yoan Germain	Available
16.03.2021 - 14.10.2021	Dissolved ^{25}Magnesium	GoFlo Bottle	Bottom	Every 3 or 4 days	Valentin Siebert - Yoan Germain	Available
16.03.2021 - 14.10.2021	Dissolved ^{31}Phosphorus	GoFlo Bottle	Surface	Every 3 or 4 days	Valentin Siebert - Yoan Germain	Available
16.03.2021 - 14.10.2021	Dissolved ^{31}Phosphorus	GoFlo Bottle	Bottom	Every 3 or 4 days	Valentin Siebert - Yoan Germain	Available
16.03.2021 - 14.10.2021	Dissolved ^{51}Vanadium	GoFlo Bottle	Surface	Every 3 or 4 days	Valentin Siebert - Yoan Germain	Available
16.03.2021 - 14.10.2021	Dissolved ^{51}Vanadium	GoFlo Bottle	Bottom	Every 3 or 4 days	Valentin Siebert - Yoan Germain	Available
16.03.2021 - 14.10.2021	Dissolved ^{52}Chromium	GoFlo Bottle	Surface	Every 3 or 4 days	Valentin Siebert - Yoan Germain	Available
16.03.2021 - 14.10.2021	Dissolved ^{52}Chromium	GoFlo Bottle	Bottom	Every 3 or 4 days	Valentin Siebert - Yoan Germain	Available
16.03.2021 - 14.10.2021	Dissolved ^{55}Manganese	GoFlo Bottle	Surface	Every 3 or 4 days	Valentin Siebert - Yoan Germain	Available
16.03.2021 - 14.10.2021	Dissolved ^{55}Manganese	GoFlo Bottle	Bottom	Every 3 or 4 days	Valentin Siebert - Yoan Germain	Available
16.03.2021 - 14.10.2021	Dissolved ^{56}Iron	GoFlo Bottle	Surface	Every 3 or 4 days	Valentin Siebert - Yoan Germain	Available
16.03.2021 - 14.10.2021	Dissolved ^{56}Iron	GoFlo Bottle	Bottom	Every 3 or 4 days	Valentin Siebert - Yoan Germain	Available
16.03.2021 - 14.10.2021	Dissolved ^{59}Cobalt	GoFlo Bottle	Surface	Every 3 or 4 days	Valentin Siebert - Yoan Germain	Available
16.03.2021 - 14.10.2021	Dissolved ^{59}Cobalt	GoFlo Bottle	Bottom	Every 3 or 4 days	Valentin Siebert - Yoan Germain	Available
16.03.2021 - 14.10.2021	Dissolved ^{61}Nickel	GoFlo Bottle	Surface	Every 3 or 4 days	Valentin Siebert - Yoan Germain	Available
16.03.2021 - 14.10.2021	Dissolved ^{61}Nickel	GoFlo Bottle	Bottom	Every 3 or 4 days	Valentin Siebert - Yoan Germain	Available
16.03.2021 - 14.10.2021	Dissolved ^{63}Copper	GoFlo Bottle	Surface	Every 3 or 4 days	Valentin Siebert - Yoan Germain	Available
16.03.2021 - 14.10.2021	Dissolved ^{63}Copper	GoFlo Bottle	Bottom	Every 3 or 4 days	Valentin Siebert - Yoan Germain	Available
16.03.2021 - 14.10.2021	Dissolved ^{66}Zinc	GoFlo Bottle	Surface	Every 3 or 4 days	Valentin Siebert - Yoan Germain	Available
16.03.2021 - 14.10.2021	Dissolved ^{66}Zinc	GoFlo Bottle	Bottom	Every 3 or 4 days	Valentin Siebert - Yoan Germain	Available
16.03.2021 - 14.10.2021	Dissolved ^{75}Arsenic	GoFlo Bottle	Surface	Every 3 or 4 days	Valentin Siebert - Yoan Germain	Available
16.03.2021 - 14.10.2021	Dissolved ^{75}Arsenic	GoFlo Bottle	Bottom	Every 3 or 4 days	Valentin Siebert - Yoan Germain	Available
16.03.2021 - 14.10.2021	Dissolved ^{88}Strontium	GoFlo Bottle	Surface	Every 3 or 4 days	Valentin Siebert - Yoan Germain	Available
16.03.2021 - 14.10.2021	Dissolved ^{88}Strontium	GoFlo Bottle	Bottom	Every 3 or 4 days	Valentin Siebert - Yoan Germain	Available
16.03.2021 - 14.10.2021	Dissolved ^{95}Molybdenum	GoFlo Bottle	Surface	Every 3 or 4 days	Valentin Siebert - Yoan Germain	Available
16.03.2021 - 14.10.2021	Dissolved ^{95}Molybdenum	GoFlo Bottle	Bottom	Every 3 or 4 days	Valentin Siebert - Yoan Germain	Available
16.03.2021 - 14.10.2021	Dissolved ^{111}Cadmium	GoFlo Bottle	Surface	Every 3 or 4 days	Valentin Siebert - Yoan Germain	Available
16.03.2021 - 14.10.2021	Dissolved ^{111}Cadmium	GoFlo Bottle	Bottom	Every 3 or 4 days	Valentin Siebert - Yoan Germain	Available
16.03.2021 - 14.10.2021	Dissolved ^{137}Barium	GoFlo Bottle	Surface	Every 3 or 4 days	Valentin Siebert - Yoan Germain	Available

16.03.2021 - 14.10.2021	Dissolved ^{137}Barium	GoFlo Bottle	Bottom	Every 3 or 4 days	Valentin Siebert - Yoan Germain	Available
16.03.2021 - 14.10.2021	Dissolved ^{138}Barium	GoFlo Bottle	Surface	Every 3 or 4 days	Valentin Siebert - Yoan Germain	Available
16.03.2021 - 14.10.2021	Dissolved ^{138}Barium	GoFlo Bottle	Bottom	Every 3 or 4 days	Valentin Siebert - Yoan Germain	Available
16.03.2021 - 14.10.2021	Dissolved ^{206}Lead	GoFlo Bottle	Surface	Every 3 or 4 days	Valentin Siebert - Yoan Germain	Available
16.03.2021 - 14.10.2021	Dissolved ^{206}Lead	GoFlo Bottle	Bottom	Every 3 or 4 days	Valentin Siebert - Yoan Germain	Available
16.03.2021 - 14.10.2021	Dissolved ^{207}Lead	GoFlo Bottle	Surface	Every 3 or 4 days	Valentin Siebert - Yoan Germain	Available
16.03.2021 - 14.10.2021	Dissolved ^{207}Lead	GoFlo Bottle	Bottom	Every 3 or 4 days	Valentin Siebert - Yoan Germain	Available
16.03.2021 - 14.10.2021	Dissolved ^{208}Lead	GoFlo Bottle	Surface	Every 3 or 4 days	Valentin Siebert - Yoan Germain	Available
16.03.2021 - 14.10.2021	Dissolved ^{208}Lead	GoFlo Bottle	Bottom	Every 3 or 4 days	Valentin Siebert - Yoan Germain	Available

Table 2 – List of parameters measured within the shells of *Pecten maximus* collected at Lanvéoc in 2021.

Parameter	Sediment/Cage	Number of shells	Principals investigators	Processed
Daily growth rate	Sediment	6	Lukas Fröhlich – Valentin Siebert	Available
Daily growth rate	Cage	6	Lukas Fröhlich – Valentin Siebert	Available
^{7}Li / $^{43}Ca_{shell}$	Sediment	3	Lukas Fröhlich – Valentin Siebert	Available
^{11}B / $^{43}Ca_{shell}$	Sediment	3	Lukas Fröhlich – Valentin Siebert	Available
^{23}Na / $^{43}Ca_{shell}$	Sediment	3	Lukas Fröhlich – Valentin Siebert	Available
^{25}Mg / $^{43}Ca_{shell}$	Sediment	3	Lukas Fröhlich – Valentin Siebert	Available
^{43}Ca / $^{43}Ca_{shell}$	Sediment	3	Lukas Fröhlich – Valentin Siebert	Available
^{51}V / $^{43}Ca_{shell}$	Sediment	3	Lukas Fröhlich – Valentin Siebert	Available
^{55}Mn / $^{43}Ca_{shell}$	Sediment	3	Lukas Fröhlich – Valentin Siebert	Available
^{57}Fe / $^{43}Ca_{shell}$	Sediment	3	Lukas Fröhlich – Valentin Siebert	Available
^{88}Sr / $^{43}Ca_{shell}$	Sediment	3	Lukas Fröhlich – Valentin Siebert	Available
^{95}Mo / $^{43}Ca_{shell}$	Sediment	3	Lukas Fröhlich – Valentin Siebert	Available
^{97}Mo / $^{43}Ca_{shell}$	Sediment	3	Lukas Fröhlich – Valentin Siebert	Available
^{135}Ba / $^{43}Ca_{shell}$	Sediment	3	Lukas Fröhlich – Valentin Siebert	Available
^{137}Ba / $^{43}Ca_{shell}$	Sediment	3	Lukas Fröhlich – Valentin Siebert	Available
^{208}Pb / $^{43}Ca_{shell}$	Sediment	3	Lukas Fröhlich – Valentin Siebert	Available
^{238}U / $^{43}Ca_{shell}$	Sediment	3	Lukas Fröhlich – Valentin Siebert	Available
^{7}Li / $^{43}Ca_{shell}$	Cage	3	Lukas Fröhlich – Valentin Siebert	Available
^{11}B / $^{43}Ca_{shell}$	Cage	3	Lukas Fröhlich – Valentin Siebert	Available
^{23}Na / $^{43}Ca_{shell}$	Cage	3	Lukas Fröhlich – Valentin Siebert	Available
^{25}Mg / $^{43}Ca_{shell}$	Cage	3	Lukas Fröhlich – Valentin Siebert	Available
^{43}Ca / $^{43}Ca_{shell}$	Cage	3	Lukas Fröhlich – Valentin Siebert	Available
^{51}V / $^{43}Ca_{shell}$	Cage	3	Lukas Fröhlich – Valentin Siebert	Available
^{55}Mn / $^{43}Ca_{shell}$	Cage	3	Lukas Fröhlich – Valentin Siebert	Available
^{57}Fe / $^{43}Ca_{shell}$	Cage	3	Lukas Fröhlich – Valentin Siebert	Available
^{88}Sr / $^{43}Ca_{shell}$	Cage	3	Lukas Fröhlich – Valentin Siebert	Available
^{95}Mo / $^{43}Ca_{shell}$	Cage	3	Lukas Fröhlich – Valentin Siebert	Available
^{97}Mo / $^{43}Ca_{shell}$	Cage	3	Lukas Fröhlich – Valentin Siebert	Available
^{135}Ba / $^{43}Ca_{shell}$	Cage	3	Lukas Fröhlich – Valentin Siebert	Available
^{137}Ba / $^{43}Ca_{shell}$	Cage	3	Lukas Fröhlich – Valentin Siebert	Available
^{208}Pb / $^{43}Ca_{shell}$	Cage	3	Lukas Fröhlich – Valentin Siebert	Available
^{238}U / $^{43}Ca_{shell}$	Cage	3	Lukas Fröhlich – Valentin Siebert	Available

CHAPTER 2

IMPACTS OF PHYTOPLANKTON DYNAMICS ON SEAWATER CHEMISTRY

PREAMBLE/PRÉAMBULE

The general introduction of this manuscript states that many studies have used the concentrations of barium and molybdenum incorporated into the shells of the scallop, *P. maximus*, to trace past phytoplankton dynamics. Previous investigations have found correlations between the variations in the concentrations of these elements incorporated into their shell and variations in the abundance of phytoplankton in the water column. However, none of them have established the links between high-frequency variations in phytoplankton assemblages and the bioavailability of these elements in the water column. In this chapter, we will set aside the study of the shells and focus solely on the relationship between variations in the concentrations of barium and molybdenum measured in the water column and the dynamics of phytoplankton (i.e., temporal variations in micro-algae assemblages, formation of aggregates) during one year. For this purpose, we will use the data collected as part of the HIPPO environmental monitoring program carried out in 2021 in the Bay of Brest (France), which was presented in the previous chapter. This second chapter is a scientific article and has been recently submitted in *Estuarine, Coastal and Shelf Science*.

Comme nous l'avons mentionné dans l'introduction générale de ce manuscrit, de nombreuses études ont utilisé les concentrations de baryum et de molybdène incorporées dans les valves de la coquille St-Jacques, *P. maximus*, comme proxy des dynamiques phytoplanctoniques dans la colonne d'eau. Ces études ont en effet découvert des corrélations entre les variations des concentrations de ces éléments incorporés dans la coquille et la structure des communautés micro-algales. Cependant, aucune de ces études n'a réellement dressé les liens qui existent entre les variations dans les assemblages phytoplanctoniques et biodisponibilité de ces éléments dans l'environnement. Par conséquent, dans ce chapitre, nous laisserons l'étude des coquilles de côté et nous nous concentrerons uniquement sur les relations qui existent entre les variations de concentration en baryum et molybdène mesurées dans la colonne d'eau et les dynamiques phytoplanctoniques durant une année. Pour cela, nous utiliserons les données recueillies dans le cadre du programme de surveillance environnemental HIPPO, réalisé en 2021 en rade de Brest (France), qui ont été présentées dans le chapitre précédent. Ce deuxième chapitre a fait l'objet d'un article scientifique qui a été soumis récemment dans le journal *Estuarine, Coastal and Shelf Science*.

Dynamics of barium and molybdenum in the Bay of Brest (France) explained by phytoplankton community structure and aggregation events

Valentin Siebert[1], Lukas Fröhlich[2], Julien Thébault[1], Bernd R. Schöne[2], Gaspard Delebecq[1], Marc Picheral[3], Matthieu Waeles[1], Brivaëla Moriceau[1]

[1]*Univ Brest, CNRS, IRD, Ifremer, LEMAR, F-29280 Plouzané, France*

[2]*Institute of Geosciences, University of Mainz, Johann-Joachim-Becher-Weg 21, 55128 Mainz, Germany*

[3]*Sorbonne Université, Centre National de la Recherche Scientifique, Laboratoire d'Océanographie de Villefranche (LOV), Villefranche-sur-Mer, FranceUniv Brest, CNRS, IRD, Ifremer, LEMAR, F-29280 Plouzané, France*

ABSTRACT

Primary producers are essential organisms for marine ecosystems because they form the basis of food webs, produce nearly half of atmospheric oxygen (Field et al., 1998) and are involved in various biogeochemical cycles. At the end of a bloom event, phytoplankton cells are known to produce organic compounds that act as a 'cement', allowing the cells to stick together and form large structures called aggregates. These aggregates are microenvironments with chemical properties that are very different from the surrounding water. The main objective of this study was to determine how the temporal variations in cell assemblages over time and the formation of aggregates following a bloom affect the concentrations of molybdenum (Mo) and barium (Ba) in the water column. For this purpose, we monitored the environment from March to October 2021 at Lanvéoc in the Bay of Brest (France) and measured several biological, chemical, and physical parameters at high frequency. Here, our results show that Mo-rich dinoflagellate cells from the genus *Gymnodinium* were responsible for the variations in Mo concentration in the water column. In addition, large phytoplankton aggregates transported a significant amount of Mo to the seafloor. In contrast, the temporal variations in Ba concentration were strongly influenced by the formation of diatom blooms. There was a significant shift in Ba from the dissolved to the particulate fraction during the largest diatom bloom of the year, apparently associated with the adsorption of this element onto diatom frustules. This bloom event was also associated with significant transport of Ba to the seafloor. This study therefore highlights the impacts of phytoplankton dynamics on the variations of these elements in coastal ecosystems.

1 INTRODUCTION

Marine phytoplankton are among the most important organisms of the biosphere. They are responsible for roughly 45% of the global primary production (Field et al., 1998). One fourth of this primary production occurs in coastal ecosystems (Boyce et al., 2010), although they represent only 2% of the earth surface (Charpy-Roubaud and Sournia, 1990). Moreover, microalgae are at the base of the trophic network and are involved in several biogeochemical cycles. In light of the events caused by their seasonal development (bloom, appearance of harmful algae, etc.), phytoplankton strongly modify the physical and chemical conditions of the water column on long-term scales (Redfield, 1958) and these changes strongly affect organisms and ecosystems.

Under stressful conditions such as nutrient limitation due to a bloom event, high hydrodynamic energy or changes in temperature or light conditions, phytoplankton cells can excrete large amounts of extracellular polysaccharides (EPS) (Myklestad, 1995). In particular, one form of EPS has been studied and is now well-documented: transparent exopolymer particles (TEPs) (e.g., Alldredge et al., 1993; Passow and Alldredge, 1994; Passow, 2002). The presence of TEPs in the water column appears to be essential for the formation of most phytoplankton aggregates, because they act as an organic 'cement' that will bind the cells together along with other inorganic particles of the environment (Passow & Alldredge, 1994; Dam & Drapeau, 1995; Logan et al., 1995; Engel, 2000). These so-called aggregates, also known as 'marine snow', can reach a few centimetres in diameter (Alldredge & Silver, 1988). Due to their fast sinking rates that average 50 $m.d^{-1}$ - but can reach several kilometers per days in the open ocean (Diercks & Asper, 1997; McDonnell et al., 2015; Toullec et al., 2019; Laurenceau-Cornec et al., 2020b), these aggregates have a major impact on ecosystems, being important vectors of organic matter export to the seafloor in shallow water as well as in the open ocean and also affect the biological carbon pump (Turner, 2015). These structures form 'microenvironments' that are highly porous and are known to transport not only particulate matter, but also dissolved elements when sinking through the water column (Carlson et al., 1994; De La Rocha et al., 2008; Moriceau et al., 2014).

Phytoplankton aggregates have their own internal chemical and biological dynamics that are quite different from those of the surrounding water (Alldredge et al., 1986; Alldredge & Cohen, 1987; Alldredge & Gotschalk, 1990; Kiørboe & Jackson, 2001; Garvey et al., 2007; Moriceau et al., 2007; Ploug et al., 2008). Several studies have recorded high heterotrophic activity and high phytoplankton cell viability within aggregates, which may explain their lower oxygen concentrations and pH values in comparison with surrounding water (Alldredge & Cohen, 1987). The combination of these factors, taken together with the high potential of the aggregate matrix to bind trace metals and other elements (Gutierrez et al., 2012; Tercier-Waeber et al., 2012), suggests that the elemental composition of the

water mass can be modified when aggregates form and sink through the water layers. In particular, sinking aggregates may especially affect trace elements that are sensitive to redox conditions and ligand concentrations. Aggregate formation may therefore have a significant impact on the concentration of these trace elements in water, as well as on their bioavailability for organisms and their transport toward the sediment/water interface (SWI).

Establishing the link between phytoplankton aggregate formation and element composition of seawater remains an important challenge. Over the past two decades, attempts have been made to identify links between trace elements, specifically molybdenum (Mo) and barium (Ba), incorporated into the shells of bivalves and changes in primary producer communities (e.g., Vander Putten et al., 2000; Barats et al., 2009; Thébault et al., 2009; Tabouret et al., 2012; Doré et al., 2021; Thébault et al., 2022; Fröhlich et al., 2022a). This field is known as bivalve sclerochronology and aims to reconstruct past phytoplankton dynamics from times prior to major anthropogenic impacts on coastal ecosystems as well as times and places for which instrumental records of phytoplankton abundance are not available. However, Mo and Ba may be coupled with organisms or particles (either mineral or biological) other than phytoplankton cells. For example, Mo may be bound to phytoplankton aggregates (Dellwig et al., 2007), which can thus contribute significantly to the transport of Mo toward the seabed. Similarly, particulate Ba is most commonly found in the water column in the form of barite crystals, mineral particles that precipitate when high concentrations of Ba or sulphide are present in the environment (Dehairs et al., 1980).

The specific objective of this paper is to assess potential links between phytoplankton dynamics and the chemical composition of seawater, specifically Mo and Ba, in the Bay of Brest, a well-studied coastal ecosystem. We explored the processes related to phytoplankton dynamics that control the distribution of these elements between the particulate and dissolved compartments and their transport to the SWI throughout the productive season. For this purpose, we set up a high-frequency monitoring survey of the environment between March and October 2021.

2 MATERIAL AND METHODS

2.1 Study site

The Bay of Brest, France, is a semi-enclosed, macrotidal marine ecosystem of 180 km^2 with a connection to the Iroise Sea to the west, separated by a narrow (2 km width) and deep strait (40 m max. depth). Freshwater input occurs from the east via two main rivers: the Aulne flows from the south and the Elorn from the north of the bay. The present study was carried out in 2021 and took place at Lanvéoc (48°17'39"N, 004°27'12"W), a site located in the southern part of the Bay of Brest

(Figure 5A). This site was chosen because several biogeochemical and ecological studies have already been conducted at this locality, making it possible to compare our new data with those from the past 10 years. Lanvéoc is characterized by shallow waters (6 to 13 m depending on tides, with a mean depth of approx. 10 m at mid-tide) and a seafloor consisting of sandy and silty sediment.

2.2 Environmental samples for chemical analyses

The study covered the year 2021 during which several chemical, physical and biological parameters were recorded at Lanvéoc. From 16 March to 14 October 2021, water samples were collected by SCUBA diving in surface (approx. 1 m depth) and bottom waters (approx. 20 cm above the sediment) using two different types of sampling bottles placed horizontally in the water column. Firstly, two 5 L Niskin bottles (one for surface water and the other for bottom water) were used to collect seawater dedicated to measurements of nutrients, biogenic silicate (BSi), particulate organic carbon (POC), chlorophyll a (Chl) and pheophytin a (Pheo) as well as to phytoplankton species determination and cell counts. As detailed in the Results section, on some days, bottom water samples were collected with a benthic syringe, which was positioned closer to the sediment than the Niskin bottle. Secondly, two 5 L GO-Flo water samplers were used to collect water to measure particulate and dissolved trace elements. After collection and before filtration, 2 L PTFE bottles were filled with water samples to prevent the adsorption of elements on the bottle walls risking the loss of elements. Due to the high sampling frequency (twice per week), we were not able to collect all samples at the same tide level. In parallel, two Sambat NKE probes continuously recorded dissolved oxygen (DO) concentration close to the seafloor at 20-minute intervals.

Macronutrients **-** During this monitoring experiment, concentrations of silicate ($Si(OH)_4$), phosphate (PO_4^{3-}) and dissolved inorganic nitrogen (DIN) were measured in the surface layer of the water column. DIN includes ammonium (NH_4^+), nitrate (NO_3^-) and nitrite (NO_2^-). For NH_4^+, a 100 mL glass vial was filled with seawater and immediately placed in the freezer (-20 °C) until analysis. For the other nutrients, 1 L of water was filtered through a 0.6 µm polycarbonate filter (Merck) within 3 h after sampling. The filtrate was recovered and was divided into several 15 mL polypropylene tubes and stored at 4 °C for $Si(OH)_4$ analysis and at -20 °C for the analysis of NO_3^-, NO_2^- and PO_4^{3-}. Then, the concentrations of all nutrients were measured using a SEAL (Bran+Luebbe) AA3 HR AutoAnalyzer for colorimetric (for NO_3^-, NO_2^-, $Si(OH)_4$ and PO_4^{3-}) and fluorometric (NH_4^+) analysis following the method of Aminot and Kérouel (2007). Results are given in $\mu mol.L^{-1}$. The limit of detection (LOD) of the measurements were 0.015 µM for NH_4^+ and NO_3^-, 0.003 µM for NO_2^-, 0.010 µM for $Si(OH)_4$and 0.020 µM for PO_4^{3-}. Episodes of nutrient limitation were then defined by comparing *in-situ* concentrations to the half-saturation constant for nutrient uptake (Km). Values below this threshold correspond

to stressful nutrient conditions limiting phytoplankton development (Km = 2.0 µmol.L^{-1} for DIN and $Si(OH)_4$; Km = 0.2 µmol.L^{-1} for PO_4^{3-}; Del Amo et al., 1997).

Particulate organic carbon (POC) - To measure the organic carbon content in the particulate fraction, 500 mL of seawater was filtered with pre-combusted (450 °C for 4 h) Whatman GF/F filters. Filters were then dried in the oven at 50 °C and analysed for their POC concentration using the combustion method on a CHN elemental analyser (Thermo Fisher Flash 2000) (Aminot and Kérouel, 2004). The collected data had an error rate of 5%.

Chlorophyll a and pheophytin a (Chl and Pheo) - For chlorophyll a and pheophytin a measurements, 500 mL of seawater was filtered through glass fibre filters (GF/F Whatman), which were pre-combusted for 4 h in a muffle furnace at 450 °C. Chl was extracted in 6 mL of 90% acetone and kept in the dark at 4 °C for 12 h. Samples were then centrifuged and fluorescence was measured with a Turner AU-10 fluorometer using the equation provided by Lorenzen (1966) and an LOD of 0.2 µg.L^{-1}.

Biogenic silicate (BSi) - The BSi content of seawater was measured by filtering approx. 1 L of seawater through a 0.6-µm polycarbonate filter (Merck) within 3 h after sampling. Filters were then dried and stored in a dry and dark place before completing the measurements. BSi analyses were carried out following the method developed by Ragueneau and Tréguer (1996). The measurement error was 4 %.

2.3 Phytoplankton dynamics, temporal variations in particle abundance and water chemistry

Phytoplankton determination and counts

For phytoplankton species determination, a 250 mL surface water was carefully transferred to a silicon tube, avoiding insofar as possible turbulence and disintegration of phytoplankton cells. The phytoplankton cells were immediately fixed with 2 mL of acidic Lugol's iodine solution and stored in a dark and cold (4 °C) place to avoid UV damage and evaporation. Phytoplankton taxa were identified and cell concentrations were determined within 1 month after sample collection using an aliquot of 50 mL of the water sample that was filled into a sedimentation column combined with a plate chamber (Hydrobios Kiel), according to the Utermöhl method (Edler & Elbrächter, 2010). After 24 h of sedimentation in the column, the phytoplankton cells settled on a microscope glass slide. The cells were identified and counted using an Axio Observer.A1 inverted light microscope (Zeiss) at 160x and 640x magnification. Furthermore, for most species, the surface area (i.e., the contact zone

between the water and the cells) and the biovolume (i.e., the volume occupied by the cells in the water column) were calculated based on the specific average surface and volume established by following the equations described by Smayda (1965).

Particle chemistry

A HYDRO-BIOS Multi Sediment Trap with 12 collecting bottles (total volume: 290 mL) was deployed during the survey to measure chemical parameters on particles sinking to the seafloor. Its catchment area was 153.86 cm². The rotation frequency was set to 3.d-1 between 2 March and 25 May, and 4.d-1 between 26 May and 29 July. Before deployment, each bottle was poisoned with mercury chloride (180 µM $HgCl_2$, Lee et al., 1992) to prevent any biological activity and thus the degradation of organic matter. Measured parameters included the particulate trace element concentration, POC and BSi following the methods described in the previous and following sections. Prior to filtration, samples were shaken to break up aggregates and passed through a 1 mm mesh screen to avoid clogging the filter with large mineral particles or zooplankton.

Aggregate dynamics

Aggregate dynamics were measured throughout the year by using a compact and autonomous underwater imaging system initially constructed and developed at the Laboratoire d'Oceanographie de Villefranche-sur-Mer (LOV – France), i.e., the Underwater Vision Profiler 6 (UVP6) (see Picheral et al., 2021 for a complete description of the instrument). The device consists of a camera coupled to a light source that can take pictures of particles in a precisely defined volume of water (0.65 L) at a pre-defined frequency (Fig, 15A). While this instrument has been designed for intermittent profile measurements, here it was used to measure particle dynamics as a continuous time-series, thus, the design of the UVP6 has been modified accordingly. Several environmental parameters may have influenced measurements and biased the results such as sun exposure, bioturbation, particle resuspension from the sediment and hydrodynamic conditions. To limit these potential biases, the UVP6 was placed in a PVC cylinder (diameter = 50 cm; height = 70 cm) which was open at the top and closed at the bottom. To prevent large organisms from entering the cylinder and to ensure that constant hydrodynamics prevailed within the cylinder, a 5 cm thick grid with a 1x1 cm mesh size was placed on top of the cylinder (Figure 15B).

The UVP6 was deployed on the seafloor at Lanvéoc on 16 March 2021. Data acquisition took place every hour for 30 min. During that time, the UVP6 took pictures of particles every 20 seconds and stored the images. With the chosen settings, the UVP6 worked autonomously for approx. 21 days. Every 3 weeks, the UVP was recovered, data were downloaded and the batteries were recharged. The

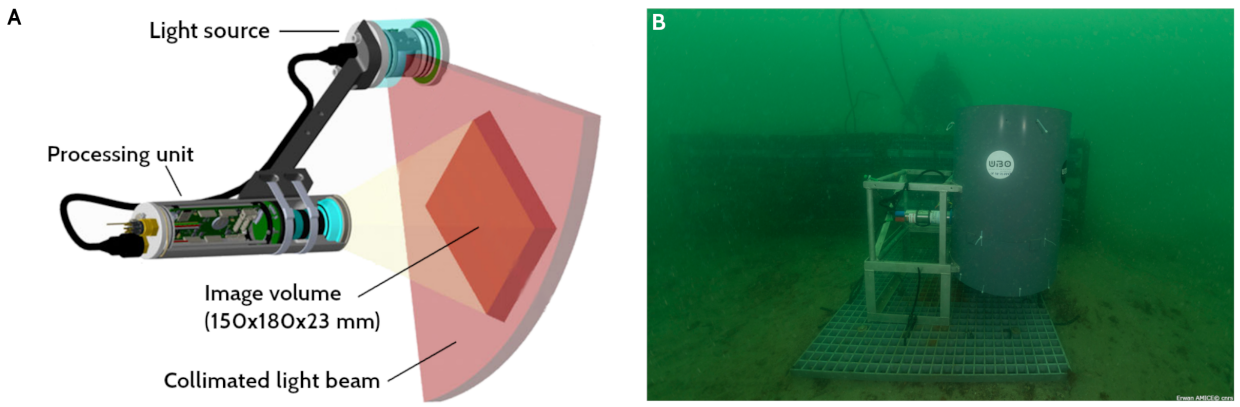

Figure 15 – (A) Expanded view of the UVP6 showing the main features of the instrument. (B) Picture of the UVP6 deployed at Lanvéoc showing the modifications made to adapt the UVP deployment for continuous measurements in a coastal ecosystem.

pictures were later processed using the UVP app, which can automatically detect particles on pictures, count them and measure their size in equivalent spherical diameters (ESD - Jennings and Parslow, 1988). After processing, the database contained measurements of particle concentration divided into 25 particle size classes ranging from 80.6 µm to 26 mm (ESD).

A first overview of aggregate dynamics was obtained by calculating the sum of particles larger than 512 µm (ESD). We thus avoided including large phytoplankton cells that can reach this size; for example, cells of Coscinodiscus sp. (among the largest phytoplankton species) can have a cell diameter of up to 500 µm (Kühn & Raven, 2008). We also excluded particles larger than 26 mm to avoid counting debris or macroparticles other than organic aggregates. Following these rules, an event was considered as an aggregation episode when the maximum value (peak) of the particle concentration exceeded the width of its base peak by two-fold.

To better characterize the aggregation episodes, particle size spectra were obtained by computing the concentration of particles as a function of their size range on each day of monitoring, as previously done for aggregates artificially produced in rolling tanks (Laurenceau-Cornec et al., 2015). For each spectrum, the slope of the linear regression between particle size and concentration was then calculated, providing information on a potential transition between small and large particles, and therefore, on the occurrence of on aggregation event. For instance, higher slope values (close to 0 since slopes are negative) indicate that a high amount of small particles have agglomerated with each other to form larger particles. This indicates the presence of large aggregates occurring at high concentrations, thereby revealing an aggregation event. Combined with the previous method, these daily measurements of aggregate dynamics were very useful because they identified other aggregation episodes that were composed of larger particles, likely otherwise undetectable due to their low concentrations. For every detected aggregation event based on these two methods, their slopes were

compared using an analysis of covariance (ANCOVA) to observe differences in the structure of the aggregation episodes.

2.4 Trace element measurements

Water samples collected with GO-Flo bottles were filtered through MF-Millipore™ mixed cellulose ester filters within 3 h after collection (1 L of water per filter). Filters were air-dried and stored in a dark and a dry place to measure the trace elements in the particulate fraction. The filtrates, dedicated to trace element analyses in the dissolved phase, were stored in 15-mL polypropylene tubes at 4 °C. The filters were pre-washed by soaking them for at least 24 h in a pH 1 solution made with nitric acid (HNO_3, Suprapur, Merck, Darmstadt, Germany) and ultrapure water (UP) from a Milli-Q element system. The filters were then soaked in UP and thoroughly rinsed with UP before use. The tubes were also pre-washed with pH 1 HNO_3 solutions and then thoroughly rinsed with UP.

Trace element analysis of particulate matter - For the analyses of particulate Mo (PMo) and particulate Ba (PBa), the filters were digested at 80 °C for 3 h in closed 30 ml PTFE screw-cap vials (Savillex, Minnetonka, MN, USA) by adding 2 mL of 65% HNO_3 (Suprapur, Merck) and 500 µL of 30% hydrogen peroxide (Suprapur, Merck). The elemental analyses of ^{95}Mo and ^{138}Ba isotopes were then conducted on diluted mixtures (2.3% HNO_3) with a X-series II, quadrupole inductively coupled plasma mass spectrometer (Q-ICP-MS) (Thermo Scientific) at the Pôle Spectrométrie Océan (Plouzané, France). The data were corrected for machine drift by inserting multi-element standard solutions every two samples. The LODs were determined based on the 3σ criterion, using the standard deviation of the signals obtained after digestion of cleaned filters and analyses of the resulting solutions. The obtained LODs were 0.01 nM for Mo and 0.03 nM for Ba. All PBa data exceeded the LOD, but 76% of the PMo data reached this threshold. Only values above the LOD were interpreted.

Trace element analysis of dissolved matter - Measurements of dissolved ^{95}Mo (DMo) and dissolved ^{138}Ba (DBa) were carried out using an Element XR HR-ICP-MS at IFREMER (Plouzané – France). Seawater samples were dilu ted 100 times with 2% HNO_3 solutions in order to preserve the instrument from the salt matrix. The drift of the machine was also taken into account and the data were corrected accordingly. The accuracy of the method was verified using a NASS 6 (National Research Council, Canada) certified reference seawater. LOD values were 0.04 nM and 0.01 nM for DMo and DBa, respectively, and 100% of the dataexceeded these LODs.

2.5 Data presentation

All data are available on SEANOE (https://www.seanoe.org/data/00808/92043/ - Siebert et al., 2023). To characterize the organic matter, understand its composition and detect episodes of degradation, the above-mentioned parameters were used to compute ratios that are commonly calculated in ecological studies. Through the calculation of the Chl:Pheo ratio (expressed in $g.g^{-1}$), it was possible to quantify the degree of phytoplankton degradation. According to Savoye (2001), a ratio below 1 indicates degraded organic matter (which can be considered as detrital if the value drops below 0.5), and a ratio greater than 2 describes fresh phytoplankton. Furthermore, the value of the POC:Chl ratio (expressed in $g.g^{-1}$) provides information on photosynthesis efficiency: values greater than 200 are used as a threshold to detect time intervals during which the efficiency of photosynthesis is reduced and mixotrophy and heterotrophy dominate (Bentaleb et al., 1998). Finally, the BSi:POC ratio (expressed in mol.mol-1) measured in the water column, as well as in the samples from the sediment trap is representative of phytoplankton composition. In fact, more than 88% of diatom species have a Si:C signature between 0.05 and 0.19 (average = 0.14) (Sarthou et al., 2005). Thus, the occurrence of these values measured in the water column or in sediment trap samples indicated a phytoplankton community dominated by diatom cells. Table 3 gives an exhaustive list of all parameters that were measured and that were used for this study.

3 RESULTS

3.1 Temporal variability of chemical and biological parameters in the water column

Temporal variation in nutrients

At Lanvéoc in 2021, all macronutrients followed more or less the same general trend (Fig, 16). The maximum concentrations were observed during winter, followed by a rapid decrease to low concentrations in mid-spring. Concentrations remained low until mid-summer before they gradually increased until the end of the monitoring survey (Figure 16A). PO_4^{3-} was the first limiting nutrient with concentrations below the Km (0.2 $\mu mol.L^{-1}$) between 25 March and late summer. DIN was physiologically limiting a few weeks after PO_4^{3-}, between mid-April and late summer, i.e., when concentrations began to rise. NO_3^- constituted most of the DIN (80% throughout the year; Figure 16B), but all three nitrogen co-products showed the same trends. Silicate had the shortest limitation period (from 6 April to 21 June), which was interrupted by a low enrichment at the end of May, before becoming limiting again from early to mid-June.

Table 3 – Summary of the parameters that were measured during the survey.

Parameter	Date of first acquisition	Date of last acquisition	Frequency	Surface/bottom water	Sampling method
Dissolved Oxygen (DO)	01 January 2021	31 December 2021	Every 20 minutes	Bottom water	Sambat probes
Nutrients	16 March 2021	14 October 2021	- Twice per week (from 16 March to 28 June) - Once per week (from 05 July to 14 October)	Surface water	SCUBA diving Niskin bottle
BSi	16 March 2021	14 October 2021	- Twice per week (from 16 March to 28 June) - Once per week (from 05 July to 14 October)	Surface water Bottom water Sediment trap	SCUBA diving Niskin bottle
Chl and Pheo	16 March 2021	14 October 2021	- Twice per week (from 16 March to 28 June) - Once per week (from 05 July to 14 October)	Bottom water	SCUBA diving Niskin bottle
POC	16 March 2021	14 October 2021	- Twice per week (from 16 March to 28 June) - Once per week (from 05 July to 14 October)	Surface water Bottom water Sediment trap	SCUBA diving Niskin bottle
Phytoplankton determination and counts	07 January 2021	13 December 2021	Bi-weekly	Surface water	SCUBA diving Niskin bottle
Particulate ^{95}Mo and ^{138}Ba concentrations	16 March 2021	14 October 2021	- Twice per week (from 16 March to 28 June) - Once per week (from 05 July to 14 October)	Surface water Bottom water Sediment trap	SCUBA diving Niskin bottle
Dissolved ^{95}Mo and ^{138}Ba concentrations	16 March 2021	14 October 2021	- Twice per week (from 16 March to 28 June) - Once per week (from 05 July to 14 October)	Surface water Bottom water Sediment trap	SCUBA diving Niskin bottle
Size-dependent particle concentration	16 March 2021	14 October 2021	Every hour	Bottom water	UVP6

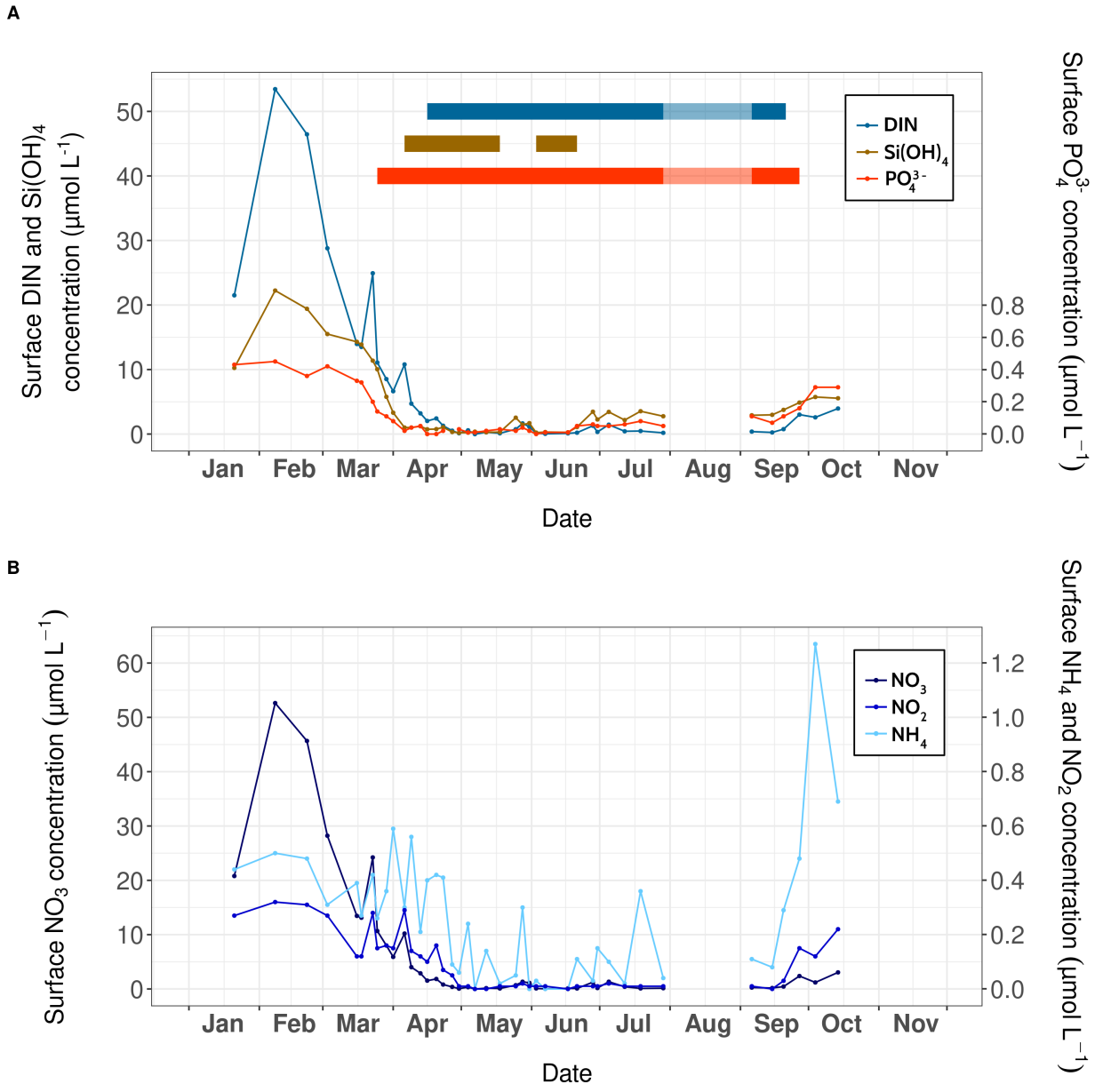

Figure 16 – (A) Dissolved inorganic nitrogen (DIN – blue line), silicate (brown line), phosphate (red line) concentration with their respective periods of limitation (thick solid lines) and (B) nitrate, nitrite and ammonium concentrations recorded at Lanvéoc in 2021.

Phytoplankton dynamics

Every fortnight, seawater was sampled at Lanvéoc to monitor the evolution of the phytoplankton community throughout the year. On 21 January 2021, phytoplankton cell concentrations were at their lowest (8,440 cell.L^{-1}) and remained stable until 20 March (Figure 17). A small peak appeared on 20 April (340,980 cells.L^{-1}) before values dropped to 127,540 cells.$^{l-1}$ on 18 May. The main phytoplankton bloom occurred a few days later on 3 June with a concentration of 2,258,580 cells.L^{-1}. This was the highest cell concentration recorded at Lanvéoc in 2021. Then, values returned to a

relatively low level of approx. 250,000 cells.L^{-1} for the rest of the summer before increasing again, attaining the third maximum on 15 September (1,516,940 cells.L^{-1}). Over the year, the phytoplankton community was largely composed of diatoms (88.45 %), with dinoflagellates (3.91 %) and other species (7.64 %) remaining a minority.

Through the calculation of the biovolumes of certain cells, it was possible to detect five dominant diatom species that occurred successively and formed a total of six significant blooms: *Coscinodiscus wailesii* (23 March), *Cerataulina pelagica* (20 April), *Guinardia flaccida* (18 May), *Leptocylindricus danicus* (3 June and 15 September) and *Chaetoceros* spp. (21 June). Dinoflagellate species were mainly represented by three species, namely *Gymnodinium* spp. which bloomed three times (end of April, 17 June and 15 September), *Protoperidinium* sp. (3 June) and *Prorocentrum triestinum* (15 September) (Figure 17C).

Chemical composition of the particulate organic matter

The biochemical composition of the organic matter provides information on its quality and how aggregates are formed. Figure 18 shows the data on Chl:Pheo, POC:Chl and BSi:POC in surface and bottom waters, which serve as indicators for phytoplankton freshness, photosynthesis efficiency and diatom composition, respectively (Savoye, 2001; Bentaleb et al., 1998; Sarthou et al., 2005).

Chl:Pheo ratios were almost constantly greater than 2 in the surface layer, proving the active phytoplankton growth with the exception of two dates: 7 June (1.69) and 27 September (1.00). In the bottom layer, this ratio occasionally fell below 1, e.g., on 23 March (0.82) and 6 April (0.76). Moreover, around the main diatom bloom on 3 June (Figure 17), a Chl:Pheo ratio close to 1 was also recorded in the bottom layer (1.16; 6 June), but a minimum of 0.15 was recorded a few days later, on 17 June. Finally, from 19 July to 6 September, a period of low Chl:Pheo was detected in bottom water, with values below 1. With the exception of the minimum value recorded on 17 June, it is important to note that all these low values in the bottom water were obtained on samples collected with a benthic syringe, thus closer to the sediment than with the Niskin bottle.

In surface water, the POC:Chl ratio remained relatively constant throughout 2021, with values oscillating between 64.68 and 251.08. However, values barely exceeded the threshold of 200 four times, i.e., on 25 May (210), 7 June (221), 17 June (251), and 19 July (245). The POC:Chl signals in bottom water followed more or less those recorded in the surface layer, with the same low values (fluctuating between 55.3 and 173) interrupted by episodic sharp peaks. These peaks were much higher than those recorded in surface water and sometimes occurred at different dates. The POC:Chl values in bottom water exceeded 200 on 18 May (570), 3 June (344), 17 June (861), 19 July (1860) and 29 July (1351) (Figure 18). As for Chl:Pheo, it is noteworthy that all the cited dates corresponded

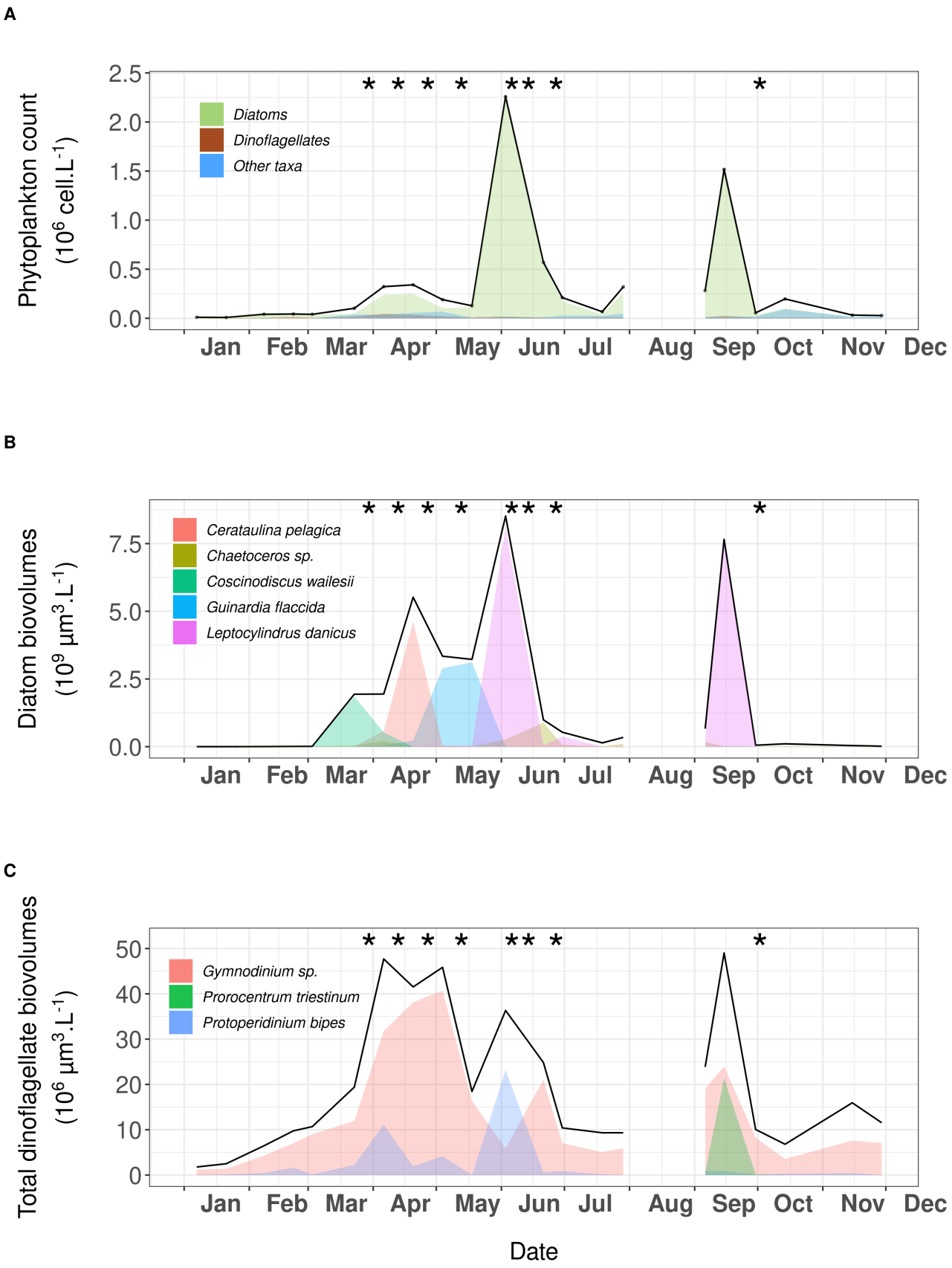

Figure 17 – (A) Phytoplankton dynamics recorded at Lanvéoc in 2021. Relative presence of the main (B) diatoms and (C) dinoflagellate species expressed as cell biovolumes. Black asterisks represent the eight aggregation events that were defined in the Section 3.3.

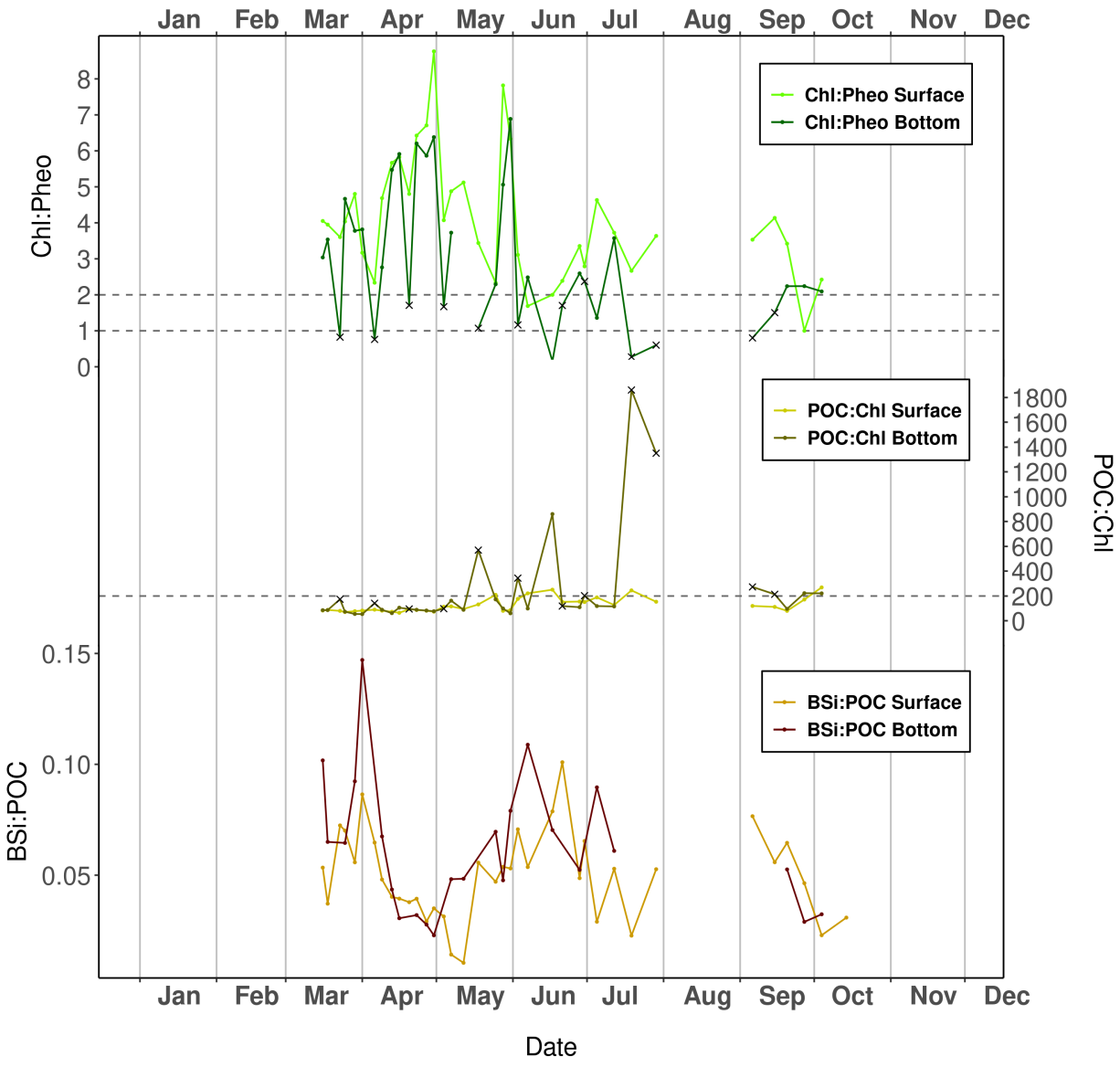

Figure 18 – Chl:Pheo, POC:Chl and BSi:POC ratios measured at Lanvéoc in bottom and in surface waters. Horizonal dashed grey lines represent the threshold values defined in Section 2.5. for the Chl:Pheo and POC:Chl ratios.

to a high POC:Chl ratio in water samples collected with a benthic syringe, with the exception of 17 July, when the bottom seawater sample was collected with a Niskin bottle.

The BSi:POC ratios oscillated between 0.01 and 0.09 in surface water, and 0.02 and 0.15 in bottom water. In surface water, two main episodes of elevated BSi:POC ratios were detected. The first reached its maximum on 1 April with a value of 0.086, and the second one on 21 June with a value of 0.101. In bottom water, the first and most important BSi:POC peak occurred on 1 April (0.147). Thereafter, values fell back and fluctuated around 0.05 until the end of May. Then, a second BSi:POC maximum was detected, reaching a value of 0.109 on 7 June before returning to the initial

value prior to this peak. Finally, a third, smaller BSi:POC elevation was observed on 5 July (0.090). Afterward, the signal remained relatively constant at a value of approximately 0.06.

Particle transport chemistry

The sediment trap provided information on the chemical composition of the particles that sedimented at the SWI. The POC signal obtained throughout the year showed episodes of low and high fluxes of organic carbon toward the SWI (Figure 19). In total, five main episodes of high carbon flux were detected. The first occurred between 26 March and 2 April (5.67 $mmol.h^{-1}.m^{-2}$), the second between 26–29 April (3.72 mmol.h-1.m-2), the third between 24–28 May (4.56 $mmol.h^{-1}.m^{-2}$), the fourth between 19–27 June (5.03 $mmol.h^{-1}.m^{-2}$) and a fifth, smaller peak between 10–15 June (1.89 $mmol.h^{-1}.m^{-2}$). Although the latter was less important than the other four, the difference between the base of this peak and the maximum value was still significant. Figure 19 also shows the BSi:POC signal recorded in the sediment trap at Lanvéoc in 2021. It oscillated between 0.01 $mol.mol^{-1}$ and 0.44 $mol.mol^{-1}$ and was quite variable throughout the year. As explained above, this ratio can be used to detect whether the sedimented organic matter corresponds to the presence of diatoms. Two long time intervals of significant diatom transport were identified. The first occurred between early and mid-May, with a BSi:POC value ranging between 0.12 and 0.18 and the second one between early and late June, with a ratio varying between 0.09 and 0.12 (Figure 19).

3.2 Trace element concentrations

Molybdenum - Results show no significant differences (Spearman's rank correlation) between surface and bottom water for PMo ($rho = 0.87$, $p < 0.001$) or for DMo ($rho = 0.50$, $p < 0.01$) (Figure 20A). During the monitoring experiment, the PMo concentrations were at a baseline value of 0.02 nM. However, two notable events with concentrations above this threshold appeared simultaneously in surface and bottom waters. The first and most important one started around 1 April and rose gradually to a maximum of 2.49 nM in bottom water and 2.71 nM in surface water (27 April and 4 May, respectively). PMo concentrations then fell back to the baseline value on 28 May and remained stable before a second, weaker peak developed in surface and bottom waters. This latter elevation started on 21 June and ended on 12 July with maximum concentrations of 0.24 nM (in bottom water) and 0.27 nM (in surface water) attained on 28 June. The concentration of DMo remained relatively constant during the studied time interval, with values generally oscillating in the range 70–80 nM, both in surface and bottom waters. However, two significant decreases in DMo were observed on 27 April and 30 June, i.e., during the same time as the PMo peaks, with values dropping from 76.1/76.8 nM to 63.5/65.5 nM on 27 April and from 77.9/79.4 nM to 69.9/71.5 nM on 30 June in bottom/surface waters.

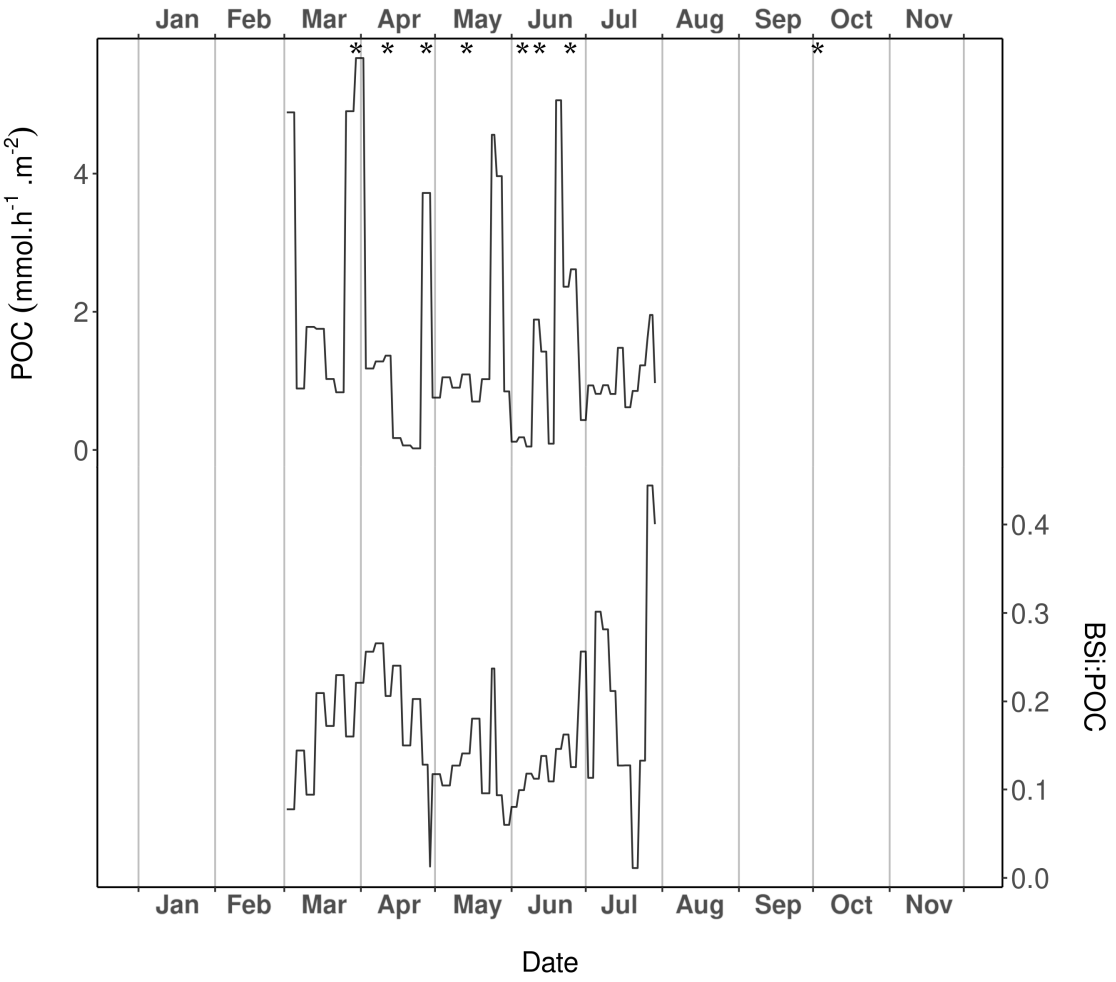

Figure 19 – POC (upper tracing) and BSi:POC (lower tracing) measured in the sediment trap samples during the experiment at Lanvéoc in 2021. The asterisks indicated the aggregation episodes that were defined in Section 3.3.

Barium - Similar to Mo, PBa (rho = 0.73, $p < 0.001$) and DBa (rho = 0.84, $p < 0.001$) followed the same trends in surface and bottom waters. Furthermore, there was a significant negative correlation between PBa and DBa for the surface (rho = -0.37, $p < 0.05$) and bottom (rho = -0.56, $p < 0.001$) waters. PBa in the water column showed baseline values of approx. 0.5 nM interrupted by strong peaks (Figure 20C). One major PBa peak stood out from the others and reached 11.70 nM in surface water and 11.88 nM in bottom water on 7 June. Aside from that event, several minor increases in PBa were observed in the surface water on 6 April (4.9 nM), 13 April (5.4 nM), 4 May (2.9 nM), 25 May (4.7 nM), 21 June 21 (4.5 nM), 30 June (2.9 nM) and 6 September (18.2 nM), whereas in the bottom layer, increases were measured on 6 April (4.6 nM), 13 April (2.4 nM), 4 May (3.5 nM) and 30 June (6.5 nM). With values ranging from 133 to 304 nM, DBa concentrations were higher than those of

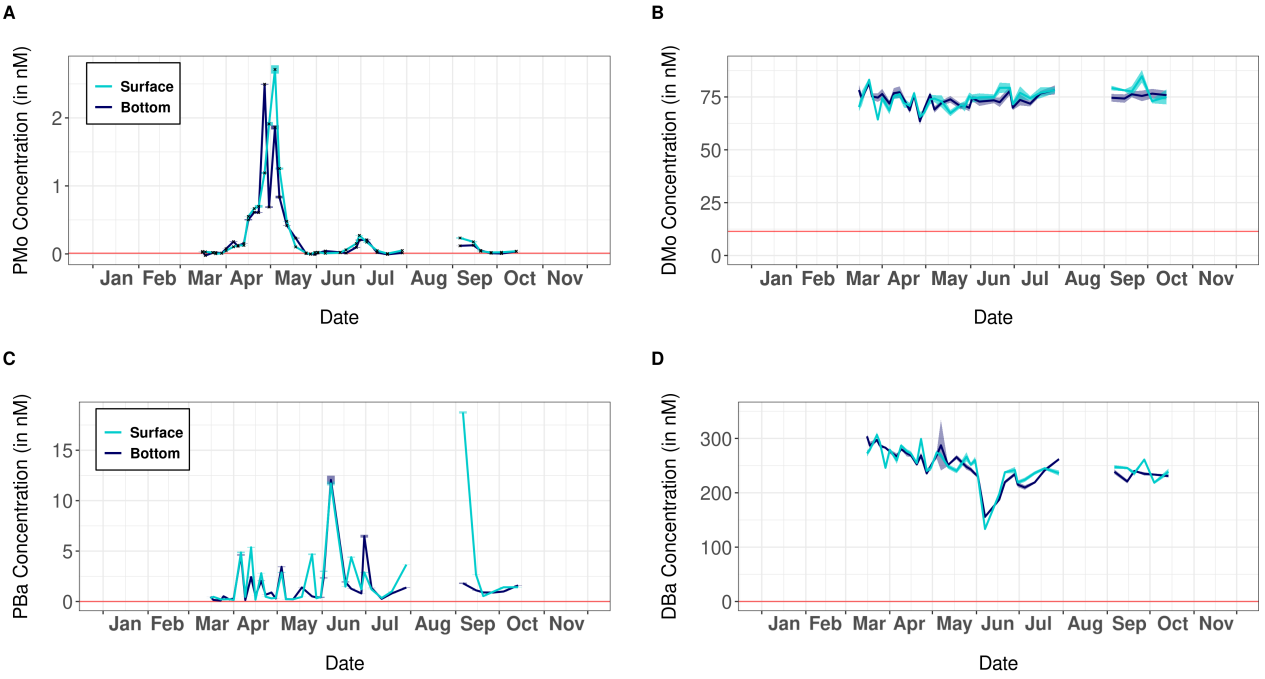

Figure 20 – Particulate (A) and dissolved (B) molybdenum (PMo and DMo) as well as particulate (C) and dissolved (D) barium (PBa and DBa) measured at the study site during 2021. Horizontal red lines represent the LOD values.

PBa. During the survey, a gradual decline in DBa was first observed between 16 March (304/272 nM) in bottom/surface waters. Then, a sharp depletion, concomitant to the main PBa peak, was observed on 7 June with minimum values of 155/133 nM in bottom/surface water. After this event, the DBa values were relatively constant and values fell to the range of 200-260 nM.

To detect Mo and Ba enrichment episodes in the water column, ratios of these elements relative to POC were computed (Figure 21). The two PMo peaks were also found at the same time in the PMo:POC data, both at the sea surface and near the seafloor. In bottom water, PMo:POC ratios attained maxima on 27 April (59.6 µmol.mol^{-1}) and on 5 July (12.4 µmol.mol^{-1}). In addition, two smaller peaks, with maxima of 3.2 µmol.mol^{-1} and 4.2 µmol.mol^{-1} emerged on 7 June and 15 September, respectively. In surface waters, PMo:POC ratios followed the same trend as near the seafloor, with the exception of early June for which the small peak observed at the bottom did not develop in surface water (Figure 21A). To detect episodes of Mo enrichment in sinking particles, the PMo:POC ratio was also calculated from the sediment trap samples (PMo:POC$_{trap}$) (Figure 21A). The single large PMo:POC$_{trap}$ increase observed in early June was uncoupled from the high PMo:POC peaks measured in the water column. This PMo:POCtrap increase lasted 27 days (26 May to 19 June) and reached a maximum of 51.8 µmol.mol-1. Three smaller increases were observed on the PMo:POC$_{trap}$ profile, one that occurred on 30 April–03 May (16.2 µmol.mol^{-1}), another on 16–19 May (16.7 µmol.mol^{-1}) and finally one on 22–24 June (21.9 µmol.mol^{-1}).

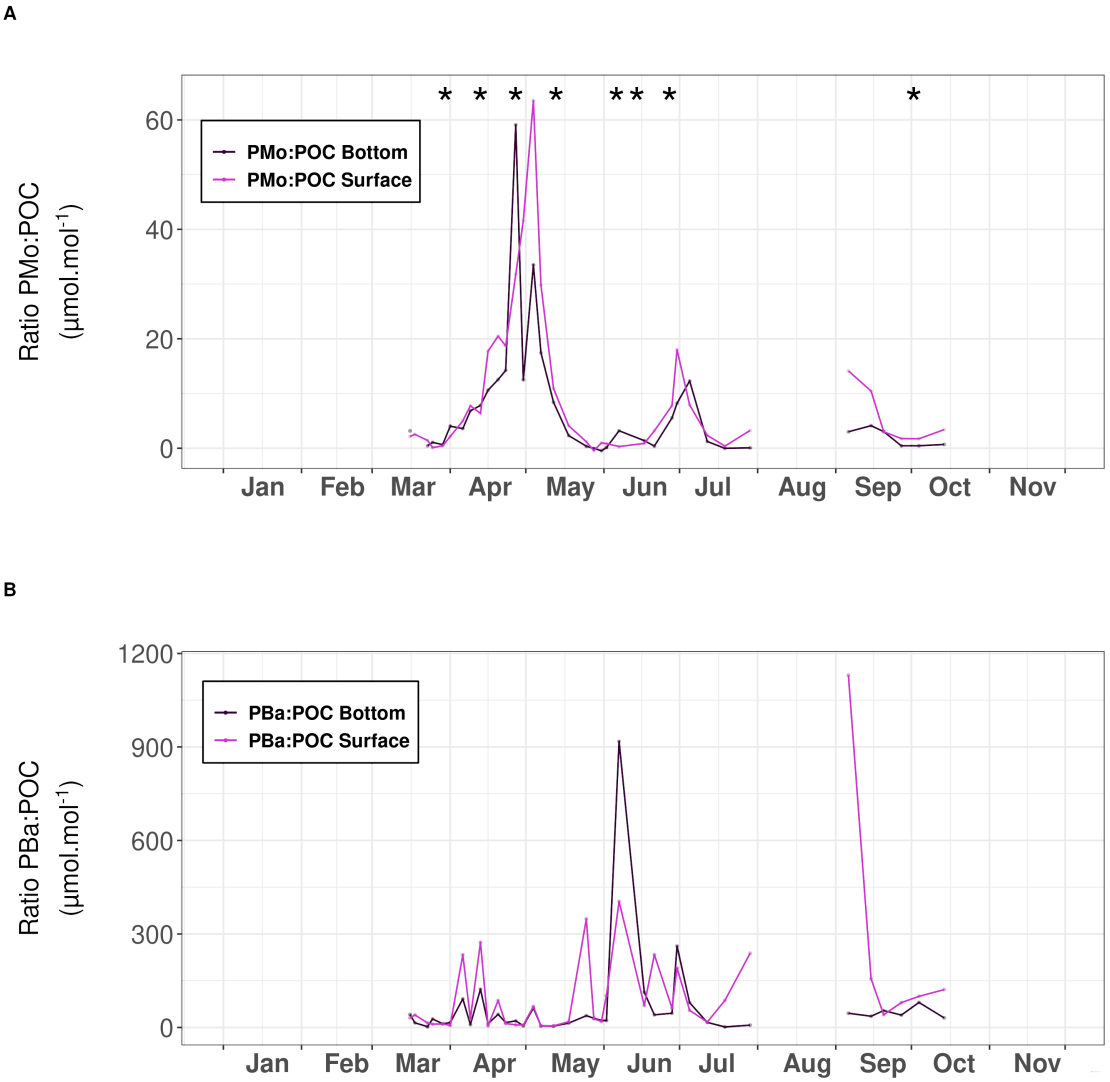

Figure 21 – PMo:POC (A) and PBa:POC (B) ratio measured at Lanvéoc in surface water (light purple line), bottom water (dark purple line) and in the sediment trap (orange line).

PBa:POC ratios closely followed the PBa trends in the water column. Six PBa:POC peaks were observed in surface water and occurred on 6 April (233 µmol.mol^{-1}), 13 April (273 µmol.mol^{-1}), 25 May (348 µmol.mol^{-1}), 7 June (404 µmol.mol^{-1}), 21 June (234 µmol.mol^{-1}) and 30 June (191 µmol.mol^{-1}). A seventh peak (1131 µmol.mol^{-1}) observed in the beginning of September was only detected in surface water. Four of these seven enrichments occurred simultaneously in bottom and surface waters, but attained different values near the seafloor (6 April: 91.76 µmol.mol^{-1}, 13 April: 123 µmol.mol^{-1}, 7 June: 918 µmol.mol^{-1}, 30 June: 261 µmol.mol^{-1}) (Figure 21B). Apart from these four peaks, no other high PBa:POC values were identified in the bottom layer. The PBa:POC$_{trap}$ values oscillated sharply between 1 and 132 µmol.mol^{-1} until 29 May. However, a small PBa:POC$_{trap}$ peak was detected between 30 April and 3 May, when PBa:POC$_{trap}$ reached 132 µmol.mol^{-1}, whereas the concentrations

measured just before and after that peak were 0.66 and 26 µmol.mol^{-1}, respectively. In addition, a strong, sharp PBa:POC$_{trap}$ increase was recorded between late May and mid-June (29 May–19 June) that culminated at a value of 437 µmol.mol^{-1} on 4–6 June, indicative of a strong Ba transport event that occurred contemporaneously to the main PBa:POC peak recorded in the water column.

3.3 Aggregate dynamics

Between 16 March and 14 October 2021, the daily mean concentration of particles above 512 µm (ESD) at Lanvéoc showed a succession of high and low values, with a minimum concentration of 4.9 part.L^{-1} (23 March) and a maximum value of 151 part.L^{-1} (30 March) (Figure 22A). Four aggregation periods occurred, with peaks in particle concentration exceeding the baseline value by more than two-fold (vertical grey areas on figure 22A and B). The first and highest peak was observed on 30 March (151 part.L^{-1}), with a value 30 times higher than the baseline. The second elevation reached its maximum on 27 April (128 part.L^{-1}). The third increase started on 5 May (28 part.L^{-1}) and reached a maximum on 13 May (78 part.L^{-1}). Finally, the fourth and last significant peak occurred on 6 June with a maximum of 113 part.L^{-1}.

From the slope of the regression line between daily particle size and concentration, four additional aggregation episodes were detected (red vertical areas on Figures 22A and B). It is noteworthy that each of the four periods established above corresponded to a peak or at least a change in the slope of the regression lines. These four new aggregation events were identified, occurring on 12 April, 14 June, 26 June and 2 October 2021 (Figure 17B). Even if the concentration of particles above 512 µm remained relatively low during these dates, the concentrations of large particles were high relative to the concentration of smaller particles. Figure 22C shows the particle size spectra obtained for the eight days during which aggregation events were detected, offering a better picture of the aggregate structure during these dates. Interestingly, each of these eight aggregation episodes was preceded by an increase in the number of diatom species (Figure 17B). The slopes of these eight spectra were then compared pairwise using ANCOVA (Figure 23). Accordingly, three aggregation episode groups can be distinguished: one including the dates of 03 March, 12 April and 13 May; another on with the dates of 14 June, 27 June and 02 October; and a last group with the dates of 06 June and 27 April. The slopes recorded on 30 March, 12 April and 13 May were significantly lower than those obtained on 14 June, 27 June and 02 October. This indicates that the aggregation events that occurred on 30 March, 12 April and 13 May were characterized by aggregates that were significantly smaller than those observed on 14 June, 27 June and 02 October, which showed the largest aggregates. Finally, aggregation events of 27 April and 06 June had an intermediate status and were similar to all other events. Therefore, they were either mainly composed by aggregates of intermediate size or evenly

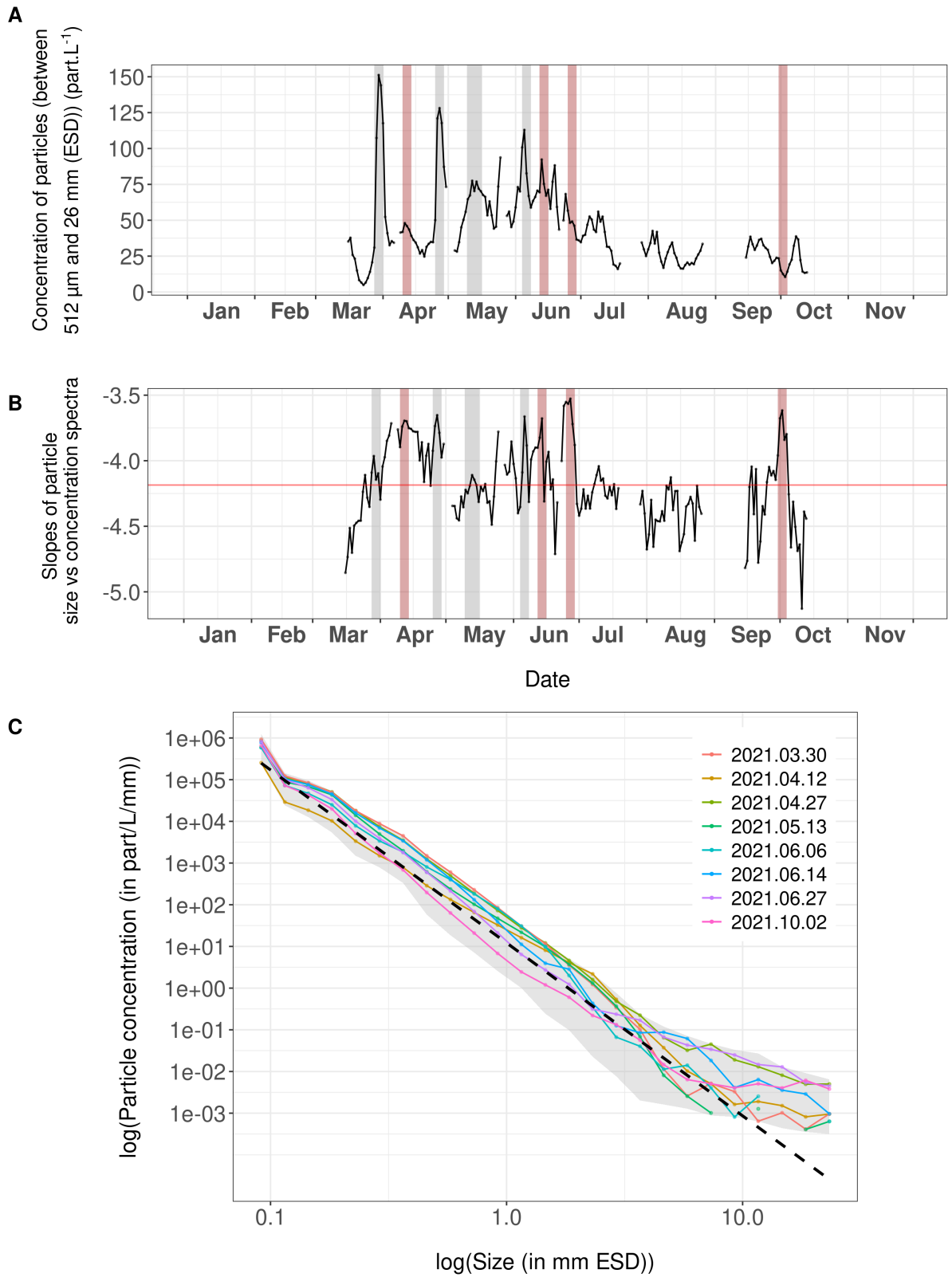

Figure 22 – (A) Average daily concentration of particles > 512 µm recorded at Lanvéoc with the UVP6. (B) Slope of the daily size spectra of particles (black line) with the annually averaged slope value (horizontal red line). Vertical grey intervals represent the four aggregation events that were detected by calculating the sum of particle concentrations larger than 512 µm, while the vertical red areas correspond to the four aggregation events that were detected with the size spectra method. (C) Size spectra of the eight dates when aggregation episodes were observed. Dashed black line represents the average slope of daily size spectra.

distributed aggregate sizes.

Figure 23 – Pairwise comparison of slopes obtained for the eight detected aggregation episodes (see Figure 22). Red cells indicate significant differences between the slopes according to an ANCOVA analysis at a 0.01 level.

4 DISCUSSION

4.1 Phytoplankton dynamics: triggers of aggregation episodes

Before discussing the involvement of phytoplankton dynamics on the variation of molybdenum and barium concentrations in the water column, some information will be first provide on their dynamics in the Bay of Brest during 2021 and the potential factors that could have led to the of aggregation events as well as the way they were detected.

To our knowledge, this is the first study to use the UVP6 as a continuous recorder. Typically, this instrument is used for discrete particle measurements in the open ocean (Stemmann et al., 2012). This novel application of the UVP6 not only required several structural adaptations as outlined in the Material and Methods section, but also precautions when processing the results. Firstly, it was necessary to remove the measurements acquired 1 h before and 2 h after deployment to prevent potential bias induced by the divers, i.e., artificial resuspension of particles that would then enter the device. Furthermore, to validate the data generated by this instrument, we compared them with other measured water column parameters that can indicate the presence of aggregates, such as the carbon transport toward the seafloor measured with a sediment trap. Carbon fluxes are not exclusively related to the formation and sedimentation of aggregates, but can also be associated with, for instance, free phytoplankton cells or detrital material (Durkin et al., 2016). Nonetheless, several major POC transport events (Figure 19) took place at the same time as detected aggregation events (Figure 22), such as the events that occurred on 30 March, 27 April, 14 June and 27 June. On the other hand, the POC transport that took place at the end of May may have been caused, for example, by the collapse of the

G. flaccida bloom (Figure 17B). This feature corroborates the interpretation of the data on aggregate concentration produced by the UVP.

By using the UVP as a recorder of aggregation episodes, eight major periods were detected during which significant amounts of aggregates were present in the water column. Each of these episodes occurred a few days after the formation of a phytoplankton bloom. For example, the first event occurred on 30 March following a *C. wailesii* bloom that occurred on 23 March, and the third aggregation event occurred on 27 April, a few days after a *C. pelagica* bloom (Figure 17). These results are consistent with the observation that aggregates are formed by phytoplankton cells at the end of a bloom, which is also in line with the validation based on UVP6 data.

As explained above, the formation of aggregates took place at the end of the phytoplankton bloom, i.e., when the cells decayed under highly stressful conditions (e.g., Alldredge et al., 1993; Passow and Alldredge, 1994; Passow, 2002). Several factors can explain the formation of these aggregates in the water column at Lanvéoc in 2021. Firstly, nutrient limitation preceded most aggregation events. For instance, the first aggregation episode occurred when phosphate became the limiting factor in the water column at the end of March. Similarly, the second and third aggregation episodes occurred when DIN and $Si(OH)_4$ became limiting in early and mid-April, respectively (Figure 16A). Finally, the main bloom of *L. danicus* detected on 3 June was likely initiated by a re-enrichment in $Si(OH)_4$. Then, this nutrient became limiting again, leading to the collapse of the bloom, triggering the formation of the subsequent diatom aggregates. However, nutrient stress is not the only parameter that can explain the formation of aggregates in the water column. When several phytoplankton species develop at the same time, some of them can have a negative effect on the development of others, becoming a source of stress contributing to their collapse and the subsequent formation of aggregates (Legrand et al., 2003). Some species of mixotrophic or heterotrophic dinoflagellates are known to have so-called allelopathic effects, specifically species in the genus *Gymnodinium* (*G. impudicum*, Band-Schmidt et al., 2020, and *G. nagasakiense* (now named *Karenja mikimotoi*), Legrand et al., 2003). In the present study, the most frequently encountered dinoflagellates belonged to *Gymnodinium* (55%), a common dinoflagellate genus found in the Bay of Brest (e.g., Chauvaud et al., 1998; Fröhlich et al., 2022a). Although the first aggregate episodes occurring in late March and in April could have been caused by nutrient limitation stress, the simultaneous development of *Gymnodinium* may also have favoured cell agglomeration (Figure 17C). This phenomenon can also be observed for the aggregates that formed in mid-June, when a significant development of *Gymnodinium* spp. took place at the same time as the bloom of the diatom *Chaetoceros* spp. (Figure 17B). It is thus important to study variation in phytoplankton assemblages as well as the chemical conditions of the water column to better understand what triggers aggregation.

4.2 Relationship of molybdenum dynamics with primary producers

Mo concentrations in the dissolved and particulate fractions measured at Lanvéoc during 2011 (Waeles et al., 2013; Thébault et al., 2022) were comparable to data collected in 2021. PMo and DMo concentrations showed similar values in 2011 and 2021 (PMo range: 0-3 nM, DMo range 60-100 nM). Although the DMo concentrations measured at Lanvéoc in 2021 remained below values observed in other coastal ecosystems (for example, 101.6 nM in Liverpool Bay - Morris, 1975), Waeles et al. (2013) reported lower values in 2011 and attributed this result to DMo removal occurring within the inner Aulne estuary. At Lanvéoc in 2021, several episodes of PMo enrichment as well as two major episodes of high Mo transport (Figure 21A) were detected in surface and bottom waters. The reasons behind these signals are discussed below.

Impacts of phytoplankton cells on the Mo enrichment in the water column

Given that the phytoplankton community structure changed on short time-scales, the chemistry of the water column is expected to be strongly affected by the succession of microalgal species. Here, we aimed to identify one or several species that would explain PMo:POC peaks (Figure 21A). The best candidate was *Gymnodinium*, which bloomed three times (late April, 17 June and 15 September). PMo:POC peaks were recorded on 27 April, 26 June and 6 September, i.e., the dates between *Gymnodinium* blooms and PMo:POC peaks almost match exactly (Figure 24). The main reason may be that the frequency of phytoplankton identification and counts was too low to accurately capture the exact timing of the bloom maximum. Previous studies have suggested that *Gymnodinium* cells play a major role in Mo dynamics of the water column. For instance, Fröhlich et al. (2022b) proposed that the Mo peaks measured in *Pecten maximus* shells are linked to the presence of *Gymnodinium* spp., especially cells smaller than 20 µm. Here, we consider all *Gymnodinium* cells together, regardless of their size. Many different reasons can explain the link between Mo and *Gymnodinium* cells. Firstly, the cells from this genus have been reported to be naturally enriched in Mo relative to other phytoplankton taxa (Ho et al., 2003). For example, in this latter study *Gymnodinium chlorophorum* (renamed *Lepidodinium chlorophorum*) showed an Mo content 3.6 times higher than the second most Mo-rich phytoplankton species (Ho et al., 2003). The unique features of the physiology of this species (probably close to *Gymnodinium* genus), may explain why it is more enriched in Mo than other taxa. Unlike other microalgae, *Gymnodinium* cells preferentially feeds on nitrate (Yamamoto et al., 2004), which is the nitrogen source that supports fastest growth; in contrast, ammonium leads to a growth rate that is two times lower (Yamaguchi & Itakura, 1999). The assimilation of nitrate requires the synthesis of an enzyme, nitrate reductase, of which Mo is an essential co-factor (e.g., Nicholas and Nason, 1955; Eppley et al., 1969). At Lanvéoc in 2021, the first two *Gymnodinium* blooms collapsed

when nitrate concentrations fell below 0.1 µmol.L^{-1} (0.06 µmol.L^{-1} on 30 April and 0.09 µmol.L^{-1} on 21 June; Figure 16B), which is the concentration below which nitrate uptake is likely impossible for some phytoplankton species (Rhee, 1974). This relationship may explain why DMo concentrations decreased during the first two *Gymnodinium* blooms, simultaneously to the increase in PMo, suggesting a Mo uptake for the synthesis of nitrate reductase. Other parameters, such as sulphate concentrations, which were not assessed in this study, may be involved in controlling the Mo content of seawater and its uptake by phytoplankton (Marino, 2003). Furthermore, Thébault et al. (2022) also recorded one high PMo:POC peak at Lanvéoc on 19 May 2011 and compared this with phytoplankton data. Based on their results, coupled with those from Fröhlich et al. (2022b), PMo:POC peaks co-occurred with the *Gymnodinium* spp. bloom, which is in line with our assumptions here. However, other *Gymnodinium* blooms occurred before this date and did not correspond to an increase in PMo:POC. This discrepancy can be attributed to the difference in the methods for determining *Gymnodinium* between 2011 and 2021. Only cells larger than 20 µm were counted in 2011, but all cells were counted in 2021, regardless of their size. However, one of the main issues for the discrepancies between water chemistry and phytoplankton blooms is likely that the monitoring of the primary producer community structure was not sufficiently frequent, hindering the determination of the exact timing of bloom maxima. Moreover, the complex hydrodynamic conditions of the Bay of Brest may also cause mismatches in these patterns.

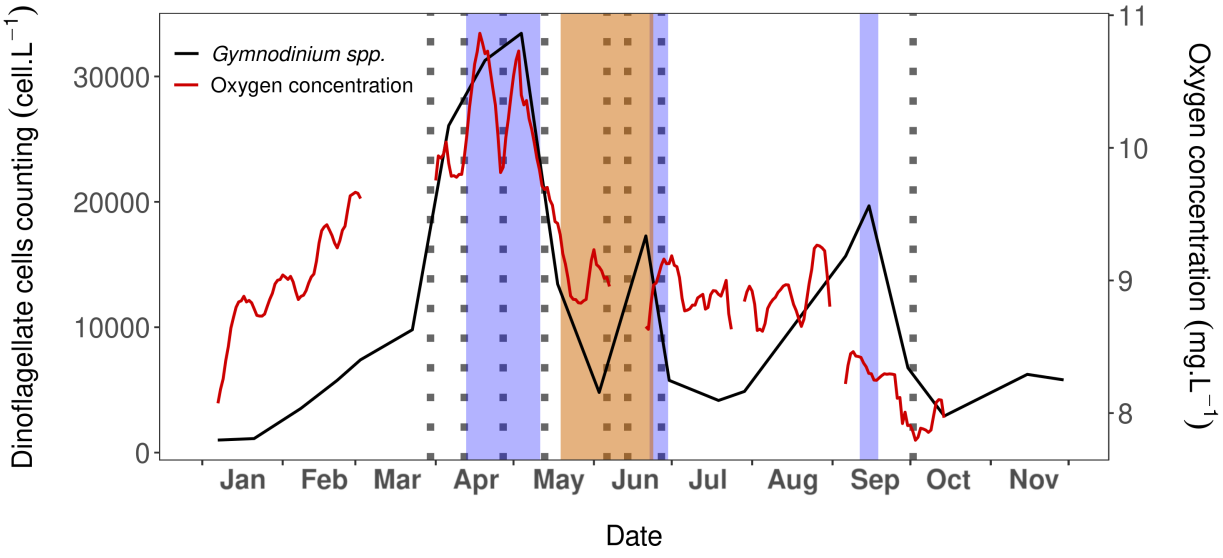

Figure 24 – Oxygen (red curve) and *Gymnodinium* spp. cells concentration (black curve) relationship with aggregation episodes and Mo downwards transport. Vertical grey dotted lines correspond to the eight days when an aggregation episode occurred. Large orange area denotes the interval of high molybdenum transport toward the seafloor, whereas the blue areas correspond to the main PMo:POC elevations.

Aggregate involvement in molybdenum transport

While *Gymnodinium* spp. cells may explain the PMo peaks, aggregate dynamics may be linked to the main Mo flux toward the SWI (Figure 21A). One of the first hypotheses regarding this aspect was formulated by Dellwig et al. (2007). In the present study, the aggregate dynamics were assessed using the UVP6 (Figure 22). However, three of the eight aggregate enrichments (6 June, 14 June and 27 June) led to the transport of Mo toward the seafloor (as detected by the sediment trap; Figure 21). In contrast, the aggregation events that occurred on 27 April and 13 May are also related to less weaker Mo transport events. Therefore, not all aggregates appear to transport Mo in the same way and other processes may be involved, resulting in different affinities for Mo between different types of aggregates.

First of all, each aggregation episode was composed of different main phytoplankton species. For instance, the first aggregation episode was mainly composed of *C. waileisii*, and the second was dominated by *C. pelagica* (Figure 17B). Because the element composition of phytoplankton differs between species (e.g., Ho et al., 2003), this may explain the differences in Mo concentration. For example, phytoplankton species that use a higher amount of Mo than others for their physiological activities may form aggregates enriched in Mo. Although the aggregation events during early June and early October were dominated by the same species, i.e., *L. danicus*, it was impossible to attribute the Mo enrichment in October to this species, due to the dysfunction of the sediment trap after the end of July and missing information on the element composition of *L. danicus*. Moreover, if there is a link between Mo enrichment and this species, an enrichment of PMo in the water column would have been detected during and shortly after the bloom of *L. danicus*, which was not observed. Regardless of the phytoplankton community structure, the chemical, physiological and biological properties of aggregates all point to high Mo transport in June.

Mo is among the best documented redox-sensitive element and its behaviour in coastal waters is fairly well known (Smrzka et al., 2019). The dominant Mo compound found in well-oxygenated water is the molybdate ion (MoO_4^{2-}), which becomes reduced and can then be found enriched in anoxic sediments (Helz et al., 1996; Morford & Emerson, 1999; Chaillou et al., 2002; Waeles et al., 2013). Based on this assumption, suspended anoxic particles such as aggregates accumulating on the seafloor, may also concentrate Mo. In fact, Alldredge and Cohen (1987) recorded a high oxygen depletion of 45.8% within a 4 mm aggregate in comparison with the surrounding water. Furthermore, oxygen depletion is weaker in smaller aggregates. For instance, a 2.1 mm diameter aggregate showed an oxygen depletion of 21.1% in comparison with the ambient environment (Alldredge & Cohen, 1987). These size-related trends have also been observed in other investigations (Ploug et al., 1997; Ploug, 2001). Based on these studies, the oxygen concentration of seawater coupled with the size

of the aggregates appear to control the oxygen content within aggregates and therefore play a role in their Mo concentration. Here, the oxygen concentration in the environment was measured in bottom water with a Sambat/NKE probe every 20 min. The aggregation episode at the end of April was accompanied by a high oxygen content in the water, but the June aggregation episodes occurred at a time when oxygen concentration was lower (Figure 24). Mo would then have been more available for aggregates in June due speciation dynamics of the element that were different due to the lower oxygen concentration in the water column, and therefore an even lower oxygen content within aggregates.

As stated above, the oxygen content in aggregates is linked to their size (Alldredge & Cohen, 1987; Ploug et al., 1997; Ploug, 2001). With the deployment of the UVP6, it became possible to determine the main size of the aggregates composing each aggregation episode. Apparently, the main Mo transport to the SWI via sinking particles occurred when larger particles dominated the particle flux (Figure 21B, 23, 24). This suggests that the largest, most oxygen-depleted aggregates were the most Mo enriched, which is consistent with the hypothesis that Mo is being more frequently scavenged in low-oxygen environments. In late April, the aggregation episode was composed of aggregates as large as those in June (Figure 23), but with a weaker associated Mo transport. This difference in Mo transport can be linked to the oxygen concentration in the water column, which was higher in April than in June (Figure 229), thereby preventing the formation of less oxygenated aggregates and, in turn, Mo scavenging. On the other hand, the oxygen concentration recorded in seawater on 13 May was similar to the concentration measured in June (Figure 24), but recorded Mo transport was weak at this date (Figure 21). Here, this divergence can be explained by a difference in the size of aggregates: the aggregates found on 13 May were significantly smaller than those formed in June (Table 23), thus leading to the formation of more highly oxygenated aggregates and, in turn, preventing the scavenging of Mo.

The relationship between Mo and aggregates remains poorly understood and the associated chemical processes still need to be addressed. To better understand the underlying mechanism, the trace metal content of differently sized aggregates and data on their exact oxygen content is needed. However, in the natural environment, this type of study may be very challenging or even impossible, because sampling single aggregates is extremely difficult. Aggregates are very fragile and prone to disaggregate even with small disturbances, e.g., by SCUBA diver bubbles, sampling turbulence, etc. Laboratory studies using rolling tanks can investigate the initiation of the formation of aggregates in a controlled environment (e.g., Moriceau et al., 2007; De La Rocha et al., 2008). Experiments using monospecific and/or plurispecific phytoplankton strains can assess the interaction of Mo and other elements with phytoplankton aggregates as well as the chemical processes involved (i.e., precipitation, adsorption, scavenging etc.). Mo may also be bound to TEPs that form the 'cement' of the aggregates, because some elements are linked with organic ligands (Decho, 1990). Establishing the relationship

between TEPs and Mo can therefore help to refine the hypothesis formulated herein regarding the chemical mechanisms behind the accumulation of Mo in phytoplankton aggregates.

4.3 Barium dynamics linked with primary producers

In the Bay of Brest, Ba concentrations have never been measured or reported. However, total Ba values measured at Lanvéoc during the current study (on average, approx. 250 nM) are in agreement with the range commonly observed in coastal shelf ecosystems, i.e., approx. 100 to 300 nM (Coffey et al., 1997). Here, successive periods of enrichment in PBa were detected in bottom and surface waters including a major event that took place on 2 June, and a drastic increase in PBa and a drop in DBa were detected (Figure. 20B - 21B).

Ba is not known to be an essential element for the proper functioning of phytoplankton cells (Sternberg et al., 2005). Nonetheless, several studies have recorded an accumulation of Ba in various species, generally attributed to the adsorption of Ba onto the silica matrix of diatoms (Dehairs et al., 1980; Fisher et al., 1991; Ganeshram et al., 2003; Sternberg et al., 2005). It appears that adsorption can also be carried out by ferric hydroxides (as long as the environmental parameters allow their precipitation), which are associated with the surface of the diatom cells (Sternberg et al., 2005). DBa would then move into the particulate fraction when diatoms form (adsorption of Ba by diatom frustules) and return into the dissolved phase when the diatoms decay. Some Ba would remain in the particulate fraction, because barite crystals are formed (Dehairs et al., 1980). For example, in the present study, the main PBa:POC peak recorded on 2 June corresponded to the timing of the *L. danicus* bloom, along with a peak in PBa in both surface and bottom waters (Figure 20C): Ba was likely bound to *L. danicus* cells (Fig, 4A). A few days later, the bloom collapsed and the cells decayed, which was accompanied by a low Chl:Pheo ratio and a high Chl:POC value on 17 June (Figure 19). These values indicated a high phytoplankton degradation rate and a reduction in the effectiveness of photosynthesis, respectively, especially in bottom waters after the bloom. Most of the diatom-linked Ba would then have returned to the dissolved fraction, with approx. 2 to 4% forming barite crystals (Ganeshram et al., 2003). These dynamics are also revealed by the DBa data of surface and bottom waters. Before the depletion (260 nM in surface and 231 nM in bottom water), concentrations were 7% and 4.9% higher than after depletion, in surface (242 nM) and bottom (220 nM) water. Some of the Ba released by the phytoplankton may thus remain in the particulate fraction and form barite crystals. That is also the reason why the PBa concentration did not retrieve its initial value after the main peak, but remained slightly higher. Even if the Ba that precipitated as barite crystals remained at a higher proportion than that recorded by Ganeshram et al. (2003), the values from our study represent approximations, because the method used here is not appropriate to accurately capture the amount of

Ba that precipitates as barite crystals. In addition to this main event, other PBa:POC elevations may be related to diatom blooms. In particular, the PBa:POC peaks that occurred on 6 and 13 April were synchronous to the first elevation in the diatoms counts (Figure 17A), and that on 23 June in surface water was synchronous to the *Chaetoceros* spp. bloom (Figure 17B). The adsorption process may be similar to the mechanism described above, but lower in scale, because the recorded blooms were not as intense as the early June blooms. However, some other PBa:POC peaks (e.g., 25 May, 30 June) were not strictly aligned with a diatom peak.

Because the presence of diatoms in the water column has an impact on the temporal variation of Ba in the ecosystem, diatom are likely involved in the transport of that element to the SWI. Based on the $PBa:POC_{trap}$ data (Figure 21B), it appears that a major Ba transport event took place simultaneously with the *L. danicus* bloom. To verify this hypothesis, the $BSi:POC_{trap}$ ratio was used to assess if the main Ba transport was induced by diatoms, especially *L. danicus*. The typical Si:C value of a monospecific culture of *L. danicus* is 0.11 (Brzezinski, 1985),which roughly corresponds to the BSi:POC value measured in the sediment trap at the same time (0.08 during 1–3 June, 0.10 during 4–6 June and 0.12 during 7–9 June). This pattern suggests that the main episode of Ba transport was linked to the main *L. danicus* bloom. A second, smaller PBa transport event was detected at the beginning of May which was associated with the presence of *C. pelagica*. At this time, the BSi:POC ratio measured in the particle trap equalled 0.12, which is a ratio typical of other diatoms. Paasche (1980) reported a Si:C ratio in *C. pelagica* oscillating between 0.28 and 0.38, depending on the temperature. Nonetheless, Ba transport occurred approximately 10 days after the *C. pelagica* bloom, a lag that may be too long for Ba transport to be correlated with the occurrence of this species. Also, in early May, the *G. flaccida* bloom was initiated (Figure 17B). However, its Si:C ratio is undocumented to date. Again, these results call for a more frequent monitoring of phytoplankton abundances, because several intermediate blooms may have been missed. Nonetheless, our results suggest the presence of diatoms at the onset of the Ba transport to the SWI. This event may be more important if the other diatom species are involved, because the Ba content of cells varies among species (Fisher et al., 1991).

Our results also indicate that phytoplankton alone is insufficient to explain all peaks and differences in the PBa:POC signal between bottom and surface waters. Specifically, the PBa:POC peak measured in early June was twice as high in bottom water as in surface water and our data cannot be used to explain the underlying reason. Nevertheless, the presence of a phytoplankton species, possibly not detected with the current sampling method, may be present at the onset of the Ba enrichment in the water column. For example, coccolithophorids are phytoplankton organisms with an external calcium carbonate skeleton (see Paasche, 2001 for review) that is known to partition Ba (Langer et al., 2009). We did not detect coccolithophorids in this study, but this does not necessarily mean that there were absent. Cell counts were only measured in the surface layer, and due to the high density of the

cell skeleton, their sedimentation rate is much higher than that of other phytoplankton taxa (Young, 1994). Coccolithophorids are therefore more common in bottom waters, which may explain why the Ba peak in early June was twice as high near the seafloor than in surface water. In addition, the use of acidic Lugol's rather than neutral Lugol's, may have partially degraded the coccoliths prior to analysis, making them unidentifiable under the microscope. Finally, other organisms such as zooplankton may also have the ability to adsorb Ba onto their skeletons and cause the formation of barite crystals, e.g., acantharians (Bernstein and Byrne, 2004). Nonetheless, their presence and dynamics have never been reported or studied in the Bay of Brest.

5 CONCLUSION AND PERSPECTIVES

The present study reported high-resolution Mo and Ba content in the water column in the Bay of Brest between mid-March and mid-October 2021. We corroborated the hypothesis that Mo is linked to aggregation episodes, although our results suggest that not all aggregates transport significant amounts Mo toward the SWI. Apparently, Mo is coupled with large-sized aggregates when DO concentrations in the water column are low. Moreover, *Gymnodinium* spp. seem to be present at the onset of the changes in Mo content in the water column. Verifying this link and detecting if the bloom occurs contemporaneously with Mo enrichment in the water column requires more frequent sampling of phytoplankton cells. The enrichment of PBa and depletion of DBa was most likely associated with phytoplankton cells, especially diatoms. However, other taxa such as coccolithophorids or zooplankton (e.g., acantharians) may also influence Ba dynamics (e.g., Bernstein and Byrne, 2004; Langer et al., 2009). Further studies must therefore consider other organisms to properly interpret Ba variation in the water column. Furthermore, aggregation episodes may also be vectors facilitating the transport of Ba to the sediment , because barite crystals were found within diatom aggregates (Dehairs et al., 1980; Bishop, 1988). Understanding the processes behind the enrichment of Mo and Ba in the water column requires future monitoring surveys including other parameters, allowing comparisons between years and thus the detection of common patterns. Furthermore, aggregates should be artificially generated in the laboratory using rolling tanks to test the hypotheses raised by our results.

CHAPTER 3

TRACE ELEMENT ACCUMULATION WITHTIN PHYTOPLANKTON AGGREGATES

PREAMBLE/PRÉAMBULE

In the previous chapter, we highlighted that phytoplankton aggregates can influence the dynamics of chemical elements (especially molybdenum) in the water column. However, due to the numerous environmental parameters that could be involved in that process, it is difficult to determine the mechanisms explaining the accumulation of molybdenum in phytoplankton aggregates. In the precedent chapter, we proposed the hypothesis that the size of aggregates, combined to the concentration of oxygen in the water column, could influence the accumulation of molybdenum within aggregates. To limit the numerous biological, chemical, or physical parameters inherent in *in situ* studies, we conducted a laboratory experiment in which we produced aggregates from monospecific strains, as well as natural communities, of phytoplankton via the use of rolling tanks. These aggregates were then individually sampled, and their trace element concentrations were measured along with other parameters (size, POC, etc.). These experiments were conducted as part of the Master's thesis of Tom RAINBOW which I supervised alongside Brivaëla Moriceau. This chapter presents the results obtained during these experiments. We made the choice to conduct this study through a multi-element approach in order to obtain an overview of the relationship between phytoplankton aggregates and several elements.

Dans le chapitre précédent, nous avons vu que la formation d'agrégats phytoplanctoniques pouvaient influencer la dynamique des éléments chimiques (en particulier le molybdène) dans la colonne d'eau. Cependant, en raison des nombreux forçages environnementaux qui peuvent expliquer cela, il est difficile de déterminer précisément les processus et les mécanismes qui expliquent l'accumulation de cet élément dans ces agrégats. Dans le chapitre précédent, nous avons alors proposé l'hypothèse que leur taille, combiné à la concentration en oxygène dans la colonne d'eau, pourraient influencer les concentrations en molybdène au sein des agrégats. Afin de limiter les nombreux paramètres biologiques, chimiques ou physiques inhérents aux études *in situ*, nous avons réalisé des expérimentations en laboratoire durant lesquelles nous avons produit des agrégats à partir de cultures monospécifiques, ainsi que d'une communauté naturelle, de phytoplancton. Ces agrégats ont ensuite été échantillonnés individuellement et leurs concentrations en éléments traces ont été mesurées, ainsi que d'autres paramètres (taille, POC, etc.). Ces expériences ont été menées dans le cadre du stage de Master de Tom RAINBOW, que j'ai supervisé au côté de Brivaëla Moriceau. Ce chapitre présente alors les résultats obtenus durant ces expérimentations. Pour cette étude, nous avons choisi d'aborder cette problématique à travers une approche multi-éléments, afin d'obtenir une vue d'ensemble de la relation entre les agrégats phytoplanctoniques et plusieurs éléments chimiques.

Behaviour of trace elements in the vicinity of phytoplankton aggregates

Valentin Siebert[1], Tom Rainbow[1], Julien Thébault[1], Matthieu Waeles[1], Lukas Fröhlich[2], Bernd R. Schöne[2], Brivaëla Moriceau[1]

[1]*Univ Brest, CNRS, IRD, Ifremer, LEMAR, F-29280 Plouzané, France*

[2]*Institute of Geosciences, University of Mainz, Johann-Joachim-Becher-Weg 21, 55128 Mainz, Germany*

ABSTRACT

Phytoplankton aggregates are large particles that play a significant role in the vertical fluxes of organic matter in the ocean due to their fast sinking rates and sticking properties. When micro-algae are under stressful conditions, they tend to aggregate with each other or with other biotic or abiotic particles by excreting extracellular polysaccharides (EPS), which are known for their stickiness properties. These EPS, precursors for transparent exopolymer particles (TEP), have been suggested to be organic ligands of some trace elements or metals, and may play an important role in the accumulation of these elements in aggregates. Metals and trace elements in the environment are important due to their essential and/or toxic functions. It would therefore be interesting to study to what extent phytoplankton aggregates accumulate them, as well as the mechanisms and processes involved. The aim of this study was to compare the behaviour of a large range of elements in aggregates. Two model species were chosen (*Chaetoceros* sp. and *Rhodomonas salina*) and compare to natural community in order to unravel the processes involved in trace elements or metals interactions with aggregates. Here, aggregates were formed in the laboratory using rolling tanks and were individually sampled for various chemical (trace elements, particulate organic carbon and TEP concentrations) and structural (size) measurements. Results showed that phytoplankton aggregates significantly accumulate several elements in comparison with the surrounding water, but the accumulated ones differed across the three experiments. This suggests that different mechanisms were involved depending on the species used and the characteristics of the aggregates formed. To understand these accumulations and their differences, adsorption mechanics (size effect for example) and TEP concentrations were compared with the accumulated elements. It was found that the processes that could explain these accumulations are unique to each element. This study can serve as a basis for many other studies dealing with the impacts of aggregate formation and sedimentation on various biogeochemical cycles.

1 INTRODUCTION

The role of the biological carbon pump is becoming increasingly important as the concentration of carbon dioxide (CO_2) in the atmosphere continues to rise (Houghton, 1996). The biological carbon pump refers to the process in which CO_2 and nutrients are converted into organic carbon, which sinks into the deep ocean and decomposes at depth (Turner, 2015). This process helps to control the concentration of CO_2 in the atmosphere by exporting carbon from the surface to the deep ocean, thus limiting ocean acidification. Phytoplankton, such as diatoms, are particularly effective at transporting carbon to the depths by forming large, fast-sinking particles called aggregates (Smetacek, 1985; Turner, 2015).

When phytoplankton cells experience stress conditions, such as limited light or nutrients that occur at the end of a bloom, they tend to stick with themselves or with other biotic or abiotic particles present in the water column. This process is facilitated by the excretion of extracellular polysaccharides (EPS) by micro-algae, which are precursors to transparent exopolymer particles (TEP) (Passow and Alldredge, 1994). TEP are gels, ligands, which exist at the interface between particulate and dissolved material (Passow, 2002), that have high stickiness properties and thus act as a natural 'cement'. These compounds are crucial to the formation of most phytoplankton aggregates (Passow and Alldredge, 1994; Dam and Drapeau, 1995; Jackson, 1995; Logan et al., 1995) and can favor their sedimentation toward the seafloor. Thus, TEP also act as a 'cleaner' of the water column by gathering all categories of particles present in the environment, which enlarges the aggregate (Smetacek, 1985). These aggregates therefore alter the chemical composition of the water column and can transport both particulate and dissolved matter from the pelagic zone to the mesopelagic or benthic zone.

With their matrix made of TEP, aggregates create small, isolated 'micro-environments' with a solid interface. Their chemical and physical properties can drastically differ from the seawater (Alldredge and Cohen, 1987). For example, studies have found that the oxygen concentration can be 46% lower within aggregate than in the surrounding water, and pH levels seem to follow the same trend with losses up to ΔpH = 0.91 (Alldredge and Cohen, 1987). This difference could impact the concentration of chemical element within these large particles, specifically those that are sensitive to redox conditions. This the case for manganese (Mn) of which Mn(IV) are reduced under oxygen-limited conditions resulting in the formation of Mn(II) and thus changing their bio-availability for surrounding organisms (Majithiya et al., 2018). It has also been shown that molybdenum (Mo) can accumulate within aggregates, leading to a significant transport of this element toward the sediment (Dellwig et al., 2007; Mori et al., 2021). It was hypothesized that low oxygen concentrations within aggregates could enhance the scavenging of Mo on these particles (Dellwig et al., 2007; see chapter 2 of this manuscript). Furthermore, at lower pH value, certain trace elements and heavy metals

have shown to be altered, such as iron for which acidification enhances the amount of bioavailable Fe species (Hirose, 2011). Taking all these factors into account and as certain metals and trace elements have a high affinity for ligands (Decho, 1990), many chemical elements are likely to accumulate in these micro-environments. In coastal ecosystems, the relationships between aggregate dynamics and water column chemistry have been the object of a few investigations (Dellwig et al., 2007; chapter 2). However, the mechanisms behind metal accumulation in these micro-environments remain unclear and are still to be adressed.

Despite extensive research into the role of aggregates in carbon export, little is known about their influence on the cycling of trace elements and heavy metals, with the exception of thorium (Crocker and Passow, 1995). However, gaining knowledge in this area would be a crucial step in fully understanding the role of aggregates in ecosystems. Certain trace elements, due to their involvement in metabolic reactions and enzymatic activities, such as photosynthesis and nitrogen reduction, can significantly impact productivity and marine algal communities (Sunda, 1989). High concentrations of some metals, such as copper, can also be toxic (Sunda, 1975; Debelius et al., 2011). Aggregates may therefore increase or decrease the availability of these elements in surface and deep waters, thereby playing a significant role in ecosystems (as illustrated in Figure 25 - Jackson and Burd, 2015). Understanding the relationship between trace elements and aggregates is therefore essential.

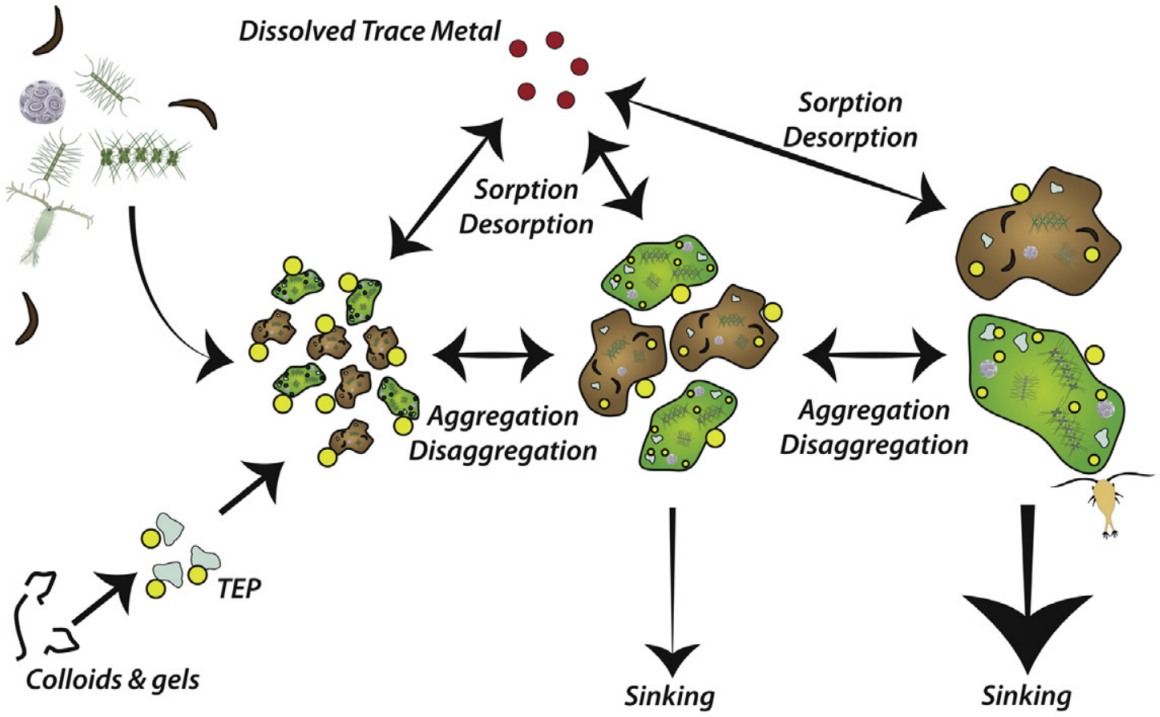

Figure 25 – Conceptual diagram of trace elements and metals behavior towards aggregates (from Jackson and Burd, 2015). Yellow dots represent dissolved trace metal (red dots) that are adsorbed on aggregates.

The invention of rolling tanks has facilitated the sampling and the study of aggregates which are formed in the laboratory in a controlled environment (e.g., Passow and De La Rocha, 2006; Moriceau et al., 2007; Long et al., 2015; Ploug et al., 2008; Laurenceau-Cornec et al., 2015). These cylindrical aquariums rotate on themesleves and increase the chance of collisions between cells, promoting the production of TEP and the subsequent aggregation. Consequently, the kinetics of aggregates can be better characterized, and various processes that could promote the formation of aggregates can be tested. However, the sampling of individual aggregate has never been done before for the purpose of analyzing and quantifying the accumulation of chemical elements within these structures. This would provide a better understanding of the mechanisms involved in the accumulation or the non-accumulation of these elements within aggregates.

Based on this assumption, the primary goal of this study was to investigate whether phytoplankton aggregates indeed accumulate metals and trace elements. To achieve this, a multi-element approach was utilized to cover the broadest possible range of information that can be extracted. The analyzed aggregates were created in the laboratory using various microalgae strains and a natural community collected *in-situ*. The trace element concentrations in the aggregates were then compared to other parameters, such as their concentration in TEP or their size, to identify the underlying process driving this accumulation.

2 MATERIAL AND METHODS

2.1 Experiments

Initation of the experiments

The experiments were carried out in climatic rooms located in the LEMAR laboratory (UMR 6539, Plouzané, France). In total, three experiments were performed in triplicate, each using a different strain of phytoplankton, in order to see whether metal accumulation is also dependent on the species forming the aggregate. For the first experiment, a diatom strain of the species *Chaetoceros* sp., a diatom, was used (CCAP 1010.3). A strain of *Rhodomonas salina* (CCMP 1319), a cryptophycae, was used in the second experiment. These monospecific strains were provided by the Argenton station (IFREMER). Finally, natural seawater was collected from Lanvéoc with a Niskin bottle on 28 March 2022 (when a bloom occurred) to form aggregates from a natural community in the third experiment. For this latter, a community analysis was performed to establish the phytoplankton assemblage. The phytoplankton community was mainly composed of *Chaetoceros* sp. (diatom - 66%), *Thalassiosira* sp. (diatom - 29%), *Skeletonema* sp. (diatom - 1%), *Gymnodinium* sp. (dinoflagellate - 1%) and other species (3%).

Each experiment were performed in triplicate in order to verify the repeatability of the results. For this purpose, three 4L flow-through rolling tanks were used in parallel, with identical initial conditions for each experiment. These tanks are a combination of a rolling tank and a flow-through reactor, which are used to control/renew their internal environment (e.g., Long et al., 2015). These 4L cylindrical tanks were connected to a peristaltic pump that renewed water at a constant flow of seawater (input/output). Flow-through rolling tanks tend to be more representative of *in-situ* conditions due to the constant renewal of the medium and the turbulence created by this flow. This technique also facilitated the sampling of the surrounding water without fragmenting the aggregates by manipuating the rolling tanks and creating turbulence.

At the beginning of each experiment, phytoplankton cultures or natural seawater were used to fill three flow-through rolling tanks. Nonetheless, because cell concentrations for the natural community are lower than for monospecific experiments, six additionnal enclosed 1 L rolling tanks (without flow) were also used, in order to increased the number of analysed aggregates (Table 4). The initial concentration of phytoplankton cells that were introduced within the tanks has been measured with a cytometer. Once they were filled with monospecific strains or natural community, the rolling tanks were placed on roller tables that maintained their rotation at a constant speed of 2 rpm. Experiments performed on flow-through rolling tanks were injected with a continuous flow of filtered (1 µm) seawater directly pumped from the bay of Brest at a constant inflow of approx. 2 L per day using a peristaltic pump, allowing a complete renewal of tanks every 48h.

Execution of the experiment

Before the aggregate formation, surrounding water was analyzed every 24 h to follow the evolution of cell concentration and chemical parameters including particulate organic carbone (POC), TEP, and trace element concentrations in the particulate fraction ($TE_{particulate}$). The methods followed to measured each chemical parameter will be provide in section 2.2. The phytoplankton cells were also counted every 24 h via the use of a cytometer (LUMINEX GUAVA EasyCyte 5HT)). This instrument counted individual particles based on to their forward scatter (FSC), their side scatter (SSC) and their fluorescence, which are related to particle size, complexity and chlorophyll content respectively. This analysis provides an insight into cell concentration within each rolling tank, allowing us to follow the aggregation process and to adjust the inputs and outputs of seawater if necessary. The principal purpose was to keep the concentration of phytoplankton cells relatively constant throughout the experiments, at least before aggregation. For the six additional enclosed roller tanks (without input/output), only an initial (T0) and final (TF) sampling of water and aggregates were undertaken (this concerns only the natural community experiment). Table 4 gathers and summarizes all the

information concerning each experiment.

Table 4 – List of the three experiments that were carried out, their characteristics and the chemical parameters that were measured in the surrounding water (SW) and in aggregates (A) at each date.

Species	Photoperiod conditions	Type of rolling tank	Initial cell count (cell.mL^{-1})	Measured parameters	Sampling
Chaetoceros sp.	12h/12h	Flow-through	C_0 = 1.18x10^5	$TE_{particulate}$ POC TEP	-T0 (28/02) : SW -T1 (01/03): SW -T2(02/03) : SW -T3(03/03) : SW -TF(04/03) SW + A
Rhodomonas salina	12/12h	Flow-through	C_0 = 4.04x10^4	$TE_{particulate}$ POC TEP	-T0 (21/03) : SW -T1 (22/03) : SW -T2 (23/03) : SW + A
Natural community	24h Light	Flow-through	C_0 = 3.03x10^2	$TE_{particulate}$ POC TEP	-T0 (28/03) : SW -T1 (29/03) : SW -T2(30/03) : SW + A -T3 (31/03) : SW + A -T4(31/03) : SW + A -TF(01/04) : SW + A
	24h Light	Enclosed	C_0 = 3.03x10^2	$TE_{particulate}$ POC TEP	-T0 (28/03) : SW -TF (30/03) : SW + A
	24h Dark	Enclosed	C_0 = 3.03x10^2	$TE_{particulate}$ POC TEP	-T0 (28/03) : SW -TF (30/03) : SW + A

Final sampling analysis

After formation of the aggregates, the rolling tanks were then stopped and placed laying sideways, allowing aggregates to settle on the bottom. Photos were taken allowing the measurements of the size of the aggregates. Aggregate size has been expressed in equivalent spherical diameter (ESD) following equation (2) and (3) (Long et al., 2015), where V is the volume of aggregates, d their diameters and h their heights (h > d).

$$V = \frac{\pi}{6} \times d^2 \times h \tag{2}$$

$$ESD = \sqrt[3]{\frac{6 \times V}{\pi}} \tag{3}$$

Secondly, surrounding water was sampled at the surface of each tanks in order to measure the final concentration of $TE_{particulate}$, POC and TEP (TF). Aggregates that were photographed were then carefully collected using a graduated burette, whilst minimizing sampling of the surrounding water and placed in a 50 mL tube. The sampled volume of each aggregates was carefully noted. Filtered seawater (0.2 µm) was then added to achieve a final volume of approx. 50 mL. This solution was then shaken vigorously in order to break and homogenize the aggregate in the medium. Finally, aggregates were analyzed for POC, TEP and $TE_{particulate}$ concentrations following the protocols described in 2.2. The full experimental protocol is summed up in Figure 26.

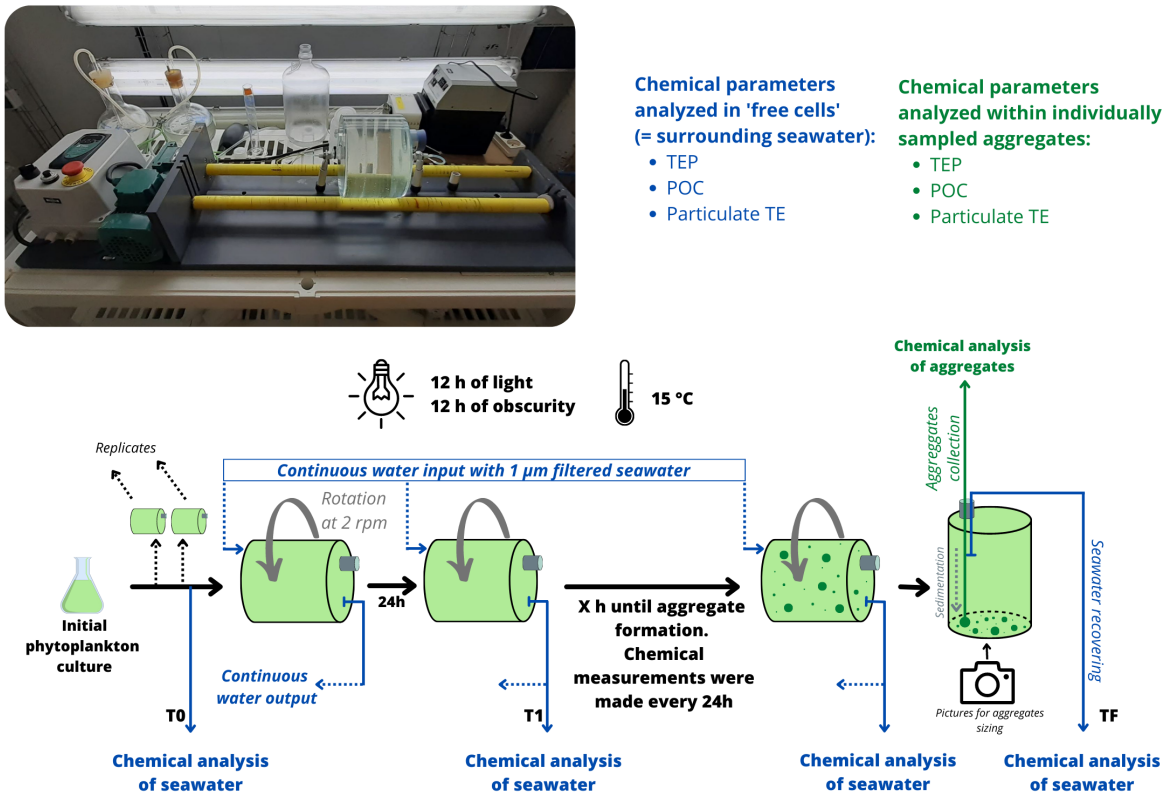

Figure 26 – Experiment design of the study. The use of enclosed tank (only for the natural community experiment) required the same protocoles but without water sampling between the initial and final time (direct passage from T0 to TF).

2.2 Chemical Analyses

Particulate organic carbon (POC) - POC is commonly used to characterize the quality and quantity of organic matter (state of decay, composition, origin, etc.). The surrounding water and aggregates were filtered through GF/F 25mm filters that were pre-conbusted for 4 hours at a temperature of 450 °C. Filters are then dried in an oven at 50°C, stored in a dark and dry place and analyzed via a CHN elemental analyzer (Themo fisher flash 2000) following the protocol established in Aminot and

Kérouel (2004). POC concentration was then used to normalize our metal concentrations in free cells and in aggregates, allowing comparison between these two compartments.

Trace elements measurements - For analysis of $TE_{particulate}$, water and aggregates were filtered through MF-Millipore™ mixed cellulose ester filters. Filters were then air-dried and stored in a dark and a dry place prior to measurements of trace elements in the particulate fraction. Before filtration, all the filters were pre-washed by soaking them for at least 24 h in a pH 1 solution made with nitric acid (HNO_3, suprapur, Merck) and ultrapure water (UP) from a Milli-Q element system. The filters were then soaked in UP and thoroughly rinsed with UP before use.
For the analysis of $TE_{particulate}$, the filters were digested at 80 °C for 3h in closed 30 mL-PTFE screw-cap vials (Savillex, Minnetonka, MN, USA) by adding 2 mL of HNO_3 65% (Suprapur, Merck, Darmstadt, Germany) and 500 µL of 30% hydrogen peroxide (Suprapur, Merck, Darmstadt, Germany). The elemental analyses of $TE_{particulate}$ were then conducted on diluted mixtures (2.3% HNO_3) with a X-series II, quadrupole inductively coupled plasma mass spectrometer (Q-ICP-MS) (Thermo Scientific) at the Pôle Spectrométrie Océan (PSO - Plouzané, France). The data were corrected for machine drift by inserting multi-element standard solutions every two samples. Here is the list of all the isotopes that were measured during this study: ^{7}Li, ^{25}Mg, ^{27}Al, ^{43}Ca, ^{51}V, ^{55}Mn, ^{56}Fe, ^{59}Co, ^{63}Cu, ^{66}Zn, ^{88}Sr, ^{95}Mo, ^{111}Cd, ^{138}Ba, ^{208}Pb.

Transparent Exopolymer Particles (TEP)

TEP analysis was done following the protocol elaborated by Bittar et al. (2018). This method consists of filtering the TEP, dyeing them with Alcian blue and finally digesting the filters onto sulfuric acid before absorbance measurement by spectrometry. Alcian blue selectively stains acidic polysaccharides by ionically binding with COOH and O-SO_3 groups, making TEP visible and enabling quantification (Bittar et al., 2018). Prior to measurements, a calibration range was created using a diluted series of a Xanthan gum solution (75 $mg.L^{-1}$) known for the same characteristics of TEP, dyeing it with alcian blue and measuring the corresponding absorbance after similar digestion. This calibration permitted us to draw the relation between absorbance and a mass of xanthan gum. This calibration curve allowed the estimation of the mass of TEP in the sample in units of mass equivalent gum xanthan (gGXeq). For each sample, 5 to 10 mL were filtered through a 0.4 µm plycarbonate filter using a hand pump and not exceeding 23 kPa. The filters were kept wet with the samples and then TEP are dyed by adding 500 µL of a Alcian blue solution (400 $\mu g.L^{-1}$) for 2-3 seconds. Afterwards, the filters are rinsed two to three times with ultra-pure water in order to assure the removal of the excess of Alcian blue. Filters were then transferred to a 15 mL Falcon Tube and can either be stored in a cold environnement (-20°C) or analyzed directly. For the analysis, 6 mL of sulfuric acid (80%) was added

to each tube, and left to agitate in a shaking water bath at room temperature for a duration between 2 and 20 hours to allow the full extraction of Alcian blue. A volume of 1-2 mL was sampled from the tubes and analyzed using a spectrometer (SECOMAM PRIM) set at 787 nm, with milli-Q water used as a blank. Absorbance was then noted, and plotted onto the calibration slope to estimate the concentration of TEP within aggregates, regarding their volume (in µgGXeq.L_{agg}^{-1}).

2.3 Data presentation

Concentrations of chemical parameters measured within individually sampled aggregates were given in concentration units per liter of filtered aggregates (taking the volume of each aggregate and the filtered volume of each sample into account). A comparison between the concentrations of elements in the aggregates and the surrounding water at TF (also refered as 'free cells') was made. To allow this comparison, the chemical element concentrations will be expressed as element-to-POC ratios. This allowed a first overview of the elements that significantly accumulate in the agregates in comparison with surrounding water. Furthermore, a comparison of the accumulation factor will then be made to determine whether larger aggregates accumulate a higher concentration of each element than smaller aggregates. To verify the adsorption hypothesis, the element-to-POC ratios of aggregates were compared with their surface-to-volume ratio. Finally, in order to determine which element is bound with these organic ligands, linear regressions between the concentration of $TE_{particulate}$ and TEP were calculated. A Wilcoxon-Mann-Whitney test with a significance level of α = 0.05 was used to compare averages and Pearson's rank correlation coefficients were calculated to verify if a correlation exists between two parameters.

3 RESULTS

The experiment that used *Chaetoceros* sp. provided 14 dense aggregates within 96 h, with an average size of approx. 0.17 cm (ESD) within the three rolling tanks. These aggregates, with ESD ranging between 0.08 and 0.54 cm (ESD), were individually sampled and analyzed for the multiple parameters quoted beforehand. TEP concentrations for *Chaetoceros* sp. varied between 3.41 and 715 gGXeq.L_{agg}^{-1}, averaging at 165 gGXeq.L_{agg}^{-1} (Figure 27) and POC concentrations were found to be between 197 and 9512 µmol.L_{agg}^{-1}, with an average of 2658 µmol.L_{agg}^{-1}.

Rhodomonas salina provided 18 larger, less dense aggregates within 48 h, with an average size of 0.46 cm over the three rolling tanks. These aggregates were sizing between 0.1 and 1.1 cm (ESD) and were sampled and analyzed. TEP concentration was lower for *R. salina*, with values between 0.4 and 28 gGXeq.L_{agg}^{-1} (Figure 27), like POC concentration with values varying between 114 and 8680 µmol.L_{agg}^{-1}, with an average of 2470 µmol.L_{agg}^{-1}.

Finally, the natural community resulted in three filamentous aggregates for the three flow-through rolling tanks. To increase the amount of analyzed aggregates for this experiment, the decision was made to incorporate the measurements made on the aggregates formed within the six additionnal enclosed rolling tanks (Table 4). From these latter, five aggregates were individually collected and analysed for their TEP, POC and $TE_{particulate}$ concentrations. In total, eight aggregates sized between 0.08 and 0.53 cm (ESD) were sampled and analyzed. Average TEP and POC concentrations were 5.94 $gGXeq.L_{agg}^{-1}$ (Figure 27), and 763 $\mu mol.L_{agg}^{-1}$, respectively, for the natural community experiment. For all the experiments, results showed that TEP concentrations decreased when aggregates became larger (Figure 27).

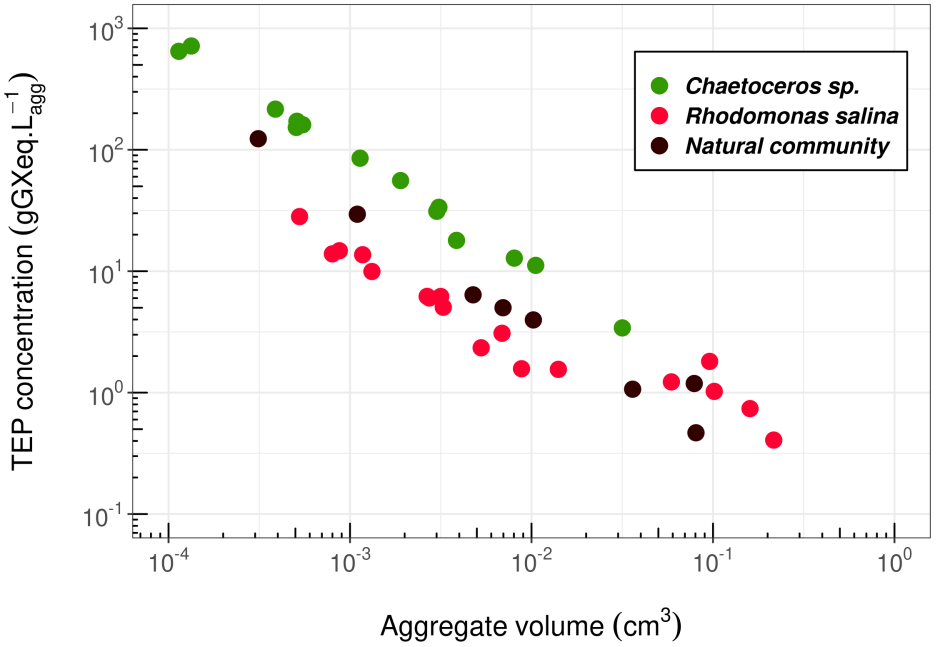

Figure 27 – TEP concentration as a function of aggregate volumes for the three experiments (in logarithmic scales).

3.1 Metal accumulation in aggregates

Elemental concentration in the 'free cells' (= surrounding water) was assessed in flow-through rolling tanks until the aggregation. Average element-to-POC ratio of the 'free cells' at TF were compared to the element-to-POC concentrations within individually sampled aggregates to visualize whether aggregate accumulate trace elements compared to freely suspended cells. As an example, particulate Cu:POC (PCu:POC) ratio measured in the 'free cells' remained globaly constant during the three experiments, despite their difference in the initial level of PCu:POC at T0. Values ranged between 0.03 and 0.4 $\mu mol.mmol^{-1}$ and between 0.01 and 0.1 $\mu mol.mmol^{-1}$ for *Chaetoceros* sp. and

R. salina, respectively. The natural community 'free cells' PCu:POC ratios slightly decreased during the experiment, and values ranged between 0.3 and 1.28 µmol.mmol^{-1} (Figure 28).

Aggregates mean PCu:POC ratio was approx. 0.90 µmol.mmol^{-1} for *Chaetoceros* sp., 0.17 µmol.mmol^{-1} for *R. salina* and 1.80 µmol.mmol^{-1} for the natural community. For the three experiments, the average PCu:POC ratios of aggregates were significantly higher, based on Wilcoxon-Mann-Whitney tests (p-value < 0.05), than in 'free cells' at TF, suggesting an accumulation of Cu within aggregates (Figure 28).

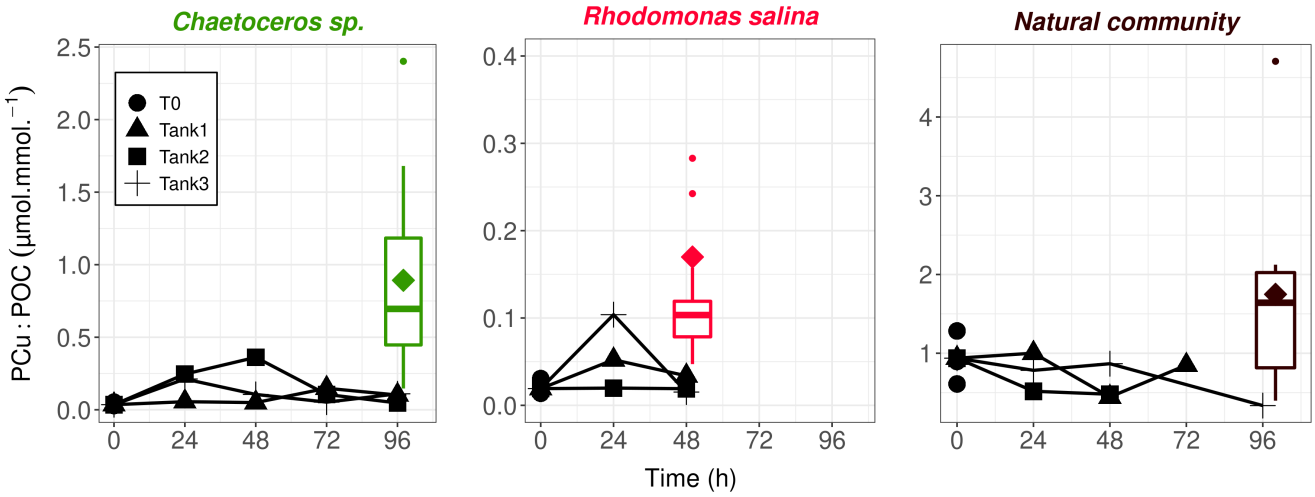

Figure 28 – Mean PCu:POC ratio measured in 'free cells' (black lines) and aggregates (boxplot) within the three tanks for each experiment. Coloured diamond represents the averaged value of PCu:POC ratio recorded in aggregates.

The list of elements that are significantly accumulated within aggregated, in comparison to the 'free cells' at TF, is given in table 5. From that table, it is important to note that only three elements are significantly enriched in all experiments, whatever the phytoplankton species that formed the aggregates: copper (Cu), zinc (Zn) and molybdenum (Mo). Moreover, *R. salina* aggregates exhibited a lower number of accumulated elements in comparison to the two other experiments.

Table 5 – List of the trace elements that are significantly accumulated within aggregates in comparison with the 'free cells' at TF (based on Wilcoxon-Mann-Whitney tests ($\alpha = 0.05$)) in the three experiments.

	Chaetoceros sp.	*Rhodomonas salina*	Natural community
Accumulated	Li, Mg, Ca, Co, Cu, Zn, Sr, Mo, Cd, Ba, Pb	V, Cu, Zn, Mo	Mg, Al, Ca, Mn, Fe, Co, Cu, Zn, Sr, Mo, Cd, Ba
Not accumulated	Al, V, Mn, Fe	Li, Mg, Ca, Sr, Al, Cd, Mn, Fe, Co, Ba, Pb	Li, V, Pb

3.2 Effect of aggregate volume on trace element accumulation

The previous table (Table 5) states that molybdenum accumulates significantly in aggregates compared to 'free cells' at TF for the three experiments. PMo:POC values within aggregates were ranging between 0.9 and 81 µmol.mol^{-1} for *Chaetoceros* sp., 0.04 and 2.56 µmol.mol^{-1} for *R. salina* and 20 and 339 µmol.mol^{-1} for the natural community (Figure 29). At the end of the experiments, the PMo:POC ratios of the 'free cells' were found to be 2, 0.4 and 26 µmol.mol^{-1} for *Chaetoceros* sp., *R. salina* and the natural community, respectively. Some aggregates exhibited PMo:POC values lower than the PMo:POC value recorded in the 'free cells' (Figure 29). This concerns only small aggregates for the *Chaetoceros* sp. and *R. salina* experiments, but also larger aggregates in the case of the natural community experiment. However, the majority of the aggregates had much higher PMo:POC values than 'free cells' at TF. By relating the PMo:POC values of these Mo-enriched aggregates to the their volumes, the same trends can be observed for the three experiments, with PMo:POC ratios that exponentially decreased as the aggregate volume increased (Figure 29).

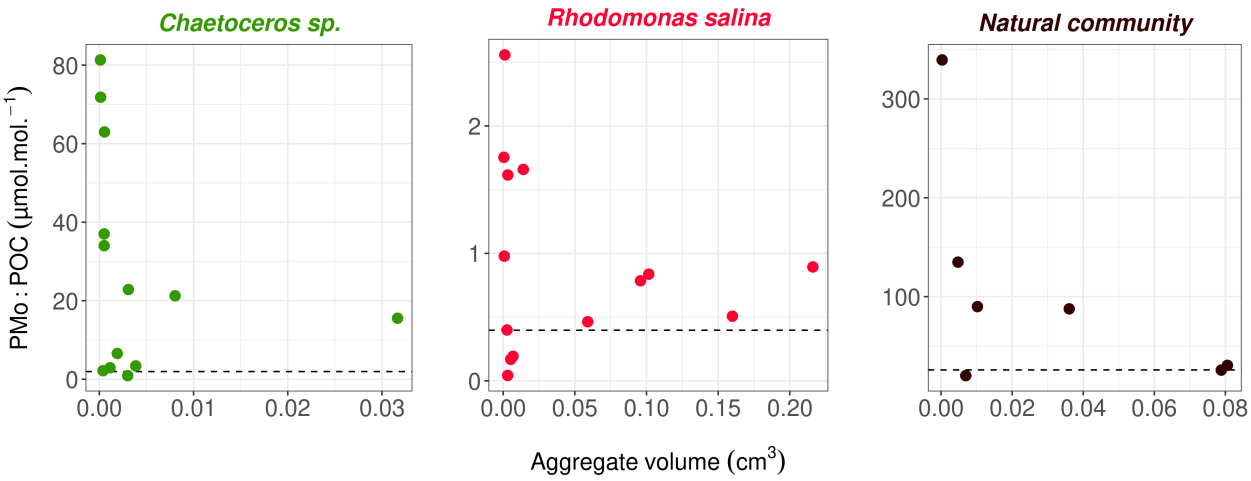

Figure 29 – PMo:POC ratios measured within aggregates samples for the three experiments (dots) in comparison to their volume. The averaged PMo:POC ratio of the 'free cells' at TF is represented by the horizontale dashed lines.

The results concerning all the elements are given in Table 6. Here, the difference between the large and the small aggregates was not based on a specific size criterion, but simply on the observed trends. If for a given element, the element-to-POC ratios between the aggregates and the 'free cells' showed similar or lower values, we simply assumed that these aggregates were not enriched with that element. For *Chaetoceros* sp. and the natural community, it can be seen that elements are mainly accumulated in smaller aggregates, since no element are enriched only in large aggregates (Table 6). Concerning *R. salina*, all four elements are accumulated in the small aggregates and only Zn is not accumulated in the large aggregates (Table 6).

Table 6 – List of the elements that are enriched within aggregates regarding their size.

	Chaetoceros sp.	*Rhodomonas salina*	Natural community
Elements accumulated in small aggregates	Li, Mg, Ca, Co, Cu, Zn, Sr, Mo, Cd, Ba, Pb	V, Cu, Zn, Mo	Mg, Al, Ca, Fe, Co, Cu, Zn, Sr, Mo, Ba
Elements accumulated in large aggregates	Li, Mg, Ca, Co, Cu, Sr	V, Mo, Cu	Al, Ca, Fe, Co, Cu, Zn, Sr, Mo, Ba

3.3 Trace element concentrations *vs* surface-to-volume ratio

Adsorption mechanisms are influenced by the particle surface in contact with the surrounding medium. To investigate if this process explains the accumulation of trace elements in the aggregates, elements-to-POC ratios were compared against the surface-to-volume ratios. However, it is important to note that adsorption alone cannot fully explain the enrichment of trace elements in aggregates, as their concentrations in 'free cells' would be the highest due to their smallest surface-to-volume ratio. For *Chaetoceros* sp., *R. salina*, and natural communities, as the surface-to-volume ratios increased from approximately 5 to 35 cm^{-1}, 2 to 16 cm^{-1}, and 3 to 26 cm^{-1}, respectively, PMo:POC ratios increased to reach values of 0.08, 0.0025, and 0.34 $\mu mol.mmol^{-1}$, respectively (Figure 30). In all experiments, the aggregates with the highest surface-to-volume ratio exhibits the highest PMo:POC ratios. Pearson's rank correlation test was conducted for all elements listed in Table 7 to examine if a correlation exists between the element-to-POC ratio and the surface-to-volume ratio of the aggregates. As an example, a correlation exists (p-value < 0.05) between PMo:POC and surface-to-volume ratio for the three experiments (coefficient correlation (cor) = 0.78 for *Chaetoceros sp.*; cor = 0.61 for *R. salina*; cor =0.70 for the natural community). However, this is not the case for all analyzed elements. On opposition, cobalt (Co) is not significantly correlated (p-value > 0.05) with surface-to-volume ratio for the *Chaetoceros* sp. (cor = 0.14) and the natural community (cor = 0.42) experiments. The three elements which significantly accumulated within aggregates in the three experiments (i.e., Cu, Mo and Zn) (5) are also correlated with the surface-to-volume ratios in the three experiments (Table 7).

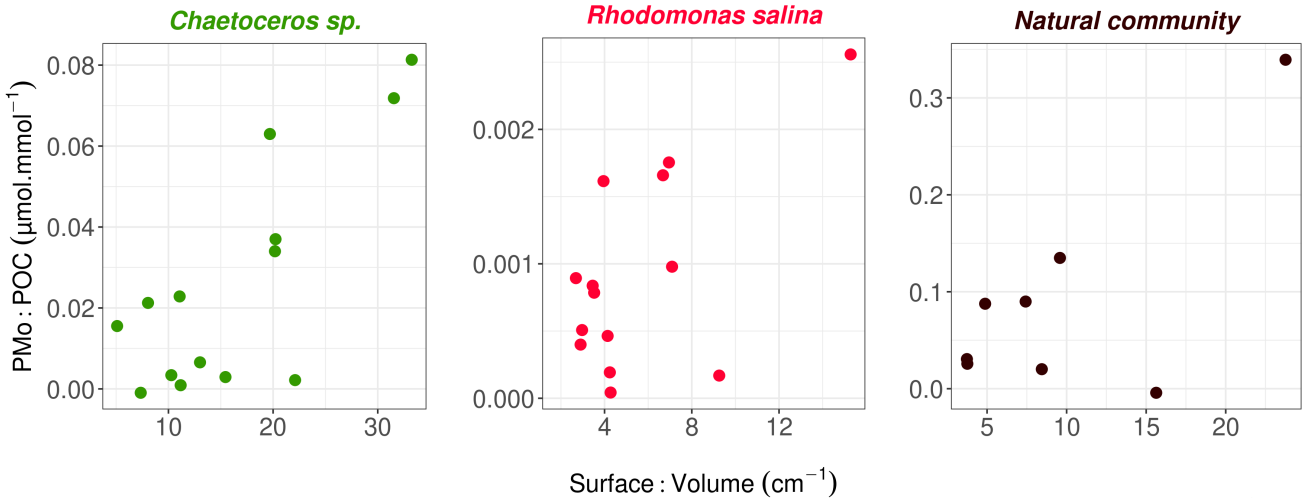

Figure 30 – PMo:POC concentration of aggregates as a function of their surface-to-volume ratios for each experiment.

Table 7 – List of the trace elements enriched in aggregates compared to freely suspended cells that are significantly correlated with exchange surface (based on Pearson's correlation (α = 0.05)) throughout all three experiments.

	Chaetoceros sp.	*Rhodomonas salina*	Natural community
Correlated	Li, Mg, Ca, Cu, Zn, Sr, Mo, Ba	Cu, Zn, Mo	Mg, Ca, Cu, Zn, Sr, Mo
Uncorrelated	Co, Cd, Pb	V	Al, Mn, Fe, Co, Cd, Ba

3.4 Trace element *vs* TEP concentrations

To test our hypothesis that TEP may also be the reasons for element accumulation, a linear regression was build between the analyzed element concentrations (in µmol.L_{agg}^{-1}) and their corresponding TEP concentrations (in gGXeq.L_{agg}^{-1}). TEP concentrations increased from a value close to 0 to 715 gGXeq.L_{agg}^{-1}, 28 gGXeq.L_{agg}^{-1}, and 125 gGXeq.L_{agg}^{-1}, for *Chaetoceros* sp., *R. salina*, and natural communities respectively (Figure 31). Particulate Mo (PMo) concentrations increased proportionally to TEP concentrations within aggregates. PMo concentration values varied between 0 and 683 µmol.L_{agg}^{-1} (for *Chaetoceros* sp.), between 0 to 13 µmol.L_{agg}^{-1} (for *R. salina*) and between 0 to 74 µmol.L_{agg}^{-1} (for the natural community). Mo concentration is shown to correlate with TEP for the three experiments, achieving R^2 up to 0.94 for *Chaetoceros* sp., 0.87 for *R. salina* and 0.93 for natural communities (Figure 31). However, it is important to note that for the natural community experiment, a lot of point are gathered close to the origine of the graph, and only one aggregates

seemed to create that slope. Each element was then submitted to a Pearson's correlation test, to see statistically if they correlate with TEP. This is how elements were sorted in Table 8. It can be seen that for the *Chaetoceros* sp. and the natural community experiments, all the accumulated element are significantly correlated with TEP concentrations. However, concerning *R. salina*, only Mo is significantly correlated with TEP (cor = 0.94) while V, Cu and Zn showed no significant correlation (cor = 0.41 for vanadium; cor = 0.31 for copper; cor = 0.37 for zinc).

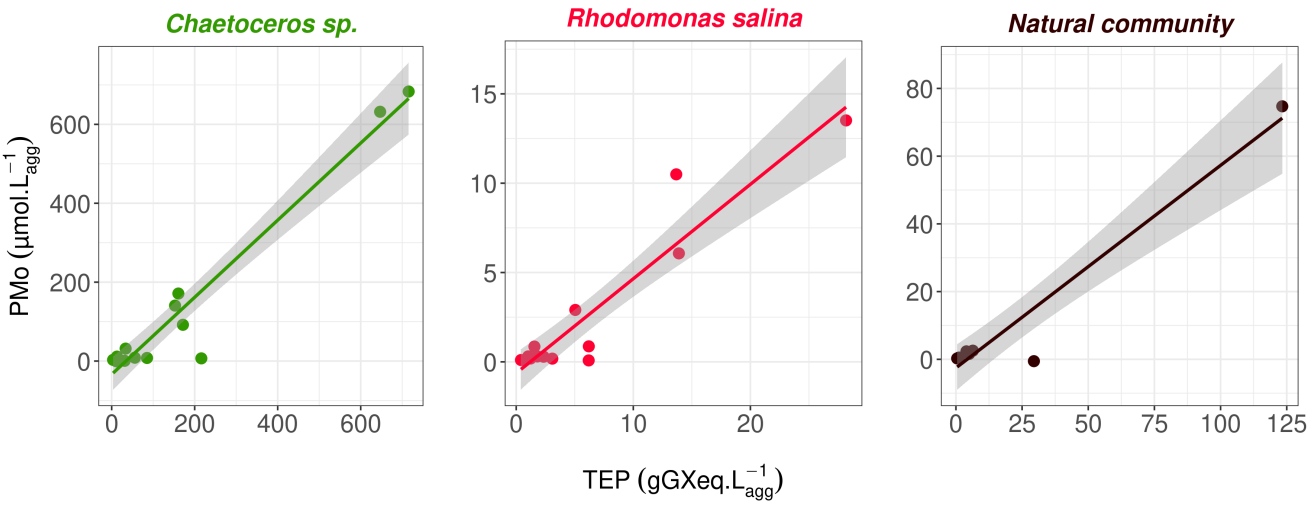

Figure 31 – Linear regression between the particulate Mo (PMo) content of aggregates and their concentrations of TEP measured for each experiment.

Table 8 – List of trace elements enriched in aggregates that are significantly correlated with TEP concentrations (based on Pearson's correlation (α = 0.05)) throughout all three experiments.

	Chaetoceros sp.	*Rhodomonas salina*	Natural community
Correlated	Li, Mg, Ca, Co, Cu, Zn, Sr, Mo, Cd, Ba, Pb	Mo	Mg, Al, Ca, Mn, Fe, Co, Cu, Zn, Sr, Mo, Cd, Ba
Uncorrelated	-	V, Cu, Zn	-

4 DISCUSSION

During this study, many samples were analyzed and numerous chemical elements were measured. It will therefore be impossible to provide a detailed discussion for each of them. This discussion will focus specifically on the mechanisms and processes that are involved and that could explain the

accumulation of certain elements within phytoplankton aggregates. In term of size, the aggregates formed here are of the same order of size as those measured by Long et al. (2015), who used the same phytoplankton strains, which validate our size measurements. To summarize, the elements that were found to accumulate within aggregates regardless their respective size were Li, Mg, Ca, Co, Cu, Zn, Sr, Mo, Cd, Ba, Pb for *Chaetoceros* sp., V, Cu, Zn, Mo for *R. salina* and Mg, Al, Ca, Fe, Co, Cu, Zn, Sr, Mo, Cd, Ba for the natural community (Table 5). However, since molybdenum was previously assumed to be linked with aggregates (see chapter 2 of this manuscript), a specific paragraph was dedicated to this elements at the end of this section.

4.1 Processes that could drive elemental accumulation in aggregates

The accumulation of metals or trace elements into larger particles can be explained by a variety of processes such as (i) assimilation, which can be either made by active biological processes or by passive diffusion, (ii) adsorption or (iii) precipitation. Assimilation is the biological absorption of certain elements used for metabolic reactions, such as photosynthesis or N_2 fixation. Some elements are essential for the growth of phytoplankton, and are essential for the survival of organisms. Assimilation can occur via a passive diffusion across biological membranes, which takes place when the concentration of an element is higher than that normally found in the natural environment (Leynaert et al., 2009). It follows a concentration gradient and involves the transport of molecules or elements from a site of higher concentration to a site of lower concentration (inside a cell for example). The adsorption of an element can be either reversible or irreversible depending on the chemical bonds involved. While reversible adsorption depends on the surrounding concentration, the irreversible enrichment will take place regardless of the concentration in the surrounding medium and the elements will persist in the particle. Its accumulation in the particle wall therefore depends on the concentration of the sites to which the metal is bonded. Finally, precipitation is the process of converting an element from a soluble to a precipitated form. Precipitation can also occured because of another element, while the first element would combine with an other one to form a less soluble compouds as is the case with Si and Al under acidic conditions (Doucet et al., 2001). For example, changes in O_2 and pH are found in aggregates as well as in sediments in comparison to seawater (Alldredge and Cohen, 1987; Ploug, 2001). Under these conditions, the chemical forms of the elements can be altered, resulting in their ability to bind differently with other elements, ligands or organic matter, creating insoluble molecules that can accumulate in the environment (Bourg & Loch, 1995).

Here, the mecanisms of assimilation and precipation were not studied since the experimental scheme followed was not intended to obtain information about them. Moreover, metal enrichment due to a higher amount of organic matter was discarded as metal concentration was corrected by POC. We

therefore hypothesized that the reasons behind these accumulations are more likely chemistry-based. Looking into this accumulation from a chemical perspective, elements binding to functional sites found on ligands, or changing form/solubility or adsorbing to larger particles could be an explanation to these observed enrichments. Given the results, the decision to class each of the elements into two main groups were made: trace elements that adsorp in link with the surface of contact of the particles and trace elements that tend to bind with organic ligands such as TEP.

Adsorption

In the present study, the first hypothesis put forward was related to adsorption, which involves the attachment of dissolved elements onto molecules. For example, certain elements, such as thorium, are known to adhere to the surfaces of large particles (Nozaki et al., 1987). Adsorption can also occur directly onto the phytoplankton cell wall. Thus, metal enrichment is assumed to be dependent on the surface area and size of particles. Our results, portrayed in table 6, indicate that element enrichment is higher towards small aggregates formed with a *Chaetoceros* sp., *R. salina* strains as well as the natural community. This can be explained by two processes: smaller particles have a higher surface-to-volume ratio, resulting in a large exchange surface available for adsorption, while larger particles have a lower surface-to-volume ratio, leading to a low exchange surface available for adsorption. The experiments showed that metal concentration correlates with the exchange surface size for several elements (Mg, Ca, Cu, Zn, Sr, Mo) in *Chaetoceros* sp. and natural communities (Table 7). However, for *R. salina*, three elements (Cu, Zn and Mo) correlate with the surface-to-volume ratio. Although adsorption could be a plausible hypothesis for certain elements, such as Cu, Zn, Mo, which accumulate in all experiments, it is not the case for some elements, such as V which did not accumulate in aggregates formed with the *Chaetoceros* sp. strain and the natural community, unlike the *R. salina* experiment (Table 5). Furthermore, even if correlation between surface-to-volume ratio and element-to-POC ratio are statistically significant, the scatter point remains rather widespread, preventing the construction of a proper linear regression. Thus, other parameters explaining this accumulation may be involved. Aggregate size has a direct influence on metal accumulation, but it also has an indirect influence through TEP concentrations, which follows a logarithmic trend when plotted against aggregate volume (Figure 27). Size may therefore influences accumulation indirectly through adsorption of trace elements on TEP.

TEP

Since some elements are known to bind to exopolymers (i.e. precursors of TEP) (Decho, 1990), a closer examination of the relationship between trace elements and TEP seems an interesting approach.

Organic ligands such as TEP have many functional groups such as rhamnose, fucose and galactose, all of which are binding sites of several elements which is the case for Cu, Ba, Sr, Ca, Ni, Zn, Mg, etc. (Güven et al., 1995). As shown on table 8, all elements have a high correlation coefficient with TEP concentrations for the *Chaetoceros* sp. and the natural community experiments. However, only Mo were significantly correlated with TEP in the *R. salina* aggregates. For example, Sr, Mo, Li and Mg exhibit a correlation coefficient with TEP, with a R^2 higher than 0.85 for each experiment. The high stickiness of TEP is due to the sulfate ester groups (Zhou et al., 1998), which give them the ability to form cation bridges (Kloareg & Quatrano, 1988) and hydrogen bonds (Mopper et al., 1995; Chin et al., 1998), which may also explain the relationship with some elements. The high cohesion of TEP strongly contributes to the formation of aggregates, allowing increased collisions with all surrounding particles, including metals. However, metal binding to TEP has been shown to reduce stickiness (Mari & Robert, 2008). The TEP concentration decreases significantly as the aggregate volume increases, which could mean that the smaller aggregates have a higher concentration of TEP. Therefore, the high binding capacity of small aggregates with other particles, unlike large aggregates which present lower binding capacity, may explains the lower enrichment in larger aggregates. For *R. salina*, the TEP concentrations were significantly lower than those of *Chaetoceros* sp. (Figure 27), and only Mo was found to be correlated with TEP. One interesting aspect to consider is how metal binding to TEP differs between species. For example, in the case of Zn, it has a correlation coefficient of $R^2 = 0.87$ for *Chaetoceros* sp. and 0.99 for the natural community, whereas for *R.salina*, $R^2 = 0.08$. This difference may be due to the fact that TEP composition varies depending on the species and physiological status of the phytoplankton releasing TEP precursors (Myklestad, 1995). The chemical structures of the EPS are often species-specific (Aluwihare & Repeta, 1999), and changes in TEP functional sites between species could explain the differences in metal binding (Güven et al., 1995). Studies have shown that the main composition of Cryptophytes EPS is fucose, mannose and N-acetyl glucosamine (Giroldo et al., 2005), whereas for diatoms it's rhamnose, fucose, and galactose. Zinc has been shown to bind with polysaccharides (Baldrian et al., 2005), notably MFP4P, a polysaccharide composed of arabinose, rhamnose, and galactose (Wang et al., 2019). Two of these are found in diatom's TEP and not in cryptophytes, explaining why zinc accumulates in *Chaetoceros* sp. and natural community (mainly composed with *Chaetoceros* sp. cells) aggregates, and not in *R. salina*.

The analysis of TEP described in section 2.2 was only performed using a semi-quantitative analysis in gum xanthan equivalent to determine correlation. However, this analysis does not indicate the precise composition of TEP nor which ligands are present and which ones are bonded to metals or trace elements. Therefore, it can be concluded that metal accumulation depends not only on TEP concentrations but also on TEP composition, which is determined by the composition of their precursors (EPS). Due to TEP high correlation with the analyzed elements for the *Chaetoceros* sp. and the

natural community experiments, they are believed to be the primary reason for elemental accumulation for Li, Mg, Ca, Co, Cu, Zn, Sr, Mo, Cd, Ba, Pb in diatom aggregates. Additionally, TEP could represent the main route for trace elements and metals in the pelagic marine food web (Grossart et al., 1998; Ling & Alldredge, 2003; Mari & Rassoulzadegan, 2004; Passow & Alldredge, 1999) and play a significant role in the vertical export of trace elements.

Other parameters

For the *R. salina* experiment, certain elements do not correlate with either the exchange surface or TEP concentration, which is the case for vanadium, prompting us to conduct a literature review to understand how chemical element behave towards organic matter and under different oxic conditions. Some elements have been found to bind to specific organic compounds within phytoplankton. For instance, aluminum has been shown to bind to the cell walls (frustules) of marine diatoms (Beck et al., 2002), which could explain its accumulation in the natural community and not in *R. salina* (Table 5). The frustule is a distinct characteristic of the diatom group, which is an envelop made of siliceous material. Lithium and baryum are also known to be adsorbed on diatom frustules (Dehairs et al., 1980; Coplen et al., 2002), potentially explaining the accumulation in *Chaetoceros* sp. and the natural community experiments but not in non-silicifying species like *R. salina*. The results showed different behaviors from Al and Li across the three experiments, suggesting that frustule adsorption alone cannot explain accumulation in aggregates mainly composed with diatoms. Further analysis of biogenic silicat (BSi) would therefore be necessary to better understand the role of diatom frustule on the accumulation of Al, Li, Ba or other elements. For this purpose, several diatoms strains, with cell that exhibit different size or shape should be used and compared, in order to better understand this phenomenon.

Other elements such as vanadium and molybdenum are highly sensitive to redox conditions and can precipitate. The fate of molybdenum in the water column is not only dependent on its redox state, but also influenced by the availability and supply of organic matter/ligands. Our results showed that molybdenum accumulation can be explained by the TEP concentrations, suggesting a relationship between Mo and TEP. To fully understand which elements accumulate due to ligands, adsorption, or redox conditions, further experiments are needed to test the real impact of oxygen conditions and pH levels of aggregates, which were note done here.

4.2 Implications for natural ecosystems

Aggregates as factors of metal vertical transport

The vertical flux of particle-reactive elements is strongly influenced by sinking biogenic debris (Collier & Edmond, 1984), such as aggregates. As shown on table 5, most of the analyzed element accumulate in aggregates, meaning that the dissolved pool in surface waters could decrease, while deeper water concentrations could increase. Taking this into account, metal limitations in the euphotic zone of the ocean can be linked to the formations of aggregates. In approximately 50% of the ocean, iron (Fe) limits phytoplankton growth (Lelong et al., 2013). In the cultures of microalgae (*Chaetoceros* sp. and *R. salina*), iron did not accumulate within monospecific aggregates. However, iron did accumulate for the natural community's aggregates (Table 5). Interpretation became therefore complex, and the limitation of iron in natural sea waters may be accentuated by *in-situ* aggregate formation. However, it should be noted that artificially formed aggregates from a monospecific strain of microalgae are markedly different from those formed from seawater collected in the environment. This is mainly due to the presence of other micro-particles such as mineral particles, feces, or bacteria that accompagnied phytoplankton cells taken from the water column and introduced into the roller tank (which is not the case for sterile monospecific strains). Such heterogeneity can significantly impact the chemistry of the aggregates and may account for the observed differences in some element behaviors between aggregates from the natural community and those formed from *Chaetoceros* sp. and *R. salina*. In the case of Fe, further studies, involving other phytoplankton species, would therefore be necessary to understand the role of aggregates on its bioavailability in the ecosystems.

Other elements, such as Cu, which has been shown to accumulate in aggregates for the three experiments, are known to have an essential/toxic behavior depending on their concentrations (Maldonado et al., 2006; Debelius et al., 2011; Richon and Tagliabue, 2019). With the presence of aggregates, dissolved Cu concentrations found in surface waters could drop below the concentrations necessary to maintain a healthy ecosystem. On the contrary, as Cu at high concentrations can be toxic (Debelius et al., 2011; Suratno et al., 2015), a loss of this dissolved pool may be beneficial to surface waters but detrimental to ecosystems found in deeper waters, where aggregates fragment. High concentrations of trace elements, including many essential elements, can cause toxic effects (Rainbow, 2007). Elements such as mercury, which is also known for its toxicity (Rice et al., 2014), would be interesting to analyze to understand if aggregates can serve as accumulators and "detoxify" surface waters. As aggregates have a higher sinking rate than free cells, elements found to accumulate in aggregates can reach the ocean floor at a faster rate, such as what have been hypothesized for microplastics from the results obtained in similar experiments (Long et al., 2015). The transport of these metals throughout the water also depends on the loss rates during their descent (Fisher & Wente, 1993).

Aggregates as a food source

Marine snow has been demonstrated to serve as a food source for various species of zooplankton, crustaceans, and fish (e.g., Lampitt et al., 1993; Toullec et al., 2019; Toullec et al., 2021). When animals consume this matrix, they will also consume adsorbed/absorbed trace elements and organic compounds coincidentally while they feed on sediments, cells, or flocs. EPS have proven to be an effective trophic-transfer vehicle for adsorbed metals in amphipods (Schlekat et al., 1998, 2000; Selck et al., 1999). Concentrations of trace elements in various animal tissues can affect their survival by altering functions such as metabolism, immune response, and ability to respond to sensory cues (Bennett et al., 2001; Lal Shah, 2010; Williams et al., 2016). From a biological perspective, understanding the importance of aggregates as potential sources of metals would require studies on the chemical form of metals present in the aggregates. Depending on their form in the water column or within the aggregate, metals could be bioavailable to organisms. However, bioavailable metals, whether essential or toxic, could have positive or negative effects on consumers. Organisms such as the great scallops, *Pecten maximus*, tend to accumulate some elements in their tissues and incorporate them into their shells (e.g., Metian et al., 2008b; Metian et al., 2009). If aggregates export metals and trace elements in high concentrations, traces of their formation and sinking could be detected in their shells. This is the assumption followed by the sclerochronologist community, that used molybdenum incorporated into scallops shells to track aggregation events (e.g., Barats et al., 2009; Thébault et al., 2009; Fröhlich et al., 2022a; Thébault et al., 2022).

4.3 The case of molybdenum

Molybdenum is an element that is sensitive to redox reactions and has been extensively studied (Smrzka et al., 2019). Previous investigations suggested that molybdenum might be more abundant in phytoplankton aggregates (Dellwig et al., 2007; Mori et al., 2021). Dellwig et al. (2007) also observed that the formation of oxygen-depleted aggregates, which favor the fixation and the accumulation of Mo, could also be at the origin of a release of Mn by chemical or biological processes. This trend can be observed here, since Mo is accumulated in all aggregates formed whatever the phytoplankton strain, while Mn was an element that was almost never accumulated, with the exception of the natural community experiment (Table 5). However, this latter experiment suffered from a low number of analyzed aggregates. To overcome this issue, using a plankton net for sampling, rather than a simple Niskin bottle, would allow higher initial cell concentrations and thus form a greater amount of aggregates. Furthermore, due to external constraints, the six additionnal rolling tanks were placed in different light conditions, which could have impacted the oxygen concentrations in the aggregates, and thus biased these results.

Recently, Siebert et al., (2023 - see chapter 2 of this manuscript) observed the same trend in Mo enrichment within *in situ* aggregates in the Bay of Brest (France). During a year when multiple aggregation events occurred, it became evident that not all aggregates accumulated molybdenum in the same way as the transport of this element to the seafloor was not always associated to an aggregation episode. This latter assumption was also visible here, since some aggregates (which represented a minority) were not enriched with Mo in comparison to the 'free cells' (Figure 29). However, Siebert et al., (2023 - see chapter 2 of this manuscript) suggested that only large aggregates with low internal oxygen concentrations were responsible for Mo downwards transport. Contrarily, the results of this study do not support this hypothesis, as small aggregates (< 0.17 cm (ESD)) of both *Chaetoceros* sp. and natural communities were found to be more enriched than large ones (Figure 29). This difference in enrichment could be due to the wider size range of the aggregates formed in the environment (0.5-26 mm (ESD)) compared to those formed in rolling tanks (0.8-5 mm (ESD)). In comparison, aggregates formed in the rolling tank are on the whole smaller than those found in nature. Aggregates that were refered as "large" in this study may be considered as "small" in the environment (chapter 2 of this manuscript). Finding a valid threshold size value would thus make it possible to better classify aggregates according to their size. This could have been done by establishing size classes (e.g., Laurenceau-Cornec et al., 2015), but this was relatively complicated to apply in our study due to the small number of aggregates that were sampled. The main limitation of this study is that the oxygen concentrations in each aggregate were not measured. It would have been interesting to have access to this parameter, in order to verify our hypotheses. Differences in aggregate morphological caracteristics may also impact the behavior of elements that bind to them. Aggregates formed from monospecific cultures tend to be very compact and dense, while those observed in nature are more elongated, less dense, and contain a more visible organic matrix, which increases the contact surface with surrounding water. This study has shown that Mo is strongly bound to transparent exopolymer particles (Figure 31), suggesting that TEP may be the main vector of Mo accumulation within aggregates. Unfortunately, Siebert et al. (2023 - see chapter 2 of this manuscript) did not measure TEP concentration in the environment, which could have helped refine this hypothesis. In order to compare the Mo accumulation within marine snow, the sampling and analysis of individual aggregates from a natural ecosystems may provide new insights. However, this remains a complicated task, given the fragility of aggregates and their tendency to collapse when exposed to turbulence. Developing a sampling scheme would therefore be necessary for this purpose. Other factors may also play a role, such as the concentration of oxygen within the aggregates, which was not measured in this study. Using microelectrode, as it was done in previous reports (e.g., Alldredge and Cohen, 1987), it could help refine hypotheses about the processes driving the accumulation of molybdenum and other redox-sensitive elements within the aggregates.

5 CONCLUSION AND PERSPECTIVES

The main objective of this study was to identify which trace elements accumulate in aggregates and to start to unravel the mechanisms involved. Our study proved that most elements accumulated within *Chaetoceros* sp. aggregates, whereas only a few accumulated in *Rhodomonas salina*. Metal accumulations is therefore related to the phytoplankton species. Nonetheless, some elements, such as Mo, Zn and Cu, significantly accumulated in the three experiments, suggesting that their enrichment might be due to the aggregation process and is independent of the species. These elements might therefore be proxies for aggregation events. In order to confirm this assumption, renew that type of experiment by using other species would be interesting. Most trace elements accumulate proportionnaly to the TEP content of the aggregate, highlighting the fact that most of the aggregate matrix, especially when diatoms are dominant, may bound to metals. TEP composition varies between species, and each one has different functional groups that allow trace elements to attach to them or not, explaining the diffeences observed. The second hypothesis was simple adsorption on cell wall, a phenomenon that has been widely studied in numerous domains. Both of these assumptions were shown to be true for the majority of the studied elements.

This study answers some questions but raises even more, such as (i) why accumulation seems to affect diatoms more than cryptophycae (presence of a frustule, TEP composition)? (ii) how oxygen levels affect metal accumulation? or (iii) what would be the impacts of more toxic elements such as mercury, chromium, or arsenic? More experiments are needed to fully understand the relationship between trace elements and aggregates, including experiments using other taxa such as dinoflagellate (an other important group of phytoplankton) with different light conditions or testing oxygen and pH levels inside aggregates via the use of a microelectrode. Analyzing the TEP composition could also provide a clearer insight into which functional groups are present (depending on the species) and which elements are likely to bind to them. Enhancing our knowledge on the relationship between aggregates and trace elements remains an important issue due to the intensification of human activities. Via the formation of aggregates that accumulate several trace elements as well as metals (toxic or not) and their sedimentation, these activities would impact not only surface waters but also the ocean seafloors.

CHAPTER 4

SHELLS FROM THE HIPPO MONITORING - CALIBRATION OF PROXIES

PREAMBLE/PRÉAMBULE

The previous two chapters of this manuscript have enhanced our comprehension of how phytoplankton dynamics (i.e., seasonal variations in phytoplankton assemblages and/or formation of aggregates) can influence the bioavailability and the transport of diverse trace elements to the seafloor. It is now time to investigate how *P. maximus* specimens, which lived on the sediment, incorprated these elements within their calcitic structures in response to these dynamics. Therefore, this chapter presents the analysis of *P. maximus* shells collected at the end of the HIPPO environmental monitoring which was introduced in chapter 1. The previously proposed hypotheses have enabled us to gain better insights into the trace element profiles (Li/Ca, Mo/Ca, Ba/Ca) recorded in these shells. In addition, the impact of sediment on the incoropration of these elements was also studied. This, in turn, allowed us to calibrate the different tracers with the ultimate aim of applying the acquired knowledge to older shells that developed in past environments, of which biological, chemical, and physical parameters remain unknown. Similar to chapter 2, this chapter is scientific article that were mainly written by Lukas Fröhlich which were recently submitted in *Limnology and Oceanography*.

Les deux précédents chapitres de ce manuscrit ont permis de mieux comprendre comment les dynamiques phytoplanctoniques dans la colonne d'eau (à savoir les variations saisonnières des assemblages phytoplanctoniques et/ou la formation d'agrégats), peuvent influencer la biodisponibilité et le transport des différents éléments traces vers le sédiment. Il est maintenant temps d'examiner comment les coquilles Saint-Jacques intègrent ces différents éléments dans leurs structures calcaires en réponse à ces dynamiques. Ce chapitre présente donc l'étude des coquilles de *Pecten maximus* collectées dans le cadre du suivi environnementale HIPPO, que nous avons présentée dans le chapitre 1. Les hypothèses avancées précédemment ont alors permis d'obtenir une meilleure compréhension des profils en éléments traces (Li/Ca, Mo/Ca, Ba/Ca) mesurés au sein de ces coquilles. De plus, l'impact du sédiment sur l'incorporation de ces éléments a également été étudié. Nous avons ainsi pu calibrer les différents traceurs avec pour objectif final d'appliquer les connaissances acquises ici à des coquilles plus anciennes, qui se sont développées dans des paléoenvironnements dont les paramètres biologiques, chimiques et physiques nous sont aujourd'hui inconnus. De la même manière que le chapitre 2, ce chapitre correspond à un article scientifique, écrit principalement par Lukas Fröhlich, et qui a récemment été soumis dans le journal *Limnology and Oceanography*.

Uptake of barium, molybdenum and lithium and incorporation into the shell of *Pecten maximus*: refining proxies for primary production dynamics

Lukas Fröhlich[1], Valentin Siebert[2], Qian Huang[1], Julien Thébault[2], Brivaëla Moriceau[2], Klaus Peter Jochum[3], Bernd R. Schöne[1]

[1]*Institute of Geosciences, University of Mainz, Johann-Joachim-Becher-Weg 21, 55128 Mainz, Germany*

[2]*Univ Brest, CNRS, IRD, Ifremer, LEMAR, F-29280 Plouzané, France*

[3]*Climate Geochemistry Department, Max Planck Institute for Chemistry, Mainz, Germany*

ABSTRACT

Ba/Ca_{shell}, Mo/Ca_{shell} and Li/Ca_{shell} chronologies of *Pecten maximus* can provide information on past phytoplankton dynamics. Distinct Ba, Mo and Li peaks in the shells are associated with algal blooms. This study evaluated the underlying hypothesis that respective element profiles are mainly controlled by processes occurring in the water column rather than at the sediment-water-interface (SWI). Therefore, the chemical content of scallops from the Bay of Brest, France, that lived on the sediment surface was compared to conspecific specimens living in a cage above the SWI, and contextualized with the phytoplankton abundance and the physicochemical properties of the water column. As demonstrated, Ba/Ca_{shell} and Mo/Ca_{shell} peaks occurred contemporaneously in specimens within the cage and on the sediment, but were higher in the latter. Furthermore, element/Ca peaks agreed with the timing of particulate Ba and Mo enrichments in the seawater. These data support the assumption of a dietary uptake of both elements. Differences in peaks heights between cage and sediment shells were controlled by rates of filtration and biomineralization. While the timing and magnitude of Ba/Ca_{shell} peaks was linked to Ba-containing diatoms, Mo/Ca_{shell} peaks were related to blooms of a Mo-enriched dinoflagellate and diatom aggregation events. Two episodes of slight Li enrichment occurred synchronously in cage and sediment shells. Although the exact mechanism causing such Li increases remains unresolved, the findings suggest a link to large diatom blooms or presence of a specific diatom taxon. This study refines previously hypothesized relationships between trace element enrichments in scallop shells and phytoplankton dynamics.

1 INTRODUCTION

The health of aquatic ecosystems is strongly influenced by phytoplankton. Besides playing an important role in oxygen production and atmospheric CO_2 sequestration (Field et al., 1998; Westberry et al., 2008), phytoplankton also impacts marine food webs (e.g., Turner and Tester, 1997). Increasing surface water temperature (Winder and Sommer, 2012), ocean acidification (Iglesias-Rodriguez et al., 2008; Wu et al., 2014) and imbalanced levels of nutrients caused by inputs of anthropogenic pollutants and artificial fertilizers (Vitousek et al., 1997) can affect the phytoplankton species abundance and community structure. Nearshore areas that provide the habitat for many organisms and serve as valuable sites for human activities (e.g., Worm et al., 2006; Barbier et al., 2011) are particularly vulnerable to eutrophication-induced changes of the phytoplankton species composition. For example, the transition from a phytoplankton community dominated by diatoms to such largely dominated by non-siliceous species such as dinoflagellates (e.g., Wasmund et al., 2017; Spilling et al., 2018) can lead to an increase in harmful algal blooms (Hallegraeff, 1993; Lewitus et al., 2012). To evaluate future trends in phytoplankton community structures, it is crucial to understand the pre-industrial phytoplankton dynamics, i.e., prior to enhanced anthropogenic forcings. Such an approach requires temporally well-constrained archives, e.g., shells of bivalve mollusks, that reliably record ephemeral variations in phytoplankton species dynamics.

Bivalves record paleoenvironmental information in their shells at high temporal resolution, specifically in the form of geochemical properties including stable isotopes (e.g., Schöne et al., 2003; McConnaughey and Gillikin, 2008; Huang et al., 2023) as well s well as trace and minor elements (e.g., Vander Putten et al., 2000; Thébault et al., 2009; Marali et al., 2017; Zhao et al., 2017; Schöne et al., 2021). Daily, fortnightly and annual growth increments and lines (e.g., Chauvaud et al., 1998; Clark, 2005; Peharda et al., 2021), can be used to temporally contextualize these geochemical properties. Temporally constrained barium-to-calcium ratios in shells (Ba/Ca_{shell}) of different bivalve species, e.g., *Arctica islandica*, *Mytilus edulis*, *Callista chione*, *Mercenaria mercenaria*, *Comptopallium radula* and *Pecten maximus*, were identified as proxies for phytoplankton dynamics (e.g., Stecher et al., 1996; Gillikin et al., 2006; Barats et al., 2009; Thébault et al., 2009; Markulin et al., 2019; Doré et al., 2020; Poitevin et al., 2022). Respective time-series were characterized by a low background that was interrupted by sharp, erratic peaks. Notably, Ba/Ca_{shell} peaks occurred highly synchronously among specimens growing at the same locality and time (e.g., Gillikin et al., 2008; Barats et al., 2009; Thébault et al., 2009). Whereas Ba/Ca_{shell} peaks typically correlate only weakly with chlorophyll a concentration (e.g., Gillikin et al., 2008; Fröhlich et al., 2022a; Schöne et al., 2023), they seem to be strongly linked to blooms of specific phytoplankton taxa, especially diatoms containing species-specific loads of cellular Ba (e.g., Riley and Roth, 1971; Fisher et al., 1991; Sternberg et

al., 2005). Furthermore, profiles of molybdenum-to-calcium ratios (Mo/Ca) and lithium-to-calcium ratios (Li/Ca) in scallop shells exhibited similar patterns as Ba/Ca_{shell}, i.e., a low background level interrupted by sharp peaks, and were likewise associated with phytoplankton dynamics (Thébault et al., 2009; Barats et al., 2010; Thébault & Chauvaud, 2013; Thébault et al., 2022). However, the underlying mechanisms leading to the formation of Mo/Ca_{shell} and Li/Ca_{shell} peaks differed notably from that of Ba/Ca_{shell} peaks. An enhanced dietary uptake of Mo by *P. maximus* (Barats et al., 2010; Tabouret et al., 2012) seems to be related to the ingestion of small Mo-enriched aggregates of phytoplankton cells (Thébault et al., 2022) and specific dinoflagellates with a high load of cellular Mo (Fröhlich et al., 2022b). The timing of Li/Ca_{shell} peaks in shells of *P. maximus* suggested a relationship to blooms of diatoms adsorbing Li from the water column (Thébault & Chauvaud, 2013; Thébault et al., 2022). Thus, Ba/Ca_{shell}, Mo/Ca_{shell} and Li/Ca_{shell} profiles of scallops seem to serve as highly valuable sclerochronological tools to derive information about past phytoplankton dynamics. However, despite an increasing number of implications for a trophic uptake of Ba, Mo and Li, uncertainties remain to what extent the complex dynamics of phytoplankton contribute to the shell geochemistry and which pathways (uptake of these elements, transport within the body and incorporation into the shell) are involved. For instance, the large variation of cellular Ba reported in various marine phytoplankton taxa (e.g., Fisher et al., 1991; Masuzawa et al., 1999; Lobus et al., 2021) makes it difficult to precisely attribute Ba/Ca_{shell} peaks to the presence of specific phytoplankton taxa. Furthermore, it remains unresolved if phytoplankton aggregations episodes and/or dinoflagellate blooms can sufficiently explain the formation of Mo/Ca_{shell} peaks (Fröhlich et al., 2022b; Thébault et al., 2022). In order to use Ba/Ca_{shell}, Mo/Ca_{shell} and Li/Ca_{shell} as qualitative and quantitative proxies for phytoplankton dynamics, more detailed information is required on the elemental uptake and shell incorporation, which control the formation of peaks in the trace element-to-calcium profiles.

This study combines highly resolved time-series of Ba/Ca_{shell}, Mo/Ca_{shell} and Li/Ca_{shell} measured in contemporaneous *P. maximus* specimens (Bay of Brest, France) with detailed environmental monitoring data (Siebert et al., 2023), aiming to verify and refine proposed hypotheses about the uptake of Ba, Mo and Li from the ambient environment into the shells. By comparing element chemical properties of scallops that thrived naturally on the sediment surface to such of specimens that lived inside a cage deployed above the seafloor, the underlying assumption was tested that the main sources for Ba, Mo and Li originate from the water column, i.e., related to phytoplankton, rather than from the sediment (e.g., trace element-enriched pore waters or microphytobenthos) (Thébault and Chauvaud, 2013; Thébault et al., 2022). Geochemical data from the two settings (sediment floor and cage) were also contextualized with the physicochemical properties of the ambient seawater and the prevailing phytoplankton dynamics. Together with specimen-specific physiological parameters, i.e., growth rate, shell height and approximated filtration rate, the molar element-to-calcium ratios were used to

deduce absolute concentrations of trace elements that were potentially taken up by the scallops, aiming to quantitatively evaluate if the proposed uptake mechanisms provide sufficient quantities of trace elements to explain their enrichment in the shells. Results of this study can increase the understanding of how Ba/Ca_{shell}, Mo/Ca_{shell} and Li/Ca_{shell} of *P. maximus* respond to variations in the ambient environment and facilitate the use of the shells as archives for past phytoplankton dynamics.

2 MATERIAL AND METHODS

2.1 Study locality, shell collection and experimental setup

In October 2021, living specimens of *P. maximus* were collected by SCUBA divers in the southern part of the Bay of Brest (Pointe de Lanvéoc, 48°17'39"N, 004°27'12"W [WGS84]), a shallow and semi-enclosed coastal ecosystem in northwestern France (Figure 32A). Six specimens were collected from their natural habitat, i.e., the sediment (at approx. 8 m below sea surface; hereafter referred to as 'sediment shells'), and six specimens were retrieved from cages (hereafter referred to as 'cage shells') positioned about 1 m above the sediment-water interface (SWI) (see Supplementary Table S1). These large-meshed (ca. 0.5 cm mesh size) cages (60×80×25 cm) were deployed on 22 February 2021 and juvenile scallops (obtained from the Tinduff hatchery in Plougastel-Daoulas, France, with a shell height between 2.5 and 3 cm) placed inside (30 scallops per cage). All specimens used in this study have encountered one winter (age class 1) and therefore showed one prominent winter growth line on the outer shell surface (Figure 32). *P. maximus* precipitate most of the shell carbonate during the second year of life. The respective shell portion therefore provides the highest temporal resolution for sclerochronological analyses. After collection, the bivalves were dissected, eviscerated and epibionts gently removed with a nylon brush. For shell growth pattern and element chemical analyses, only the left (flat) valves were utilized, because these valves show the most distinct daily growth patterns (increments and lines, aka 'striae'; Chauvaud et al., 1998). In all cage specimens, shell portions representing the beginning of the growing period, i.e., March/April, were infested by epibionts leading to difficulties in the identification of individual growth increments and in-situ element analyses. Accordingly, only shell portions without epibionts were used in this study.

2.2 LA-ICP-MS analysis

The *P. maximus* shells were measured for their Ba, Mo and Li (^{137}Ba, ^{97}Mo and ^{7}Li as analytes) content by means of a Laser Ablation – Inductively Coupled Plasma – Mass Spectrometry (LA-ICP-MS) system (Max Planck Institute for Chemistry in Mainz, Germany). To fit the shell samples into the ablation chamber of the laser system, a ca. 5 mm broad slab was cut from the left valves along

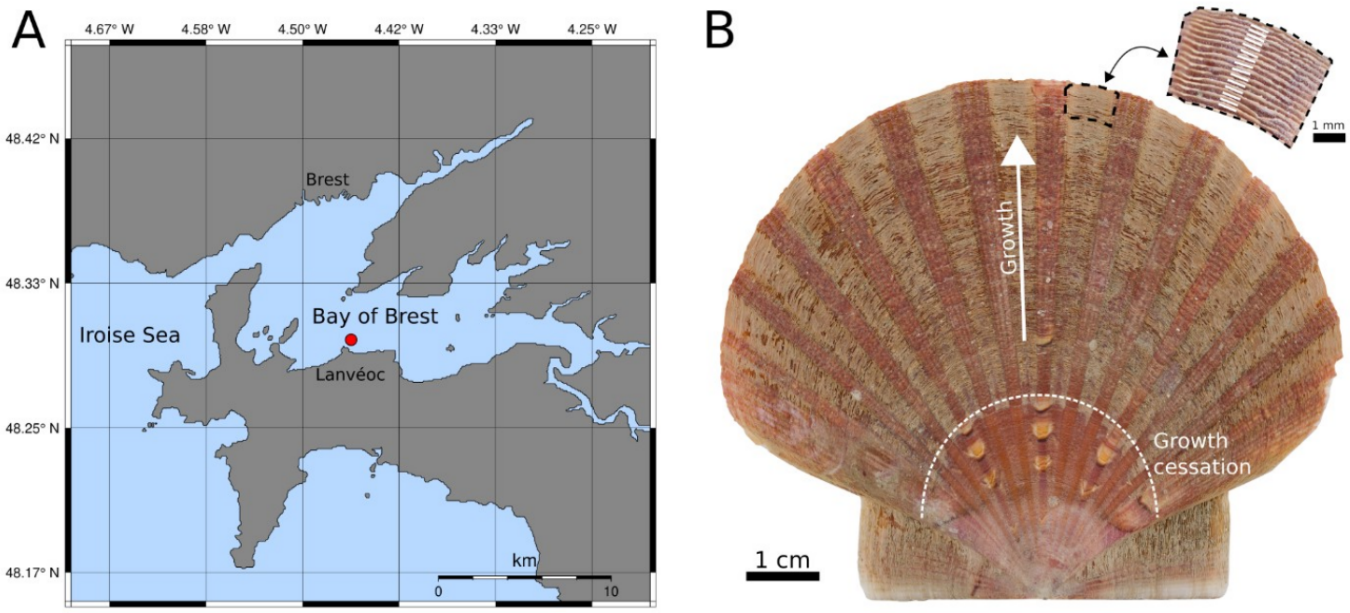

Figure 32 – Map showing the Bay of Brest (northwest France) and study locality where the scallop specimens were hatched and collected (red circle; Pointe de Lanvéoc) (A). Left valve of a *P. maximus* specimen (prior to the removal of overlapping calcitic striae) and magnification of a shell portion close to the ventral margin (after removing overlapping striae) with white lines indicating how individual LA-ICP-MS scans were positioned on the shell surface (B).

the axis of maximum growth using a 150 µm-thin, diamond coated (galvanically bonded) disk (Art. Number.: 6911H.-104.220, Komet – Dental Gebr. Brasseler GmbH & Co. KG) connected to a manual drilling device. Measurements were accomplished between two radial ribs and the focus was placed on the portion between the first winter growth mark and the ventral margin (Figure 32B). Prior to the chemical analysis, shell slabs were immersed in 10 vol% acetic acid for ca. 1 min and ultrasonically cleaned with deionized water for about 3 min. This procedure removed unwanted sediment grains and epibionts that were trapped within the surface sculpture of the scallop shells. In addition, the laser performed a pre-ablation procedure (line scan) to avoid potential surface contamination by ablating at a speed of 80 µm.s^{-1}, with a laser spot size of 100 µm. Measurements were conducted in line scan mode (length of 600 µm) at a constant speed of 5 µm.s^{-1} and a spot size of 80 µm on the outer surface of the shell, perpendicular to the direction of growth (Figure 32B). Signal intensities measured from each scan were averaged because a homogeneous distribution of the studied elements within individual striae has been demonstrated (Barats et al., 2007). The daily periodicity of shell formation (Chauvaud et al., 1998; Lorrain et al., 2000) allowed to extract elemental time-series with a temporal resolution between one and two days.

The laser system (NewWave Research UP-213 Nd:YAG laser) operated at a repetition rate of 10 Hz and a laser energy density of approx. 15.8 J.cm^{-2}, using helium (quality 5.0) as a carrier gas (0.57 L.min^{-1}). With a Thermo Fisher Element 2 single collector sector-field ICP-MS system, the ion

intensities were measured after each ablation, with argon (quality 5.0) as a carrier gas (0.77 L.min^{-1}). To calibrate the obtained raw signals, a synthetic silicate glass (NIST SRM 612) was used as an external standard, ^{43}Ca as an internal standard and a pressed carbonate powder pellet (USGS MACS-3) was analyzed as blind sample to account for quality control. Reference materials were analyzed similar to the shell samples (i.e., in a line scan mode using similar laser system settings) and reference values derived from the GeoReM database (version 33; http://georem.mpch-mainz.gwdg.de/; last access: 16 August 2022; Jochum et al., 2011).

An in-house script (C++) (by Lukas Fröhlich, 2023, unpublished) was used to process raw signal intensities following the equations provided by Longerich et al. (1996) and Jochum et al. (2007, 2011) and convert them into element-to-calcium ratios, i.e., Ba/Ca, Mo/Ca and Li/Ca (in µmol.mol^{-1}). Based on the 3σ criterion, the detection limits (LOD) were calculated from the blank signal of the calibration material (NIST SRM 612) obtained from 15 s before the laser started to ablate. Values below average LODs (Supplementary Table S1) were discarded. To account for a potential time-dependent machine drift, each sequence was processed following a batchwise calibration, i.e., a batch of shell and quality control samples was calibrated using repeated measurements of reference materials (NIST SRM 612). Based on these replicate measurements of the external reference material, the relative standard deviation in percent (RSD%) was calculated to report the uncertainty of reproducibility for each measurement. For Ba and Li measurements, the average RSD% was 1.2 % and 1.3 % for Mo (Supplementary Table S1). The blindly measured quality control material (USGS MACS-3) exhibited average deviations from the reference values of 6 % for Ba and Mo and 17 % for Li (Supplementary Table S1). These deviations are potentially induced by an uneven ablation behavior of the pressed synthetic carbonate powder pellet (heterogeneity of particle sizes) which can lead to ionization differences and/or uncertainties in reported values of the non-certified quality control material (Jochum et al., 2019).

2.3 Temporal contextualization of measured shell data

The outer shell surface was photographed with a Canon EOS 600 DSLR camera mounted to a binocular microscope (Wild Heerbrugg) equipped with sectoral dark field illumination (Schott VisiLED MC 1000, reflected light). Photographs were used to measure pixel-distances between successive microgrowth lines (daily striae) and converted into µm-distance (reported in µm.day^{-1}). Since the specimens were collected alive, the last growth increment at the ventral margin corresponds to the date of death allowing to assign precise calendar dates to each shell portion. Visually identifying individual striae was not always unambiguous (Thébault et al., 2006; Thébault et al., 2009) and fractures, mainly occurring at the ventral margin, led to uncertainties in the shell growth reading procedure and

to inter-reader differences. To account for these discrepancies, the growth curves of multiple specimens were crossdated to form an average chronology which was used to temporally constrain the growth record. In this study, six specimens from the cage and six specimens from the sediment were used for growth pattern analysis (Supplementary Table S1). Since elemental analyses were conducted on the outer shell surface, each LA-ICP-MS scan could be visually associated with a specific growth increment (Figure 32) and thus assigned to a calendar date.

2.4 Environmental monitoring

Water samples (250 mL) from approx. 1.5 m below the sea surface were analyzed for their phytoplankton content. After biweekly water collection, the samples were transferred into silicon tubes and 8 mL of Lugol's solution was added to fix the phytoplankton cells. The phytoplankton content from a 50 mL aliquot was then analyzed (identification and cell counting) with an inverted microscope (Axio Observer.A1-ZEISS) after the cells sedimented on a glass slide for about 24 h, according to the Utermöhl method (Edler and Elbrächter, 2010). The samples for analyzing particulate Ba (PBa), Mo (PMo) and Li (PLi) content were collected from the surface water (approx. 1 m below sea surface) and from the bottom water (approx. 0.20 m above the SWI). Samples were obtained by SCUBA diving twice per week between March and June and once per week from July to October. The water was filtered (using MF-MilliporeTM mixed cellulose ester filter, mesh size 0.45 µm) and the particulate trace element content was analyzed by means of ICP-MS (inductively coupled plasma mass spectrometry; Thermo Scientific Quad XSERIES 2). In addition, the filtered fraction of the water samples (using Whatman GF/F filters; mesh size 0.7 µm) were dried at 50 °C and analyzed for their particulate organic carbon (POC) content using a CHN elemental analyzer (Thermo Fisher Flash 2000). The pheophytin pigment concentrations were calculated based on the method described by Lorenzen (1966). A detailed description about the entire environmental monitoring is provided by Siebert et al. (2023) (see chapters 1 and 2 of this manuscript).

2.5 Trace element uptake by scallops and relation to phytoplankton

Based on the molar trace element-to-calcium ratios measured in the scallop shells, the absolute amount of trace elements incorporated into the shell per day was approximated following the method described by Thébault et al. (2009). Additionally, the quantity of a trace element (TE) contained in each liter of filtered seawater was estimated (hereafter referred to as $TE_{\text{filtered seawater}}$). Briefly, the approximations (described and illustrated in the Supplementary material and Figure S1A) were based on the following steps: (1) The shell height at each day was calculated from shell growth rates and combined with the shell height-to-soft tissue dry weight and the shell height-to-shell weight relation-

ships of *P. maximus* (Lorrain et al., 2004) to approximate the soft tissue dry weight as well as the shell weight. (2) This information was used to estimate the daily filtration rates using the soft tissue dry weight standardized filtration rate of approx. 5 $L.h^{-1}.g^{-1}$ (Palmer, 1980; Laing, 2004; Thébault et al., 2009) and the amount of shell material that was precipitated each day. (3) Considering a relative Ca content of 38 wt% in the shell (e.g., determined for *P. maximus* by Richard (2009), and *A. islandica* shells by Marali et al., 2017), the absolute amount of a trace element incorporated into the shell during each day was estimated according to the measured trace element-to-calcium ratios. Note, for the Ba/Ca_{shell} and Mo/Ca_{shell} profiles a background subtraction was performed to remove the influence of dissolved Ba and Mo on the measured element-to-calcium ratios. Accordingly, the Ba/Ca and Mo/Ca ratios measured in the seawater were used to estimate the Ba/Ca_{shell} and Mo/Ca_{shell} background levels using the partition coefficient for Ba (D_{Ba} = 0.11 (Barats et al., 2009)) and Mo (D_{Mo} = 1.5×10^{-4} (Barats et al., 2010)). The relationship between daily growth rates and Li/Ca_{shell} background was used to account for excess Li/Ca_{shell} (Thébault and Chauvaud, 2013). (4) By considering the total load of trace elements incorporated each day (i.e., assuming that 63 % of the total Ba and 27 % of the total Mo ends up in the shell matrix according to preliminary data from Barats, 2006) and the daily filtration rate, the amount of trace element that was contained in each liter of ingested seawater was approximated.

To estimate the phytoplankton-associated trace element content as well as to address potential relationships between trace element incorporation rates and phytoplankton dynamics, the approximated trace element requirements were combined with the measured phytoplankton cell concentration data. Since the patterns of the Ba/Ca_{shell} profiles were previously hypothesized to be controlled by the dynamics of multiple phytoplankton species, primarily diatoms (Thébault et al., 2009; Fröhlich et al., 2022a; Fröhlich et al., 2022b), the measured profile was numerically approximated using the pseudo-random Monte Carlo (MC) approach described in Fröhlich et al. (2022a). Note that uncertainties in the temporal alignment of the geochemical shell data as well as the low sampling frequency of the phytoplankton data (i.e., the exact timing when a phytoplankton bloom reaches the highest cell concentration remains unknown) largely influences the direct assignment of a given phytoplankton bloom to a Ba/Ca_{shell} peak during the MC calculations. Additionally, a short time lag of up to 12 days between the occurrence of a given phytoplankton species and a Ba/Ca_{shell} peak had to be assumed (Fröhlich et al., 2022a; Fröhlich et al., 2022b). Therefore, a stepwise testing of different time windows (i.e., 4-days window) was necessary to determine the combination of different phytoplankton species that agreed best to the measured Ba/Ca_{shell} profile. As no phytoplankton data were available for the time between late July and early September, the MC approximations were performed excluding this time interval. The MC-estimated species-specific weighting coefficients served as relative Ba-enrichment factors and were used together with $Ba_{filtered\ seawater}$ to account for the minimum con-

tent of diatom-associated Ba in one liter of seawater that was potentially ingested by the scallops (see Supplementary Figure S1B).

2.6 Statistics

To statistically evaluate differences between the average shell growth patterns of cage and sediment specimens, a two-way factorial analysis of variance (i.e., two-way ANOVA test) was used. Sample site, i.e., cage vs sediment, and the timing of shell growth, i.e., comparison of monthly pooled growth rates (May to September), were considered as orthogonal and fixed factors. Shapiro-Wilk tests were performed to satisfy the underlying assumption of normally distributed data, and Bartlett tests were used to check for the homogeneity of variance. Finally, a Tukey's post-hoc test identified which specific groups were significantly different. The average trace element-to-calcium chronologies were analyzed for statistical differences in the background levels (Ba/Ca_{shell} and Mo/Ca_{shell}) or mean profiles (Li/Ca_{shell}) between cage and sediment specimens. To separate episodes of pronounced trace element peaks from the background, any period longer than one week with values exceeding the median was treated as an episode of trace element enrichment and not considered as background. The trace element-to-calcium profiles were evaluated using the non-parametric Kruskal-Wallis test given the normality or homogeneity of variation was not fulfilled. All statistical analyses were performed using the programming language Python (version 3.7.4).

3 RESULTS

3.1 Growth rates of sediment and cage shells

According to growth pattern analysis, the main growing season of sediment scallops started in early March (Figure 33). In cage shells, epibionts made the reliable identification of striae formed between early March and mid-April impossible. Between March and April, sediment shells grew approx. 70 to 175 $\mu m.day^{-1}$ with gradually increasing rates until mid-April and values fluctuating around 150 $\mu m.day^{-1}$ until the end of April. The first visible daily growth increments of cage shells measured around 190 µm (end of April). At the beginning of May, growth rates in cage shells remained high (up to 240 $\mu m.day^{-1}$) while a growth rate reduction was observed in contemporaneous specimens from the sediment (< 140 $\mu m.day^{-1}$ in early May). Growth rates in sediment shells progressively increased until July, reaching a maximum of 220 $\mu m.day^{-1}$, and slowly decreased until early October. Cage shells experienced a reduction in growth rate at the end of May (reaching 170 $\mu m.day^{-1}$) followed by a steady increase until mid-July (up to 267 $\mu m.day^{-1}$) and a moderate decline until October. Month-wise (May to September; Figure 33) testing for statistical differences in the growth rates between sediment and

cage shells (Supplementary Table S2 and S3) indicated that the position (i.e., sediment surface or 1 m above the substrate) as well as the timing of growth caused a significant difference in growth (ANOVA: $F = 14.26$, $df = 4$, $p < 0.001$). Furthermore, the growth rates between May and August were significantly different between cage and sediment shells (Tukey multiple comparison test, $p < 0.001$). Accordingly, shells grown 1 m above the SWI grew faster (except in September) compared to shells that lived on the sediment surface (Figure 33).

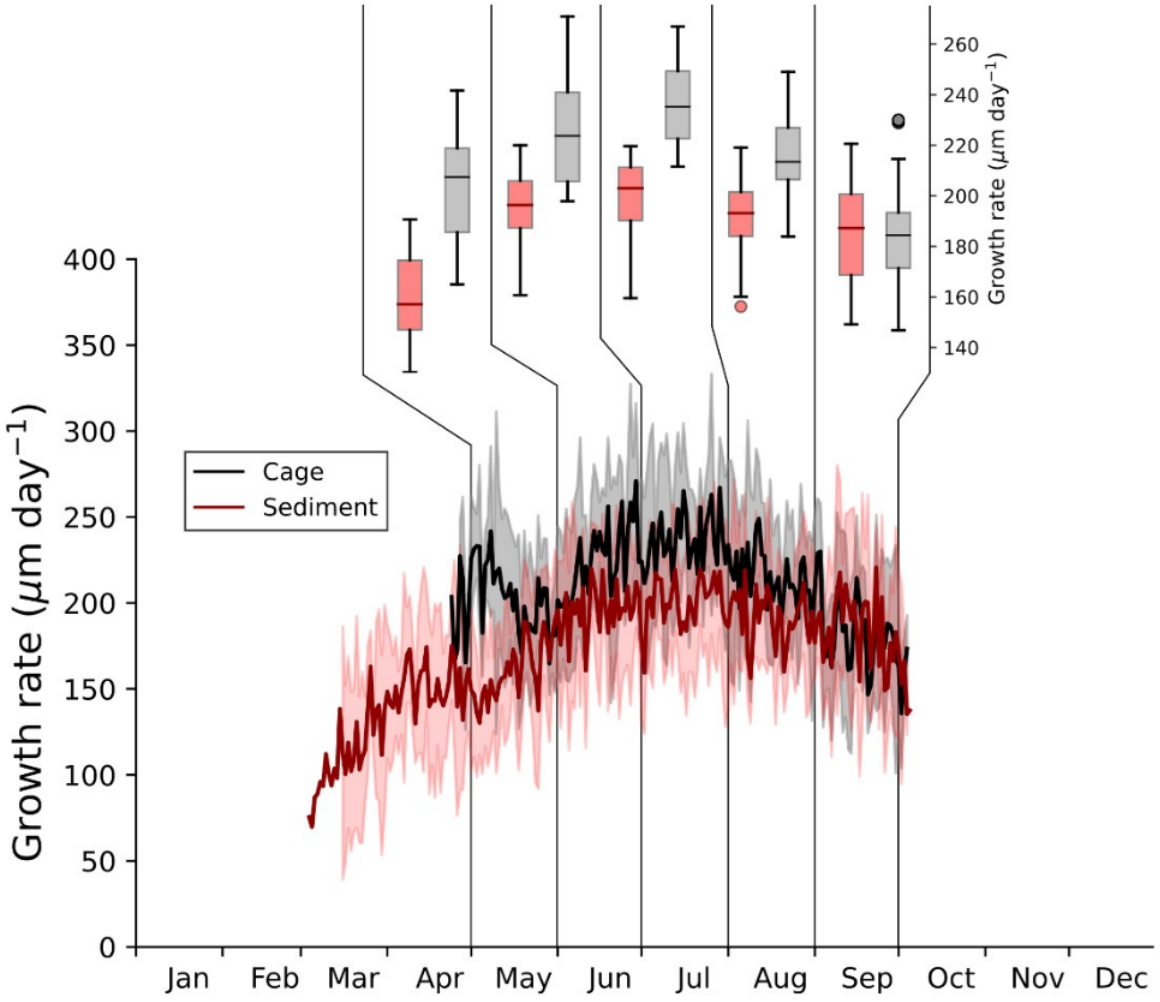

Figure 33 – Growth rates measured in six specimens of *P. maximus* shells living in a cage (1 m above the sediment) and six specimens grown on the sediment surface. Bold lines correspond to the average growth rates ($\pm 1\sigma$) for cage and sediment shells and box plots indicate for monthly differences in measured growth rates.

3.2 Ba in shells, seawater and relation to diatom blooms

All studied cage shells showed one prominent Ba/Ca_{shell} peak at ca. 08 June that occurred contemporaneously in all specimens from the cage (on average, 5.23 ± 0.79 µmol.mol^{-1}) (Figure 34A). This peak was followed by another, smaller Ba/Ca_{shell} enrichment (04 July; on average 2.37 µmol.mol^{-1}),

which was, however, only well-pronounced in one of the three studied specimens (Shell B; Figure 34A). Similarly, in late July, another Ba/Ca_{shell} peak was only observed in one of the three specimens (Shell C; Figure 34A). On average, the measured Ba/Ca_{shell} background in cage shells equaled approx. 1.73 ± 0.41 µmol.mol^{-1}. In the ontogenetically older shell portions (starting from mid-August), larger deviations from this background level were observed, e.g., short-term (< 2 days) enrichments showing Ba/Ca_{shell} ratios reaching up to 8.23 µmol.mol^{-1} on 05 September in Shell A; (Figure 34A).

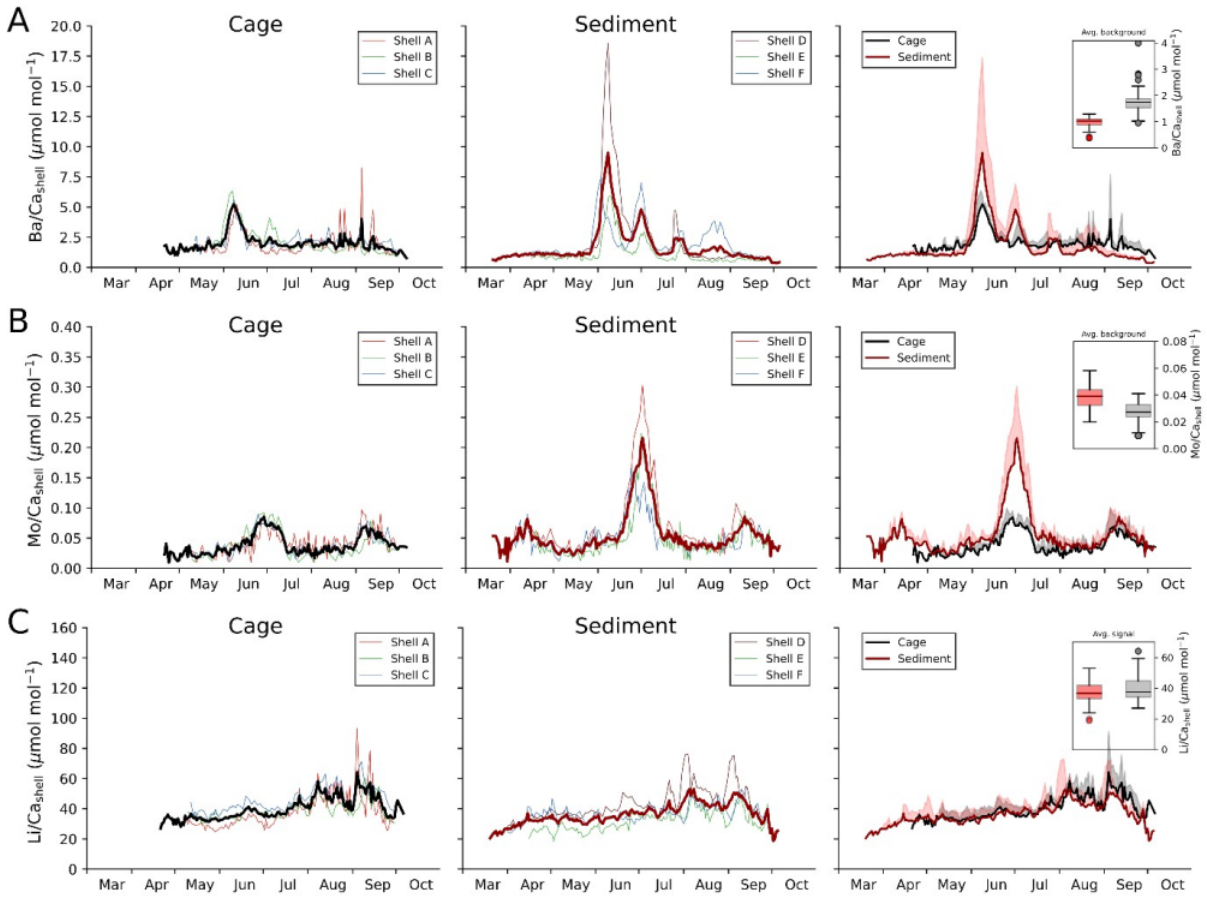

Figure 34 – Ba/Ca_{shell} (A), Mo/Ca_{shell} (B) and Li/Ca_{shell} (C) measured in three *P. maximus* specimens grown inside a cage (Shell A-C; left panel) and on the sediment surface (Shell D-F; center panel) during 2021. Average molar element-to-calcium chronologies represented as bold lines. For better visualization, the average profiles ($+1\sigma$) from cage and sediment shells were plotted together (right panel). Box plots indicate for differences in the background signals between cage and sediment shells of average Ba/Ca_{shell} and Mo/Ca_{shell} profiles and the average signal of Li/Ca_{shell} ratios.

In contrast to the cage shells, the Ba/Ca_{shell} profiles of sediment specimens revealed a more stable background level of about 0.96 ± 0.20 µmol.mol^{-1} (Figure 34A). This background was interrupted by a large double peak between late May and end of June, with average values of 9.50 and 4.80 µmol.mol^{-1} on 08 June and 01 July, respectively (Figure 34A). Although the first Ba/Ca_{shell} peak occurred nearly synchronously in all three specimens (i.e., within a few days), the peak magnitude of Shell D (18.58 µmol.mol^{-1}) was notably larger than that of Shell E and F (5.95 and 7.43 µmol.mol^{-1},

respectively). In late July, another Ba/Ca_{shell} enrichment episode was observed in all three shells with average values of up to 2.43 µmol.mol^{-1} (25 July). The fourth and last Ba/Ca_{shell} enrichment (3.86 µmol.mol^{-1}) was recorded in August in only one specimen from the sediment (Shell F), while no peak was present in the other two shells (Shell D and E). The average background signals differed significantly between cage and sediment shells (approx. 80 % higher median in cage shells than in sediment shells), as indicated by a Kruskal-Wallis test ($p < 0.001$, $H[chi^2] = 135.7$).

Ratios of PBa to POC (PBa/POC) range from 1.86 to 904.58 µmol.mol^{-1} in bottom waters and 5.23 to 1098.04 µmol.mol^{-1} in surface waters (Figure 35). PBa/POC profiles at both settings (surface and bottom) were characterized by a very low and flat baseline episodically interrupted by sharp peaks. Largest values were recorded on 07 June in bottom waters and 06 September in surface waters. Notably, all episodes of enhanced PBa/POC ratios that were measured in bottom waters occurred contemporaneously with PBa/POC peaks in surface waters, although to different magnitudes. A significant correlation existed between Ba/Ca_{shell} profiles (cage and sediment) and PBa/POC ratios of bottom waters (see Supplementary Figure S2).

The different Ba/Ca_{shell} enrichments were associated with unique diatom assemblages (Figure 35). For instance, the two large Ba/Ca_{shell} peaks in shells from the sediment (i.e., in early June and early July; Figure 36A) occurred contemporaneously with blooms of the diatom genus *Leptocylindrus* (i.e., *L. danicus* on 03 June and *L. danicus* + *L. convexus* on 30 June, respectively), while different diatoms of the genus *Chaetoceros* made up the majority of diatom cells on 21 June that coincided with only a very small Ba/Ca_{shell} enrichment in the cage shells (Figure 35). No apparent correlation existed between bulk diatom dynamics and Ba/Ca_{shell} profiles. Instead, the pseudo-random MC method (considering time lags and species-specific weighting factors) revealed potential patterns between Ba/Ca_{shell} profiles and the main abundant diatom taxa (see caption Figure 35). The MC results (i.e., using the Pearson correlation coefficients as a metric) showed the strongest correlation (0.91 with $p < 0.05$; Figure 36B) for a time lag of 5 to 8 days (Figure 36). However, the timing and magnitude of the diatom occurrences agreed better with the Ba/Ca_{shell} profiles at a shorter time lag of 4 to 7 days (with slightly lower Pearson correlation coefficients). According to this, the best diatom combination (hereafter referred to as "scenario 1", containing the diatom species *Lennoxia faveolata*, *C. socialis* and *C. laciniosus* and *T. belgicus*) coincide with the timing of the two large Ba/Ca_{shell} peaks in June and July and the smaller enrichment at the end of July (Figure 36B, C).

In a second, slightly modified set of MC calculations, the cell concentration data of *L. danicus* were forced to be included in each tested combination performed by the pseudo-random simulation (set 2; Figure 36B). The reason for considering set 2 is that the mass occurrence of this specific diatom taxon, by far the most abundant diatom species in the studied year (Figure 35), coincided with the timing of the largest Ba/Ca_{shell} peak in cage and sediment shells and thus suggested to be related to the

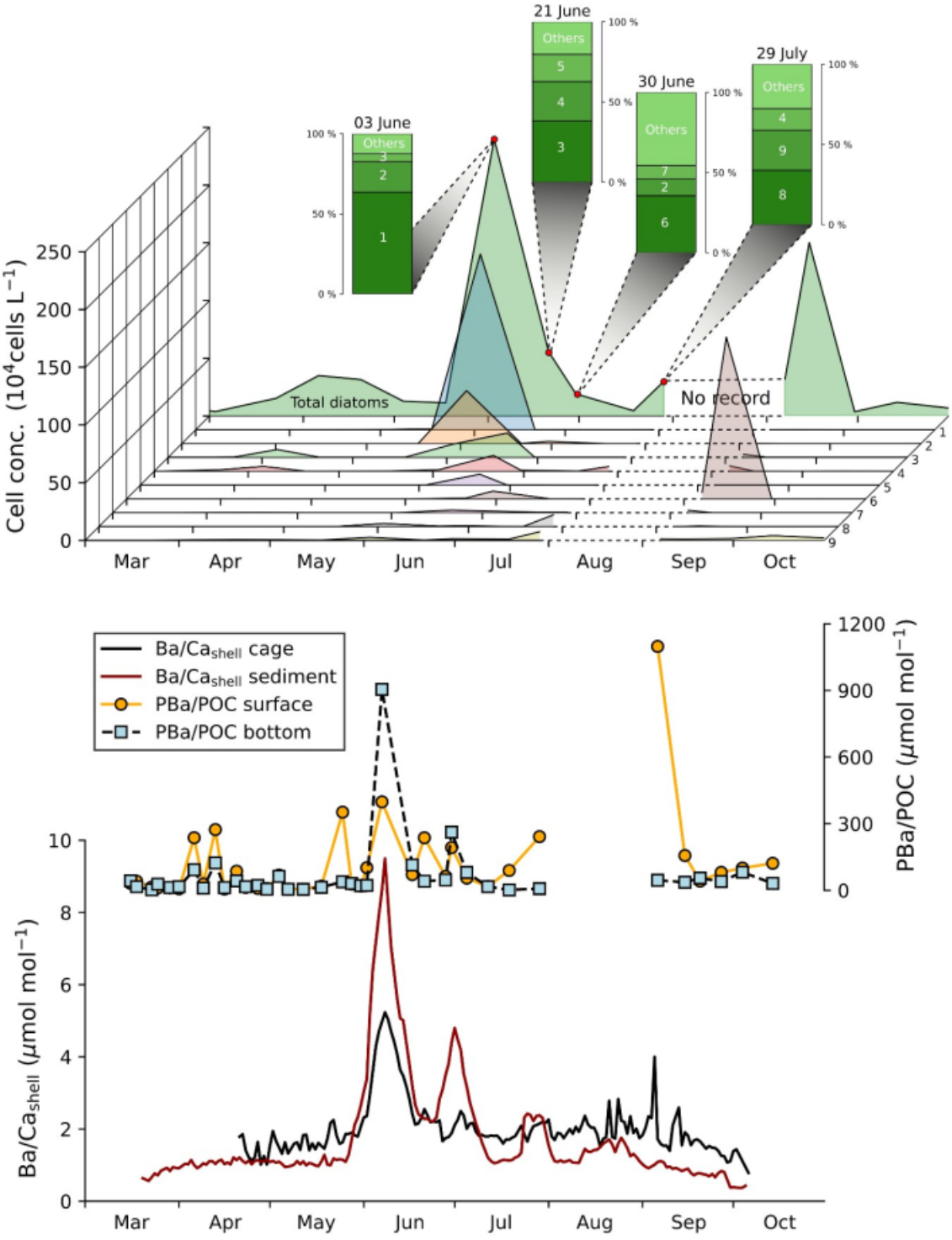

Figure 35 – Average Ba/Ca_{shell} profiles from cage and sediment shells (from 2021), the temporal variation in the PBa/POC ratios measured in surface and bottom waters and the cell concentration time-series of the most abundant diatom species that were recorded in the water column (at the studied locality in Lanvéoc, France). The vertical bar plots in the upper panel indicate the relative community compositions at four different dates with the three most abundant diatom taxa (1 – *Leptocylindrus danicus*, 2 – *Tenuicylindrus belgicus*, 3 – *Chaetoceros curvisetus*, 4 – *Chaetoceros* spp., 5 – *C. laciniosus*, 6 – *L. danicus* and *L. convexus*, 7 – *C. socialis*, 8 – *Pseudo-nitzschia delicatissima*, *P. pseudodelicatissima* and *P. cuspidata*, 9 – *Lennoxia faveolata*).

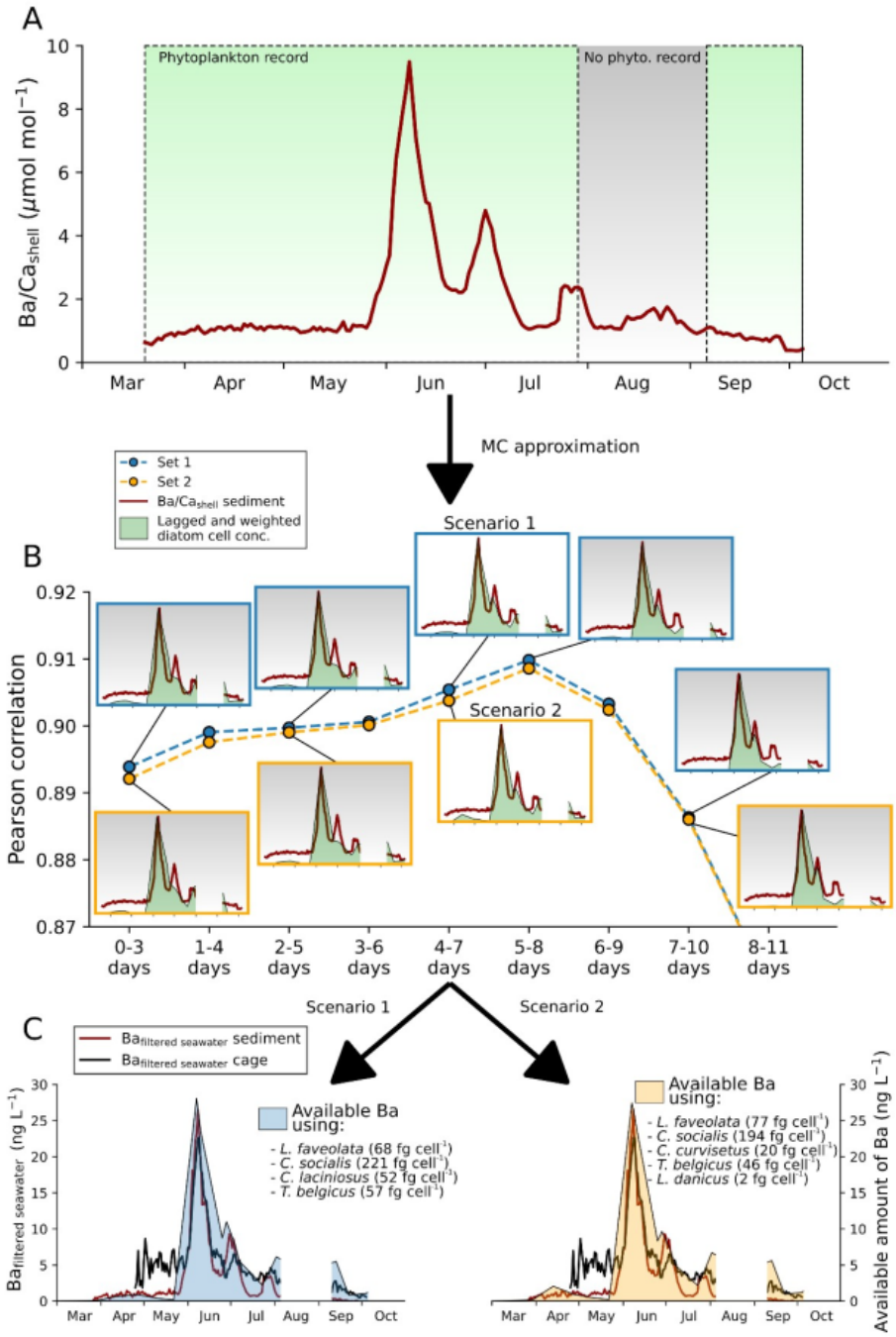

Figure 36 – The average Ba/Ca$_{shell}$ profile obtained from sediment grown shells (A) was used to approximate the potential contribution of the most abundant diatom taxa observed in the water column to the Ba/Ca$_{shell}$ peaks. Since no phytoplankton record was available between late July to early September, the Monte Carlo (MC) approximations were performed by excluding this time period (gray area in A). Pearson correlation coefficients indicated for the best combination (small subplots illustrating the respective result of the temporally shifted and weighted diatom time-series) that were tested for different time lags (B). Considering the growth rates and filtration rates (i.e., 5 L.h^{-1}.g^{-1} soft tissue dry weight), the Ba$_{filtered\ seawater}$ concentration was estimated (C). Using scenario 1 and scenario 2, the diatom-associated amount of Ba was estimated following the assumption that the ingestion of diatoms triggered the formation of the measured Ba/Ca$_{shell}$ peaks (see calculations described in Supplementary Figure S1).

Ba enrichment in the shell. In agreement with simulations of set 1, the most suitable combination was detected for a potential time lag of 4 to 7 days (in the following referred to as "scenario 2" considering *L. faveolata*, *C. socialis*, *C. curvisetus*, *T. belgicus* and *L. danicus*; Figure 36B, C). Because the obtained species-specific weighting factors were affected by the time lag that was artificially applied to each diatom species, various tested time lags produced slightly different outcomes (Figure 36B). In this study, the short time lag (i.e., in the expected range which was previously approximated between phytoplankton bloom and geochemical response; Fröhlich et al., 2022b) was exclusively used to determine the potential phytoplankton combination (with weighting factors) that best matched the Ba/Ca_{shell} profile. As depicted in Supplementary Figure S3, the daily amount of Ba that ended up in the bivalve varied considerably between specimens in the cage (maximum of 1.6 $\mu g.day^{-1}$) and on the sediment (maximum of 3.6 $\mu g.day^{-1}$). However, an almost equal amount of Ba in one liter of ingested seawater was needed to trigger the formation of the largest Ba/Ca_{shell} peaks in early June (Supplementary Figure S3) for shells from the cage (approx. 23 $ng.L^{-1}$) and the sediment (approx. 27 $ng.L^{-1}$) after taking the shell growth and filtration rates into consideration. Following the approximations performed for scenario 1 (Figure 36C), the hypothetically calculated amount of Ba (see Supplementary Figure S1) ranged between 52 and 221 $fg.cell^{-1}$ (for the diatom taxa *T. belgicus* and *C. socialis*, respectively). Based on the estimates of scenario 2, an adequate amount of phytoplankton-associated Ba was potentially abundant in the seawater if the diatom cells contained between 2 (*L. danicus*) and 194 (*C. socialis*) $fgBa.cell^{-1}$ (Figure 36C).

3.3 Mo in shells, seawater and its potential environmental sources

Mo/Ca_{shell} profiles (Figures 34B and 37) of the cage shells showed two episodes of elevated Mo content, i.e., at 29 June (0.08 ± 0.01 $\mu mol.mol^{-1}$) and 08 September (0.07 ± 0.02 $\mu mol.mol^{-1}$). Peak heights were nearly identical between the three specimens and clearly stood out from the background (approx. 0.03 ± 0.01 $\mu mol.mol^{-1}$). In specimens from the sediment, a large Mo/Ca_{shell} peak occurred at around the same time of the year, i.e., on 02 July, but was nearly threefold larger than in cage specimens (0.22 ± 0.09 $\mu mol.mol^{-1}$). As in the cage shells, another Mo/Ca_{shell} enrichment was observed in early September with an average magnitude of 0.09 ± 0.01 $\mu mol.mol^{-1}$. Sediment specimens also revealed elevated Mo/Ca_{shell} values (approx. 0.08 $\mu mol.mol^{-1}$) in shell portions deposited in early April. The contemporaneous shell portions could not be studied in cage shells due to epibiont overgrowth. Sediment specimens contained on average approx. 25 % higher Mo/Ca_{shell} values (0.04 ± 0.01 $\mu mol.mol^{-1}$) than cage shells (Kruskal-Wallis test; $p < 0.001$, $H[chi^2] = 74$). The total (shell plus soft tissue) daily Mo incorporation ranged between 3 and 63 $ng.day^{-1}$ for cage specimens and 8 and 147 $ng.day^{-1}$for sediment specimens (Figure 38A). Considering the daily filtered water volume

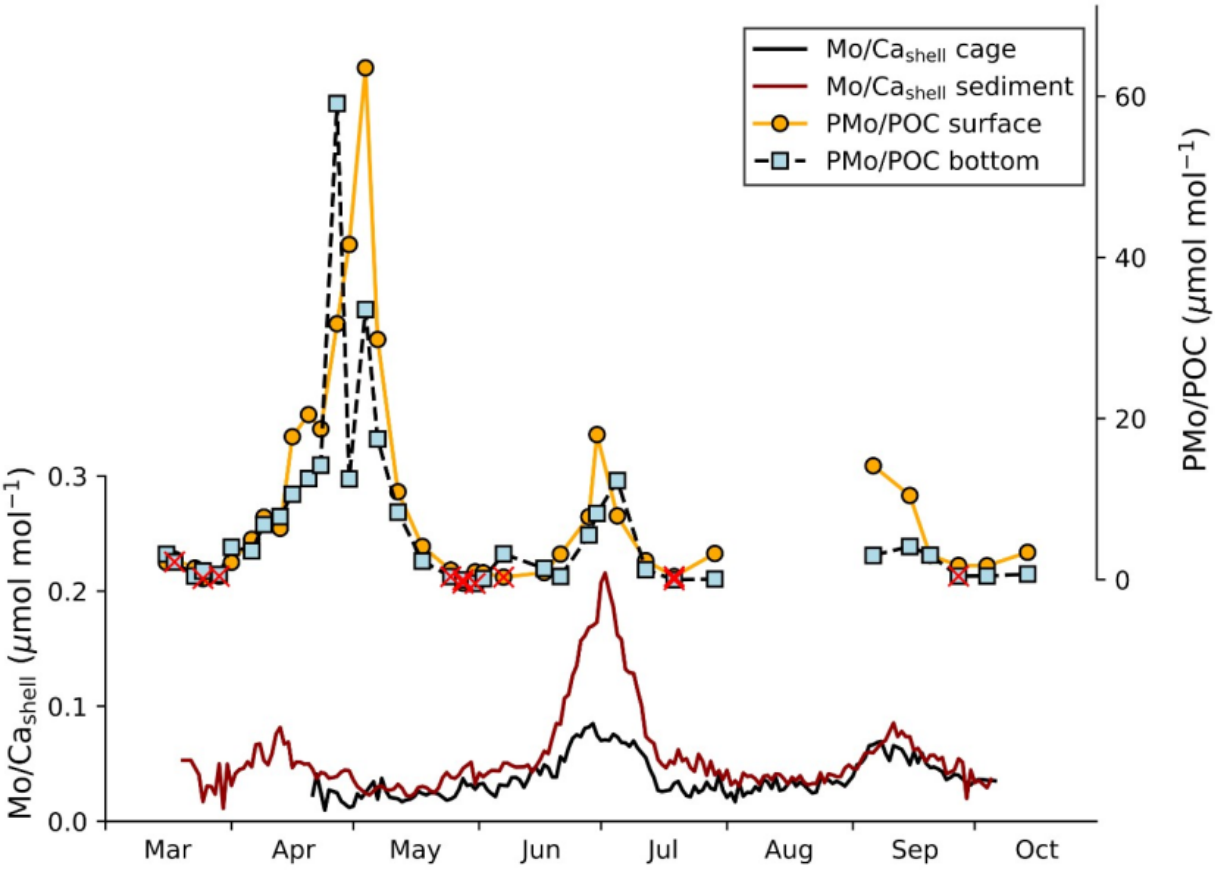

Figure 37 – Average Mo/Ca$_{shell}$ profiles from cage and sediment shells (from 2021) and the variation in PMo/POC ratios measured in surface and bottom waters. Note that some analyses of PMo remained below the limit of detection (indicated with a red cross).

(Figure 38A), one liter of seawater contained 0.03 to 0.78 ngMo (Figure 38B). Three episodes of enhanced Mo concentrations in the filtered seawater were determined for cage specimens (i.e., early May, early July, September) and sediment scallops (i.e., mid-April, early July, September) (Figure 38B).

Levels of PMo/POC ratios likewise showed a flat baseline (note that low PMo/POC levels were slightly below the detection limit obtained for particulate Mo) with episodes of enhanced PMo/POC levels (Figure 37). In both bottom and surface waters, three PMo/POC events were observed, i.e., in late April to early May (up to 59.10 and 63.53 µmol.mol^{-1}, respectively), late June (reaching 12.29 and 18.01 µmol.mol^{-1}, respectively) and early to mid-September (mainly occurring in surface water samples with ratios of 14.13 µmol.mol^{-1}). Siebert et al. (see chatper 2 of this manuscript) determined eight aggregation events occurring in the water column during the studied year (30 March, 12 and 27 April, 13 May, 06, 14 and 27 June, 02 October) and indicated that the aggregates in June were enriched in Mo (Figure 38). The most abundant dinoflagellate species identified in 2021 belonged to the genus

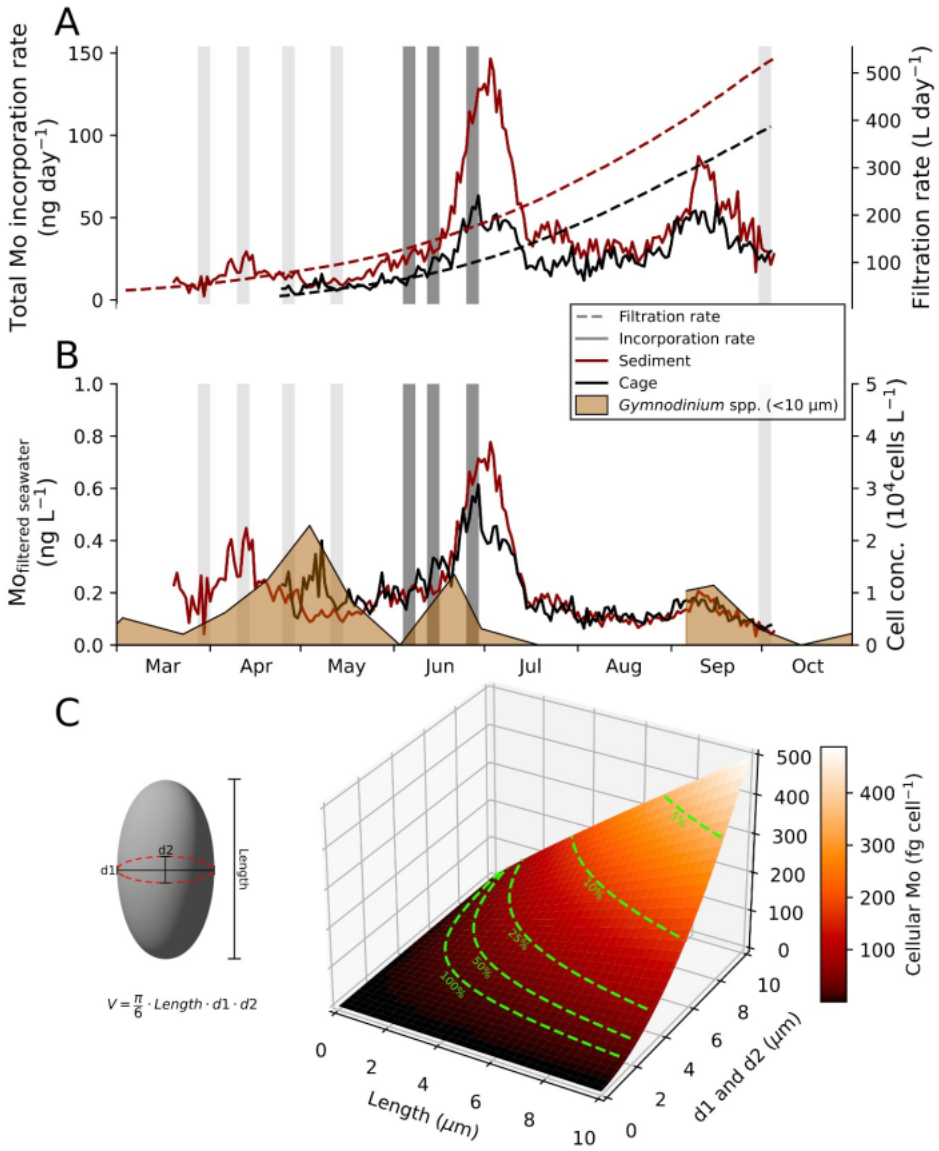

Figure 38 – Approximated total Mo incorporation rate into the scallops and filtration rate (at 5 $L.h^{-1}.g^{-1}$ of soft tissue dry weight) for cage and sediment shells (A). The $Mo_{filtered\ seawater}$ concentration (based on the total Mo incorporation rate, growth and filtration rate) and the temporal dynamics of the dominant dinoflagellate *Gymnodinium* spp. monitored at the studied locality (B). Periods of aggregate formation (determined by Siebert et al., see chatper 2 of this manuscript) indicated as light grey, vertical bars (A and B). Dark grey bars depict aggregation episodes during which significant loads of Mo were transported from the water column toward the SWI (Siebert et al.; see chatper 2 of this manuscript). The cellular Mo content at various cell volumes (C) was estimated using the cell geometry for *Gymnodinium* (Hillebrand et al., 1999; Sun and Liu, 2003), the volume-to-carbon relationship for dinoflagellates (Menden-Deuer and Lessard, 2000) and the elemental Mo/P (phosphorous) and C/P composition determined for the dinoflagellate *G. chlorophorum* (Ho et al., 2003). The green graphs in the 3D plot (C) illustrates potential values for cell parameters (if 100, 50, 25, 10 or 5 % of the *Gymnodinium* spp. cells per liter were ingested by the scallops) that are required to provide an adequate amount of cellular Mo to meet the trace element requirement in the ingested seawater (estimated in B) to explain the observed Mo/Ca_{shell} peaks.

Gymnodinium with a maximum cell concentration of 33,440 cell.L^{-1} on 04 May (cf., Siebert et al., see chapter 2 of this manuscript). More than half of these cells (68 %) were smaller than 10 µm. Distinct blooms of this dinoflagellate occurred in early May, mid-June and mid-September (Figure 38B), contemporaneously with PMo/POC enrichments. Theoretical approximations (described in Discussion) of the cellular Mo content of individual *Gymnodinium* spp. cells smaller than 10 µm (in length and diameter) yielded amounts of up to 500 fg $cell^{-1}$ (Figure 38C; see discussion for calculations).

3.4 Li in shells and seawater

Cage and sediment shells revealed similar Li/Ca_{shell} profiles (Figure 34C) that were characterized by low values in early 2021 (on average, 32.65 ± 2.04 and 30.61 ± 3.71 µmol.mol^{-1} until June in cage and sediment shells, respectively) and steadily increasing ratios during the main growing season in June and July (on average, 37.70 ± 3.35 µmol.mol^{-1} in cage and 36.97 ± 2.98 µmol.mol^{-1} in sediment specimens). Between August and mid-September, Li/Ca_{shell} values were slightly higher in cage shells (49.20 ± 5.77 µmol.mol^{-1}) than in sediment shells (45.40 ± 3.74 µmol.mol^{-1}). Although no large, distinct peaks were observed in the Li/Ca_{shell} chronologies (Figure 34C), two smaller enrichment episodes were present during late summer (August to mid-September) with average values reaching 58.20 to 64.18 µmol.mol^{-1} in cage shells and 50.73 to 52.99 µmol.mol^{-1} in sediment shells. Until the end of shell growth in early October, Li/Ca_{shell} ratios decreased rapidly in both groups (cage: 40.51 µmol.mol^{-1}, sediment: 31.52 µmol.mol^{-1}). Li/Ca_{shell} data differed significantly between cage and sediment shells (Kruskal-Wallis test, $p < 0.05$, $H[chi^2] = 6.0$). It is noteworthy that similar results were obtained after removing the estimated background signal from the measured Li/Ca_{shell} data by using the daily growth rates-to-Li/Ca_{shell} background dependency that was previously introduced by Thébault and Chauvaud (2013).

Ratios of PLi to POC exhibited values ranging between 1.15 and 1289.74 µmol.mol^{-1} in bottom and surface waters (Figure 39). Aside from a large PLi/POC peak in March, two additional enrichments occurred in bottom PLi/POC ratios on 07 June (656.47 µmol.mol^{-1}) and 15 September (384.88 µmol.mol^{-1}). The latter coincided with maximum PLi/POC ratio in surface waters.

4 DISCUSSION

Shell Ba/Ca and Mo/Ca profiles of *P. maximus* differed among specimens grown on the sediment surface and in a cage 1 m above the sediment-water interface. This was particularly the case for the magnitudes of synchronous peaks. A close link existed between elements bound to organic particles in the water column and Ba/Ca_{shell} and Mo/Ca_{shell} data, supporting previously proposed hypotheses on the trophic uptake of those elements by scallops. Computing the trace element concentrations in the

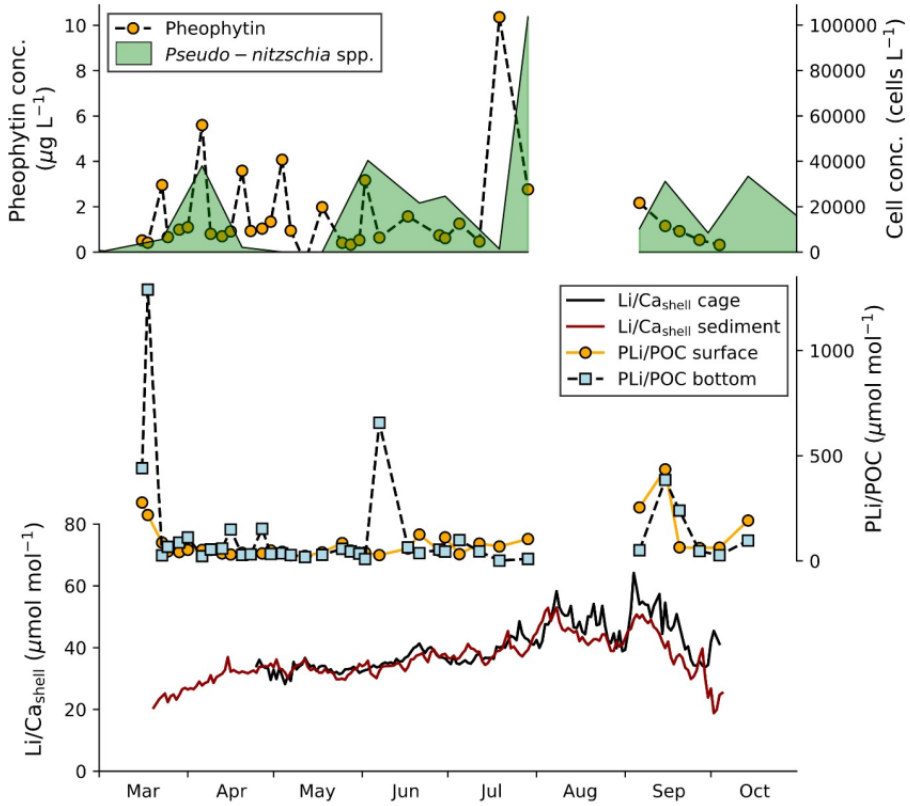

Figure 39 – Cell concentration time-series of the diatom *Pseudo-nitzschia* spp. and pheophytin pigment concentration in 2021. Temporal variation of PLi/POC recorded in surface and bottom waters with averaged Li/Ca_{shell} profiles measured in cage and sediment shells.

seawater filtered by the scallops, considering shell height, growth rate and filtration rate, revealed that the theoretical filtered Ba and Mo loads in the seawater were nearly identical between sediment and cage scallops during Ba/Ca_{shell} and Mo/Ca_{shell} peak formation. The measured differences in the geochemical signals were rather related to growth conditions than different food or water conditions. The approximations show that the timing and magnitude of Ba/Ca_{shell} peaks can be quantitatively modeled by blooms of specific diatom species containing different amounts of cellular Ba. The Mo/Ca_{shell} profiles appeared to be related to the timing of Mo-enriched dinoflagellate species as well as to the occurrence of aggregate forming diatoms transporting particulate Mo towards the SWI. Li/Ca_{shell} profiles did not show distinct peaks. However, two small Li enrichments occurred in all studied shells contemporaneously with elevated particulate Li concentration in the water, supporting assumptions according to which Li is derived not only from the dissolved phase but also from the particulate fraction (Thébault et al., 2022). These findings add new insights into uptake mechanisms of Ba, Mo and Li from the seawater into the shells of scallops, allowing to further refine Ba/Ca_{shell}, Mo/Ca_{shell} and Li/Ca_{shell} ratios as proxies for short-term phytoplankton dynamics. As demonstrated herein, the strong influence of specimen-specific physiological parameters (e.g., filtration rate, growth rate and

shell height) on shell chemistry requires the normalization of element chemical data before they can serve as quantitative paleoenvironment proxies.

4.1 Ba/Ca_{shell} profiles

The synchronicity of the Ba/Ca_{shell} peaks (in cage and sediment specimens) and PBa/POC ratios of the water column (Figure 35) suggests that shell Ba enrichments likely originated from the particulate phase (PBa), which is derived from the ambient water rather than the sediment. This finding corroborates the hypothesized trophic uptake of Ba-enriched suspended particles by scallop shells (e.g., Gillikin et al., 2008; Barats et al., 2009; Tabouret et al., 2012), that either originate from Ba accumulated on phytoplankton cell walls (Sternberg et al., 2005) or from enhanced barite precipitation (during the decay of phytoplankton blooms or the presence of acantharians in the water column) (e.g., Bishop, 1988; Ganeshram et al., 2003). A direct ingestion of cellular Ba from living phytoplankton cells provides a reasonable explanation for elevated shell Ba levels, because Ba/Ca_{shell} peaks occur contemporaneously with blooms of certain diatom species and a strong increase in the PBa/POC ratio in early June (Figure 35). This agrees to previous findings demonstrating that the occurrence of Ba/Ca_{shell} peaks is linked to the formation of phytoplankton blooms (i.e., mainly diatom blooms) (Thébault et al., 2009; Fröhlich et al., 2022a; Fröhlich et al., 2022b). During the blooms, dissolved Ba from the ambient water is adsorbed onto phytoplankton cell walls (Sternberg et al., 2005) and the ingestion of those Ba-enriched cells by scallops leads to an elevated Ba concentration in the shell calcite after a few days. The hypothesis is further substantiated by a negative correlation between dissolved Ba and PBa in the seawater (Siebert et al.; see chatper 2 of this manuscript). While large phytoplankton blooms generate microenvironments facilitating the precipitation of barite (e.g., Dehairs et al., 1980; Bishop, 1988), the ingestion of such particles could not sufficiently explain the formation of Ba/Ca_{shell} peaks in the scallop, *Comptopallium radula* (Thébault et al., 2009). Moreover, the ingestion of rapidly sinking barite particles in decaying phytoplankton (Stecher and Kogut, 1999) would have caused a larger Ba uptake by sediment specimens than by cage specimens because of the accumulation of large amounts of barite crystals at the SWI. However, after normalizing the Ba/Ca_{shell} peaks based on shell precipitation and filtration rates, the $Ba_{filtered\ seawater}$ was nearly identical between cage and sediment shells (see Supplementary Figure S3), indicating that barite ingestion played only a minor role in the formation of shell Ba enrichments. Although the development of barite particles potentially contributed to the observed enrichments of PBa/POC in the water column, a pathway via barite uptake leading to the formation of the observed Ba/Ca_{shell} peaks in cage and sediment shells is less likely.

Consistent with previous findings (e.g., Barats et al., 2009; Fröhlich et al., 2022a), the variation

in bulk phytoplankton or gross diatom abundance (Figure 35) provided no striking similarities to the Ba/Ca_{shell} chronologies within the studied year (except the large peak in early June), reinforcing the assumption that phytoplankton or diatoms as a whole cannot explain the variability of Ba/Ca_{shell} peaks. This complicates the applicability of Ba/Ca_{shell} as a direct paleoproductivity proxy. The quantity of cell-associated Ba varies significantly between different phytoplankton species (Riley and Roth, 1971; Fisher et al., 1991), indicating that the ingestion of some phytoplankton taxa contributes more to the measured Ba/Ca_{shell} peaks than other species (Fröhlich et al., 2022a). The pseudo-random MC approximations (considering species-specific amounts of cell-associated Ba) returned two possible scenarios (Figure 36) which qualitatively illustrated that the dynamics of only four (scenario 1; Figure 36C left subplot) or five (scenario 2; Figure 36C right subplot) diatom species are sufficient to explain the observed Ba/Ca_{shell} patterns. Although both scenarios include chain-forming diatoms (i.e., *C. socialis* and *L. danicus*) which can potentially inhibit the shell growth of scallops due to gill clogging (Chauvaud et al., 1998; Lorrain et al., 2000), these diatom species cannot be excluded as potential food sources because no distinct reductions in growth rate were observed during the formation of Ba/Ca_{shell} peaks. Aside from the diatom genus *Chaetoceros*, a well-known dietary component of *P. maximus* (e.g., Laing, 2004), no further information about feeding preference or gut content was available for the studied scallops. Therefore, none of the potential diatom scenarios can be ruled out. Moreover, the small discrepancy in the estimated time lag (4 to 7 days; Figure 36B) compared to the previously reported delay between phytoplankton blooms and geochemical response in the Ba/Ca_{shell} profiles (8 to 12 days; Fröhlich et al., 2022a; Fröhlich et al., 2022b) were most likely due to the low temporal resolution of the phytoplankton record and small uncertainties in the temporal alignment of the geochemical data. In fact, estimating the required cellular Ba content for the selected diatom species from $Ba_{filtered\ seawater}$, which provided a sufficient amount of this trace element to induce the formation of Ba/Ca_{shell} peaks (see Supplementary Figure S3), exhibited species-specific Ba quantities between 2 and 221 $fg.cell^{-1}$ (Figure 36C). These values fall in the range of cellular Ba content in different marine phytoplankton species (up to 245 $fg.cell^{-1}$; Fisher et al., 1991). In particular, a cell-associated Ba load of 60 $fg.cell^{-1}$ can be approximated for *Chaetoceros*, considering an average Ba concentration of 75.33 $\mu g.g^{-1}$ of dry weight (Lobus et al., 2021) at a maximum cellular dry weight for *C. gracilis* of approx. 0.8 $ng.cell^{-1}$ (Tachihana et al., 2020), which is notably consistent with the cellular Ba range computed in the present study. Such combinations of qualitative and quantitative approaches provide ecologically reasonable estimates and suggest that the cell abundance of only a few diatom species containing a reasonable amount of Ba can induce the formation of maxima in the Ba/Ca_{shell} chronology of *P. maximus*.

Interestingly, the significant difference in peak magnitudes of the elemental Ba/Ca_{shell} ratios between cage and sediment shells in early June (Figure 35) was diminished after normalization, i.e., after

considering the individual filtration and shell precipitation rates (to approximate the $Ba_{filtered\ seawater}$ content; Figure 36C and Supplementary Figure S3). This suggests that the filtered seawater for both cage and sediment scallops contained nearly the same amount of Ba (during the formation of Ba/Ca_{shell} peaks), which could be induced by the same external event, e.g., a diatom bloom in the ambient water. The higher Ba/Ca_{shell} peaks of sediment shells, on the other hand, seem to be mainly controlled by higher filtration and shell precipitation rates (Supplementary Figure S3). Aside from the difference in the averaged Ba/Ca_{shell} ratios of cage and sediment shells, a relatively large inter-specimen variation existed in the Ba/Ca_{shell} peak heights among sediment shells (i.e., the most distinct difference occurred between Shell D and Shell E in early June during the formation of the largest Ba/Ca_{shell} peak with 3.1 times higher values measured in Shell D; Figure 34A). By computing the $Ba_{filtered\ seawater}$ contents for Shell D and Shell E according to their individual growth rate and filtration rate, this *in-situ* measured Ba/Ca_{shell} discrepancy became less pronounced and differed by approx. 16 $ng.L^{-1}$ (1.7 times higher in Shell D compared to Shell E; Supplementary Figure S4). Nevertheless, it needs to be noted that an equal weight standardized filtration rate of 5 $L.h^{-1}.g^{-1}$ was considered for normalizing the Ba/Ca_{shell} data of Shell D and Shell E. Given that asynchronous, short-term changes in individual filtration activities have been observed for scallops, even when cultured in the same tank at identical conditions (Strohmeier et al., 2009), it is likely that individual variations in filtration rate might have induced such differences in peak heights. Alternatively, if the same amount of Ba (i.e., $Ba_{filtered\ seawater}$) was available in the water for Shell D and Shell E in early June, the filtration rate should have been slightly higher in Shell D to explain the larger Ba/Ca_{shell} peak magnitude (e.g., given a scenario in which Shell D possessed a higher, yet realistic (see discussion below), relative filtration rate of about 8.6 $L.h^{-1}.g^{-1}$ instead of 5 $L.h^{-1}.g^{-1}$, both specimens exhibited similar $Ba_{filtered\ seawater}$ levels after normalizing the Ba/Ca_{shell} profiles; Supplementary Figure S3). Therefore, small individual differences in growth rate and filtration rate can result in significant differences in the measured Ba/Ca_{shell} profiles which could affect the inter-specimen reproducibility of Ba/Ca_{shell} profiles. These findings suggest to normalize elemental Ba/Ca_{shell} ratios measured in *P. maximus* for filtration rate and shell growth rate before the data can be used as a potential quantitative indicator of past phytoplankton dynamics.

The Ba/Ca_{shell} background level of cage shells was significantly higher than that of sediment shells (Figure 34A), even after approximating the $Ba_{filtered\ seawater}$ content (Figure 36C). This finding is potentially coupled to the observation of higher growth rates measured in cage-grown specimens (Figure 33), a phenomenon previously reported for other scallop taxa, e.g., *Crassadoma gigantea* (Leighton, 1979), *Placopecten magellanicus* (MacDonald, 1986) and *Lyropecten nodosus* (Mendoza et al., 2003). The higher growth rate in cage grown scallops may be primarily associated with higher food availability (MacDonald, 1986), because the cage was placed within the water column where bi-

valves had better access to living planktonic organisms, such as diatoms. Thus, the constant provision of Ba-containing cells, selectively retained by scallop gills (Shumway et al., 1997; Beninger et al., 2004), potentially led to elevated Ba/Ca_{shell} background levels. Sediment particles within the digestive tract of scallops from the sediment (as reported by Shumway, 1987) could also affect the bivalves to efficiently assimilate their food, e.g., by altering the gut pH and/or the retention time of food particles in the gut (e.g., Wang et al., 1995). This potential influence might have contributed to the observed differences in Ba/Ca_{shell} background, yet needs to be confirmed in future studies by analyzing the gut content of scallops. The high variability in the Ba/Ca_{shell} profiles observed in cage shells compared to the more stable Ba/Ca_{shell} background measured in sediment shells (Figure 34A) could be related to an enhanced competition for resources between the cage scallops, given the high specimen density in the cage and the fact that scallops were reported to actively avoid high spatial population densities (e.g., MacDonald and Bajdik, 1992). An inter-species food competition for cage scallops is also likely, as a large number of naturally growing, filter-feeding ascidians colonized the cage. Accordingly, scallops living on the sediment surface may have had limited access to large amounts of planktonic diatoms, but rather fed on a mixture of detritus and benthic microalgae. After phytoplankton bloom events, the decaying cells sank toward the SWI where they got ingested by the scallops and triggered the formation of Ba/Ca_{shell} peaks provided that the quantity of cellular Ba together with the cell abundance in the water was sufficient to cause a respective enrichment in the shells. Although it remains unknown to which extent the various factors (i.e., growth and filtration rates, food availability, resource competition, spatial distribution of food and phytoplankton dynamics) contributed to the observed differences in cage and sediment Ba/Ca_{shell} background levels, the findings indicate that *P. maximus* sensitively reacted to changes in their direct environment which subsequently affected the measured Ba/Ca_{shell} ratios.

4.2 Mo/Ca_{shell} profiles

Similar to Ba/Ca_{shell} profiles, the Mo/Ca_{shell} profiles of cage and sediment shells shared a remarkably similar pattern with the PMo/POC data recorded in the water column with three contemporaneous episodes of Mo enrichment (Figure 37). This observation supports the assumption that shell Mo originates from the particulate phase (PMo) (Tabouret et al., 2012; Thébault et al., 2022). However, the magnitude of PMo/POC elevations (e.g., during late April to early May) does not correspond to the patterns measured in the Mo/Ca_{shell} profiles, suggesting that the scallops seem to have incorporated a non-proportionate amount of Mo from the PMo pool. Interestingly, after normalizing for filtration (Figure 38A) and shell growth rate, an episode of enhanced Mo concentration in the water ($Mo_{filtered\ seawater}$) was identified for cage shells in late April to early May (Figure 38B) which was not

obvious from the original Mo/Ca_{shell} profile (Figure 37). This $Mo_{filtered\ seawater}$ enrichment exhibited very similar levels to that determined for sediment shells in April. Although a temporal offset exists, it can be assumed that the enhanced $Mo_{filtered\ seawater}$ concentrations for both cage and sediment shells was potentially induced by the same external event that occurred in the water column. The short temporal discrepancy between $Mo_{filtered\ seawater}$ of cage and sediment shells during this period (late April to early May) is likely an artifact of uncertainties in the absolute temporal alignment of the geochemical data (especially in growth increments closer to the first winter growth cessation). Furthermore, the approximation of $Mo_{filtered\ seawater}$ indicates a comparable quantity of Mo was filtered from the ingested water by cage and sediment shells in early July, making the distinctively lower Mo/Ca_{shell} peak magnitudes in cage shells less pronounced (Figure 38B). Following previous observations, Mo/Ca_{shell} peaks in scallops (*P. maximus* and *C. radula*) are associated with a transport of Mo-enriched biogenic particles towards the SWI where they got ingested by the bivalves (Thébault et al., 2009; Barats et al., 2010). More specifically, stressed phytoplankton cells (e.g., due to nutrient limitation, (Toullec et al., 2021), or grazing by zooplankton, (Toullec et al., 2019) tend to stick together, forming large particles, i.e., aggregates (e.g., Alldredge and Silver, 1988; Alldredge and Gotschalk, 1989), which were proposed to sequester Mo from the dissolved phase (Dellwig et al., 2007; Mori et al., 2021) and induce Mo/Ca_{shell} peaks after digestion by the scallops (Thébault et al., 2009; Thébault et al., 2022). Siebert et al. (see chatper 2 of this manuscript) identified multiple episodes of aggregate formations in the water column throughout the studied year (Figgure 38A, B; grey bars) and concluded that not all aggregation episodes were linked to a significant transport of PMo toward the SWI, but only three aggregation events in June were associated with an enhanced PMo transfer (Figure 38A, B; dark grey bars). Accordingly, the largest Mo/Ca_{shell} peak observed in both sediment and cage shells occurred shortly after those three Mo-associated aggregation episodes (Figures 37, 38), substantiating the aforementioned relationship between scallops and potentially ingested aggregates. However, the two remaining Mo/Ca_{shell} enrichments in April and September did not occur contemporaneously with aggregation events (Figures 37, 38). Since the phytoplankton genus *Gymnodinium* is naturally enriched in Mo (Ho et al., 2003) and is the most dominant dinoflagellate genus of the studied year, a large bloom event may have contributed to an excessive transfer of Mo from the dissolved phase to the particulate phase, which potentially accounted for the large PMo/POC ratio measured in early May (Siebert et al.; see chatper 2 of this manuscript). A compelling synchronicity in early May and September existed between the timing and magnitude of blooms of this dinoflagellate taxon (i.e., *Gymnodinium* spp. from the size fraction < 10 µm) and the variation of enhanced $Mo_{filtered\ seawater}$ levels estimated for cage and sediment scallops (Figure 38B). This is in agreement with the findings by Fröhlich et al. (2022a) reporting qualitative similarities in the occurrence of small cells (< 20 µm) of the dinoflagellate *Gymnodinium* spp. and peaks in Mo/Ca_{shell} profiles of scallop shells from three

studied years. Aside from the blooms of *Gymnodinium* spp. in early May and September, a third mass occurrence of this dinoflagellate developed in June, shortly before the largest shell Mo enrichment observed in this year (Figure 38B). Similar to Ba/Ca_{shell}, a short time lag of a few days existed between a *Gymnodinium* spp. bloom and a Mo/Ca_{shell} peak (Fröhlich et al., 2022b), but this appears to be negligible given the uncertainties in absolute dating of the shell data and the low temporal resolution of phytoplankton monitoring. Assuming a linear relationship between cell abundance and Mo uptake, the cell concentration of *Gymnodinium* spp. during this bloom would have resembled the approximated $Mo_{filtered\ seawater}$ contents, which was not observed in this study. As described above, it is therefore likely that episodes of aggregate formation observed in June resulted in loads of PMo transported toward the SWI (Dellwig et al., 2007). Furthermore, the retention of small aggregate particles (Thébault et al., 2022) in addition to the ingestion of Mo-enriched cells of *Gymnodinium* spp., led to an enhanced trace element uptake by the scallops. The contemporaneity of *Gymnodinium* spp. blooms and phytoplankton aggregation may represent an allelopathic relationship (i.e., one organism produced biochemical compounds affecting the growth or survival of another) between dinoflagellates and other phytoplankton taxa. The allelopathic relation may have stressed the phytoplankton in competition with the dominant *Gymnodinium* genus (e.g., Kubanek et al., 2005). Such a stress may either induce cell lysis or promote the excretion of large amounts of sticky polymers, both mechanisms triggering aggregation of phytoplankton cells. The small difference in the $Mo_{filtered\ seawater}$ concentration between cage and sediment shells in early July (Figure 38B) could be due to aggregate particles that sank rapidly toward the SWI and resided only shortly in the water column, making them more available to scallops living on the sediment surface. This hypothesis can hardly be validated in the current study, because the approximations contain several uncertainties (see discussion below) that potentially contributed to differences in the absolute trace element uptake. However, these findings confirm that the patterns in Mo/Ca_{shell} profiles are potentially influenced by phytoplankton dynamics within the water column, i.e., both *Gymnodinium* spp. blooms and aggregation events play a role in Mo/Ca_{shell} peak formation.

Based on the hypothesis that the formation of Mo/Ca_{shell} peaks can be triggered by the ingestion of small *Gymnodinium* spp. cells (< 10 µm), the intracellular Mo content of this dinoflagellate was approximated in order to evaluate if this pathway can provide a sufficient load of PMo to explain respective trace element enrichments in the scallop shells. Ho et al. (2003) determined the element ratios of Mo and carbon (C), both normalized to phosphorus (P), in the dinoflagellate species *G. chlorophorum*, allowing to calculate the molar Mo/C ratio, i.e., 0.8 $mol.mol^{-1}$ (using Mo/P of 0.11 $mol.mol^{-1}$ and C/P of 137 $mol.mol^{-1}$). An empirical relationship between carbon content and cell volume was defined for dinoflagellates, i.e., $pgC.cell^{-1} = 0.216 \times volume^{0.939}$ (Menden-Deuer and Lessard, 2000), where the cell volume can be estimated by a geometric model for *Gymnodinium* cells (Figure 38C;

Hillebrand et al., 1999; Sun and Liu, 2003). These features allowed to estimate the range of absolute cellular Mo content at various possibilities in the shape of *Gymnodinium* cells (i.e., length, diameter d1 and d2; Figure 38C). Considering that the total pool of *Gymnodinium* cells within each liter of filtered seawater was retained by the scallops, a cellular Mo load of 17.5 fg.cell^{-1} (Figure 38C green 100%-graph) was calculated (e.g., 0.4 ngMo.L^{-1} of filtered water at 22,880 cell.L^{-1} in early May; Figure 38B). Based on the above-described cell geometry-to-Mo content relationship, the *Gymnodinium* cell volumes would have been about 14.7 µm^3, e.g., at a cell length of 7 µm and a diameter of 2 µm for d1 and d2 (Figure 38C), which agrees will with the observed phytoplankton in this study (a length of < 10 µm of the recorded *Gymnodinium* spp. cells). Given that many species of *Gymnodinium* have been reported toxic and could hamper shell growth in bivalves (Widdows et al., 1979; Chauvaud et al., 2001), cells of *Gymnodinium* are likely not the preferred diet of *P. maximus* and only ingested by smaller amounts. In fact, a reduction in growth rate was observed for sediment scallops during the first large *Gymnodinium* bloom in early May (Figure 33). Therefore, a scenario in which only 5 % of the total *Gymnodinium* spp. cells were ingested (i.e., corresponding to a cell concentration as low as 1,144 cells.L^{-1} in early May) is likely, which would result in a cellular Mo load of up to 349.7 fg.cell^{-1} to account for the estimated $Mo_{filtered\ seawater}$ requirement of 0.4 ngMo.L^{-1} for the cage and sediment shells (in early May). Interestingly, even this high cellular Mo content can be contained in *Gymnodinium* cells with a length and diameter not exceeding 10 µm (e.g., at a length of 8.4 µm and 9 µm in diameter d1 and d2; Figure 38C green, 5 %-graph). The ingestion of cells of only a very small portion (less than 5 %) of the total *Gymnodinium* spp. (< 10 µm) pool provided sufficient $Mo_{filtered\ seawater}$ quantities to induce the formation of the measured Mo/Ca_{shell} peaks in the cage and sediment shells. Although these calculations were based on multiple assumptions, this line of evidence supports that a potential link exists between the dinoflagellate genus *Gymnodinium* and Mo/Ca_{shell} peaks.

Despite small differences observed in the Mo/Ca_{shell} background levels (Figure 34B), after accounting for growth and filtration rates (Figure 38A), the $Mo_{filtered\ seawater}$ concentration revealed closely similar levels between cage and sediment shells outside Mo enrichment episodes (Figure 38B). Compared to the significant deviations in the Ba/Ca_{shell} background levels that can be explained by small differences in the ambient environment of the scallops, the more similar Mo requirements in cage and sediment shells suggests that such small environmental variations did not affect Mo/Ca_{shell} background levels. Instead, only during distinct events in the water column (e.g., aggregation episodes and/or large dinoflagellate blooms) enhanced loads of Mo enter the scallops and lead to the formation of Mo/Ca_{shell} peaks. This is in agreement with previous findings showing that the digestive gland is the most Mo-enriched organ (about 69 % of the total shell Mo content; Barats et al., 2010; Thébault et al., 2022) and that variations of dissolved Mo in seawater contribute insignificantly to the Mo/Ca_{shell} profiles (Barats et al., 2010; Tabouret et al., 2012).

4.3 Li/Ca_{shell} profiles

Unlike the Li/Ca_{shell} chronologies of *P. maximus* from previously studied years, respective profiles of cage and sediment specimens in the present study did not show large, distinct peaks (e.g., a Li/Ca_{shell} peak of approx. 159 µmol.mol^{-1} was measured in scallops by Thébault et al., 2022). However, two small Li/Ca_{shell} enrichments in August and September occurred contemporaneously in cage and sediment shells (Figure 39). These Li enrichments were even more pronounced when converted to an absolute daily Li incorporation rate (Supplementary Figure S6), using the relationship between daily shell growth rates and the Li/Ca_{shell} background (Thébault and Chauvaud, 2013) together with the daily Ca precipitation rate (Supplementary Figure S1). This indicates a common environmental forcing acting upon Li incorporation into the shells. It was previously hypothesized that Li from the dissolved phase is removed by the production of biogenic opal (Coplen et al., 2002) in diatom frustules that can lead to a transport of large quantities of Li toward the SWI triggering the formation of Li/Ca_{shell} peaks in scallops (Thébault and Chauvaud, 2013; Thébault et al., 2022). The large diatom blooms in early June and mid-September (Figure 35) occurred contemporaneously with increased PLi/POC levels in bottom waters, while increased PLi/POC values were only detected at the surface water in mid-September (Figure 39). The latter PLi/POC event (September) also coincided with a Li/Ca_{shell} enrichment, corroborating a link between diatom abundance and shell Li enrichments. However, no respective Li/Ca_{shell} peak occurred in June after the formation of the largest diatom bloom (Figure 35). A possible explanation for the absence of a respective Li/Ca_{shell} enrichment in early June is that either particulate Li was associated with a diatom species that was not ingested by the scallops or another process was involved that caused the recorded peak in PLi/POC at the SWI, such as the resuspension of Li-enriched sediment particles (Tardy et al., 1972) that were not filtered and retained by the scallops. Alternatively, Thébault et al. (2022) demonstrated that after large diatom blooms the recycling of biogenic silica at the SWI also releases frustule-associated Li into the ambient water causing distinct Li/Ca_{shell} peaks in scallops. The lack of a Li/Ca_{shell} peak following the large diatom bloom in June could potentially be linked to the observation that a large number of epifaunal brittlestars, *Ophiocomina nigra*, colonized the seabed. This omnivorous echinoderm species could have consumed most of the organic-enriched particles at the SWI including deposited diatom frustules which in turn prohibited the dissolution of Li into the water column. Unfortunately, no environmental monitoring data are available for August during the formation of the first, small Li/Ca_{shell} enrichment to further constrain these links.

Another proposed hypothesis describes a potential relationship between the diatom genus *Pseudo-nitzschia* spp. and the formation of transient Li/Ca_{shell} peaks in *P. maximus* (Thébault and Chauvaud, 2013; Fröhlich et al., 2022b). Growing under stressful conditions, i.e., nutrient limitations and en-

hanced predatory activity by zooplankton (Pan et al., 1996; Bates et al., 2018), *Pseudo-nitzschia* spp. cells were shown to produce the neurotoxin, domoic acid, which requires the presence of intracellular Li (Subba Rao et al., 1998) and the ingestion of those cells by scallops led to elevated Li/Ca_{shell} levels. In the studied year, several *Pseudo-nitzschia* spp. blooms were recorded (Figure 39) including large blooms in June, at the end of July (i.e., the most abundant diatom genus; Figure 35) and in September. However, only during the end of July, high concentrations of pheophytin pigments (an indicator for increased predation activity of zooplankton; Lorenzen, 1967) were observed when the development of *Pseudo-nitzschia* spp. initiated (Figure 39), generating conditions for *Pseudo-nitzschia* spp. to produce the Li-associated neurotoxin. Considering a short time lag between the timing of the diatom bloom and the formation of Li/Ca_{shell} enrichments (cf. Fröhlich et al., 2022b), this pathway seems to provide a possible explanation for the Li enrichment in cage and sediments shells in August. A similar pattern occurred in September, during the presence of elevated pheophytin levels (2 $\mu g.L^{-1}$) and the development of a *Pseudo-nitzschia* spp. bloom (Figure 39). This may have induced the formation of the second episode of elevated Li/Ca_{shell}. However, as blooms of this diatom also occurred prior to the two Li/Ca_{shell} enrichment episodes (i.e., in April and June) at slightly increased pheophytin pigment concentrations (Figure 39), the absence of respective trace element peaks in the scallop shells argues against the proposed link. The observed discrepancies may be explained by a species-specific filtration of scallops, because these blooms were composed of different *Pseudo-nitzschia* species.

The exact uptake mechanisms of Li from the water column to the incorporation into the scallop shells need to be further validated by longer time-series of Li/Ca_{shell} and environmental records. Nonetheless, the hypotheses of Li formation in scallop shells discussed in this study may also apply to the formation of larger, distinct Li/Ca_{shell} peaks (e.g., Thébault et al., 2022), making Li/Ca_{shell} chronologies a potent geochemical proxy recording short-term changes in the water column. A reliable approximation of the absolute amount of Li that was filtered from the water (like $Ba_{filtered\ seawater}$ and $Mo_{filtered\ seawater}$; section 4.1 and 4.2) could not be performed because no information about the relative distribution of this trace element in soft tissue and the shell was available. However, when considering differences in the volume of filtered seawater between cage and sediment specimens (Supplementary Figure S3), it can be estimated that scallops from the sediment filtered seawater that contained about 36 % less Li relative to cage scallops during the Li enrichments in August and September (Supplementary Figure S6). Accordingly, Li potentially derived from planktonic particles which might have been more accessible to the cage scallops, analogous to the observation of the enhanced ingestion of Ba-enriched phytoplankton for cage shells (see section 4.1).

4.4 Uncertainties in the trace element-related approximations

The model used to back-calculate $Ba_{filtered\ seawater}$, $Mo_{filtered\ seawater}$, total Li incorporation rates as well as the amount of cellular Ba and Mo in specific phytoplankton taxa (see Supplementary Figure S1), was based on the following presumptions that might have affected the final results. (1) The amount of daily filtered seawater was approximated using the shell height-to-soft tissue dry weight-relationship proposed by Lorrain et al. (2004) and the assumption of a relative filtration rate of about 5 $L.h^{-1}.g^{-1}$ of soft tissue dry weight, which is in the range previously determined for bay scallops (Palmer, 1980) and juvenile king scallops at optimal temperature settings (Laing, 2004). For simplification, the relative filtration rate was assumed to be constant throughout the year despite potential influences of temperatures as well as food particle density and quality on the filtration rate of the scallops (Laing, 2004). For instance, at very low seston conditions (i.e., chlorophyll a concentration below 0.88 $\mu g.L^{-1}$) the filtration rate in *P. maximus* was shown to reach 12 $L.h^{-1}.g^{-1}$ (Strohmeier et al., 2009), more than twice the rate that was considered herein. Note, according to a higher filtration scenario of scallops, the approximated cellular Ba contents for the selected diatom species would notably decrease, e.g., a maximum of 221 $fgBa.cell^{-1}$ was calculated at a filtration rate of 5 $L.h^{-1}.g^{-1}$ compared to 92 $fgBa.cell^{-1}$ at 12 $L.h^{-1}.g^{-1}$ for the diatom species *C. socialis* (scenario 1; Figure 36C). (2) Using the described relationship between the dissolved Ba/Ca and Mo/Ca ratio in the surrounding media and the Ba/Ca_{shell} and Mo/Ca_{shell} background (Gillikin et al., 2006; Gillikin et al., 2008; Barats et al., 2009; Barats et al., 2010), the influence of the dissolved phase was estimated considering constant Ba and Mo partition coefficients. As the dissolved Ba/Ca and Mo/Ca ratio in the seawater (Supplementary Figure S5) was assumed to be vertically homogenous within the range of 1 m (distance between sediment and cage), the estimated background signal was subtracted from the measured Ba/Ca_{shell} and Mo/Ca_{shell} profiles for both cage and sediment shells. However, the temporal variation and biological influence onto the partition coefficients remain uncertain, as the values were obtained from different years and small differences in reported partition coefficients exists between studies (e.g., Gillikin et al., 2008; Barats et al., 2010; Tabouret et al., 2012). (3) The species-specific amount of cellular Ba and Mo in phytoplankton was considered stable and potential environmental influences such as pH or Fe concentration in the seawater that can affect the Ba adsorption onto diatoms (Sternberg et al., 2005) were not included in the approximations. (4) It was assumed that the distribution of the totally ingested Ba and Mo pool that ended up in the shell relative to the soft tissues remained constant during shell growth. (5) To approximate the cellular Ba contents of diatoms, the total amount of phytoplankton cells per liter of filtered seawater (measured in the water column) was expected to be retained and ingested by the scallops, without considering species-specific feeding preferences.

Although these uncertainties likely contributed to deviations from actual trace element loads that

were taken up by the scallops and/or associated with individual phytoplankton cells, the approximations corroborate previously hypothesized uptake mechanisms. In the case of Ba and Mo, a sufficient amount of those trace elements was available for the scallops to induce the formation of Ba/Ca_{shell} peaks and Mo/Ca_{shell} peaks in the studied year. Moreover, the calculations demonstrated that physiological parameters of the bivalve can strongly affect the element-to-calcium ratios in its shell, which need to be considered when using trace element profiles as quantitative proxies.

5 SUMMARY AND CONCLUSIONS

Peaks in the Ba/Ca_{shell} and Mo/Ca_{shell} profiles occurred synchronously in cage and sediment specimens and contemporaneously to particulate trace element enrichments in the seawater. This suggests a dietary trace element uptake to induce the formation of Ba/Ca_{shell} and Mo/Ca_{shell} peaks, which is in agreement to previously reported findings. To quantify the absolute food-associated amount of trace elements that were potentially taken up by the scallops, shell height, growth and filtration rates were considered and combined with the element-to-calcium ratios of the shells. Despite notable differences in peak heights in the Ba/Ca_{shell} and Mo/Ca_{shell} profiles between cage and sediment shells, the formation of such peaks is likely induced by the same external event occurring in the water column, because the estimated trace element content in seawater exhibited closely similar levels. Specifically, the timing and magnitude of Ba/Ca_{shell} peaks agreed with the occurrence of specific diatom species containing different amounts of cellular Ba. In fact, the approximated phytoplankton-associated Ba content falls within the range of previously reported marine phytoplankton species, demonstrating that a trophic uptake of diatoms by scallops can provide reasonable quantities of this trace element to cause the formation Ba/Ca_{shell} peaks. Moreover, an enhanced Ba incorporation outside Ba/Ca_{shell} peak episodes as well as higher growth rates observed in cage shells were likely induced by a better access of cage scallops to living Ba-containing phytoplankton cells.

The variation of the Mo/Ca_{shell} profiles in the studied year is likely controlled by two external drivers, i.e., blooms of the dominant dinoflagellate *Gymnodinium* spp. and the occurrence of phytoplankton aggregation events. Based on the approximated amount of Mo that was filtered by the scallops during Mo/Ca_{shell} peak episodes combined with estimated cellular Mo content in *Gymnodinium* spp. cells (< 10 µm in size) indicated that the recorded blooms provided enough cell-associated Mo in the water column to induce the observed Mo/Ca_{shell} peaks even if only a small portion (< 5 %) of the cells were ingested by the scallops. Moreover, the occurrence of the largest Mo/Ca_{shell} peak in June followed the succession of phytoplankton aggregation events that were previously shown to transport PMo towards the SWI supporting the proposed relationship between aggregation periods and Mo/Ca_{shell} peaks.

Although distinct Li/Ca_{shell} peaks were lacking in the studied year, two episodes of enhanced Li uptake occurred contemporaneously in cage and sediment shells. Potential pathways that were proposed to trigger the formation of Li/Ca_{shell} peaks were examined, i.e., large diatom blooms and the presence of stressed *Pseudo-nitzschia* spp. cells, and indicated that both pathways may have contributed to the formation of Li/Ca_{shell} peaks. Accordingly, a diatom-related, environmental control on the incorporation of Li into the shells of *P. maximus* is reasonable but needs to be further validated in future studies. These findings demonstrate that patterns in the Ba/Ca_{shell}, Mo/Ca_{shell} and Li/Ca_{shell} profiles are strongly coupled to phytoplankton dynamics in the water column making them highly valuable as qualitative and quantitative paleoproductivity proxies.

CHAPTER 5

PHYTOPLANKTON PALEODYNAMICS: INSIGHTS FROM ARCHAEOLOGICAL SHELL MIDDENS

PREAMBLE/PRÉAMBULE

The journey thus far has been lengthy and has yielded numerous insights across the previous chapters of this manuscript. The time has now come to address the ultimate objective of the HIPPO project, which is to apply the knowledge gained thus far to ancient scallop shells obtained from various archaeological excavations in Brittany in order to quantify the impacts of anthropogenic activities on coastal ecosystems. A few scallop shells that are several centuries or millennia old were analyzed for concentrations of various trace elements, as well as oxygen isotope ratios. Each shell provides a unique glimpse into its respective time period, allowing for the reconstruction of past high-resolved variations in phytoplankton assemblages, and facilitating comparisons with the current environment. This experiment represents the latest that was conducted in this PhD project, and we currently believe that this chapter is not ready for publication yet. Despite this, we will still be able to discuss the results obtained. Before writing an article based on these data, we wish we could increase the number of analyzed shells, spanning several distinct time periods, to observe whether any general trends can be observed.

Le chemin parcouru jusqu'ici a été long et de nombreuses connaissances ont été obtenues au cours des précédents chapitres. Il est maintenant venu l'heure de répondre à l'objectif ultime du projet HIPPO : appliquer les connaissances acquises jusqu'à présent à des coquilles Saint-Jacques anciennes (provenant de différentes fouilles archéologiques entreprises dans la région Bretagne) afin de quantifier les impacts anthropiques sur les écosystèmes côtiers. Les concentrations des différents éléments, ainsi que des rapports isotopiques de l'oxygène, ont été mesurés au sein de quelques coquilles Saint-Jacques âgées de plusieurs siècles ou plusieurs millénaires. Chaque coquille est alors une véritable fenêtre sur son époque, et il devient possible de reconstruire les variations haute fréquence des communautés phytoplanctoniques passées et de faire des comparaisons avec l'environnement actuel. Il s'agit des dernières expérimentations qui ont été menées dans le cadre de ce projet de thèse et, à l'état actuel, nous pensons que ce chapitre ne peut pas encore faire l'objet d'un article scientifique. Cependant, cela ne nous empêchera pas de discuter des résultats obtenus. Afin de pouvoir écrire une publication à partir de ces données, nous souhaiterions augmenter le nombre de coquilles analysées dans le but de couvrir plusieurs époques distinctes et de voir si des tendances générales peuvent être observées au cours du temps.

High resolution reconstruction of past phytoplankton dynamics through the sclerochemical study of archaeological *Pecten maximus* shells

Valentin Siebert[1], Lukas Fröhlich[2], Brivaëla Moriceau[1], Bernd R. Schöne[2], Klaus Peter Jochum[3], Yvan Pailler[4], Julien Thébault[1]

[1]*Univ Brest, CNRS, IRD, Ifremer, LEMAR, F-29280 Plouzané, France*

[2]*Institute of Geosciences, University of Mainz, Johann-Joachim-Becher-Weg 21, 55128 Mainz, Germany*

[3]*Climate Geochemistry Department, Max Planck Institute for Chemistry, Mainz, Germany*

[4]*Chaire ArMeRIE (University of Brest / Inrap), UMR 6554 LETG, F-29280 Plouzané, France*

ABSTRACT

Due to the crucial role of phytoplankton in marine ecosystems (oxygen production, carbon sequestration, base of food webs etc.), many studies investigated their long-term temporal dynamics. In recent years, changes have been observed in these dynamics, including modification in the phenology of blooms as the emergence of toxic algae species. However, the historical data on phytoplankton are not sufficient to quantify the actual impact of human activities on these changes, as they do not go back far enough back in time. Shells of the fast-growing bivalve, *Pecten maximus*, are a valuable archive for past environmental conditions. This pioneer study analyzed and applied geochemical proxies obtained from two shells of *P. maximus*, collected within two different shell middens distributed along the Brittany coasts to elucidate the climate and ecosystem functioning of the past. These two samples were dated to 4500 years BP and to the 13th century. For this purpose, the stable isotope content of oxygen ($\delta^{18}O$) were measured and combined with trace element chemical properties of the shell (Sr:Ca_{shell}, Ba:Ca_{shell}, Mo:Ca_{shell} and Li:Ca_{shell}) to (i) evaluate and reconstruct the water temperature in which the bivalves grew, (ii) approximate the daily growth rates of the shells (using Sr:Ca_{shell}) and (iii) gain insights into the phytoplankton dynamics (using Ba:Ca_{shell} , Mo:Ca_{shell} and Li:Ca_{shell}) that prevailed in the water column during shell lifespan. According to the results obtained during this study, the shell geochemistry of archeological shells deviated to some extent to that of modern scallops which can be indicative for different phytoplankton community compositions and dynamics, or differences in the physicochemical properties of the water column in paleoenvironements (e.g., salinity). On the other hand, comparable variations in the Mo:Ca_{shell} profiles suggest that the phytoplankton taxon *Gymnodinium* (or another taxon showing similar characteristics) has been the dominant dinoflagellate genus in the Bay of Brest since the last 4500 years. Moreover, the data

indicate that diatom aggregation events and further nutrient limitations and/or enhanced zooplankton activity occurred in the water column hampering the growth of scallops. These findings demonstrate the potential, but also the limitations, of *P. maximus* shells as high-resolution multiproxy biogenic archives and lays the foundation for subsequent sclerochronological studies aiming to reconstruct past phytoplankton dynamics.

1 INTRODUCTION

The emergence of photosynthetic primary production on Earth billions of years ago was a significant biological process that allowed for the evolution of complex life forms. Nowadays, phytoplankton contributes significantly to oxygen production, accounting for nearly half of the global primary production, with one-third of this production occurring in coastal zones (Field et al., 1998; Boyce et al., 2010). Furthermore, they are essential for marine food webs and play a critical role in the biogeochemical cycles of carbon and associated elements. For several decades, qualitative and quantitative changes in phytoplankton dynamics have been monitored in various ecosystems and trends and changes have been observed (e.g, Edwards, 2004a; Boyce et al., 2010; Hinder et al., 2012; Rousseaux and Gregg, 2015). However, the existing time-series observations of phytoplankton dynamics (such as *in situ* monitoring and satellite measurements) have limitations. These limitations include insufficient temporal resolution to capture ephemeral and spatially localized phytoplankton blooms, the inability to distinguish between anthropogenic and natural influences on primary production, and propose an incomplete coverage of photo-autotrophic taxa.

Within the context of studying coastal ecosystems, the utilization of biological records presents a valuable opportunity to extend existing datasets over prolonged time periods, enabling the differentiation of natural climate variability and anthropogenic activities while providing comprehensive spatial coverage to evaluate ecosystem responses to global change. Bivalve shells, coralline red algae and corals are among the most commonly used biological records of ecosystem variability (Gillikin et al., 2019; Peharda et al., 2021). The growth of these carbonate structures often generates periodic marks, offering an accurate sclerochronological record of environmental changes. Notably, the king scallop, *Pecten maximus*, displays daily concentric rings in its valves (Antoine, 1978; Chauvaud et al., 1998), allowing for precise temporal dating. Furthermore, biomineralization processes frequently incorporate minor and trace elements into these structures in proportion to environmental conditions, such as temperature but also the amount of phytoplankton (Barats et al., 2009; Thébault and Chauvaud, 2013; Thébault et al., 2022; Fröhlich et al., 2022a; Fröhlich et al., 2022b).

In the past years, variations in the concentrations of barium (Ba), lithium (Li), and molybdenum (Mo) measured on the surface of *P. maximus* shells have proven to be effective tracers of past primary production (e.g., Gillikin et al., 2008; Barats et al., 2009; Barats et al., 2010; Thébault and Chauvaud, 2013; Fröhlich et al., 2022a; Fröhlich et al., 2022b; Thébault et al., 2022; see also chapter 4 of this manuscript). The hypothesis is based on the fact that these elements would be linked, through various mecanisms, with phytoplankton cells or aggregates (see chapters 2 and 3 of this manuscript). An increase in the concentration of these elements measured within the *P. maximus* shell would then follow the ingestion and digestion of these enriched phytoplankton cells. The high concentrations of

Ba and Li recorded within some portions of the shell (corresponding to a specific time of the year) would then be due to the ingestion of a high amount of diatom cells, which are known to adsord these elements onto their frustules (Barats et al., 2009; Thébault and Chauvaud, 2013; Fröhlich et al., 2022a; see chapters 2 and 4 of this manuscript). On the other hand, Mo would be linked to specific dinoflagellate cells, notably species of the genus *Gymnodinium* (Fröhlich et al., 2022a; see chapter 4 of this manuscript), which are naturally enriched in Mo (Ho et al., 2003). In addition, this element has been reported to be a good tracker of the formation of phytoplankton aggregates, which follows the collapse of a bloom (Thébault et al., 2022; see chapter 4 of this manuscript). Several tools are therefore available to get insights into past primary producers dynamics in coastal ecosystems.

The analyses of mollusc shells recovered within shell middens in the framework of archeological excavations is particularly useful for paleoenvironmental reconstruction (e.g., Carré et al., 2021). Shell middens are real mounds of dead shell materials, that correspond to waste depot built by past human population. Over the past two decades, the interest of archaeologists in these middens has increased, since they have access to a large amount of archaeological materials that allow them to better understand the customs and habits of past human communities. This has been shown by previous sclerochronological and sclerochemical investigations which tracked mollusc collection seasons throught the measurement of oxygen stable-isotope ratios ($^{18}O/^{16}O$ ratios refered to as $\delta^{18}O$ values) on several species (e.g., Killingley, 1981; Bailey et al., 1983; Andrus, 2012; Burchell et al., 2013; Eerkens et al., 2013; West et al., 2018). This is derived from the fact that the variation of $\delta^{18}O$ is an effectiv proxy of sea water temperature (Grossman and Ku, 1986).

For scientists interested in the reconstruction of past environmental parameters, access to this archaeological material is also facilitated, as they are often part of public archaeological programs and are referenced in collections. Moreover, archaeologists can date the shells based on their proximity to other dated materials or on their position in the stratigraphic layer. Thus, radiocarbon dating (which remains expensive) is not essential to date each sample. Shell middens discovered in Brittany have already provided archeological shell material, especially shells from the gastropod *Patella vulgata* (Dreano et al., 2007). Recent investigations studied the growth and the chemical composition of recent limpet shells with the aim of applying this knowledge to archaeological ones collected in the shell midden discovered on the Béniguet island (Brittany, France) (Cailleux, 1950; Dreano et al., 2007) in order to gaining knowledge on past environments (Cudennec and Paulet, 2021, 2022). However, given its morphological difference with the latter gastropod specie, the collection of *Pecten maximus* shells within this midden or during other archaeological excavations has the potential to bring new insights about paleoenvironments. Combined with the previous findings (Thébault et al., 2022; Fröhlich et al., 2022a; Fröhlich et al., 2022b; see chapter 4 of this manuscript), it allows to access the high-resolved past primary production dynamics, which has never been done before. Quantifying the impact of

anthropogenic activities on coastal shelf ecosystems then becomes possible.

The main objectif of this study is to assess the impact of recent human activities on coastal shelf ecosystems by comparing the dynamics of primary producers in past and present environments. To achieve this goal, the Sr:Ca, Li:Ca, Mo:Ca, Ba:Ca, as well as $\delta^{18}O$ profiles, have been measured on the shell of two archaeological *P. maximus* specimens collected at two excavation sites in Brittany (France). The trace element signals, including the amplitude and timing of observed peaks, were compared to those of contemporary shells from the Bay of Brest, collected during the HIPPO monitoring program (Siebert et al., 2023; chapter 4). Therefore, this study aims to bring new insights on the long-term impacts of anthropogenic activities on phytoplankton dynamics in coastal ecosystems.

2 MATERIAL AND METHODS

In the context of this study, two archaeological *Pecten maximus* specimens were analyzed. These two shells were collected during two archaeological excavations at two distinct sites, and come from different time periods. The first shell has been collected on the shell middens of the island of Béniguet while the second one comes from the Landévennec Abbey (Figure 40).

2.1 Presentation of shell materials

Shell from Béniguet island

One *P. maximus* shell was collected in the shell midden located in the island of Béniguet (site Béniguet-03), an island that is part of the Molène archipelago situated in the Iroise Sea (Figure 40 - Brittany, France). This shell midden has been dated to the late Neolithic, i.e., ca. 4500 years before present (BP), via radiacarbon methods (Stéphan et al., 2011). The shell is a well-preserved left (flat) valve and since no radiocarbon dating have been performed on this sample, it has been assumed to come from the late Neolithic (4500 years BP), like the shell midden where it was found. The Molène archipelago was once a plateau attached to the continent during the last glacial maximum, but it gradually became an isolated island with the rise of sea level during the Holocene period (11000 years BP). The archipelago has a high concentration of archaeological sites, indicating that some of the geomorphological changes occurred in the presence of humans. The fragmentation of the island space had various consequences such as reduced accessibility to the islands, isolation, reduction of territories, lifestyle changes, resource availability, changes in the apprehension of the territory, and communication with the continent (Pailler et al., 2011). It is important to note that the sea level was approximately 5-6 meters lower than the current level at the time the *P. maximus* shell was dated (Pailler et al., 2014).

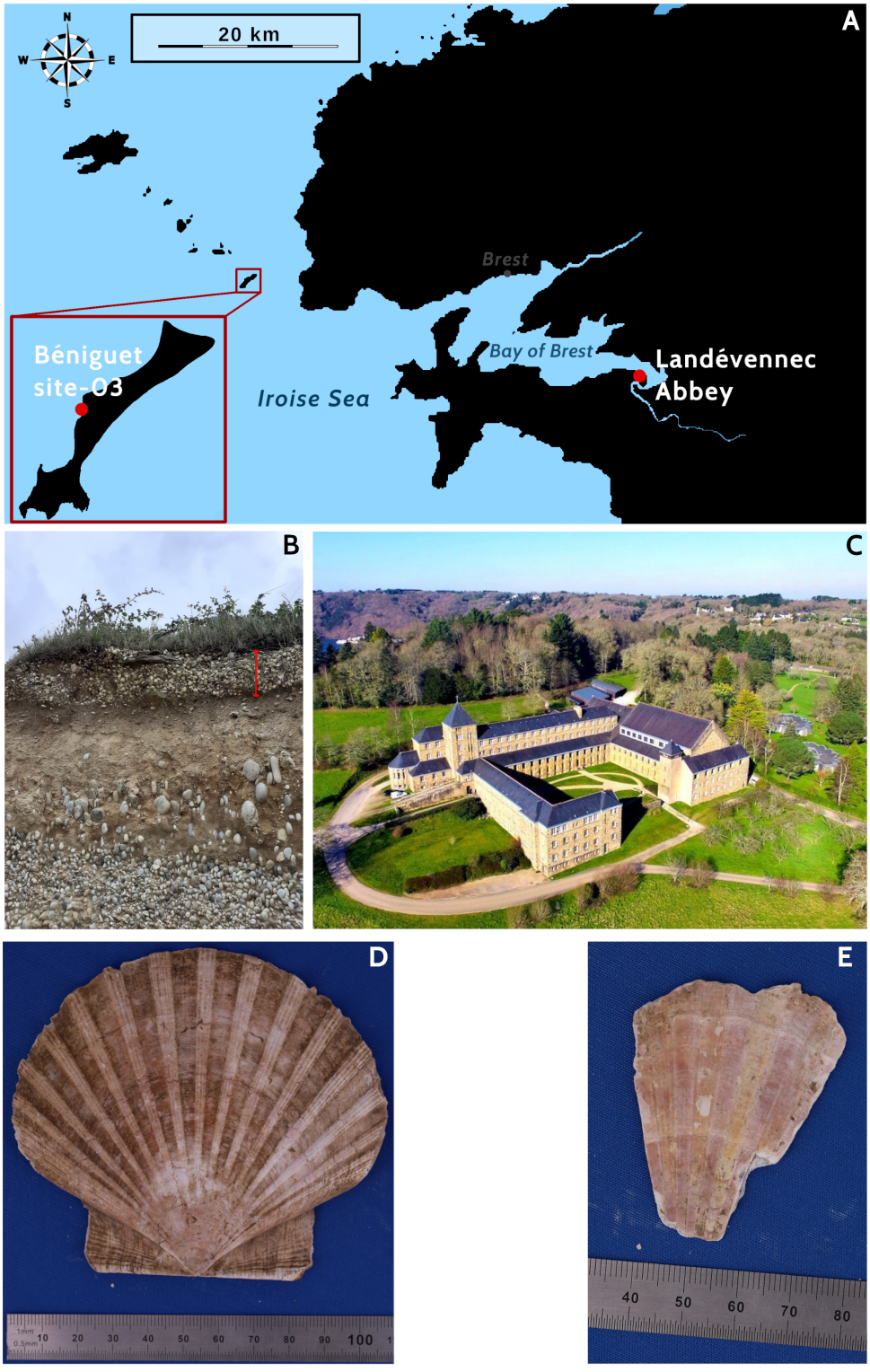

Figure 40 – (A) Location of the two excavation sites from which the analysed shells were collected. (B) Pictures of the shell midden from the site Béniguet-03 of the island of Béniguet (the layer corresponding to the shell midden is symbolised by the red line - approx. 40 cm thick) and (C) the Landévennec Abbey (picture from: https://divinebox.fr/abbaye-landevennec/). The shells collected in the shell midden from Béniguet (D) and at the Landévennec Abbey (E) are also presented.

Shell from the Landévennec Abbey

The second shell was collected during archaeological excavations carried out at the Saint-Guénolé Abbey in Landévennec (Figure 40 - Brittany, France). It is a fragment of a left valve that was dated to the 13th century. The Abbey St-Guénolé of Landévennec is an ancient abbey located in the south of the Bay of Brest. It was founded in the 5th century by Saint Guénolé, a Breton monk. The abbey played an important role in the Christianization of the region and in preserving knowledge during the medieval era. Over the centuries, the abbey has been destroyed and rebuilt several times. For example, it suffered from pillaging and fires during Viking invasions and was also damaged during the French Revolution. Today, the Landévennec Abbey is a center for research and studies on Brittany history, culture, and religion. It also houses a religious community and is open to visitors.

2.2 Shell analyses

Both shells have been lent by the Centre Départemental d'Archéologie du Finistère (Le Faou, France). First, the surface of the samples was gently cleaned with tap water and a plastic brush in order to remove sediment grain. Two adjacent radial ribs were then selected in order to perform trace element measurements on the first one, and oxygen isotope analyses on the second one (Figure 41). Since their exact fishing date remained unknown, the latter parameter was measured to obtain an estimation of the seawater temperature variations during the lifespan of each specimen, which enable the differentiation of seasons and the determination of a temporal context for the geochemical signals.

LA-ICP-MS analyses

To fit the shell samples into the ablation chamber of the laser system, a 5 mm broad slab was cut from the left valves along the axis of maximum growth using a 150 µm-thin, diamond coated (galvanically bonded) disk (Art. Number.: 6911H.-104.220, Komet - Dental Gebr. Brasseler GmbH & Co. KG) connected to a manual drilling device (Figure 41). Afterwards, the surface of the shell slabs was again gently cleaned with a plastic brush and tap water to remove calcite grains. Two successive ultrasonic cleanings that lasted 5 minutes were then applied to the shell slabs. Afterwards, the samples were analyzed for their Sr:Ca, Li:Ca, Mo:Ca, and Ba:Ca ratios using a Laser Ablation (NewWave Research UP-213 Nd:YAG laser) - Inductively Coupled Plasma Mass Spectrometry (Thermo Fisher Element 2 single collector sector-field)(LA-ICP-MS) system operating at the Max Planck Institute for Chemistry (Mainz, Germany). Here, the Li:Ca, Mo:Ca and Ba:Ca ratios were used to reconstruct past phytoplankton dynamics, based on the hypotheses put forward in previous studies (e.g., Thébault and Chauvaud, 2013; Fröhlich et al., 2022a; Fröhlich et al., 2022b; see chapter 4 of this manuscript). As the shell surface of the archaeological materials was frequently damaged (especially for the shell

from the Landévennec Abbey), it was difficult to accurately identify each stria and measure the daily growth rate (DGR - in µm.day^{-1}). Nevertheless, a correlation between the Sr:Ca ratio and the DGR has been established in a previous study and has was used to access the growth variations of our samples (Lorrain et al., 2005) :

$$DGR = \frac{Sr : Ca(\mu mol.mol^{-1}) - 1364}{0.002} \tag{4}$$

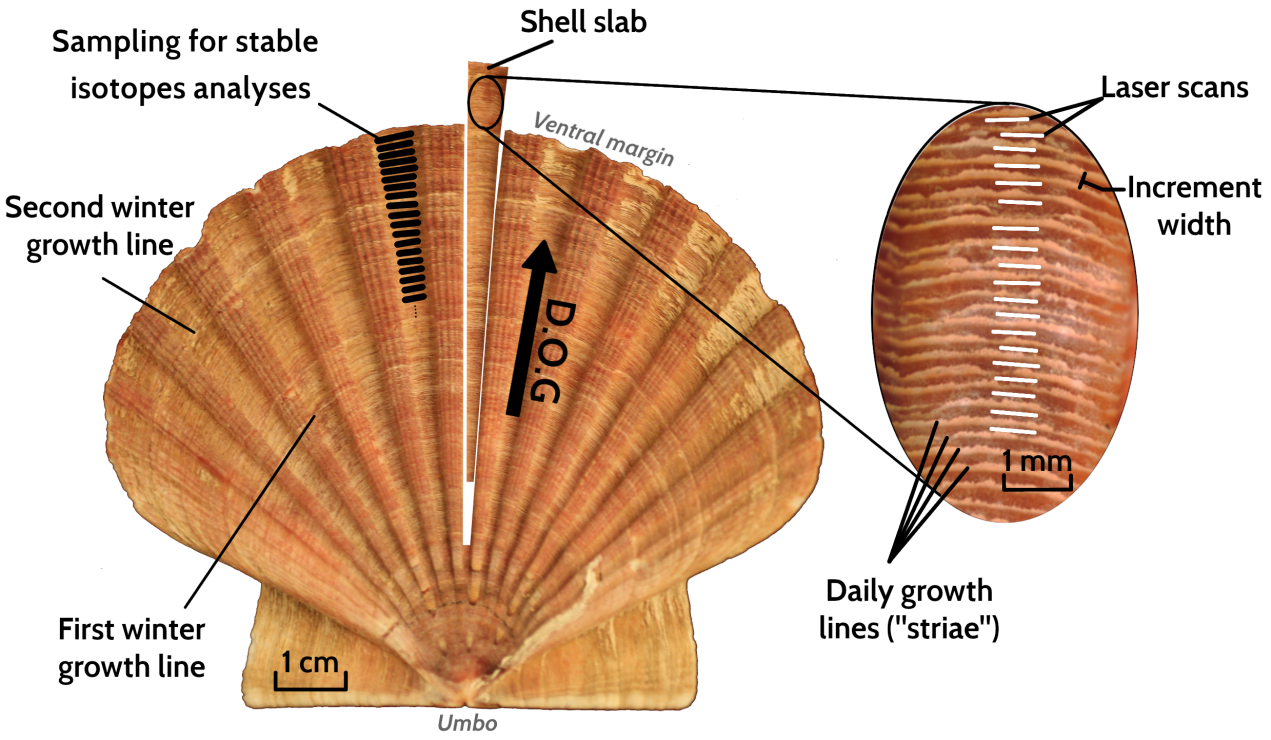

Figure 41 – Surface of a left valve of a recent *P. maximus* shell showing how the analyses were carried out. Black lines represent the sampling transect for stable isotope analyses. A magnification of the surface also showed the laser scans (white lines) that were performed for trace element measurements. DOG = direction of growth.

The laser system was used at a repetition rate of 10 Hz and a laser energy density of approximately 15.8 J.cm^{-2}, with helium (quality 5.0) as the carrier gas at a flow rate of 0.76 L.min^{-1}. To ensure accuracy, a synthetic silicate glass (NIST SRM 612) was used as an external standard, with ^{43}Ca as an internal standard. Quality control was maintained by analyzing a blind sample of pressed carbonate powder pellet (USGS MACS-3). Reference materials were analyzed similarly to the shell samples, and reference values were obtained from the GeoReM database (version 33; http://georem.mpch-mainz.gwdg.de/; (Jochum et al., 2011). To prevent surface contamination, a pre-ablation procedure was performed with a laser spot size of 100 µm and speed of 80 µm.s^{-1} just before the analyses. Measurements were performed in line scan mode with a constant speed of 5 µm.s^{-1} and spot size of 80 µm on the outer surface of the shell, perpendicular to the direction of growth (Figure 41). Signal intensities were averaged for each line scan as a homogeneous distribution of elements within individual striae was demonstrated (Barats et al., 2007).

An in-house (C++) script (by Lukas Fröhlich, 2023, unpublished) was utilized to process the raw signal intensities according to the equations provided by Longerich et al. (1996) and Jochum et al. (2011, 2007) and convert them into element-to-calcium ratios such as Sr:Ca, Li:Ca, Mo:Ca, and Ba:Ca (in µmol.mol^{-1}). The limits of detection (LOD) were calculated based on the 3σ criterion from the blank signal of the calibration material (NIST SRM 612) obtained 15 seconds before the laser ablation began. All events that will be interpreted and discussed in this article are above the LOD (LOD = 0.16 µmol.mol^{-1} for Sr:Ca; LOD = 8.55 µmol.mol^{-1} for Li:Ca; LOD = 0.008 µmol.mol^{-1} for Mo:Ca; LOD = 0.005 µmol.mol^{-1} for Ba:Ca). To account for potential machine drift over time, each sequence was processed using batchwise calibration, where a batch of shell and quality control samples was calibrated using repeated measurements of reference materials (NIST SRM 612). The quality control material (USGS MACS-3) exhibited average deviations of -5.1% for Sr, -19.75% for Li, 32.5% for Mo, 11.5% for Ba from the reference values. These deviations could potentially be induced by uneven ablation behavior of the pressed synthetic carbonate powder pellet (heterogeneity of particle sizes) leading to ionization differences and/or uncertainties in reported values of the non-certified quality control material (Jochum et al., 2019).

Oxygen isotope analyses

In order to attribute a temporal context to the trace element measurements, i.e. to identify the seasons corresponding to potential observed events, the $\delta^{18}O$ variations were measured along the growth axis, of which variation over time follows the variations of seawater temperature in Pecten shells (Chauvaud et al., 2005). These measurements were made on the radial rib adjacent to the one where the trace element measurements were performed (Figure 41). For these analyses, samples were ob-

tained by ablating calcite powder on the surface of the shell, perpendicular to the direction of growth, using a microdrilling system equipped with a 300 µm tip. The amounts of powder for each sample ranged from 50 to 120 µg. The carbonate powders were dissolved in He-rinsed borosilicate vessels at 72 °C with the addition of 99.9% phosphoric acid. The released CO_2 gas was then measured in continuous flow with a ThermoFisher MAT 253 isotope ratio mass spectrometer coupled to a Gas-Bench II. The oxygen isotope ratio was then calibrated using a reference material: IVA-Carrara ($\delta^{18}O$ = -1.91‰). Quality control was also performed using the IAEA-603 standard. The $\delta^{18}O$ results are given in ‰. In the framework of this study, we decided to use the equation provided by Chauvaud et al. (2005) who established it using recent *P. maximus* from the Bay of Brest:

$$T(^{\circ}C) = 14.84 - 3.75 \times (\delta^{18}O_{shell} - 0.164S + 5.38) \quad (5)$$

In addition to the $\delta^{18}O_{\text{calcite}}$ value, it is also necessary to assess the $\delta^{18}O_{\text{seawater}}$, which remains unknown in the case of paleoenvironments. However, this parameter can be estimated based on the salinity (S) values via the following equation (Chauvaud et al., 2005):

$$\delta^{18}O_{water} = 0.164S - 5.38 \quad (6)$$

Since *P. maximus* does not tolerate low salinity conditions (Laing, 2002; Strand et al., 1993), the water temperature was reconstructed by assuming a salinity of 31.5 and 35 psu, which corresponds to the salinity range commonly measured in marine environments.

Because profiles of trace elements and $\delta^{18}O$ were measured on two different radial ribs, it was necessary to realign the signals obtained for each shell. Given the degraded state of their surface, especially for the shell from the Landévennec Abbey, it was difficult to distinguish the daily growth lines. Furthermore, after sampling for $\delta^{18}O$ measurements, it was impossible to assign a sampling line to a specific growth increment. However, a common reference point, visible after sampling and present in both radial ribs, was used to aid in the realignment process: the first winter growth line (Figure 41). The distance of each sample (laser scans and sampling lines for $\delta^{18}O$ measurements) from this first annual growth line was measured and both signals were thus expressed as a distance to this mark. The distance values are higher for measurements near the ventral margin, and therefore lower for measurements near the umbo (Figure 41).

3 RESULTS

3.1 Oxygen isotopic composition of shells

Shell from Béniguet Island - 4500 years BP

The $\delta^{18}O$ signal was measured in *P. maximus* shells collected on the shell midden from the Béniguet Island. The $\delta^{18}O$ profile oscillated between 0.14‰ and 1.93‰, showing seasonal variations (Figure 42A). At the nearest point from the umbo, the $\delta^{18}O$ ratio was relatively low (0.79‰), and an increase in this ratio was observed as the first winter growth stop approaches. At the first winter growth line, a value close to the maxima was recorded (1.49‰). After this annual growth mark, a decrease in the $\delta^{18}O$ signal can be observed up to approximately 10 mm from the latter (in the direction of the ventral margin). The $\delta^{18}O$ value then remained stable around 0.30‰. A slight increase occurred 30 mm after the winter growth mark, with a value that reached 1.28‰ at the closest point of the ventral margin (34 mm). However, no second growth mark was visible near the ventral margin. From these $\delta^{18}O$ profiles, a reconstruction of the temperature experienced by the shell was carried out for salinities of 31.5 and 35 psu. Temperatures close to the minima (8.4 °C and 10.5 °C for a salinity of 31.5 and 35 psu, respectively) were recorded at the annual growth line while the maximum temperatures were measured farthest from this annual mark (approx. 13 °C and 15 °C recorded between 10 and 30 mm from the first winter growth line for a salinity of 31.5 and 35 psu, respectively) (Figure 42A).

Shell from the Landévennec Abbey - 13th century

The $\delta^{18}O$ signal measured in the scallop shell from the Landévennec Abbey shows similar trends to the shell from Béniguet island, with values oscillating between 0.22‰ and 2.51‰ (Figure 42B). However, this specimen showed two distinct winter growth lines, with $\delta^{18}O$ values close to the maximum recorded at their levels (1.97‰ at 0 mm and 2.14‰ at 22.1 mm of the first annual growth line). Before and after these annual growth lines, the $\delta^{18}O$ values gradually decrease and reach stable values, which are close to the minimum. For example, between both winter growth lines, the $\delta^{18}O$ profile dropped at a value of 0.34‰ at 9.1 mm from the first winter line. Depending on salinity, and similary to the previous one, the reconstructed temperatures for this shell vary between approximately 5 °C (at the level of the winter line) and 15 °C (between the two winter marks) (Figure 42B).

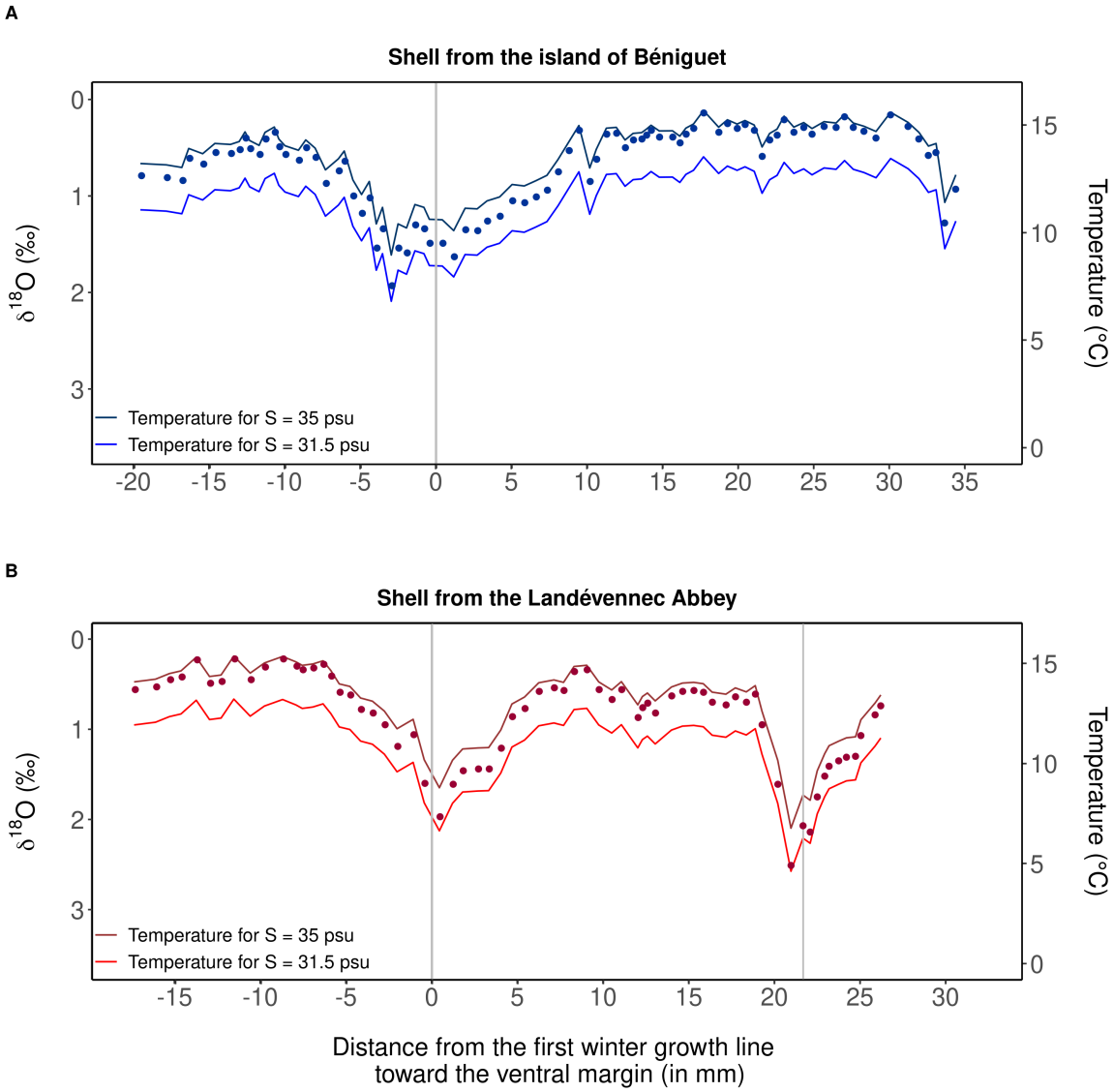

Figure 42 – $\delta^{18}O$ (inverted scale) as well as recalculated temperatures (assuming a salinity (S) of 31.5 and 35 psu - based on eq. 5) profiles for the shell from the island of Béniguet (A) and the Landévennec Abbey (B).

3.2 Ontogenetic variations of trace element ratios in shells

Shell from Béniguet Island - 4500 years BP

The $Sr:Ca_{shell}$ profile measured in the Béniguet shell follows the temperature profile (Figure 43A). The minimum Sr:Ca value (1237 µmol.mol^{-1}) was measured at the first winter line when the temperature was close to its minima. As the distance from this winter line to the ventral margin increased, $Sr:Ca_{shell}$ values progressively increased, until it reached a first plateau with values oscillating around 1500 µmol.mol^{-1} between 5mm and 16.5 mm. A second smaller increase is observed afterwards, with values oscillating around 1600 µmol.mol^{-1} from 20 mm to the ventral margin. However, although a decrease in temperature is observed near the ventral margin, no decrease in the $Sr:Ca_{shell}$ ratio is

observed in parallel (Figure 43A).

The onset of the Li:Ca_{shell} signal followed the temperature profile quite well (Figure 43B). Before the first winter growth line, the Li:Ca_{shell} values decreased from 26.8 to 13.5 µmol.mol^{-1}. The latter value corresponds to the minimum value recorded at the first winter line. After this annual growth mark, Li:Ca_{shell} signal deviated from temperature profile and values increased until they reach a value of 32.8 µmol.mol^{-1} at 6.2 mm before gradually decreasing to a value of 22.2 µmol.mol^{-1} measured at 15.6 mm. Thereafter, Li:Ca_{shell} values showed a further increase (30.3 µmol.mol^{-1} measured at 18.4 mm) which precedes a progressive decrease toward the ventral margin (23.8 µmol.mol^{-1} measured at the ventral margin).

The Mo:Ca_{shell} ratio showed a signal characterized by a baseline close to 0 µmol.mol^{-1} (Figure 43C). However, this baseline is interrupted by one significant peak measured between 10.4 and 15.3 mm, with a maximum value of 0.22 µmol.mol^{-1} measured at 11.8 mm. Between 18 and 20.3 mm, a second smaller increase in the Mo:Ca_{shell} ratio can be observed, with a maximum of 0.07 µmol.mol^{-1}. Afterwards, close to the ventral margin, the Mo:Ca_{shell} profile did not exhibit another major peak. However, it is important to note that on the other side, closest to the umbo, the end of a Mo:Ca_{shell} peak was recorded, albeit an incomplete one, with a value of 0.23 µmol.mol^{-1} measured at -13.8 mm. However, the initiation of this peak is not visible on the figure 43C.

The Ba:Ca_{shell} profile for this shell did not show any major event. The signal was very noisy, with values varying between 5.24 and 9.04 µmol.mol^{-1} (Figure 43D). The average Ba:Ca_{shell} value was 7.12 µmol.mol^{-1}.

Shell from the Landévennec Abbey - 13th century

Contrary to the previous shell, the Sr:Ca_{shell} values vary along the shell but do not followed the temperature profile (Figure 44A). Sr:Ca_{shell} values are ranging from 946 to 1330 µmol.mol^{-1}. However, low values (close to minimum) were observed near the two winter growth lines (988 µmol.mol^{-1} at 0 mm and 946 µmol.mol^{-1} at 22 mm). Between these two growth lines, where the temperature is high and stable, the Sr:Ca_{shell} profile fluctuates significantly without any noticeable trend or event. However, after the second winter line, a strong increase (from 1037 µmol.mol^{-1} at 26.53 mm to 1306 µmol.mol^{-1} at 26.75 mm) can be observed (Figure 44A).

The Li:Ca_{shell} profile showed similar fluctuations to the Sr:Ca_{shell} profile, with values ranging from 2.7 µmol.mol^{-1} to 25 µmol.mol^{-1} (Figure 44B). Low values were observed close to the winter growth line when temperatures were at their lowest. Although relatively small, three elevations in Li:Ca_{shell} values were observed while the baseline value was around 10 µmol.mol^{-1}. The first elevation occurred just after the first winter growth line, when the water temperature was increasing, with a maximum

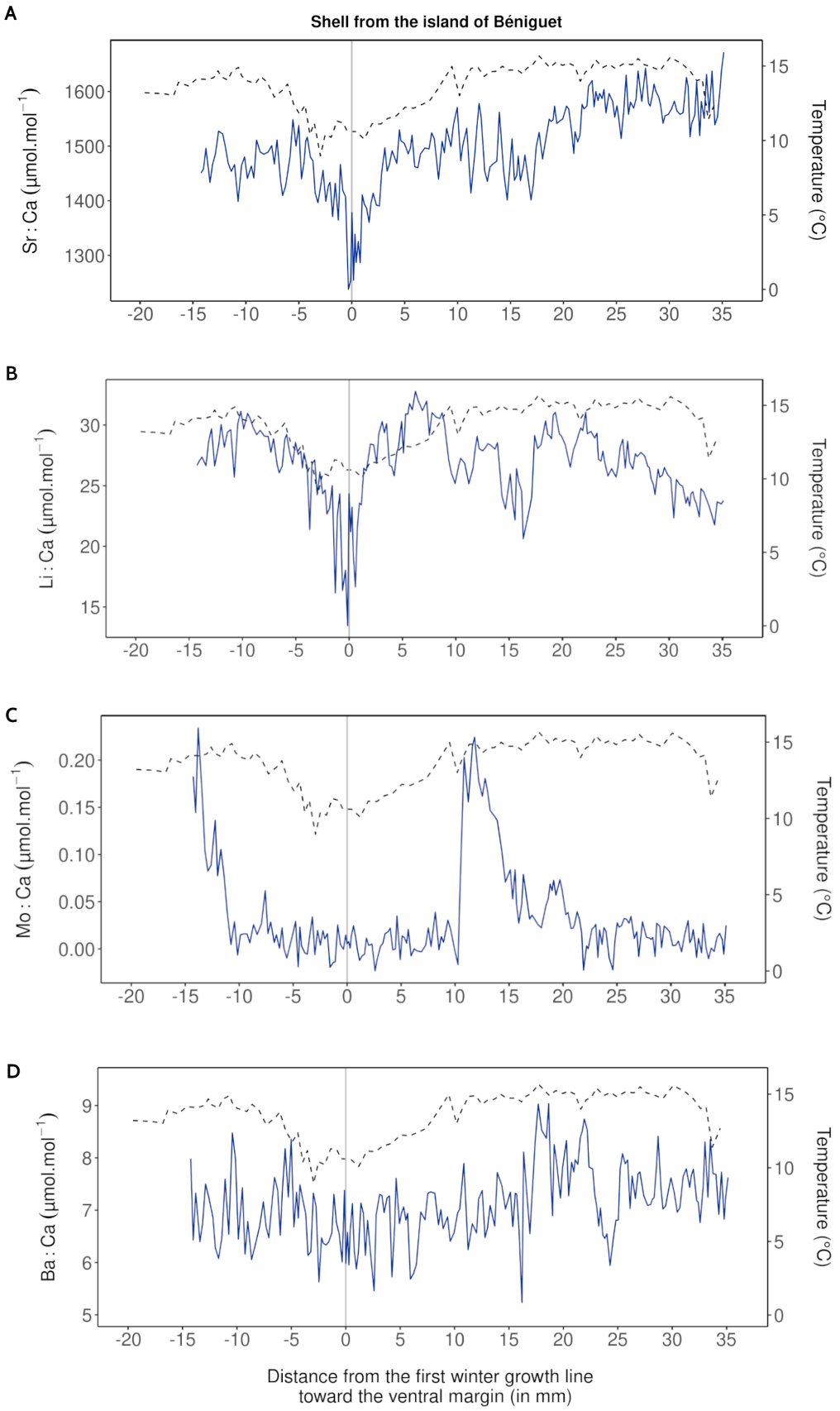

Figure 43 – Sr:Ca (A), Li:Ca (B), Mo:Ca (C) and Ba:Ca (D) profiles measured et surface of the shell of the scallop collected in the shell midden at the island of Béniguet. Temperature reconstructed from the $\delta^{18}O$ profile (dashed line) are also presented (assuming a salinity of 35 psu).

value of 17.8 µmol.mol^{-1} at 4.3 mm. The second increase occurred at 11 mm from the first growth mark, reaching a value of around 15 µmol.mol^{-1}. Finally, and similary to the Sr:Ca$_{shell}$ profile, a third peak can be observed after the second winter growth line (at 26.75 mm), with a value increasing quickly from 9.8 to 25 µmol.mol^{-1} before decreasing to around 14 µmol.mol^{-1} towards the ventral margin.

The Mo:Ca$_{shell}$ profile has a baseline with an average value of 0.1, which is interrupted by five clear and erratic peaks (Figure 44C). The first peak was observed before the first winter growth line (Mo:Ca$_{shell}$ = 0.85 µmol.mol^{-1} at -10 mm) at a time of high water temperature. The second peak (Mo:Ca$_{shell}$ = 0.35 µmol.mol^{-1}) occurred just after the winter line (between 1 and 3 mm) during the second year of shell growth when the temperature was relatively low. The third peak (Mo:Ca$_{shell}$ = 0.45 µmol.mol^{-1}) was detected in the same year of growth and it occurred at 14.5 mm when the water temperature was high. Finally, the fourth and fifth peaks appeared after the second winter growth mark. The fourth peak was recorded at 24 mm when the water temperature was increasing, with a Mo:Ca$_{shell}$ value of 0.85 µmol.mol^{-1}. The last peak (Mo:Ca$_{shell}$ = 0.54 µmol.mol^{-1}) was detected at 30.5 mm, close to the ventral margin (Figure 44C).

The Ba:Ca$_{shell}$ profile showed again a relatively noisy signal, with a baseline oscillating between 8.3 and 15.6 µmol.mol^{-1} (Figure 44D). However, a major peak was detected just after the first winter growth streak (22.5 µmol.mol^{-1} measured at 1.33 mm) when the water temperature started to increase after the winter season.

3.3 Growth rate reconstruction based on the Sr:Ca$_{shell}$ profile

The daily growth rates of each shell were recalculated using the equation of Lorrain et al. (2005) (4) and the resulting data for the three shells were combined in the figure 45. The shell from the Béniguet shell midden displays daily growth rates that range from -63 to 154 µm.day^{-1}, with the minimum value measured at the level of the winter growth band. Conversely, the shell from the Landévennec Abbey had all negative recalculated growth rate values, oscillating between -209 and -17 µm.day^{-1}. It is noteworthy that the relative amplitude between the minimum and maximum daily growth rate values is consistent across all shells, with the Béniguet island and the Landévennec Abbey shells displaying similar amplitudes of 217 and 192 µm.day^{-1}, respectively.

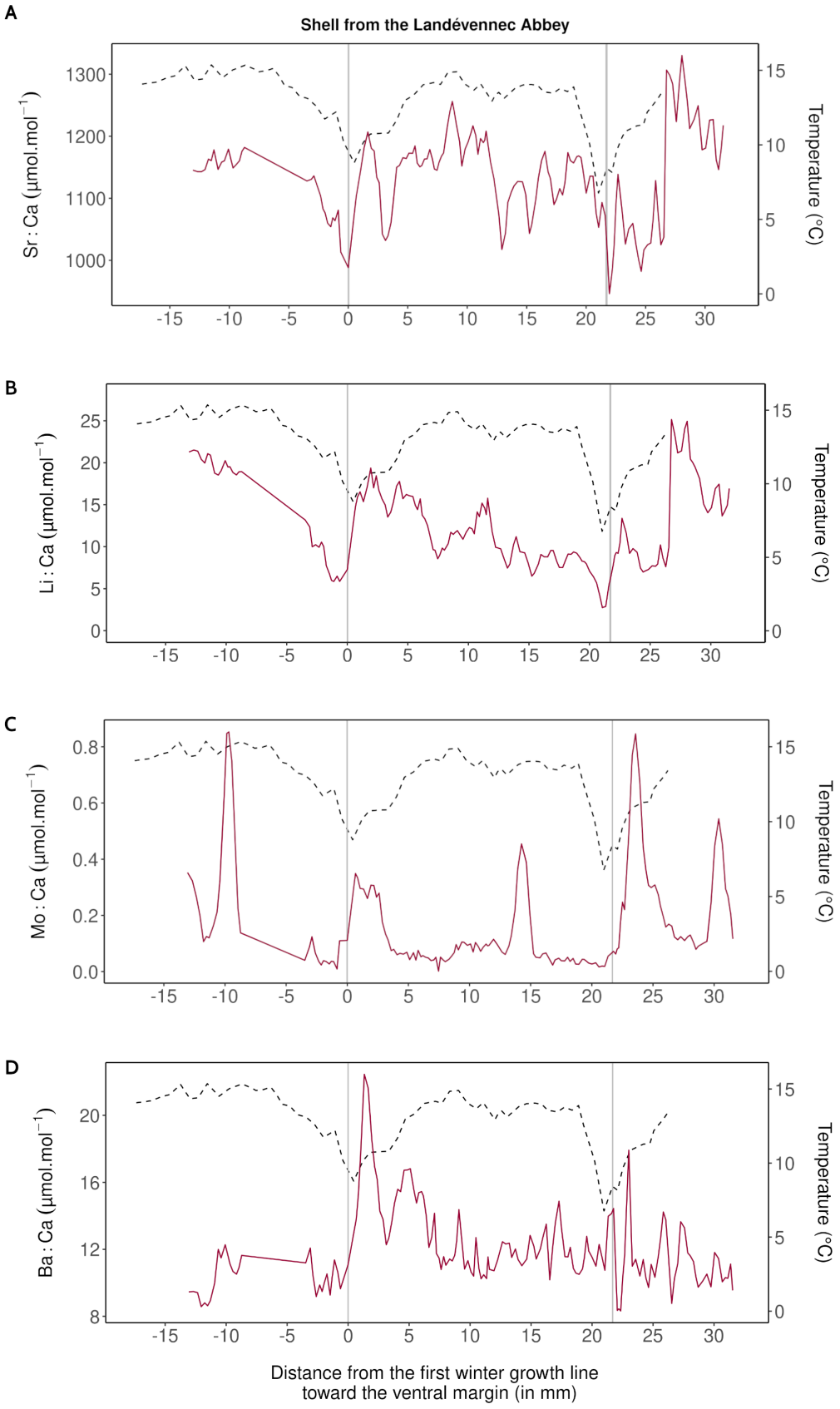

Figure 44 – Sr:Ca (A), Li:Ca (B), Mo:Ca (C) and Ba:Ca (D) profiles measured et surface of the shell of the scallop collected at the Landévennec abbey. Temperature reconstructed from the $\delta^{18}O$ profile (dashed line) are also presented (assuming a salinity of 35 psu).

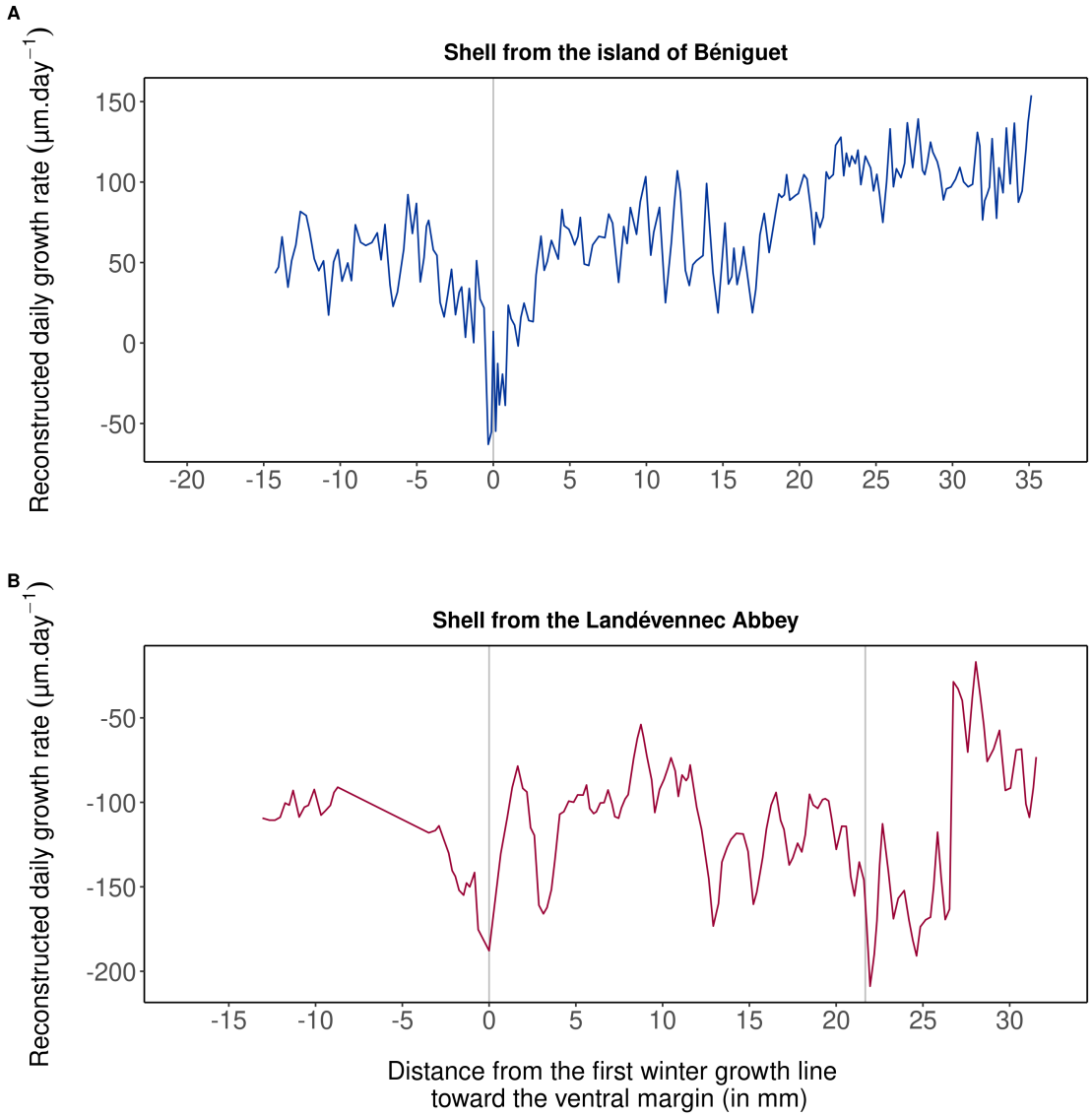

Figure 45 – Daily growth rate reconstructed from the Sr:Ca profile for the shells from the island of Béniguet (A) and the Landévennec Abbey (B).

4 Discussion

4.1 Srontium as a proxy for shell growth patterns

Accessing the daily growth rates of *Pecten maximus* specimens is crucial in an environmental perspective. This parameter is dependent on various biotic or abiotic factors such as seawater temperature, phytoplankton quantity in the water column, predation, etc. Therefore, growth pattern provides a holistic understanding of the environment that the organisms experienced but cannot quantitatively and accurately reconstruct environmental parameters. The growth data of *P. maximus* is commonly measured directly on the surface of the left valve (flat) of its shell (e.g., Chauvaud et al., 1998; Lorrain et al., 2005; Fröhlich et al., 2022a). However, due to the significant degradation of the surface of shells

analyzed in this study, especially for the specimen from the Landévennec Abbey, it was impossible to directly measure daily growth rates. This is why variations in the $Sr:Ca_{shell}$ ratio have been measured.

The study conducted by Lorrain et al. (2005) allows the calculation of daily growth rates (DGR) in archaeological shells using $Sr:Ca_{shell}$ ratio (equation 4). Here, the results indicated that the recalculated growth rates were much lower than the real ones, because of the occurence of negative values (Figure 45). This can be attributed to lower $Sr:Ca_{shell}$ ratios in archaeological shells in comparison to recent shells, which resulted in an underestimation of the actual DGR. Here, the $Sr:Ca_{shell}$ ratio ranged from approx. 1000 to 1600 $\mu mol.mol^{-1}$, while other studies mesured higher concentrations in recent shells, ranging from 1350 to 1900 $\mu mol.mol^{-1}$ (Lorrain et al., 2005; Freitas et al., 2009). Despite this, the amplitude of growth (i.e., the difference between the maximal and the minimal daily growth rate) was in accordance with previous investigations (Chauvaud et al., 1998; Lorrain et al., 2005; Thébault and Chauvaud, 2013; Fröhlich et al., 2022b), with a growth amplitude of approx. 200 $\mu m.day^{-1}$. These findings suggest that there may be a loss in the Sr content of shells over time, which could be attributed to diagenesis. Diagenesis is a term used to describe the changes that occur with time in sedimentary rocks and skeletal carbonate as a result of physical and chemical processes (Land, 1967). This can affect some trace elements such as the strontium (Brand, 1991). According to a prior research, fossil shells were found to have lower levels of Sr compared to present-day *Pecten* shells (Dauphin et al., 2007). The $Sr:Ca_{shell}$ ratios in the calcite of fossil shells were observed to be 39% lower than in recent calcite (Dauphin et al., 2007). Therefore, diagenesis could be responsible for the lower recalculated DGR values observed in the ancient shells.

Despite that loss of the Sr content within calcerous structure over time, the shell from the Béniguet shell midden exhibits a typical growth pattern with minimal growth rates in winter and maximal in summer. Nonetheless, this is not the case for the shell from the Landévennec Abbey, which showed higher variations over time. One possible explanation for this could be the differing state of degradation between these two samples. The shell from Béniguet was well-preserved and intact, whereas the one collected at the Landévennec Abbey is a fragment with a more degraded surface (the daily growth marks were not visible on it). It is possible that $Sr:Ca_{shell}$ measurements were performed not directly on the surface but on a layer deeper inside, (a few µm deeper from what was once the surface). To our knowledge, no study has measured the concentrations and the ditribution of elements on a cross-section of *P. maximus* shell. The only clue available is from Richard (2009), who measured the concentrations of a few trace elements on a cross-section at the scale of one daily growth striae and characterized their distribution over a few µm below the shell surface (150-200 µm deep) using a microprobe. It appeared that the concentrations of some elements can change significantly as we go deeper toward the inner shell layer, even after approx. 20 µm (this is the case for sodium and sulfur for example). However, the concentration of Sr seems to be the same between the surface and the shell

layer below (up to 150 µm). Nevertheless, this study did not measure the Sr concentrations throughout the entire shell's thickness and only stopped at approx. 150 µm below the shell surface. Obtaining the Sr as well as other element concentrations throughout the thickness of the shell could thus improve our understanding of the variations recorded in the specimen collected from the Landévennec Abbey. However, the degraded state of this shell does not seem to have affected the concentrations of the other elements.

Finally, a simpler explanation for these negative values, at least for the shell from the Landévennec Abbey which is more recent than that of Béniguet (and therefore less subject to diagenesis), would be that the equation given by Lorrain et al., 2005 may not be applicable to this sample. In fact, although it is only a fragment of a shell, it is probable, given the distance between the two successive winter growth lines, that the $Sr:Ca_{shell}$ measurements and calculations were made on a portion of the shell that formed between the 2nd and 3rd winters that the specimen experienced. However, the equation used here was constructed from data collected on shells that had only experienced one winter, and which therefore naturally exhibit higher DGR, since there is an ontogenic effect on growth.

4.2 Past primary production reconstruction

To our knowledge, this is the first investigation using archaeological scallop shells that aimed to track, at high temporal resolution, the past phytoplankton dynamics in a coastal ecosystems. Variations in primary production dynamics 4500 years ago and during the 13th century were reconstructed using the $Li:Ca_{shell}$, $Mo:Ca_{shell}$ and $Ba:Ca_{shell}$ profiles.

By far, the trace element that showed the most promising results is Mo. The shell from the Béniguet shell midden exhibited a $Mo:Ca_{shell}$ profile with values comparable to profiles measured within recent scallops, with a baseline close to 0 µmol.mol^{-1} and peaks culminating at values around 0.2 µmol.mol^{-1} (Thébault et al., 2022, see chapter 4 of this manuscript) (Figure 43C). However, this peak is relatively large and occurred at a time when the water temperature stopped increasing and reached a plateau of maximal values, probably at the end of spring or in early summer. Moreover, this peak occurred at a time when DGR were slightly decreasing, before increasing again once the $Mo:Ca_{shell}$ peak had passed (Figure 45A). This decrease in growth rate is also visible in the $Li:Ca_{shell}$ profile, of which variations in the shell have also been reported as an indicator of *P. maximus* growth variations (Thébault and Chauvaud, 2013) (Figure 43B). Based on the hypotheses put forward in previous investigation and on our results, it is therefore conceivable that a dinoflagellate bloom, of the genus *Gymnodinium* (or a species with similar physiological characteristics), occurred at the end of the spring season 4500 years ago. Furthermore, given the amplitude of the peak, compared to those measured in current shells, we can assume that cell concentrations during the bloom were similar

to what is observed today (approx 20,000 cell.L^{-1}). The appearance of this bloom also explains the decrease observed in growth rates, as *Gymnodinium* cells are known to produce toxic blooms, and therefore stressful conditions for scallops (Chauvaud et al., 1998). The same conclusion could be applied to the year before, with another Mo:Ca_{shell} peak that was measured. Unfortunately, this latter remained incomplete (Figure 43C).

The other hypothesis is that the occurence of these Mo:Ca_{shell} peaks could be partly due to the formation of phytoplankton aggregates (Thébault et al., 2022; see chapter 4 of this manuscript). These aggregation events often follow a diatom bloom (see chapter 2 of this manuscript). It has been reported during past investigations that the Ba:Ca_{shell} profile could be a good proxy for diatom dynamics in the water column (Barats et al., 2009; Fröhlich et al., 2022a; Fröhlich et al., 2022b; see chapter 4 of this manuscript). However, no Ba:Ca_{shell} peak could be observed on the shell from the island of Béniguet. Instead, the measured Ba:Ca_{shell} values are higher than in current shells. Here, an average Ba:Ca_{shell} value of approx. 7 µmol.mol^{-1} was measured (Figure 43D). This value is typically measured during a peak in recent shells, which showed lower baselines of approx. 1.5 µmol.mol^{-1}. This difference in Ba:Ca_{shell} baselines values is also visible for the Landévennec Abbey shell and could be due to different salinity conditions between present and past environments, since Ba concentrations in seawater depend on this parameter (Coffey et al., 1997). Along a gradient where salinity increases, Ba concentrations in seawater decrease. For instance, with a decrease in salinity from 30 to 26 psu, an increase in Ba concentrations of seawater in some estuaries was recorded, from approx. 100 to 150 nM (+50%) (Coffey et al., 1997). It can therefore be assumed that the 4500 year old and 13th century specimens experienced a lower salinity environment than today. However, no information has been found on potential reasons for the lower salinity conditions at these times in this region, but this could be explained by higher riverine inputs, wetter climate or higher precipitation rates for example. This latter hypothesis is also consistent with the lower Sr:Ca_{shell} ratios recorded in archaeological shells compared to contemporary shells, as discussed above, since Sr concentrations in seawater increase with salinity (Lawrence and Kamber, 2006). Lower salinity condition in ancient environment would therefore induce lower Sr:Ca ratios in archaeological specimens, as it was observed here. Nevertheless, with only one shell analysed for each period, it is impossible to precisely explain the actual reason for the higher Ba:Ca_{shell} (and lower Sr:Ca_{shell}) concentrations in these shells. It would therefore be interesting to verify if other specimens from the same periods and the same locations exhibit similar trends.

Concerning the shell from the Landévennec Abbey, two Mo:Ca_{shell} peaks were measured throughout one year (between the two winter growth lines). The first peak appears at the end of winter, when temperatures begin to rise in the water column (Figure 44C). The second peak occurred around mid-summer. While it is likely that this second peak may be due to the formation of a *Gymnodinium*

bloom in the environment (following the same reasoning as for the previous shell), this is not the case for the first peak, which occurred when temperatures were low, i.e., during or at the end of the winter season. In addition, this latter Mo:Ca_{shell} peak occurred at a time when a Ba:Ca_{shell} peak were also measured, which could indicate a bloom of diatoms (Figures 44C, D). Nonetheless, cells of the genus *Gymnodinium*, as well as other phytoplancton species, are not known to form important blooms in winter in the Bay of Brest (personal communication from Gaspard Delebecq). Although variations in phytoplankton communities can occur during the winter, they remain low in comparison with the summer season (Zingone et al., 2010; Trombetta et al., 2019). This winter Mo:Ca_{shell} could therefore be attributed to the formation of aggregates subsequent to a early diatom bloom, which developped exceptionally earlier due to optimal light and/or nutrient conditions. Another potential explanation for this could be that the shell from the Landévennec Abbey was harvested from another location, where phytoplankton dynamics differed from the Bay of Brest. It would have been brought there during the several pillages that the abbey underwent. Additional analyses, using other shells from the same period and site, could help to verify whether the occurrence of these winter blooms was more common during that time, and could allow us to better understand our results.

Upon analyzing both shells, it was found that the phytoplankton dynamics were similar to the present time. This is especially true for the Mo:Ca_{shell} profiles, which showed a peak at the end of spring 4500 years ago, similar to the specimens from 2011 (Thébault et al., 2022) or 2021 (see chapter 4 of this manuscript). However, the Ba:Ca_{shell} ratios measured here remain unexplained, as the only significant peak was measured during winter, when phytoplankton blooms are not typically observed. It should be noted that these results are based on only two shells from very distant times and locations, and increasing the number of specimens is necessary to accurately characterize past phytoplankton dynamics. Furthermore, radiocarbon-14 dating would allow for more precise dating of these scallops and may confirm the temporal context in which the scallops lived. Since it has not been done here, these dates could slightly deviate from the ones we assumed here (especially for the shell from the Béniguet island), as it depends on the level (in height) at which the sample was collected in the shell midden (which remain unknown). Nonetheless, given the radiocarbon datings that were carried out at different levels of the shell midden (Stéphan et al., 2011), this date value may deviate by a few hundred years (approx. 500 years), which does not significantly impact our results or interpretations. Despite the low number of analysed specimens, this investigation showed that it is possible to study archaeological material and obtain promising chemical signals that can be interpreted to reconstructed past phytoplankton dynamics.

4.3 Achaeological perspective

Scientists and archaeologists have utilized $\delta^{18}O$ signals found in various types of shells to determine when past human populations harvested particular molluscs during different seasons (e.g., Killingley, 1981; Bailey et al., 1983; Andrus, 2012; Burchell et al., 2013; Eerkens et al., 2013; West et al., 2018). This information can offer insights into the decision-making and adaptability of hunter-gatherer societies based on resource availability and potential food shortages. Additionally, it can reveal patterns of landscape use, social rituals, and economic activities that may be related to resource availability.

Our study, which presents results obtained from only two shells, each from very different historical periods, is limited in the low number of analyzed samples and therefore cannot provide the same archaeological information as the above-mentionned studies. Moreover, the occurrence of *P. maximus* shells in archaeological sites is relatively rare compared to other shellfish species. This may be because *P. maximus* is a subtidal species, and accessing it is more challenging than for intertidal species. Furthermore, the shell midden discovered on the island of Béniguet is predominantly composed of limpets *Patella* sp. (approx. 3500 *Patella* sp. discovered and only 3 *P. maximus* specimens - Dreano et al., 2007). Therefore, we suggest using shells from *P. vulgata* or other species such as mussels (*Mytilus edulis*) or abalones (*Haliotis tuberculata*), found in higher amounts in this shell midden (296 and 113 specimens, respectively - Dreano et al., 2007), for archaeological studies in the region. It would provide more robust information regarding the customs and habits of past human populations. However, *P. maximus* shells remained a more efficient archive to track variations of past phytoplankton dynamics at high temporal scales.

5 CONCLUSION AND PERSPECTIVE

This study presents the preliminary findings of the chemical composition of archaeological shells of *P. maximus*, marking the first time such results have been obtained. However, these results are not a comprehensive reconstruction of the phytoplankton dynamics of past periods. To enhance the study's validity, increasing the number of analyzed shells would be the first and more important step. Additionally, observing changes in these dynamics over time by increasing the number of temporal windows between the oldest and most recent shells would be highly beneficial. Since shells found in archaeological sites or shell middens are not always well-preserved, alternative analysis methods could be used to determine whether the chemical signals measured on the shell surface are similar to those found in cross sections. Furthermore, in sclerochronological and sclerochemical studies, only the left flat valve is typically utilized because it offers the best growth and chemical measurement

conditions. However, shell middens also contain right valves. As a result, comparing signals obtained from a left and right valve could be useful in determining the value of using the latter for these investigations. Thus, all shell materials found in the shell middens can be used in order to increase the amount of samples and refine the results and hypotheses that were put forward here. Despite these limitations, this study showed the high potential of using *P. maximus* shells to trace past phytoplankton dynamics in a coastal ecosystem through its sclerochronological and sclerochemical analysis.

DISCUSSION GÉNÉRALE, CONCLUSIONS ET PERSPECTIVES

1 SYNTHÈSE

Le principal objectif de cette thèse était de développer de nouveaux traceurs environnementaux incorporés dans les valves de *Pecten maximus* afin de reconstruire les dynamiques phytoplanctoniques passées. Cette problématique a été abordée par une approche pluridisciplinaire, combinant des domaines tels que l'écologie du phytoplancton, la biogéochimie, la sclérochronologie et l'archéologie. Les résultats et hypothèses mis en avant ont été discutés dans chaque chapitre que comporte ce manuscrit. Jusqu'à présent, les études existantes se concentraient sur les corrélations qui existaient entre les variations des concentrations en éléments traces (Li, Mo et Ba) incorporées dans les valves de la coquille St-Jacques et les variations observées dans les communautés phytoplanctoniques. Cependant, l'impact réel que provoquent les variations hautes fréquences des assemblages phytoplanctoniques sur la biodisponibilité de ces éléments pour les organismes de l'écosystème n'a jamais était établi. Afin de répondre à cette problématique, cette thèse s'est divisée en trois phases. La première a été de comprendre comment les dynamiques phytoplanctoniques impactaient les propriétés chimiques de la colonne d'eau, et comment les cellules de micro-algues pouvaient être des vecteurs de transport des éléments traces vers l'interface eau-sédiment. La seconde étape a été de calibrer les différents traceurs chimiques incorporés dans la coquille afin de retracer les variations des assemblages de phytoplancton dans la colonne d'eau. Enfin, la dernière phase a été d'appliquer les hypothèses émises à des coquilles St-Jacques collectées durant des fouilles archéologiques afin d'observer ou non des différences entre les environnements passés et l'environnement actuel.

1.1 Impact des dynamiques phytoplanctoniques sur la géochimie de la coquille de *Pecten maximus*

L'évènement majeur de ce manuscrit de thèse, ainsi que du projet HIPPO de manière générale, a été le suivi environnemental qui a été réalisé à Lanvéoc (rade de Brest) entre les mois de mars et octobre 2021 (voir chapitre 1). Ce suivi a produit un jeu de données conséquent qui a permis de mieux comprendre comment la dynamique du phytoplancton pouvait jouer un rôle sur la biodisponibilité du molybdène et du baryum pour les organismes de l'écosystème. Nous avons alors mis en évidence que les efflorescences de cellules de dinoflagellés du genre *Gymnodinium* entraînaient un accroissement des concentrations en Mo particulaire dans la colonne d'eau. Cela s'explique par le fait que ces cellules ont une affinité avec cet élément, qui est nécessaire pour leur métabolisme et l'assimilation des nutriments. L'ingestion de ces cellules par les spécimens de *P. maximus* pourrait alors engendrer un pic du rapport Mo:Ca dans la coquille. De plus, nous avons pu voir que la formation d'agrégats phytoplanctoniques, faisant suite aux principaux blooms observés, était à l'origine d'un transport significatif de Mo vers l'interface eau-sédiment. Or, il est apparu que tous les agrégats ne

transportaient pas de la même manière cet élément et que des processus chimiques plus complexes expliquant cela pouvaient rentrer en jeu. Nous avons alors émis l'hypothèse que seuls les plus gros agrégats, présentant des concentrations internes faibles en oxygène, se retrouveraient enrichis en Mo et participeraient à ce transport significatif. Ce dernier aspect a été vérifié dans le cadre du chapitre 3, durant lequel nous avons produit artificiellement des agrégats à partir de plusieurs souches phytoplanctoniques à l'aide de rolling tanks. Ces agrégats produits ont été individuellement mesurés et échantillonnés afin de vérifier s'ils se retrouvaient bien enrichis en éléments traces. Bien que nous ayons abordé cette problématique à travers une approche multi-éléments, nous avons mis en évidence que le Mo se retrouvait bel et bien accumulé au sein des agrégats phytoplanctoniques par rapport à l'eau environnante, et cela, quelle que soit la souche de micro-algue étudiée. Cela indique que l'enrichissement du Mo dans les agrégats est alors lié au processus d'agrégation et à leurs propriétés chimiques, plutôt qu'aux cellules phytoplanctoniques à partir desquelles ils sont formés. Quant au mécanisme expliquant ce phénomène, il est apparu que cet élément se retrouvait particulièrement lié aux concentrations de TEP (transparent exopolymer particles) de l'agrégat. Ces TEP sont des composés organiques produits par les cellules phytoplanctoniques qui leur permettent de s'agglomérer entre elles et qui constituent ainsi la matrice de l'agrégat. Cependant, il reste nécessaire d'entreprendre de nouvelles expériences similaires et de mesurer de nouveaux paramètres, comme la concentration en oxygène au sein des agrégats par exemple, afin d'approfondir nos hypothèses.

Concernant le baryum, les variations temporelles des concentrations de cet élément dans la colonne d'eau ont été expliquées par la succession des blooms de diatomées. En effet, au moment du bloom principal de l'année, qui a eu lieu à la fin du printemps 2021, une diminution drastique des concentrations en Ba dissous a été enregistrée, à la différence du Ba particulaire pour lequel nous avons mesuré une élévation importante au même moment. Cela suggère que le Ba passerait de la phase dissoute vers la phase particulaire en se retrouvant adsorbé sur le frustule de ces diatomées. À la fin du bloom et durant la dégradation des cellules, un transport significatif de Ba vers l'interface eau-sédiment a également été enregistré. Ce suivi environnemental a alors permis de mettre en lumière les mécanismes et les processus mis en jeu qui expliquent dans quelle mesure les variations temporelles hautes fréquences des structures des communautés phytoplanctoniques affectent la biodisponibilité du molybdène et du baryum pour les organismes benthiques, et donc pour la coquille St-Jacques.

Suite à l'établissement de ces hypothèses, il était temps de les vérifier en mesurant les concentrations de ces éléments dans les coquilles de *P. maximus* prélevées sur notre site d'étude à la fin du suivi environnemental. Brièvement, nous avons alors pu mettre en évidence que les pics de Mo:Ca mesurés dans la coquille étaient concomitants aux pics de Mo particulaire mesurés dans la colonne d'eau, et donc à la succession des différents blooms de *Gymnodinium* observés. Les hypothèses concernant le

Ba ont également pu être vérifiées, puisque les pics de Ba:Ca mesurés dans la coquille sont apparus au moment où les principaux blooms de diatomées ont été observées (voir chapitre 4). L'étude de ces coquilles a alors permis d'affiner nos connaissances sur les processus impliqués dans l'incorporation de ces éléments au sein des valves de la coquille St-Jaques. Nous avons ainsi pu calibrer ces différents traceurs chimiques des dynamiques phytoplanctoniques dans le but d'appliquer ces nouvelles connaissances à des spécimens plus anciens. Au cours de ce projet, nous avons eu la chance de pouvoir analyser quelques spécimens qui ont été collectés dans le cadre de fouilles archéologiques et qui ont vécu à des époques où l'impact des activités humaines sur les écosystèmes côtiers était inexistant.

1.2 Étude des coquilles archéologiques

À travers le dernier chapitre de cette thèse et l'étude de deux coquilles archéologiques datées d'il y a 4500 ans et du XIII^{ème} siècle, nous avons pu produire les toutes premières reconstructions à haute résolution temporelle des dynamiques phytoplanctoniques à des époques lointaines. Dans un premier temps, il est apparu qu'il était possible de mener des études sclérochimiques sur ces coquilles anciennes puisqu'elles présentent des signaux de Mo:Ca et de Ba:Ca exploitables et que les concentrations en ces éléments ne diminuent pas au cours du temps en raison de la diagenèse. Des pics significatifs de Ba:Ca, mais également de Mo:Ca, ont été mesurés au sein de ces coquilles. Les premiers résultats ont suggéré que les dynamiques phytoplanctoniques passées sont relativement similaires à celles que l'on retrouve aujourd'hui. En effet, des blooms composés d'espèces de micro-algues toxiques (comme *Gymnodinium* spp. ou d'autres espèces physiologiquement proches) ont pu être reconstruits il y a 4500 ans. Cependant, il ne s'agissait que de résultats préliminaires et une des grandes limites de cette étude a été le nombre trop faible de coquilles analysées. Les reconstructions des dynamiques phytoplanctoniques passées ne sont alors pas assez représentatives et, sans augmentation du nombre d'échantillons, il est impossible de fournir des reconstructions fiables. Afin de clairement identifier et quantifier les impacts anthropiques sur les variations des structures des communautés de phytoplancton dans la colonne d'eau, il reste encore un certain nombre d'analyses à réaliser.

2 AMÉLIORER NOS CONNAISSANCES SUR LE SUJET

À travers ce manuscrit de thèse et les conclusions qui ont été apportées, nous avons vu l'importance et l'intérêt d'utiliser la coquille de *P. maximus* dans le but d'effectuer des reconstructions à haute résolution temporelle des dynamiques phytoplanctoniques passées. Toutefois, afin de confirmer ou d'infirmer les hypothèses mises en avant ici, il est possible d'entreprendre un certain nombre d'études et d'expérimentations.

2.1 Expérimentations *in-situ*

Dans un premier temps, au vu des résultats qui ont été obtenus dans le cadre du suivi environnemental HIPPO, il serait intéressant de réitérer ce genre d'évènement en gardant la même stratégie d'échantillonnage. La répétition de ce type de suivi environnemental permettrait de déterminer s'il existe des tendances récurrentes entre les dynamiques phytoplanctoniques dans la colonne d'eau, la biodisponibilité des éléments traces et l'incorporation de ces éléments dans les coquilles de *P. maximus*. De plus, afin d'obtenir une meilleure estimation de la dynamique d'agrégation et du rôle de ces agrégats dans le transport des éléments vers l'interface eau-sédiment, il serait nécessaire d'élaborer un dispositif permettant de les échantillonner individuellement directement dans la colonne d'eau afin d'y analyser divers paramètres chimiques (concentrations en oxygène, en TEP ou en éléments traces par exemple). Les nouvelles connaissances apportées constitueraient alors une avancée majeure pour les scientifiques s'intéressant aux cycles biogéochimiques. De plus, une potentielle piste d'amélioration pour de futurs programmes de surveillance environnementale serait d'augmenter la fréquence des comptages phytoplanctoniques dans la colonne d'eau afin que le pas de temps entre les différents points de mesure soit similaire à celui des paramètres chimiques mesurés. Cela permettrait de confirmer la correspondance des différentes efflorescences avec les différents pics en éléments traces mesurés dans la colonne d'eau. Toutefois, un tel suivi nécessite une importante mobilisation de ressources humaines et financières et il paraît compliqué de pérenniser ce genre d'évènement à court terme.

Pour aller plus loin, une collection de coquilles St-Jacques, collectées quasiment chaque année depuis 1990 sous l'impulsion d'Yves-Marie Paulet à plusieurs stations de la rade de Brest, est disponible. Analyser leurs compositions chimiques permettrait de dresser une série temporelle continue à haute résolution couvrant une période d'une trentaine d'années. Une telle série fournirait des informations précieuses sur les évolutions récentes des dynamiques phytoplanctoniques et permettrait également d'affiner nos hypothèses. En effet, des comptages cellulaires ont été effectués dans le cadre de plusieurs programmes d'observations (observatoires SOMLIT et Lanvéoc, programme de science participative : Objectif plancton), notamment sur ces 10 dernières années et sur plusieurs points de la rade de Brest. Par exemple, depuis 2014, le programme de science participative 'Objectif Plancton' réalise des comptages des cellules phytoplanctoniques trois fois par an dans une quinzaine de stations situées en rade de Brest. L'analyse des coquilles disponibles permettrait donc de retracer les dynamiques phytoplanctoniques de la rade de Brest à des époques antérieures à la création de ces séries d'observations. Les hypothèses mises en avant tout au long de ce manuscrit pourrait alors se voir confirmer ou infirmer, et de nouvelles pourraient également voir le jour.

Une des limites importantes de ce genre de suivi *in-situ*, ainsi que de l'analyse de spécimens préle-

vés directement dans l'environnement, est la quantité de paramètres environnementaux, qu'ils soient biotiques ou abiotiques, qui peuvent influencer ou perturber l'incorporation des différents traceurs chimiques au sein des coquilles de *P. maximus*. Afin de les limiter au maximum, il est également possible d'entreprendre un certain nombre d'expérimentations en laboratoire dans le but de pouvoir contrôler tous ces paramètres.

2.2 Expérimentations en laboratoire

La coquille St-Jacques est une espèce qui se maintient particulièrement bien en aquarium, ce qui a permis d'effectuer plusieurs études abordant différentes problématiques par le passé. Ainsi, l'accumulation des métaux dans les tissus de la coquille (Metian et al., 2008a ; Metian et al., 2008b), les comportements d'évasion face à un prédateur (Magnesen et Redmond, 2012) ou encore les impacts de la température et de la photopériode sur la reproduction des spécimens (Saout et al., 1999) ont pu être étudiés. Dans le cadre de notre problématique, il est question de vérifier si les efflorescences phytoplanctoniques, ainsi que la formation d'agrégats, sont à l'origine des pics en éléments traces mesurés dans la coquille. Pour ce faire, maintenir des spécimens en aquarium peut s'avérer intéressant. En addition à la nourriture apportée en continu afin d'assurer les fonctions métaboliques des spécimens étudiés, effectuer un apport massif d'une grande quantité de cellules de micro-algues (afin de simuler un bloom) ou d'agrégats formés grâce à des rolling tanks, sur une courte période de temps, permettrait de vérifier comment ces évènements se retrouveraient enregistrés au sein de la coquille.

Ce genre d'expérimentation a été réalisée dans le cadre de ce projet de thèse (voir chapitre bonus dans la partie 'Annexes'). Malheureusement, les résultats obtenus n'étaient pas ceux escomptés et les interprétations restaient malheureusement pauvres. En effet, lors de l'apport de nourriture, dans notre cas un bloom de *Chaetoceros* spp. ainsi que des agrégats de diatomées, aucun enrichissement, ni en Mo, ni en Ba, n'a été enregistré dans l'eau de l'aquarium. Cela s'est alors traduit par un signal qui est resté relativement plat dans la coquille, ce qui reste logique au vu des signaux mesurés dans l'eau. Malgré cela, cette expérimentation nous a permis de fournir de potentielles pistes d'améliorations pour le futur. Premièrement, l'utilisation de jeunes coquilles St-Jacques (de classe d'âge I - qui ont vécu qu'un seul hiver) comme modèles pour ces expérimentations, et non des spécimens de classe d'âge II, serait plus adéquat. En effet, en raison des effets ontogéniques sur la croissance, les coquilles de classe d'âge I forment des incréments journaliers plus larges est plus visibles, permettant ainsi d'effectuer des mesures plus précises. De plus, alors que cette expérience s'est déroulée sur une période relativement courte (six semaines environ), il est nécessaire d'augmenter sa durée à plusieurs mois, afin de bien respecter la période d'acclimatation et de laisser le temps aux spécimens d'incorporer les éléments dans leur coquille après l'apport de nourriture. En effet, un délai de 8 à 20 jours

peut être observé entre l'apparition d'un bloom et la présence des pics en éléments traces dans la coquille (Thébault et Chauvaud, 2013 ; Thébault et al., 2022 ; Fröhlich et al., 2022b). Enfin, l'utilisation de structures et de dispositifs adéquats, assurant un apport de nourriture relativement constant pour le bon fonctionnement du métabolisme des organismes tout au long de l'expérience, permettrait une croissance optimale des coquilles sans aucune perturbation majeure. Malgré le fait que les résultats obtenus au cours de ces expérimentations ne soient pas ceux attendus, mener ce type d'expérience reste nécessaire, et même primordial, afin de mieux comprendre les processus qui influencent l'incorporation des éléments dans la coquille St-Jacques. Un autre aspect qui a pu impacter les résultats était que l'apport d'agrégats ne s'est pas fait de manière optimale. En effet, les agrégats ont été formés parallèlement en rolling tanks clos. De plus, ils ont dû être fragmentés afin de pouvoir être introduits dans l'aquarium, ce qui a pu impacter leurs propriétés chimiques. Afin de pallier ce problème, un nouvel instrument pourrait nous permettre d'apporter de manière optimale des agrégats aux coquilles St-Jacques : Le SNOWMAN (Laurenceau-Cornec et al., 2019 ; Laurenceau-Cornec et al., 2020a).

Le SNOWMAN est un nouveau dispositif qui est toujours en cours de développement, et qui consiste en une colonne rectangulaire de 2 mètres de haut environ et d'une cinquantaine de centimètres de côté. Cette colonne se remplit entièrement d'eau et est également fermée sur le dessus. Au fond de cette dernière, il est possible de venir y déposer des spécimens de *P. maximus* sur un sédiment meuble. Par des aménagements qui ne seront pas développés ici, il est possible de renouveler l'eau à l'intérieur du SNOWMAN et d'y apporter de la nourriture fraîche sans voir à déplacer où à ouvrir la colonne. Pour ce genre d'étude, l'intérêt principal du SNOWMAN est que ce dispositif présente, au sommet de la colonne, un cylindre placé horizontalement qui tourne sur lui-même (de la même manière qu'un rolling tank). En étant en rotation, il va entraîner la formation d'agrégats à l'intérieur. Une fois que ces agrégats ont atteint une taille ainsi qu'une vitesse de sédimentation suffisantes, ils vont sortir seuls du cylindre sans être fragmentés (la paroi du cylindre est pourvue de petites ouvertures) et vont sédimenter vers le fond de la colonne, et donc vont être apportés aux coquilles. Au-delà des objectifs propres à notre projet, le SNOWMAN serait un outil intéressant pour les scientifiques s'intéressant à la dynamique d'agrégation (étude des tailles et des vitesses de sédimentation de ces particules, impacts du zooplancton sur leur fragmentation, etc.). Ce dispositif permettrait alors de produire des agrégats qui atteignent naturellement le fond, sans intervention humaine, en suivant des processus similaires à ce que l'on peut observer dans la colonne d'eau.

2.3 Autres pistes à explorer

Il est très probable que la coquille St-Jacques incorpore les éléments à la suite de l'ingestion et la digestion des cellules phytoplanctoniques enrichies en ces éléments (Barats et al., 2009 ; Tabouret et

al., 2012). Afin de mieux comprendre les chemins qu'empruntent les différents éléments traces entre l'ingestion et leur incorporation dans la coquille, analyser les différents tissus mous des spécimens peut s'avérer intéressant. Cela a par exemple été fait par Thébault et al. (2022), qui ont mesuré la composition chimique du muscle adducteur, des branchies, du manteau, de la glande digestive ainsi et des gonades de spécimens de *P. maximus* durant un bloom phytoplanctonique. Ils ont ainsi pu confirmer que la principale voie d'entrée du Mo dans la coquille était clairement digestive, au vu des concentrations élevées en Mo dans la glande digestive par rapport aux autres organes. Toutefois, il est possible d'aller encore plus loin et de mesurer la composition chimique dans d'autres "compartiments" des individus. Par exemple, il serait intéressant de mesurer la composition chimique des différents fluides corporels, tels que l'hémolymphe ou le fluide extra-palléal, sachant que ce dernier joue un rôle important dans la bio-minéralisation de la coquille. Il pourrait également être intéressant de mesurer les concentrations de ces éléments dans les fèces de *P. maximus*. Analyser la composition chimique des différents organes de la coquille permettrait alors de découvrir les processus sous-jacents à l'incorporation des éléments traces dans la coquille.

Bien que mesurer la composition chimique de la coquille semble être le moyen le plus efficace de retracer les dynamiques phytoplanctoniques, d'autres paramètres peuvent également être envisagés. En effet, pour certaines espèces, comme l'ormeau *Haliotis discus*, la couleur de la coquille est dépendante de son régime alimentaire (Ju et al., 2016). Cela suggère alors que l'incorporation de pigment dans la coquille pourrait être directement dépendante des espèces de phytoplancton qu'elle a ingérées et digérées. Des études visant à identifier les pigments présents dans la coquille ont déjà été réalisées par le passé, utilisant comme modèles plusieurs espèces de mollusques (Hedegaard et al., 2006 ; Bergamonti et al., 2013). Cela se fait par des analyses à l'aide de la spectrométrie RAMAN, qui consiste à caractériser la composition moléculaire de la structure étudiée. Ces mesures présentent l'avantage d'être non destructrices pour l'échantillon, permettant de les coupler avec d'autres analyses comme les analyses LA-ICP-MS par exemple. L'utilisation du RAMAN n'a jamais été testée sur des valves de coquille St-Jacques. C'est pourquoi, afin de caractériser la composition moléculaire des coquilles, quelques échantillons ont été analysés durant ce projet. Malheureusement, les premiers spectres obtenus n'ont permis d'obtenir des informations uniquement sur les liaisons carbone-carbone, correspondant à la structure (calcite) de la coquille, et non à des liaisons traduisant la présence de pigments. Il pourrait alors être intéressant de développer une méthode d'analyse et de réaliser des tests plus approfondis afin de pouvoir identifier ces pigments. La pigmentation de la coquille pourrait ainsi être un proxy de la nature du phytoplancton (et possiblement de leurs quantités), appartenant potentiellement à d'autres taxons que ceux que les éléments traces permettent de retracer.

3 *Pecten maximus*, ARCHIVE MULTI-PROXIES, HAUTE RÉSOLUTION DE LA PRODUCTION PRIMAIRE

Au vu des différents chapitres de ce manuscrit, il est indéniable que la coquille St-Jacques est un modèle de choix pour les reconstructions à haute résolution temporelle des dynamiques phytoplanctoniques dans les écosystèmes côtiers. Ce manuscrit ouvre un grand nombre de portes pour de futures expérimentations visant à affiner les hypothèses proposées.

Notre étude s'arrête à la frontière de la rade de Brest, qui présente une dynamique phytoplanctonique qui lui est propre et qui est différente des autres écosystèmes. Toutefois, les processus et mécanismes de transport des éléments vers le benthos, ainsi que leur incorporation dans la coquille, sont probablement identiques pour des individus provenant d'autres écosystèmes. Au vu de l'aire de répartition des spécimens de *P. maximus*, s'étendant sur toute la côte ouest de l'Europe (du sud du Portugal jusqu'aux côtes norvégiennes) (Chauvaud et al., 2012), il devient possible de retracer les dynamiques phytoplanctoniques à haute résolution temporelle, en couvrant une zone géographique conséquente. Pour aller encore plus loin, bien que cette espèce ne soit présente qu'en Europe, certains taxons, que l'on retrouve dans d'autres régions du globe, sont très proches phylogénétiquement de *P. maximus*. C'est le cas par exemple de *Pecten afribenedictus* (présente sur les côtes d'Afrique du Sud), de *Pecten novaezelandiae* (présente sur les côtes de Nouvelle-Zélande), *Pecten fumatus* (présente sur les côtes sud de l'Australie), *Pecten erythraeensis* (présente en mer Rouge), *Pecten jacobaeus* (présente en mer Méditerranée), *Pecten keppelianus* (présente sur les côtes ouest de l'Afrique) ou encore *Leopecten sericeus* (présente sur les côtes ouest d'Amérique centrale), dont la ressemblance avec *P. maximus* est frappante. Appliquer toutes les hypothèses mises en avant dans ce manuscrit à ces différents modèles permettrait de comparer plusieurs écosystèmes côtiers qui sont également impactés, de manière plus ou moins importante et similaire, par l'intensification des activités anthropiques. Cela permettrait d'augmenter grandement la couverture spatiale des reconstructions hautes fréquences des dynamiques phytoplanctoniques.

Enfin, le dernier point évoqué dans ce manuscrit est l'utilisation de coquille St-Jacques provenant de sites archéologiques, afin de reconstruire les dynamiques phytoplanctoniques des paléoenvironnements. Bien que les résultats obtenus ne soient pas représentatifs de ces environnements passés, puisque chaque période est représentée par un seul échantillon, ce qui est statistiquement faible, nous avons démontré que l'analyse de ces coquilles restait possible, et que les éléments traces d'intérêt ne semblent pas souffrir du phénomène de diagenèse. Cette limitation du nombre d'échantillons est également préjudiciable pour des interprétations archéologiques, car cela ne permet pas de déterminer des saisons de collectes spécifiques, et n'apporte pas non plus de preuve concrète de consommation

de la coquille St-Jacques par des populations humaines passées. Afin d'augmenter ce nombre de coquilles archéologiques pouvant être analysées, il serait nécessaire d'entreprendre quelques études au préalable. En effet, la coquille St-Jacques possède deux valves asymétriques et toutes les études se sont concentrées jusqu'à présent sur l'analyse de la valve gauche (plate). Cependant, aucune étude n'a étudié les différences qui pourraient exister entre cette valve gauche et la valve droite (creuse). De plus, il n'est pas rare que la surface de ces coquilles soit partiellement ou entièrement dégradée. Afin de pallier cela, il serait intéressant de vérifier si les concentrations en éléments traces mesurées à la surface des valves de *P. maximus* sont similaires aux concentrations mesurées plus en profondeur, en réalisant des coupes transversales. Cela permettrait de pouvoir analyser tous les échantillons de coquilles St-Jacques que l'on retrouve dans les amas coquillers, qu'il s'agisse de valves gauches, de valves droites, ou encore de fragments de coquille dont la surface s'est retrouvée dégradée.

Il reste donc plusieurs expérimentations à mettre en place afin de répondre de manière optimale à l'objectif ultime du projet HIPPO : comparer la phénologie et les variations hautes fréquences des communautés phytoplanctoniques de l'environnement actuel avec le paléoenvironnement dans le but de quantifier l'impact de l'intensification des activités anthropiques sur les écosystèmes côtiers. Ce travail de thèse pourrait alors être un point de départ pour de futurs projets de recherche ayant pour objectif de retracer, à haute résolution temporelle, les variations dans les assemblages phytoplanctoniques à travers l'étude sclérochronologique et sclérochimique de la coquille St-Jacques, *Pecten maximus*.

ANNEXES - APPENDIX

BONUS - INCORPORATION OF TRACE ELEMENT WITHIN CALCITIC SHELLS OF *Pecten maximus* SPECIMENS: AN *in-vitro* STUDY

1 CONTEXT OF THE STUDY

This study took place one year after the end of the environmental monitoring of Lanvéoc, during which several hypotheses were put forward to explain the variations in the Li/Ca Mo/Ca and Ba/Ca ratios measured in the surface of *Pecten maximus* shells (see chapters 2 and 4). However, in order to validate the previously stated hypotheses, a laboratory experiment was carried out. Here, we added to the measurements the vanadium-to-calcium ratio (V/Ca), as this element is essential for phytoplankton (Moore et al., 1996). The interest of these experiments is to limit the environmental factors controlling the dynamics of phytoplankton and the chemistry of the water column. For about six weeks, specimens of *P. maximus* were maintained in aquariums, providing them the optimal conditions to ensure their growth. The idea of this experiment was to provide some specimens with extra food and to see how this was reflected chemically within their shells. Thus, a large quantity of diatom cells as well as aggregates formed in the laboratory from *Chaetoceros* sp. strain were supplied to some specimens. Chemical signals were then measured in the shells as well as in the aquarium water in order to observe if the element-to-calcium profiles followed the elemental enrichment in the water. This chapter presents the experimental design that was followed and the results obtained. The results will then be quickly discussed and areas of improvement will be given if future experiments with the same problematic are ever conducted.

2 MATERIAL AND METHODS

2.1 Preparation of the experiments

A total of 18 age class II shells were collected at Lanvéoc on 28 August 2022. These shells are the remaining shells from the Lanvéoc environmental monitoring and come from the cage which was located 1 m above the sediment (see chapter 1 of this manuscript). This ensured that we obtained a large number of natural shells without dredging, which could have damaged and stressed the specimens. In the laboratory, they were divided and placed in three 100 L tanks, prepared specifically for their reception (six specimens per tanks). Approximately two weeks before their arrival, a mixture of fine sand (0.5 mm - 1 mm) and larger sand grains (2 mm - 4 mm), previously cleaned, was deposited at the bottom of each tanks in order to form a layer of sediment of about 8 cm thick. Seawater, pumped from the Brest harbour (St-Anne - IFREMER), and filtered at 30 µm was added in order to renew the entire content of each tank every 24h. A photoperiod of 12 hours light and 12 hours dark was also applied. These settings will be used throughout the entire experiments. One day before the introduction of the shells, a mixture of phytoplanktonic cells composed of 70% dinoflagellate (*T-iso*) and 30% diatoms

(*Chaeteceros* sp.), produced and provided by the IFREMER station in Argenton, were introduced in each tank. An amount of 1,000,000 cells per day and per specimen was added. This mixture will be used to meet the metabolic needs of the specimens and ensure their growth throughout the entire experiments. The scallops were acclimatised in their new environment for 16 days.

2.2 Feeding source and aggregates within the cylinders

After the acclimatisation period (16 days), three of the six shells in each tank were isolated. This was done by the use of a transparent PVC cylinder (70 cm high and 30 cm in diameter), open at the top and bottom. The walls of the cylinder were incremented with slots that were 35 cm high and 10 cm wide (10 slots of this size around the circumference of the cylinders). These slots allow water to pass between the inside and outside the cylinder to ensure identical conditions (especially oxygen conditions) between both compartments. The cylinder was then placed in order to isolate three specimens without moving them, thus limiting the stress generated. Once the three scallops were isolated in each tank, a differential food supply was introduced into each cylinder. In the first tank, no special food was introduced. This tank served as an initial condition to verify if the cylinder had an effect on the incorporation of elements into the shell. This tank will be referred to as "tank$1_{control}$" for the rest of the chapter. In order to better enclose the shells, without impacting the usual food supply, a 2.5 mm mesh grid was applied around the cylinder. In the cylinder of the second tank, a large quantity of diatoms of the species *Chaetoceros* sp. has been provided to the specimens inside the cylinder. In order to prevent any exchange between the inside and the outside, the wall of the cylinder was covered with a 10 µm mesh phytoplankton net. This tank will be referred to as "tank2_{bloom}" for the rest of the chapter. In the third cylinder, aggregates formed from *Chaetoceros* sp. strain, with the use of rolling tanks, were introduced into the cylinder. These aggregates were previously photographed in order to determine their sizes. In the same way, and in order to limit the exchange between the inside and the outside of the cylinders, a phytoplankton net with a mesh size of 10 µm was applied to its wall. This tank will be referred to as "tank$3_{aggregates}$" for the rest of the chapter.

For each experiment, the cylinders were left in place for 72 hours, to give time for the shells to ingest the food provided and to ensure that nothing remained when the cylinders were removed. Thus, the removal of the cylinder will not impact the specimens outside. Once removed after 72 hours, all the specimens returned to their maintenance conditions until the end of the experiment, 19 days later. This time is very important as there can be a time lag between the ingestion of trace elements and their incorporation into the shell, estimated at 8 to 20 days (Thébault and Chauvaud, 2013; Fröhlich et al., 2022b). The experiment therefore ended 19 days after the removal of the cylinders. All shells were

then recovered, dissected, and analysed for their trace element compositions following the protocols outlined in the chapter 4 and 5. In order to facilitate the understanding of the experimental process, figure 46 shows the experimental scheme that was followed.

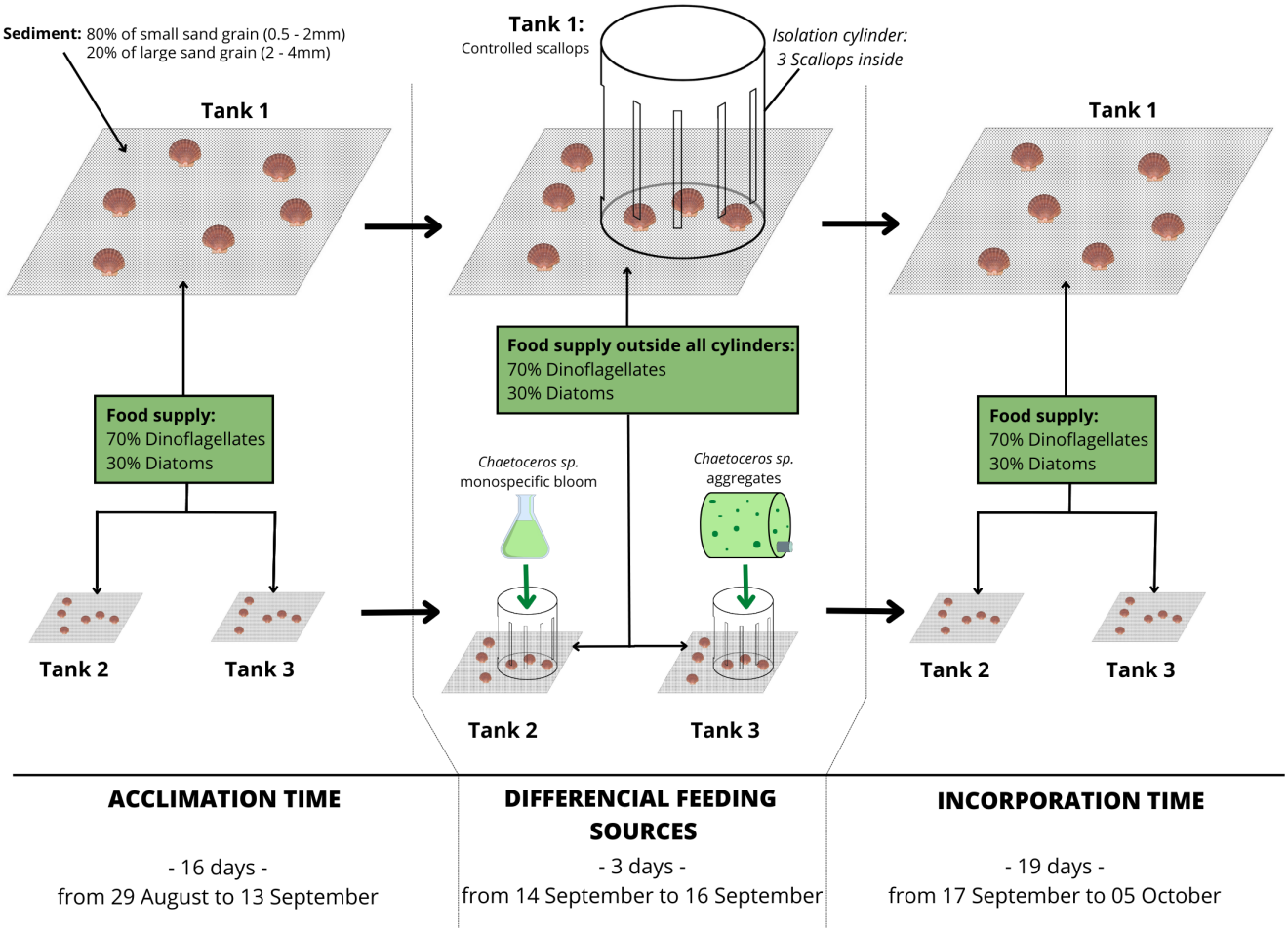

Figure 46 – Experimental design followed during this study.

2.3 seawater sampling and analyses

During the whole experiment, from the acclimatisation to the incorporation period, water samples were collected from each tank every day or every two days, in order to measure the concentrations of trace elements in the particulate and dissolved fractions as well as the particulate organic carbon (POC). In addition, a cell count was performed every day with a cytometer to monitor the phytoplankton cell concentration in each tank and adjust their input if the measured value deviated from the targeted value. These seawater samples were collected at mid-height of tanks, using a syringe to fill a 2 L PTFE bottles. At the time the cylinders were in place, these samples were collected every day, both inside and outside the cylinder for each tank.

POC and trace element concentrations were measured based on the same protocols as described

in the chapter 2 of this manuscript. The concentrations of trace elements in the particulate fraction will be expressed as an element-to-POC ratio.

2.4 Shell analyses

The *P. maximus* shells were recovered after the experiment, on 05 October, and were immediately dissected. Each sample were then photographed under reflected light (Zeiss, KL 2500 LCD) using an AxioCam MRc5 RGB camera installed on a Zeiss Lumar. V12 stereomicroscope equipped with a motorized stage. Photomosaics were constructed using AxioVision 4.9.1 software (Zeiss). Prior to chemical analyses of their calcitic material, shells slabs were obtained by cutting a 5 mm width portion between two radial ribs from the ventral margin to the second winter growth line (Figure 41) in order to fit the shell into the laser ablation chamber. For the measurements of their Li:Ca, V:Ca, Mo:Ca and Mo:Ca content, the shells were analysed following the same protocols as mentioned in the chapters 4 and 5 of this manuscript (see figure 32B, 41). However, the measurements were made only on the last 40 increments and not from the whole year of growth. Element-to-calcium profiles were then averaged between the three shells that experienced the same conditions.

3 RESULTS

3.1 Lithium profiles within seawater and shells

Lithium concentrations in the dissolved fraction (DLi) in the three tanks ranged from 27 µmol.L^{-1} to 45 µmol.L^{-1}. A tendency of progressive increase after the withdrawal of the cylinder (after 16/09) can be observed in all the aquariums, with values which changed on average from 35 µmol.L^{-1} just before the removal of the cylinders (on 16/09) to 43 µmol.L^{-1}on 05/10 (Figure 47 - blue curves). Inside the cylinders, the DLi values measured were identical, or at least very close to the values measured outside the cylinders (Figure 47 - blue bars). Only the water inside the cylinder of $tank2_{bloom}$ showed slightly higher DLi values than the seawater outside. On the other hand, the measurements of lithium in the particulate fraction (PLi) showed different patterns in the three tanks with a PLi:POC ratio that ranged from 25 µmol.mol^{-1} to 431 µmol.mol^{-1}. However, in $tank1_{control}$ and $tank2_{bloom}$, at the time the cylinder was in place, a peak in PLi:POC wa observed which reached a value of 960 µmol.mol^{-1} on 15/09 in $tank1_{control}$ and 652 µmol.mol^{-1} on 14/09 in $tank2_{bloom}$ (Figure 47 - red curves). Furthermore, the PLi:POC values measured inside the cylinders were similar to those measured outside, with the exception of $tank2_{bloom}$, where the values measured inside the cylinder were lower (65 µmol.mol^{-1} on average) than outside (482 µmol.mol^{-1} on average over the three days when the cylinder was in place) (Figure 47 - red bars).

Regarding the $Li:Ca_{shell}$ signals measured within the shells, no significant modification was recorded after the introduction of the cylinders, whatever the experiment (Figure 47 - lower panels). This was statistcally confirmed by the calculation of the Speraman's rank correlation coefficients between the $Li:Ca_{shell}$ signals for shells that were inside the cylinder and the $Li:Ca_{shell}$ measured in the shells that were outside for each tank ($tank1_{control}$: rho = 0.41 and p-value < 0.05; $tank2_{bloom}$: rho = 0.49 and p-value < 0.001; $tank3_{aggregate}$: rho = 0.73 and p-value < 0.001) (Figure 47 - lower panels). However, a common trend in all three experiments, with a progressive decrease in $Li:Ca_{shell}$ values, can be observed. Indeed, at the beginning of the experiment, the $Li:Ca_{shell}$ values measured in the shells were 27 µmol.mol^{-1} and this value dropped to 20 µmol.mol^{-1} in tanks$1_{control}$ and $tank2_{bloom}$, and to 17 µmol.mol^{-1} in $tank3_{aggregate}$ on 05/10 (Figure 47 - lower panels).

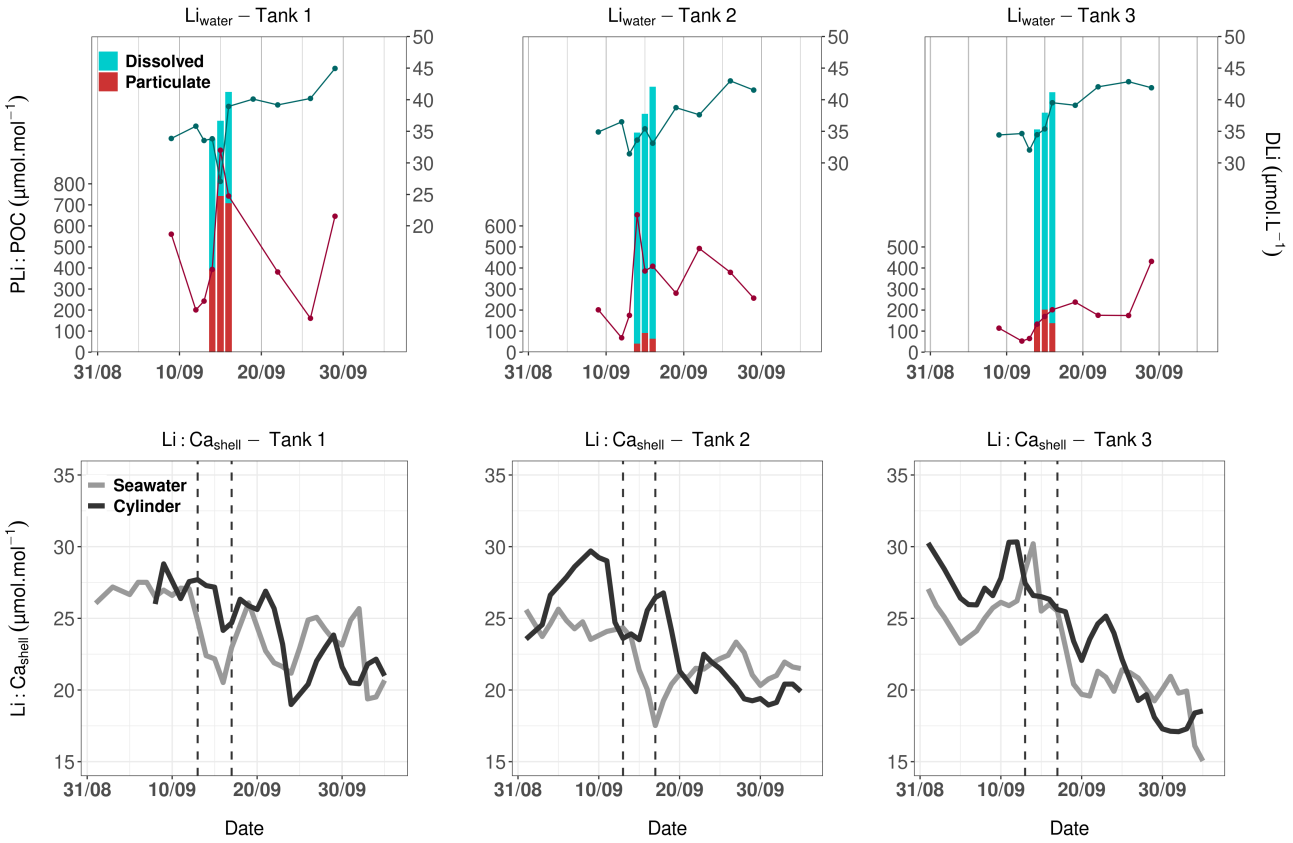

Figure 47 – (Upper panels) DLi and PLi:POC measurements of the seawater outside the cylinder (blue and red curves, respectively) as well as inside the cylinder when they were in place (blue and red bars, respectively). (Lower panels) $Li:Ca_{shell}$ measured within the *P. maximus* shells that were placed outside (grey curves) and inside (dark line) the cylinder. The time intervall during which the cylinders were in place is represented by the two vertical dashed lines.

3.2 Vanadium signals within seawater and shells

In the dissolved fraction, vanadium concentrations (DV) oscillated between 0.023 and 0.031 µmol.L^{-1} and remained relatively stable over the course of the experiment, despite a very slight decrease occur-

ring on 15/09 and 16/09 in tanks1$_{control}$ and tank2$_{bloom}$, respectively (Figure 48 - blue curves). Inside the cylinders, DV concentrations were similar to those recorded outside (0.028 µmol.L^{-1} on average in tank1$_{control}$; 0.029 µmol.L^{-1} on average in tank2$_{bloom}$; 0.031 µmol.L^{-1} on average in tank3$_{aggregate}$) (Figure 48 - blue bars). Concerning the vanadium concentrations in the particulate fraction (PV), the PV:POC values oscillated globally between 20 and 250 µmol.mol^{-1} in the three tanks (Figure 48 - red curves). Howewer, an increase can be observed and occurred only in tank1$_{control}$ on 16/09, with a PV:POC value that reached 462 µmol.mol^{-1}. Once again, the PV:POC concentrations recorded in the cylinders are relatively similar to those measured outside (Figure 48 - red bars). The PV:POC peak found in the tank1$_{control}$ also occured inside the cylinder, while the values remain stable in the cylinders of tank2$_{bloom}$ and tank3$_{aggregate}$ (on average 48 µmol.mol^{-1} and 98 µmol.mol^{-1} respectively). However, unlike the other two tanks, and like lithium, the PV:POC values measured inside the cylinder of tank2$_{bloom}$ are slightly lower than those measured in the seawater outside the cylinder.

Within the shells, no particular trend seems to emerge and no significant difference is observed between the V:Ca$_{shell}$ profils of shells that were inside the cylinder and those that were outside in tank1$_{control}$ (Spearman's rank correlation: rho = 0.55; p-value < 0.01) and tank3$_{aggregate}$ (rho = 0.56; p-value < 0.01) (Figure 48 - lower panels). In contrast, in tank2$_{bloom}$, in which a massive addition of diatoms was brought inside the cylinder, a significant difference in the V:Ca$_{shell}$ signals between the shells that were inside and outside the cylinder occurred (rho = -0.21; p-value > 0.1). Several days later, an increase in V:Ca$_{shell}$ values was observed only in the shells that were inside the cylinder, with a maximum of 0.072 µmol.mol^{-1} measured on 28/09, whereas the values oscillated between 0.020 and 0.030 µmol.mol^{-1} during the rest of the experiment. This increase in the V:Ca$_{shell}$ ratio within the shells that were outside the cylinder was not present (48 - lower panel (tank 2)).

3.3 Molybdenum signals within seawater and shells

The evolution of molybdenum concentrations in the seawater during the experiment did not show any particular pattern, as lithium and vanadium. The concentration of Mo in the dissolved fraction (DMo) fluctuated between approx. 0.125 µmol.L^{-1} and 0.175 µmol.L^{-1}(Figure 49 - blue curves). In tank1$_{control}$, a slight increase was observed between the beginning of the experiment (0.132 µmol.L^{-1}) and the end (0.182 µmol.L^{-1}). In tank2$_{bloom}$, the signal remained relatively stable, with an average value of 0.132 µmol.L^{-1} over the whole experiment. In tank3$_{aggregate}$, a strong decrease of DMo concentration was observed at the beginning of the experiment until 15/09, when the cylinder was in place (from 0.181 µmol.L^{-1} on 09/09 to 0.124 µmol.L^{-1} on 15/09). Afterwards, a slight increase can be observed until 22/09 (0.150 µmol.L^{-1}) (Figure 49 - blue curves). The DMo measurements inside the cylinders were close to the DMo values measured outside in the three tanks, with the exception of the

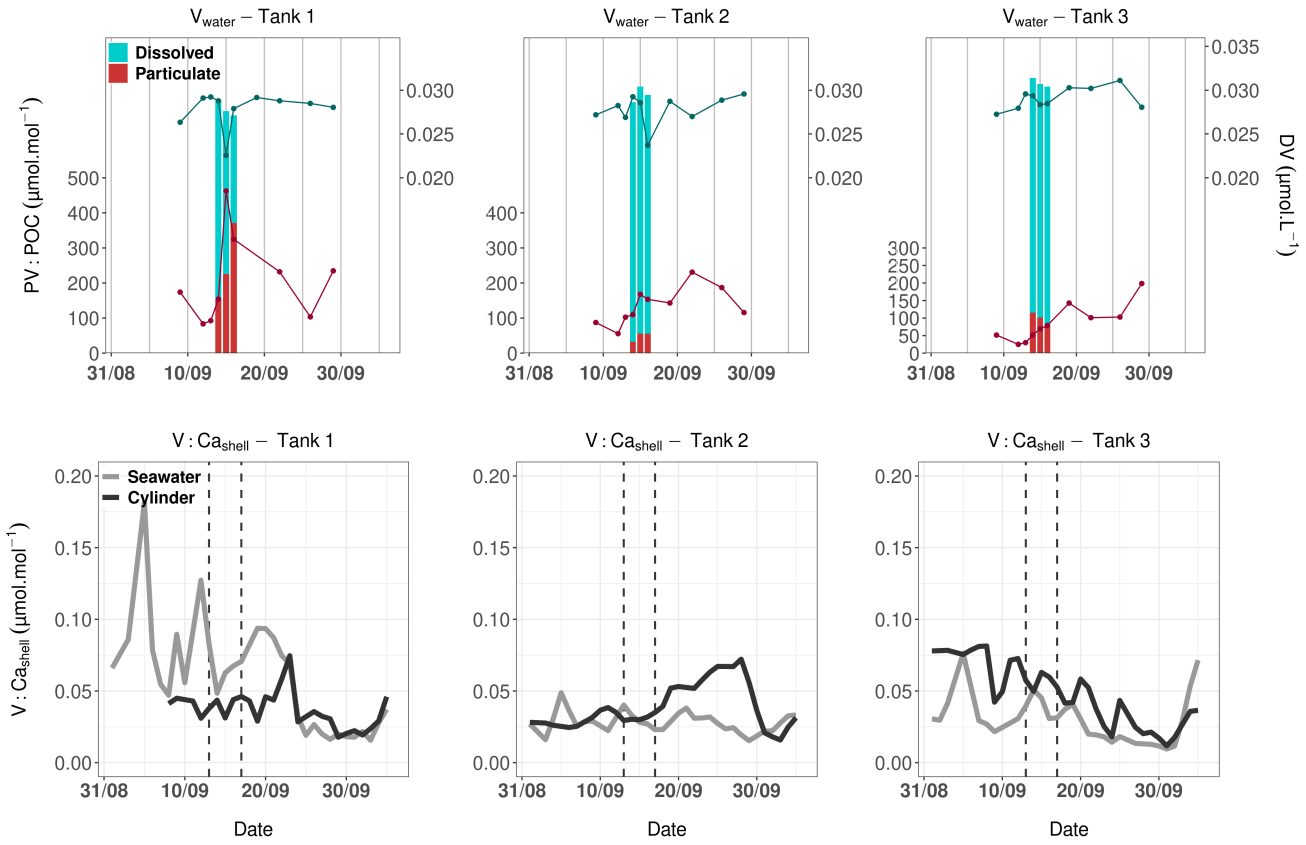

Figure 48 – (Upper panels) DV and PV:POC measurements of the seawater outside the cylinder (blue and red curves, respectively) as well as inside the cylinder when they were in place (blue and red bars, respectively). (Lower panels) V:Ca_{shell} measured within the *P. maximus* shells that were placed outside (grey curves) and inside (dark line) the cylinder. The time intervall during which the cylinders were in place is represented by the two vertical dashed lines.

value measured on 16/09 in the $tank3_{aggregate}$ only, which exceeds it largely (0.187 µmol.L^{-1}inside and 0.130 µmol.L^{-1} outside the cylinder) (Figure 49 - blue bars). Concerning Mo variation in the particulate fraction (PMo), the PMo:POC ratio remained stable and oscillated between 2 and 20 µmol.mol^{-1} in the three tanks (Figure 49 - red curves). It is important to note that a peak of PMo:POC was present when the cylinder was present only in $tank1_{control}$, with a value that reached a value of 32 µmol.mol^{-1} on 16/09. On the other hand, the PMo:POC values in the cylinders and those measured outside differed slightly in the three tanks (Figure 49 - red bars). In $tank1_{control}$ and $tank2_{bloom}$, the values measured inside the cylinders are lower than outside (15 and 24 µmol.mol^{-1} on average inside and outside in $tank1_{control}$, respectively; 7 and 16 µmol.mol^{-1} on average inside and outside in $tank2_{bloom}$, respecticely) whereas the opposite trend is observed in $tank3_{aggregate}$, with a higher value inside the cylinder (12 µmol.mol^{-1}) than outside (6 µmol.mol^{-1}) (Figure 49 - upper panels).

As lithium, none of the three experiments showed a significant difference in Mo:Ca_{shell} signals whether the shells grew inside or outside the cylinder ($tank1_{control}$: rho = 0.86, p-value < 0.05; $tank2_{bloom}$: rho = 0.91, p-value < 0.001; $tank3_{aggregate}$: rho = 0.85, p-value < 0.001) (Figure 49 -

lower panels). However, progressive decreases in Mo:Ca_{shell} ratios were also observed in the three tanks, with a decrease of about 0.02 µmol.mol^{-1} between the beginning of the experiment and the end. On the other hand, it is important to note that in tank3$_{aggregate}$, an increase was recorded between 02/10 and 05/10 with a value that changed from 0.028 to 0.043 µmol.mol^{-1} for shells that grew outside the cylinder, and from 0.028 to 0.050 µmol.mol^{-1} for shells that grew inside (Figure 49 - lower panels).

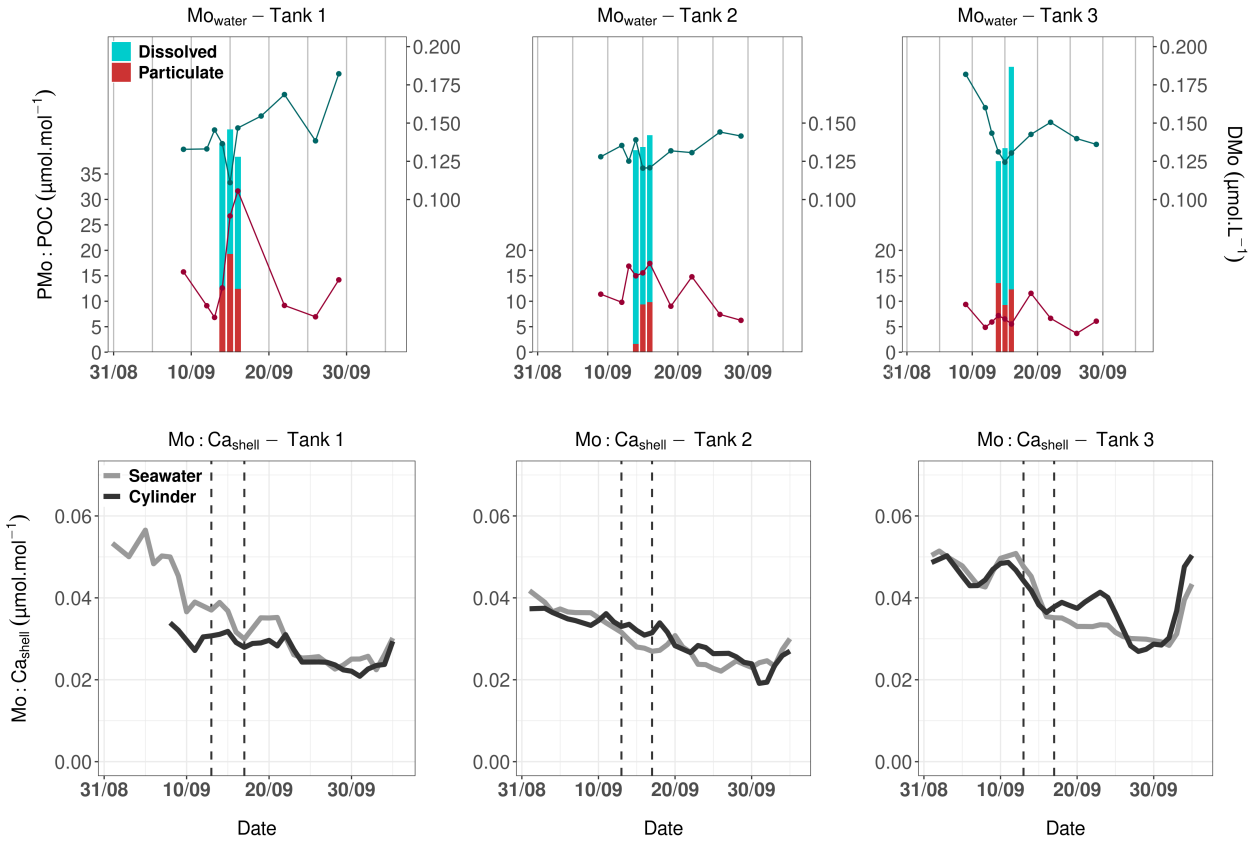

Figure 49 – (Upper panels) DMo and PMo:POC measurements of the seawater outside the cylinder (blue and red curves, respectively) as well as inside the cylinder when they were in place (blue and red bars, respectively). (Lower panels) Mo:Ca_{shell} measured within the *P. maximus* shells that were placed outside (grey curves) and inside (dark line) the cylinder. The time intervall during which the cylinders were in place is represented by the two vertical dashed lines.

3.4 Barium signals within seawater and shells

The variations of dissolevd barium (DBa) measured in the seawater during the experiments did not present any new pattern in comparison with the other elements already mentioned. The DBa values oscillated between 0.036 and 0.049 µmol.L^{-1} and remained relatively stable over the three experiments (Figure 50 - blue curves). It is important to note that a punctual decrease in DBa concentration is observed only in tank1$_{control}$ on 15/09, when the cylinder was in place. At the same time, and like other elements, a significant increase in the PBa:POC ratio was observed in tank1$_{control}$, with a value

that went from 55 to 201 µmol.mol^{-1} in one day before progressively dropping to its initial value of 50 µmol.mol^{-1} (Figure 50 - red curves). In the two other tanks, the PBa:POC signals did not show any significant peak. In tank2$_{bloom}$, the signal remains stable with values fluctuating between 24 and 81 µmol.mol^{-1} while in tank3$_{aggregate}$, this ratio showed a progressive increase between 12/09 (11 µmol.mol^{-1}) and 22/09 (123 µmol.mol^{-1}) before falling back to a value of 31 µmol.mol^{-1} on 26/09 (50 -red curves). Regarding barium in the particulate fraction (PBa), the PBa:POC measurements inside the cylinders showed no difference with the outside (Figure 50 - red bars). This was also the case for Ba concentrations in the dissolved phase (Figure 50 - blue bars). The only exception was the PBa:POC ratio measured in tank2$_{bloom}$, which has a lower value inside the cylinder (14 µmol.mol^{-1}) than outside (72 µmol.mol^{-1}).

In the Ba:Ca$_{shell}$ signals measured within the shells, this decreasing trend was again present for this element, as it was observed for the others (Figure 50 - lower panels). This is particularly noticeable in tank2$_{bloom}$ with values that dropped from 2.47 and 2.50 µmol.mol^{-1} at the beginning of the experiment to 0.84 and 1.06 µmol.mol^{-1} at the end for shells that grew inside and outside the cylinder, respectively. In addition, the Ba:Ca$_{shell}$ profiles were statistically similar for all three conditions between shells that received a differentiated food supply and shells that did not (tank1$_{control}$: rho = 0.83, p-value < 0.001; tank2$_{bloom}$: rho = 0.67, p-value < 0.001; tank3$_{aggregate}$: rho = 0.80, p-value < 0.001). However, it is interesting to note that for the shells in tank1, a shift exists between the Ba:Ca$_{shell}$ values with a mean value of 1.17 µmol.mol^{-1} for specimens that grew inside the cylinder and a mean value of 2.14 µmol.mol^{-1} for those which were outside (Figure 50 - lower panels).

4 DISCUSSION AND AREAS FOR IMPROVEMENT

Here, the results showed that no major events (in terms of water chemistry) took place at the time of the diatom bloom or the aggregate supplies. Indeed, no major enrichments in Li, V, Mo or Ba in the particulate fraction were observed in the seawater when the bloom and the aggregates were introduced. This suggests that adding a large quantity of cells at once is not enough to create a real enrichment in uor tanks. It might have been necessary to artificially enrich the phytoplankton culture, with mono-elemental solutions for example, before introducing cells into the cylinder. Moreover, the addition of aggregates did not cause any enrichment of PMo in the water of the aquarium. There are several reasons for this. Firstly, in order to make sure that the aggregates were available on the date when the feeding was supposed to take place, their formation started seven to ten days before, with the use of rolling tanks. The aggregates, which formed in a few days, remained for a long time in a closed environment (no water renewal). Therefore, the Mo pool could have been consumed during this time. Moreover, in order to be able to pour the aggregates into the cylinder, they had to be broken

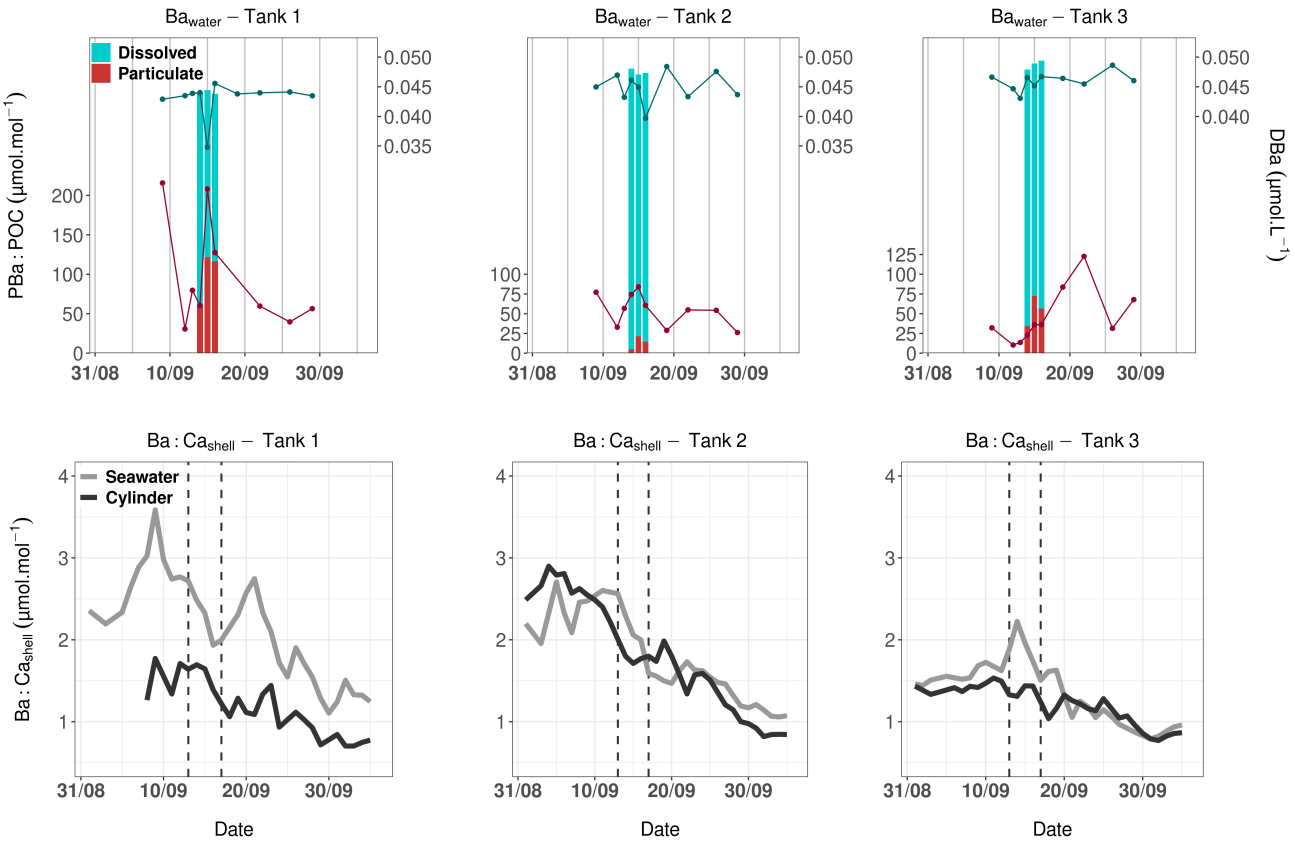

Figure 50 – (Upper panels) DBa and PBa:POC measurements of the seawater outside the cylinder (blue and red curves, respectively) as well as inside the cylinder when they were in place (blue and red bars, respectively). (Lower panels) Ba:Ca$_{shell}$ measured within the *P. maximus* shells that were placed outside (grey curves) and inside (dark line) the cylinder. The time intervall during which the cylinders were in place is represented by the two vertical dashed lines.

just before, which may have diluted the elements they transported in the water. For this purpose, the use of a new instrument, still under development, could overcome the issues we met: the SNOWMAN (Laurenceau-Cornec et al., 2019; Laurenceau-Cornec et al., 2020a).

The SNOWMAN is a new device that consists of a rectangular column of about 2 metres high and approx. 50 cm square. This column folds up entirely of seawater and is closed on top. By means of devices that will not be developped here, it is possible to renew the water inside the SNOWMAN and to bring in fresh food without having to move or open the column. At the bottom of the column, it is also possible to deposit specimens of *P. maximus* on a sandy sediment. For this type of study, the main interest of the SNOWMAN is that this device presents, at the top of the column, a horizontally placed cylinder which rotates on itself (in the same way as a rolling tank). As it rotates, it will promote the formation of aggregates inside. Once these aggregates have reached a sufficient size and sedimentation speed, they will leave the cylinder on their own without being fragmented (the wall of the cylinder presents small openings) and will sediment towards the bottom of the column, and thus will be brought to the *P. maximus* specimens. Beyond the objectives of our project, the SNOWMAN

would be an interesting tool for scientists interested in the dynamics of aggregation (study of the sizes and sedimentation speeds of these particles, impacts of zooplankton on their fragmentation, etc.). This device would then make it possible to produce aggregates that naturally reach the bottom while following processes similar to those observed in the environment.

However, we are still convinced that this kind of experiment is necessary to confirm the hypotheses put forward so far. Nonetheless, the protocol must be modified in order to obtain the best possible results. The use of the cylinders, that were designed for this experiment, seemed appropriate since no exchange occurred between the inside and the outside in tank2 and tank3 (this was visible with the cytometer measurements). However, the use of a plastic grid in tank1, to partially enclosed the specimens, might be at the origin of the element-to-POC ratio elevations for all elements (Figure 47, 48, 49, 50). This can be explained by a degradation of this grid in contact with seawater, which affected the chemistry of the water. However, no enrichment period occurred inside the cylinder, when the diatom bloom and the aggregates were provided, in comparison with the seawater outside the cylinder. Logically, this translated into trace element profiles that remained flat in the shells, without any clear peak. For this experiment, we were confronted with several time constraints, forcing us to shorten the experiments. As a first area of improvement, these experiments must take place over a longer time (during at least a few months) or even during a whole year of growth (i.e., from February to November for example), during which the shells will be maintained in a controlled environment. Moreover, we also suggest the use of age-class I shells (which experienced only one winter season) and not age-class II, in order to obtain a better resolution of the trace element measurements. In fact, the shell used here presented increments that were very narrow, and it was difficult to accurately target one specific increment for the laser ablation. The food that was provided during the entire experiments (mixture of 70% *T-iso* and 30% *Chaetoceros* sp. for the maintenance of specimens must also be continuous and constant, in order to optimise their growth (which was not the case here). With this new experimental scheme, several food supplies (that will be brought inside the cylinder) could then be provided and tested (e.g., other diatom or *Gymnodinium* sp. blooms, aggregates formed from other species, etc.). We believe that a minimum time of four weeks should be applied after the addition of food and the ingestion of cells to let time for the different elements to be incorporated into the shells. Such experiments remain important, as they would allow us to better understand the processes that drive the incorporation of trace elements into the shell of *P. maximus*, while limiting the environmental factors that can disrupt these mechanisms. The hypotheses put forward so far could thus be confirmed or invalidated, and new questions could be raised. This is particularly true if the SNOWMAN is ever used for such experiments, which would allow a better understanding of the benthic-pelagic couplings and how aggregates influence the geochemistry of shells.

SUPPLEMENTS CHAPTER 4

Relationship between phytoplankton-associated trace element load, shell physiology and shell geochemistry to approximate the trace element uptake by scallops

Episodes of trace element enrichments in scallop shells (i.e., Ba/Ca_{shell}, Mo/Ca_{shell} and Li/Ca_{shell}) were demonstrably related to phytoplankton dynamics occurring in the water column (see discussion in the main text). For instance, the timing and magnitude of Ba/Ca_{shell} peaks were attributed to blooms of various phytoplankton species (mainly diatoms) that contain species-specific amounts of cellular Ba. Based on this underlying assumption, the amount of diatom-associated Ba in the seawater is controlled by the abundance of a given diatom species (cell concentration) and the Ba load contained in each cell (Fig. S1; Step 1 and 2). The daily shell growth rate measured on the shell surface (Fig. S1; Step 3) can be converted into total daily shell height (ht_{Shell}; in mm; Fig. S1; Step 4) allowing to estimate the soft tissue dry weight ($wt_{Soft\ tissue}$; in g) according to the allometric relationship:

$$wt_{Soft\ tissue} = 2.974 \times 10^{-7} \times ht_{Shell}^{3.817} \quad (1)$$

provided by Lorrain et al. (2004). Additionally, the soft tissue dry weight (Fig. S1; Step 5) can be used to approximate the filtration rate at each day (Fig. S1; Step 6), according to the weight standardized filtration rate of 5 L h^{-1} g^{-1} of soft tissue dry weight (value discussed in the main text). On a theoretical basis, the amount of Ba that is ingested by a scallop at each day (Fig. S1; Step 7) can then be deduced using the amount of water that was filtered per day and the diatom-associated Ba concentration in the seawater (Fig. S1; Step 2), assuming that the total pool of diatoms in each liter is retained and digested by the bivalve. Aside from the soft tissue dry weight, the shell weight (wt_{Shell}; in g) can also be determined given the allometric relationship to shell height (Lorrain et al., 2004):

$$wt_{Shell} = 4.09 \times 10^{-4} \times ht_{Shell}^{2.701}. \quad (2)$$

This information about the shell weight (Fig. S1; Step 8) is required to compute the absolute amount of Ca that got precipitated at each day (Fig. S1; Step 9). Given that the shell material is composed of calcium carbonate ($CaCO_3$) as well as a small amount of carbonate bound organic matter (< 5 wt%), a pure Ca content of 38 wt% can be assumed which is in agreement to previous Ca measurements on

bivalve shells (M. Richard, 2009 and Marali et al., 2017). Accordingly, the Ca precipitation rate (Ca; in g day^{-1}) is calculated as:

$$Ca = \left[wt_{Shell(d)} - wt_{Shell(d-1)} \right] \times 0.38, \quad (3)$$

i.e., the Ca-proportion of the shell material deposited between two consecutive days (i.e., $wt_{Shell(d)}$ and $wt_{Shell(d-1)}$). Considering that about 63 % of the total Ba content of scallops (soft tissues plus shell) is located in the shell (Barats, 2006), the amount of Ba incorporated into the shell material during each day (Fig. S1; Step 10) can be approximated from the totally ingested Ba (Fig. S1; Step 7). In combination with the daily precipitated amount of Ca (Fig. S1; Step 9), the Ba/Ca_{shell} weight ratios (Fig. S1; Step 11) as well as the molar ratios (Fig. S1; Step 12) can be calculated. Finally, the theoretically measured Ba/Ca_{shell} profile can be obtained taking into consideration that apart from the Ba in the particulate phase, the dissolved Ba also contributed to the Ba/Ca_{shell} background. This Ba/Ca_{shell} background signal can be approximated from the dissolved Ba/Ca ratio in the seawater ($Ba/Ca_{Seawater}$) and a previously determined partition coefficient (D_{Ba}) of 0.11 (Barats et al., 2009):

$$Ba/Ca_{Shell} = D_{Ba} \times Ba/Ca_{Seawater}. \quad (4)$$

Note that these steps are based on the presumption that the geochemical information measured on the shell surface of a specific shell portion is representative of the entire, contemporaneously formed shell material.

In this study, the above-described dependencies between growth rate, filtration rate and available Ba in the environment and their effect on Ba/Ca_{shell} data were used to reconstruct the theoretical amount of Ba that was potentially associated with Ba-containing phytoplankton in the water filtered by the scallops. Specifically, in a first step, the Ba/Ca_{shell} background level was subtracted from the Ba/Ca_{shell} profile (Fig. S1; Step 13 to 12), to remove the influence from the dissolved Ba content in the seawater. Then, the molar ratios were converted to weight ratios (Fig. S1; Step 11) and combined with the amount of precipitated Ca (Fig. S1; Step 9) to obtain an estimate about the absolute amount of Ba that was incorporated into the shell each day (Fig. S1; Step 10) and into the bivalve including soft tissues (Fig. S1; Step 7) which was considered to be equal to the total

amount of Ba taken up by the scallop from the particulate seawater fraction at each day. This amount of Ba was then used together with the volume of daily filtered seawater (Fig. S1; Step 6) to gain an approximation of the particulate Ba content (i.e., phytoplankton associated) that was present in the filtered seawater ($Ba_{filtered\ seawater}$ Fig. S1; Step 2). For the Mo/Ca_{shell} profiles, a similar approach was used to approximate the daily Mo incorporation and $Mo_{filtered\ seawater}$ content, using different Mo/Ca_{shell} background estimations (D_{Mo} = 1.5×10^{-4}; Barats et al., 2010) and a relative Mo distribution into the shell material of 27 % (value derived from Barats, 2006). Absolute Li incorporation rates were not calculated from the Li/Ca_{hell} profiles as important information on the relative Li distribution among the soft tissues and shell material was not available.

Tables

Table S1. Information about 12 *Pecten maximus* specimens analyzed in this study. "Habitat" specifies if a specimen lived in a cage (1 m above the sediment) or directly on the sediment surface. Three cage-lived samples (Shell A-C) were analyzed for their barium, molybdenum and lithium contents using "LA-ICP-MS" and three shells from the sediment (Shell D-F). All additional shells were solely used for growth readings ("GR") in order to generate robust averaged growth curves from shells collected from the cage (n=6) and the sediments (n=6). Average limits of detection were about 0.03 µmol mol^{-1} for Ba/Ca_{shell}, 0.01 µmol mol^{-1} for Mo/Ca_{shell} and 3.17 µmol mol^{-1} for Li/Ca_{shell}. Relative standard deviation in percent ("RSD") were calculated from measurements of the certified reference material NIST SRM 612. The pressed carbonate powder pellet USGS MACS-3 was used as a quality control material and obtained values were compared with published values (59.6 µg g^{-1} for Ba, 1.21 µg g^{-1} for Mo and 62.9 µg g^{-1} Li; GeoReM database).

				Ba/Ca_{shell}		**Mo/Ca_{shell}**		**Li/Ca_{shell}**	
Sample ID	**Date of collection**	**Habitat**	**Analyses**	**RSD (%)**	**MACS3 (µg g^{-1})**	**RSD (%)**	**MACS3 (µg g^{-1})**	**RSD (%)**	**MACS3 (µg g^{-1})**
Shell A	14.10.2021	Cage	GR + LA-ICP-MS	0.7	58.0 ± 5.4	0.7	1.2 ± 0.1	1.2	52.3 ± 4.2
Shell B	04.10.2021	Cage	GR + LA-ICP-MS	1.7	55.3 ± 0.9	2.1	1.3 ± 0.1	1.8	53.1 ± 1.6
Shell C	14.10.2021	Cage	GR + LA-ICP-MS	1.1	55.1 ± 4.7	1.1	1.3 ± 0.2	0.4	54.9 ± 3.6
Shell 1	04.10.2021	Cage	GR	–	–	–	–	–	–
Shell 2	04.10.2021	Cage	GR	–	–	–	–	–	–
Shell 3	04.10.2021	Cage	GR	–	–	–	–	–	–
Shell D	04.10.2021	Sed.	GR + LA-ICP-MS	0.9	55.8 ± 1.7	1.0	1.4 ± 0.2	0.9	52.3 ± 4.2
Shell E	11.10.2021	Sed.	GR + LA-ICP-MS	1.2	55.4 ± 1.6	1.9	1.2 ± 0.1	1.4	52.3 ± 4.2
Shell F	04.10.2021	Sed.	GR + LA-ICP-MS	1.3	55.6 ± 2.2	1.2	1.2 ± 0.1	1.4	52.3 ± 4.2
Shell 4	04.10.2021	Sed.	GR	–	–	–	–	–	–
Shell 5	11.10.2021	Sed.	GR	–	–	–	–	–	–
Shell 6	11.10.2021	Sed.	GR	–	–	–	–	–	–

Table S2. Monthly Shapiro-Wilk test results to check for normality distribution of average shell growth data obtained from cage and sediment shells. Month-wise Bartlett's test for diagnosing homoscedasticity between cage and sediment shells.

	Shapiro-Wilk test Cage shells		Shapiro-Wilk test Sediment shells		Bartlett test Cage vs Sediment
Month (2021)	**Statistic**	***p***	**Statistic**	***p***	***p***
May	0.97	0.59	0.96	0.28	0.43
June	0.94	0.09	0.97	0.56	0.11
July	0.96	0.28	0.95	0.12	0.51
August	0.99	0.95	0.97	0.58	0.82
September	0.97	0.58	0.97	0.54	0.80

Table S3. Two-way ANOVA test results. "Month" accounts for the temporal influence, i.e., monthly (May to September) differences, and "Location" denotes for differences in growth rates between cage and sediment living shells.

	Degrees of freedom (df)	**Sum of squares**	**Mean squares**	**F**	***p***
Month	4	60490.13	15122.53	50.04	4.03×10^{-32}
Location	1	51827.21	51827.21	171.50	3.34×10^{-31}
Month:Location	4	17232.85	4308.21	14.26	1.19×10^{-10}
Residual	295	89147.32	302.19	–	–

Figures

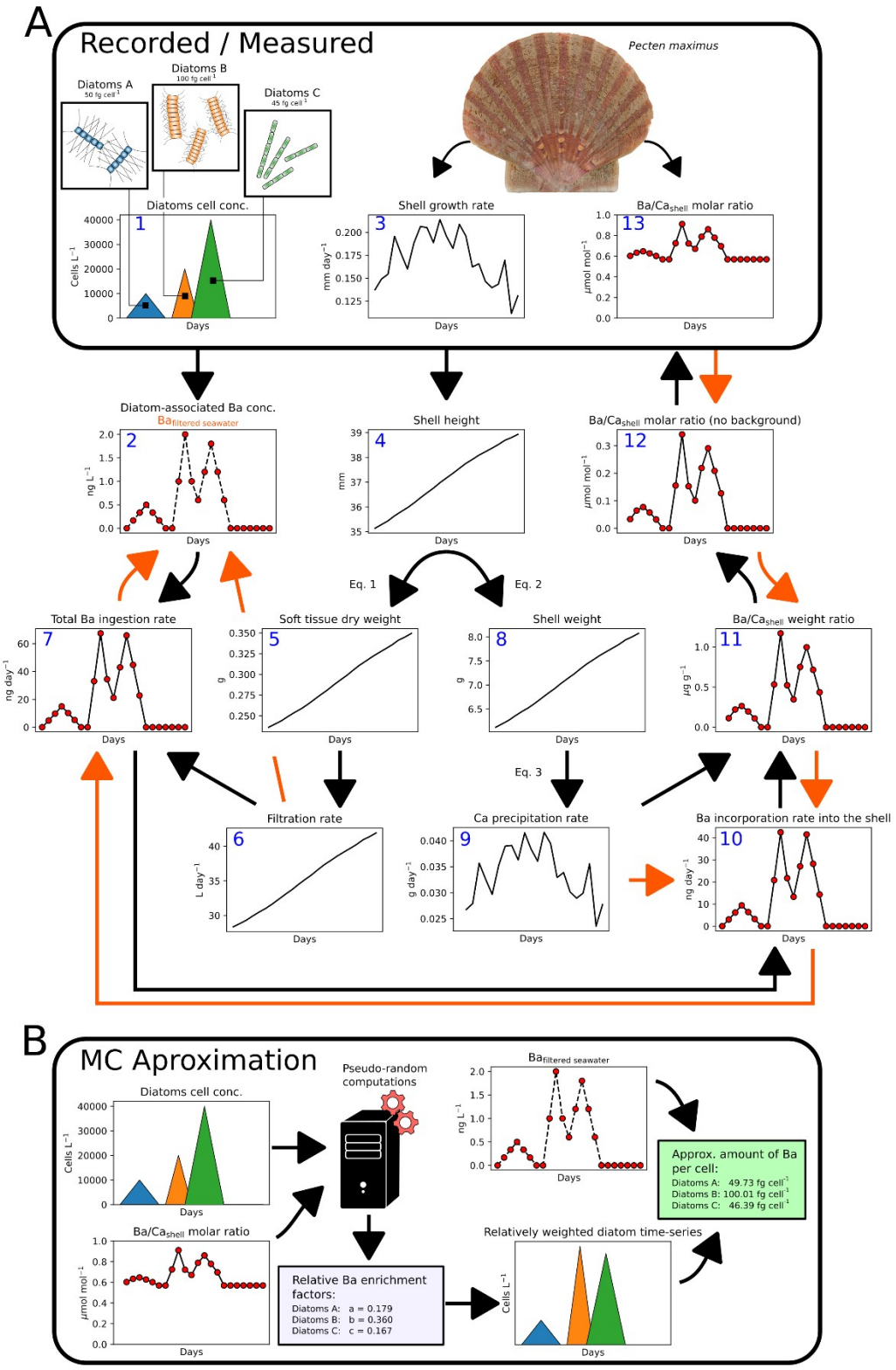

Figure S1. Simplified example of the hypothesized relationship between diatom-associated Ba (three diatom species in this example) and measured Ba/Ca$_{shell}$ profiles, modified after and based on the calculations proposed by Thébault et al. (2009). Black arrows in **A** depict the connection and contribution from cellular Ba in diatoms to the obtained Ba/Ca$_{shell}$ profiles. Orange arrows in **A**

illustrate the steps performed to approximate the total uptake of Ba by the scallops and the amount of diatom-associated Ba in the filtered seawater from the measured Ba/Ca_{shell} profile. **B** illustrates how the Monte Carlo (MC) method (described in Fröhlich et al., 2022) was included to estimate the cellular Ba content of individual diatom species, i.e., approximating the Ba/Ca_{shell} profiles by iteratively testing a large number of pseudo-randomly generated weighting factors. These species-specific weighting factors served as an indication of the relative Ba enrichment associated with each diatom species. This information was used together with the previously estimated $Ba_{filtered\ seawater}$ (**A**) to compute absolute cellular Ba concentrations of each diatom species.

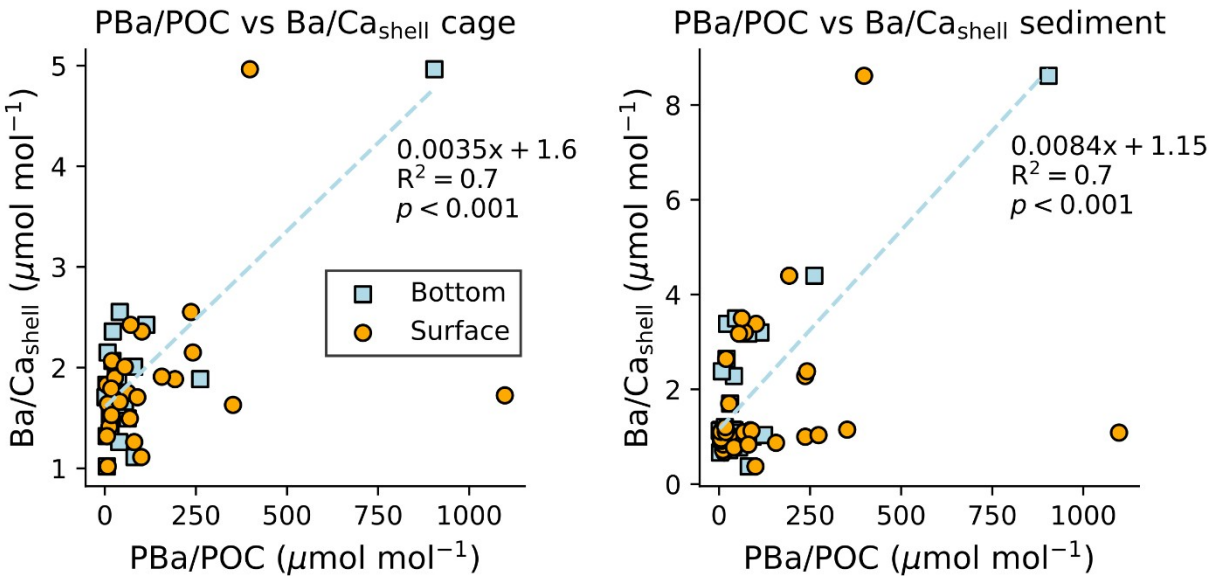

Figure S2. Cross-plots of PBa/POC ratios measured in bottom and surface waters vs average Ba/Ca_{shell} profiles from cage and sediment shells. Ba/Ca_{shell} profiles were resampled to match the resolution of the PBa/POC data. Significant (Pearson) correlations only existed between PBa/POC levels measured in bottom waters and Ba/Ca_{shell} profiles and linear regression model is indicated as blue line.

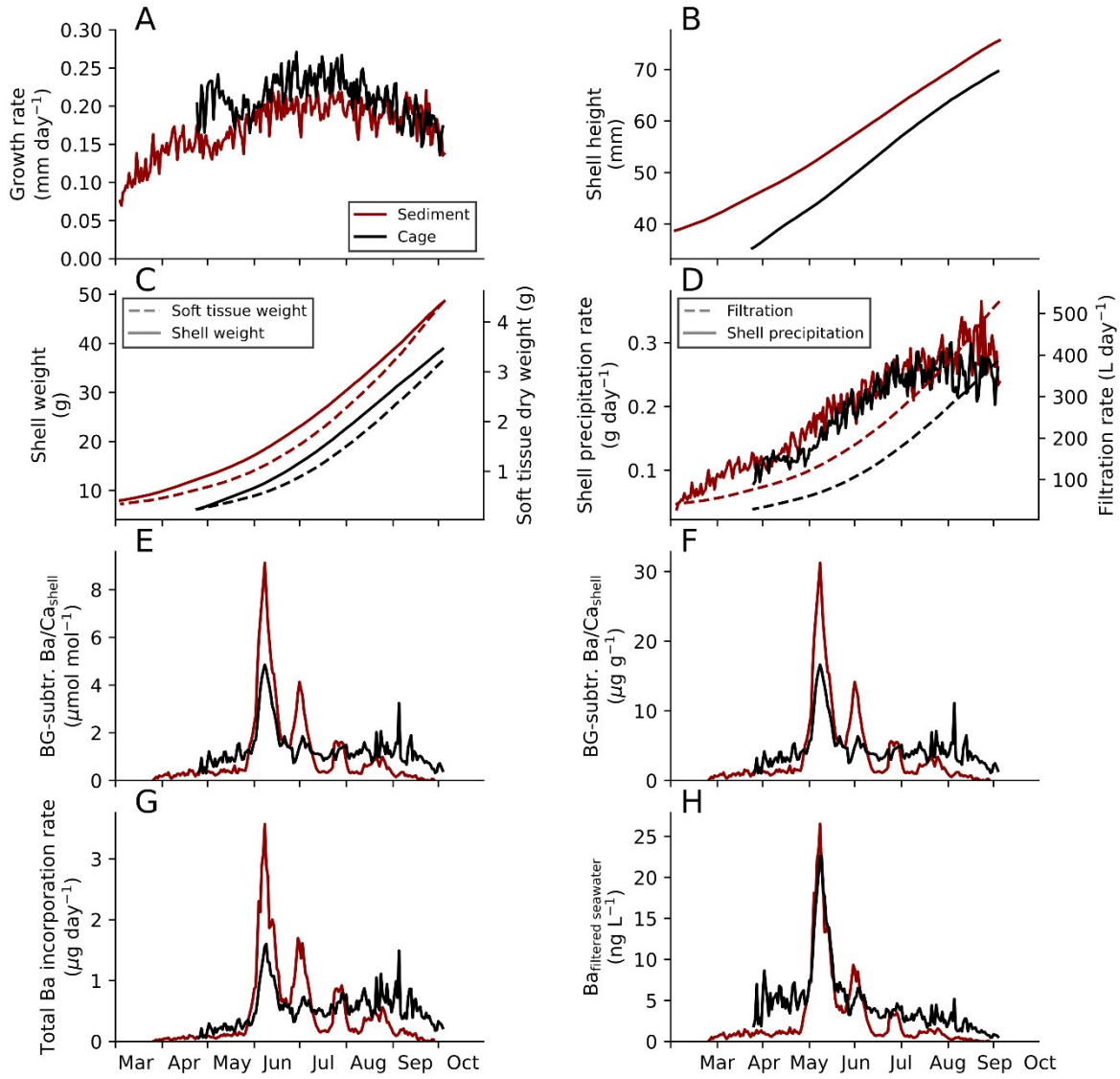

Figure S3. Average growth rates measured in sediment shells and cage shells (**A**; step 3 in Fig. S1) were used to calculate daily shell heights (**B**; step 4 in Fig. S1) and approximate the shell weight and soft tissue dry weight (**C**; step 8 and 5 in Fig. S1) following the allometric relationships from Lorrain et al. (2004). Estimated filtration rates (at 5 L h^{-1} g^{-1} soft tissue dry weight; step 6 in Fig. S1) and shell precipitation rates (**D**). Background subtracted averaged Ba/Ca_{shell} profiles (**E**; step 12 in Fig. S1) were converted into weight ratios (**F**; step 11 in Fig. S1) and used to approximate absolute Ba incorporation rates (**G**; step 7 in Fig. S1). Together with the daily filtration rate, the $Ba_{filtered\ seawater}$ was estimated (**H**; step 2 in Fig. S1).

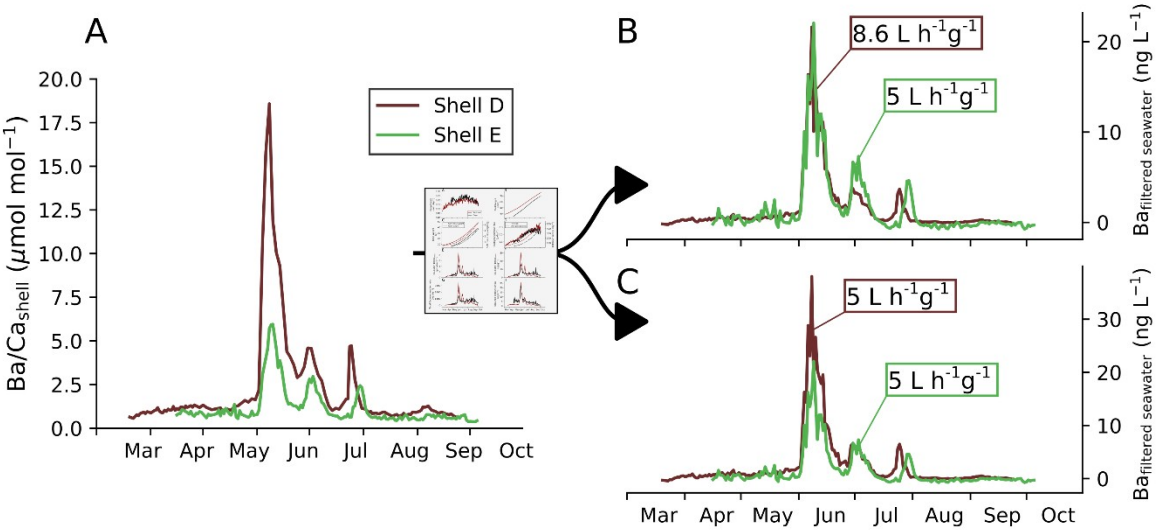

Figure S4. Differences in the Ba/Ca_{shell} profile of Shell D and Shell E that grew on the sediment (**A**). After considering the individual growth rates and filtration rates (following the steps performed in Fig. S1 and S3), the $Ba_{filtered\ seawater}$ amount was approximated (**B** and **C**). Subplot **B** illustrates a likely scenario in which Shell D possessed a slightly higher weight-standardized filtration rate compared to Shell E. According to this filtration scenario, both scallops would have filtered the same amount of Ba from the seawater during the large bloom in early June (e.g., induced by a large diatom bloom). This indicates to what extent small differences in filtration rates can affect $Ba_{filtered\ seawater}$ concentrations. For comparison, the $Ba_{filtered\ seawater}$ amount is depicted assuming a similar weight- standardized filtration rate for both shells (**C**).

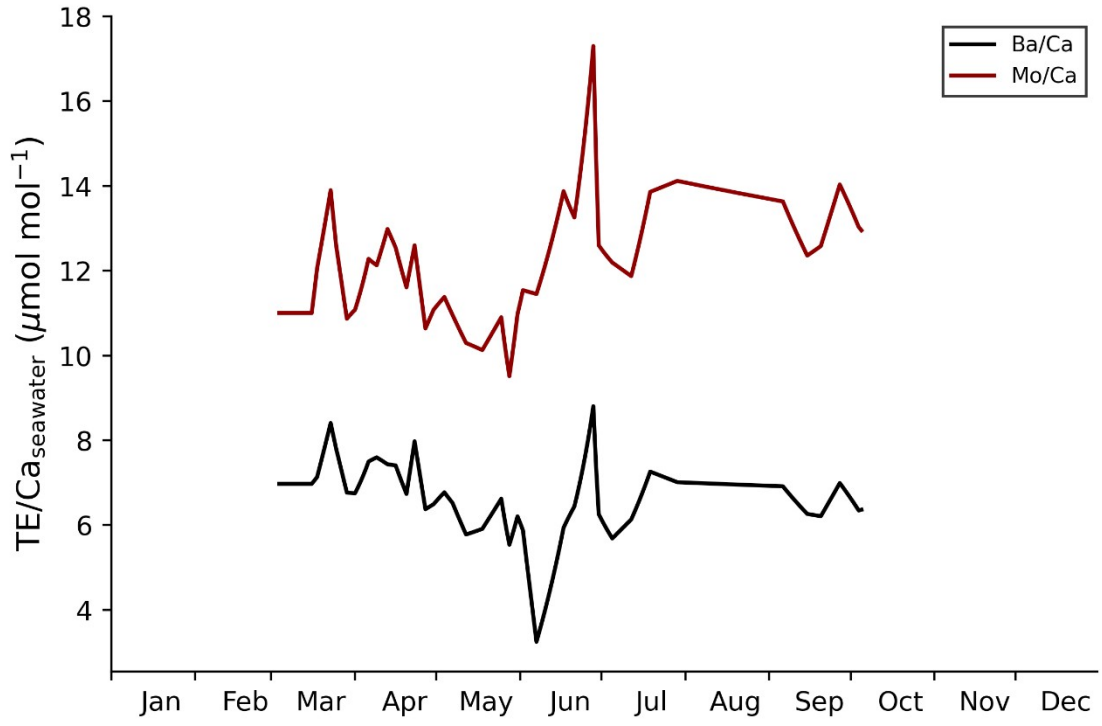

Figure S5. Dissolved $Ba/Ca_{seawater}$ and $Mo/Ca_{seawater}$ ratio measured in the water at the study locality.

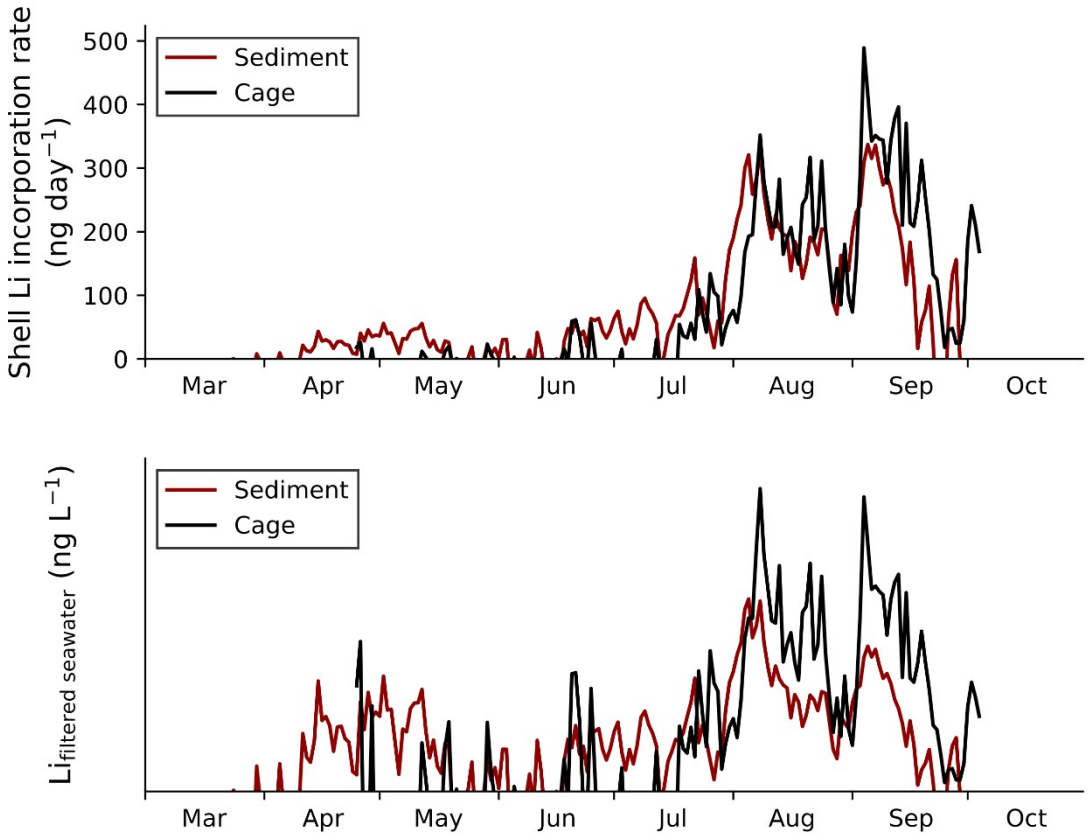

Figure S6. Estimated Li incorporation rate into the shell for cage and sediment shells (upper panel) calculated using the Li/Ca_{shell} elemental ratios together with the daily Ca precipitation rate. Note that the Li/Ca_{shell} background level was approximated, using the growth rate dependency described by Thébault and Chauvaud (2013), and subtracted from the measured Li/Ca_{shell} profiles to account for excess Li/Ca_{shell}. Relative amount of Li that was filtered by scallops from the cage and from the sediment (lower panel) considering a similar soft tissue dry weight-normalized filtration rate. Absolute values for the Li content in the filtered seawater could not be calculated as the relative Li distribution among soft tissue and shell is unknown.

References

Barats, A., 2006. Micro analyse quantitative des éléments traces dans la calcite de la coquille Saint Jacques (*Pecten maximus*) par Ablation Laser ICP-MS: une archive journalière de la biogéochimie des environnements côtiers tempérés. Diss. Université de Pau et des Pays de l'Adour.

Fröhlich, L., Siebert, V., Huang, Q., Thébault, J., Jochum, K.P., Schöne, B.R., 2022a. Deciphering the potential of Ba/Ca, Mo/Ca and Li/Ca profiles in the bivalve shell *Pecten maximus* as proxies for the reconstruction of phytoplankton dynamics. Ecol Indic 141, 109121. https://doi.org/10.1016/j.ecolind.2022.109121

Lorrain, A., Paulet, Y.M., Chauvaud, L., Dunbar, R.B., Mucciarone, D., Fontugne, M., 2004. δ13C variation in scallop shells: Increasing metabolic carbon contribution with body size? Geochim Cosmochim Acta 68, 3509–3519. https://doi.org/10.1016/j.gca.2004.01.025

Richard, M., 2009. Analyse de la composition élémentaire de *Pecten maximus* par HR-ICP-MS Element 2: développements méthodologiques et interprétations écologiques. Diss. Université de Bretagne occidentale-Brest.

Thébault, J., Chauvaud, L., 2013. Li/Ca enrichments in great scallop shells (*Pecten maximus*) and their relationship with phytoplankton blooms. Palaeogeogr Palaeoclimatol Palaeoecol 373, 108–122. https://doi.org/10.1016/j.palaeo.2011.12.014

Thébault, J., Chauvaud, L., L'Helguen, S., Clavier, J., Barats, A., Jacquet, S., Pécheyran, C., Amouroux, D., 2009. Barium and molybdenum records in bivalve shells: Geochemical proxies for phytoplankton dynamics in coastal environments? Limnol Oceanogr 54, 1002–1014. https://doi.org/10.4319/lo.2009.54.3.1002

BILAN DE THÈSE

Publications en tant que premier auteur

Article publié

Siebert, V., Poitevin, P., Chauvaud, L., Schone, B.R., Lazure, P., and Thébault, J. (2021). Using growth and geochemical composition of *Clathromorphum compactum* to track multiscale North Atlantic hydro-climate variability. *Palaeogeography, Palaeoclimatology, Palaeoecology*, 562, 110097.

Articles soumis

Siebert.V, Moriceau, B., Fröhlich, L., Schöne, B.R., Amice, E., Becker, B., Bihannic, K., Bihannic, I., Delebecq, G., Devesa, J., Gallinari, M., Germain, Y., Grossteffan, E., Jochum, K.P., Le Bec, T., Le Goff, M., Liorzou, C., Marec, C., Picheral, M., Rimmelin-Maury, P., Rouget, M.L., Waeles, M., Thébault, J. (2023). HIPPO environmental monitoring : Impact of phytoplankton dynamics on water column chemistry and the sclerochronology of the king scallop (*Pecten maximus*) as a biogenic archive for past primary production reconstructions. *Earth System Science Data*.

Siebert.V, Fröhlich, L., Thébault, J., Schöne, B.R., Delebecq, G., Picheral, M., Waeles, M., Moriceau, B. (2023). Dynamics of barium and molybdenum in the Bay of Brest (France) explained by phytoplankton community structure and aggregation events. *Estuarine, Coastal and Shelf Science*.

Publications en tant que co-auteur

Poitevin, P., Thébault, J., **Siebert, V.**, Donnet, S., Archambault, P., Doré, J., Chauvaud, L., and Lazure, P. (2019). Growth response of *Arctica islandica* to North Atlantic oceanographic conditions since 1850. *Frontiers in Marine Science*, 6, 483.

Thébault, J., Jolivet, A., Waeles, M., Tabouret, H., Sabarot, S., Pécheyran, C., Leynaert, A., Jochum, K.P., Schöne, B.R., Fröhlich, L., **Siebert, V.**, Amice, E., and Chauvaud, L. (2022). Scallop shells as geochemical archives of phytoplankton-related ecological processes in a temperate coastal ecosystem. *Limnology and Oceanography*, 67(1), 187-202.

Fröhlich, L., **Siebert, V.**, Walliser, E.O., Thébault, J., Jochum, K.P., Chauvaud, L., and Schöne, B.R. (2022). Ba/Ca profiles in shells of *Pecten maximus*–A proxy for specific primary producers rather than bulk phytoplankton. *Chemical Geology*, 593, 120743.

Fröhlich, L., **Siebert, V.**, Huang, Q., Thébault, J., Jochum, K.P., and Schöne, B.R. (2022). Deciphering the potential of Ba/Ca, Mo/Ca and Li/Ca profiles in the bivalve shell *Pecten maximus* as proxies for the reconstruction of phytoplankton dynamics. *Ecological Indicators*, 141, 109121.

Fröhlich, L., **Siebert, V.**, Huang, Q., Thébault, J., Moriceau, B., Jochum, K.P., Schöne B.R. (2023). Uptake of barium, molybdenum and lithium and incorporation into the shell of *Pecten maximus* : refining proxies for primary production dynamics. *Limnology and Oceanography*. (submitted)

Communications orales

Siebert, V., Poitevin, P., Schöne, B.R., Lazure, P., Chauvaud, L., Thébault, J. (2018). Growth patterns of *Clathromorphum compactum* from Saint-Pierre et Miquelon for paleo-envrionmental reconstructions. Présentation orale à la 6th International Rhodolith Workshop du 25 au 29 juin 2018.

Fröhlich, L., **Siebert, V.**, Huang, Q., Thébault, J., Jochum, K.P. and Schöne, B.R. (2022). High-resolution multi-proxy reconstruction of marine primary production using the short-lived bivalve *Pecten maximus*. World congress of malacology du 31 juillet au 06 Août 2022 (Munich, Allemagne).

Siebert, V., Fröhlich, L., Schöne, B.R., Moriceau, B., Waeles, M. and Thébault, J. (2022). What causes the molybdenum enrichment measured in shells of the king scallop, *Pecten maximus*?. Poster et courte présentation à la Virtual International Sclerochronology Conference (vISC) du 13 au 15 septembre 2022.

Siebert, V., Fröhlich, L., Pailler, Y., Pérennec, R., Moriceau, B., Jochum, K.P., Schöne, B.R., and Thébault, J. (2023). Reconstruction of dynamics of past primary production in the Bay of Brest from 3000 BCE to the present day, through the sclerochronological study of the King scallop, *Pecten maximus*. Présentation orale à la 6th International Sclerochronology Conference (6thISC) du 22 au 25 mai 2023.

Enseignements

Durant ma thèse, j'ai pu réaliser deux services de 64 h d'enseignement auprès d'étudiants de Licence et de Master de l'UBO au cours des années universitaire 2021/2022 et 2022/2023. Je suis notamment intervenu sur les TP/TD de ces différentes UEs :

- Biologie animale (Licence 1)
- Biologie animale (Licence BOPE 2)
- Écologie générale (Licence BOPE 2)
- Biologie animale (Licence BOPE 3)
- Archives Biogéniques du milieu marin (Master SML 2)

Encadrements de stages

- Caroline Chauvet (2021). Reconstruction des dynamiques phytoplanctoniques passées en rade de Brest à travers l'étude sclérochronologique de la coquille St-Jacques, *Pecten maximus*. Rapport de Master 1 à l'Université Sorbonne Université, Paris, France.
- Tom Rainbow (2022). Study of metal accumulation in phytoplankton aggregates. Rapport de Master 2 Science de la Mer et du Littoral (SML), mention Chimie et Sciences du Vivant (UBO), France.

Médiation et activités annexes

- Accompagnement de deux classes de primaire dans le cadre du projet "Jeunes Reporters des Arts, des Sciences et de l'Environnement (JRASE)" mené par Océanopolis.
- Encadrement d'un groupe de Master 2 dans le cadre de l'UE "Science et Société".

BIBLIOGRAPHIE

A

Alldredge, A., & Cohen, Y. (1987). Can microscale chemical patches persist in the sea? Microelectrode study of marine snow, fecal pellets. *Science*, *235*(4789), 689–691.

Alldredge, A., Cole, J., & Caron, D. (1986). Production of heterotrophic bacteria inhabiting macroscopic organic aggregates (marine snow) from surface waters. *Limnology and Oceanography*, *31*(1), 68–78.

Alldredge, A., & Gotschalk, C. (1989). Direct observations of the mass flocculation of diatom blooms: characteristics, settling velocities and formation of diatom aggregates. *Deep Sea Research Part A. Oceanographic Research Papers*, *36*(2), 159–171.

Alldredge, A., & Gotschalk, C. (1990). The relative contribution of marine snow of different origins to biological processes in coastal waters. *Continental Shelf Research*, *10*(1), 41–58.

Alldredge, A., Passow, U., & Logan, B. (1993). The abundance and significance of a class of large, transparent organic particles in the ocean. *Deep Sea Research Part I: Oceanographic Research Papers*, *40*(6), 1131–1140.

Alldredge, A., & Silver, M. (1988). Characteristics, dynamics and significance of marine snow. *Progress in Oceanography*, *20*(1), 41–82.

Aluwihare, L., & Repeta, D. (1999). A comparison of the chemical characteristics of oceanic DOM and extracellular DOM produced by marine algae. *Marine Ecology Progress Series*, *186*, 105–117.

Aminot, A., & Kérouel, R. (2004). *Hydrologie des écosystèmes marins: paramètres et analyses*. Editions Quae.

Aminot, A., & Kérouel, R. (2007). *Dosage automatique des nutriments dans les eaux marines: méthodes en flux continu*. Editions Quae.

Andrus, C. (2012). Mollusks as oxygen-isotope season-of-capture proxies in southeastern United States archaeology. *Seasonality and human mobility along the Georgia Bight*, 123–134.

Antoine, L. (1978). La croissance journalière chez *Pecten maximus* (L.)(Pectinidae, Bivalvia). *Haliotis*, *9*, 627–636.

Azzoug, M., Carré, M., Chase, B., Deme, A., Lazar, A., Lazareth, C., Schauer, A., Mandeng-Yogo, M., Simier, M., Thierno-Gaye, A., & Tito de Morais, L. (2012). Positive precipitation-evaporation budget from AD 460 to 1090 in the Saloum Delta (Senegal) indicated by mollusk oxygen isotopes. *Global and Planetary Change*, *98*, 54–62.

B

Bailey, G., Deith, M., & Shackleton, N. (1983). Oxygen isotope analysis and seasonality determinations: limits and potential of a new technique. *American Antiquity*, *48*(2), 390–398.

Baldrian, P., Valášková, V., Merhautová, V., & Gabriel, J. (2005). Degradation of lignocellulose by *Pleurotus ostreatus* in the presence of copper, manganese, lead and zinc. *Research in Microbiology*, *156*(5-6), 670–676.

Band-Schmidt, C., Zumaya-Higuera, M., López-Cortés, D., Leyva-Valencia, I., Quijano-Scheggia, S., & Hernández-Guerrero, C. (2020). Allelopathic effects of *Margalefidinium polykrikoides* and *Gymnodinium impudicum* in the growth of *Gymnodinium catenatum*. *Harmful algae*, *96*, 101846.

Barats, A. (2006). Micro analyse quantitative des éléments traces dans la calcite de la coquille Saint Jacques (*Pecten maximus*) par Ablation Laser ICP-MS: une archive journalière de la biogéochimie des environnements côtiers tempérés. (Doctoral dissertation). Université de Pau et des Pays de l'Adour, France.

Barats, A., Amouroux, D., Chauvaud, L., Pécheyran, C., Lorrain, A., Thébault, J., Church, T., & Donard, O. (2009). High frequency Barium profiles in shells of the Great Scallop *Pecten maximus*: a methodical long-term and multi-site survey in Western Europe. *Biogeosciences*, *6*(2), 157–170.

Barats, A., Amouroux, D., Pécheyran, C., Chauvaud, L., Thébault, J., & Donard, O. (2010). Spring molybdenum enrichment in scallop shells: a potential tracer of diatom productivity in temperate coastal environments (Brittany, NW France). *Biogeosciences*, *7*(1), 233–245.

Barats, A., Pécheyran, C., Amouroux, D., Dubascoux, S., Chauvaud, L., & Donard, O. (2007). Matrix-matched quantitative analysis of trace-elements in calcium carbonate shells by laser-ablation ICP-MS: application to the determination of daily scale profiles in scallop shell (*Pecten maximus*). *Analytical and Bioanalytical Chemistry*, *387*, 1131–1140.

Barbier, E., Hacker, S., Kennedy, C., Koch, E., Stier, A., & Silliman, B. (2011). The value of estuarine and coastal ecosystem services. *Ecological Monographs*, *81*(2), 169–193.

Bates, S., Hubbard, K., Lundholm, N., Montresor, M., & Leaw, C. (2018). *Pseudo-nitzschia, Nitzschia*, and domoic acid: New research since 2011. *Harmful Algae*, *79*, 3–43.

Beck, L., Gehlen, M., Flank, A., Van Bennekom, A., & Van Beusekom, J. (2002). The relationship between Al and Si in biogenic silica as determined by PIXE and XAS. *Nuclear Instruments and Methods in Physics Research Section B: Beam Interactions with Materials and Atoms*, *189*(1-4), 180–184.

Behrenfeld, M., O'Malley, R., Siegel, D., McClain, C., Sarmiento, J., Feldman, G., Milligan, A., Falkowski, P., Letelier, R., & Boss, E. (2006). Climate-driven trends in contemporary ocean productivity. *Nature*, *444*(7120), 752–755.

Bekker, A., Holland, H., Wang, P., Rumble, D., Stein, H., Hannah, J., Coetzee, L., & Beukes, N. (2004). Dating the rise of atmospheric oxygen. *Nature*, *427*(6970), 117–120.

Beninger, P., Decottignies, P., & Rincé, Y. (2004). Localization of qualitative particle selection sites in the heterorhabdic filibranch *Pecten maximus* (Bivalvia: Pectinidae). *Marine Ecology Progress Series*, *275*, 163–173.

Bennett, P., Jepson, P., Law, R., Jones, B., Kuiken, T., Baker, J., Rogan, E., & Kirkwood, J. (2001). Exposure to heavy metals and infectious disease mortality in harbour porpoises from England and Wales. *Environmental Pollution*, *112*(1), 33–40.

Bentaleb, I., Fontugne, M., Descolas-Gros, C., Girardin, C., Mariotti, A., Pierre, C., Brunet, C., & Poisson, A. (1998). Carbon isotopic fractionation by plankton in the Southern Indian Ocean: relationship between $\delta^{13}C$ of particulate organic carbon and dissolved carbon dioxide. *Journal of Marine Systems*, *17*(1-4), 39–58.

Bergamonti, L., Bersani, D., Mantovan, S., & Lottici, P. (2013). Micro-Raman investigation of pigments and carbonate phases in corals and molluscan shells. *European Journal of Mineralogy*, *25*(5), 845–853.

Bernstein, R., & Byrne, R. (2004). Acantharians and marine barite. *Marine Chemistry*, *86*(1-2), 45–50.

Bernstein, R., Byrne, R., Betzer, P., & Greco, A. (1992). Morphologies and transformations of celestite in seawater: The role of acantharians in strontium and barium geochemistry. *Geochimica et Cosmochimica Acta*, *56*(8), 3273–3279.

Bishop, J. (1988). The barite-opal-organic carbon association in oceanic particulate matter. *Nature*, *332*(6162), 341–343.

Bittar, T., Passow, U., Hamaraty, L., Bidle, K., & Harvey, E. (2018). An updated method for the calibration of transparent exopolymer particle measurements. *Limnology and Oceanography: Methods*, *16*(10), 621–628.

Blankenship, R. (1992). Origin and early evolution of photosynthesis. *Photosynthesis research*, *33*(2), 91–111.

Boehm, A., Ismail, N., Sassoubre, L., & Andruszkiewicz, E. (2017). Oceans in peril: Grand challenges in applied water quality research for the 21st century. *Environmental Engineering Science*, *34*(1), 3–15.

Bourg, A., & Loch, J. (1995). Mobilization of heavy metals as affected by pH and redox conditions. *Biogeodynamics of Pollutants in Soils and Sediments*, 87–102.

Boyce, D., Lewis, M., & Worm, B. (2010). Global phytoplankton decline over the past century. *Nature*, *466*(7306), 591.

Brand, U. (1991). Strontium isotope diagenesis of biogenic aragonite and low-Mg calcite. *Geochimica et Cosmochimica Acta*, *55*(2), 505–513.

Brocks, J., Jarrett, A., Sirantoine, E., Hallmann, C., Hoshino, Y., & Liyanage, T. (2017). The rise of algae in Cryogenian oceans and the emergence of animals. *Nature*, *548*(7669), 578–581.

Brosset, C., Höche, N., Shirai, K., Nishida, K., Mertz-Kraus, R., & Schöne, B. (2022). Strong coupling between biomineral morphology and Sr/Ca of *Arctica islandica* (Bivalvia) — Implications for shell Sr/Ca-based temperature estimates. *Minerals*, *12*(5), 500.

Brzezinski, M. (1985). The Si: C: N ratio of marine diatoms: interspecific variability and the effect of some environmental variables 1. *Journal of Phycology*, *21*(3), 347–357.

Buick, R. (1992). The antiquity of oxygenic photosynthesis: evidence from stromatolites in sulphate-deficient Archaean lakes. *Science*, *255*(5040), 74–77.

Burchell, M., Cannon, A., Hallmann, N., Schwarcz, H., & Schöne, B. (2013). Inter-site variability in the season of shellfish collection on the central coast of British Columbia. *Journal of Archaeological Science*, *40*(1), 626–636.

Butler, P., Wanamaker, A., Scourse, J., Richardson, C. A., & Reynolds, D. (2013). Variability of marine climate on the North Icelandic Shelf in a 1357-year proxy archive based on growth increments in the bivalve *Arctica islandica*. *Palaeogeography, Palaeoclimatology, Palaeoecology*, *373*, 141–151.

C

Cailleux, A. (1950). Observations archéologiques dans l'ile de Béniguet (Finistère). *Bulletin de la Société préhistorique française*, *47*(6), 353–354.

Cardona, T. (2018). Early Archean origin of heterodimeric Photosystem I. *Heliyon*, *4*(3), e00548.

Cardona, T., Sánchez-Baracaldo, P., Rutherford, A., & Larkum, A. (2019). Early Archean origin of photosystem II. *Geobiology*, *17*(2), 127–150.

Carlson, C., Ducklow, H., & Michaels, A. (1994). Annual flux of dissolved organic carbon from the euphotic zone in the northwestern Sargasso Sea. *Nature*, *371*(6496), 405–408.

Carré, M., Braconnot, P., Elliot, M., D'agostino, R., Schurer, A., Shi, X., Marti, O., Lohmann, G., Jungclaus, J., Cheddadi, R., Et al. (2021). High-resolution marine data and transient simulations support orbital forcing of ENSO amplitude since the mid-Holocene. *Quaternary Science Reviews*, *268*, 107125.

Chaillou, G., Anschutz, P., Lavaux, G., Schäfer, J., & Blanc, G. (2002). The distribution of Mo, U, and Cd in relation to major redox species in muddy sediments of the Bay of Biscay. *Marine Chemistry*, *80*(1), 41–59.

Charpy-Roubaud, C., & Sournia, A. (1990). The comparative estimation of phytoplanktonic, microphytobenthic and macrophytobenthic primary production in the oceans. *Marine Microbial Food Webs*, *4*(1), 31–57.

Chassot, E., Bonhommeau, S., Dulvy, N., Mélin, F., Watson, R., Gascuel, D., & Le Pape, O. (2010). Global marine primary production constrains fisheries catches. *Ecology Letters*, *13*(4), 495–505.

Chauvaud, L., Donval, A., Thouzeau, G., Paulet, Y., & Nézan, E. (2001). Variations in food intake of *Pecten maximus* (L.) from the Bay of Brest (France): Influence of environmental factors and phytoplankton species composition. *Comptes Rendus de l'Académie des Sciences - Series III - Sciences de la Vie*, *324*(8), 743–755.

Chauvaud, L., Lorrain, A., Dunbar, R., Paulet, Y., Thouzeau, G., Jean, F., Guarini, J., & Mucciarone, D. (2005). Shell of the Great Scallop *Pecten maximus* as a high-frequency archive of paleoenvironmental changes. *Geochemistry, Geophysics, Geosystems*, *6*(8).

Chauvaud, L., Patry, Y., Jolivet, A., Cam, E., Le Goff, C., Strand, Ø., Charrier, G., Thébault, J., Lazure, P., Gotthard, K., & Clavier, J. (2012). Variation in size and growth of the great scallop *Pecten maximus* along a latitudinal gradient. *PloS One*, *7*(5), 1–10.

Chauvaud, L., Thouzeau, G., & Paulet, Y. (1998). Effects of environmental factors on the daily growth rate of *Pecten maximus* juveniles in the Bay of Brest (France). *Journal of Experimental Marine Biology and Ecology*, *227*(1), 83–111.

Chin, W., Orellana, M., & Verdugo, P. (1998). Spontaneous assembly of marine dissolved organic matter into polymer gels. *Nature*, *391*(6667), 568–572.

Clark, G. (2005). Daily growth lines in some living Pectens (Mollusca: Bivalvia), and some applications in a fossil relative: time and tide will tell. *Palaeogeography, Palaeoclimatology, Palaeoecology*, *228*(1-2), 26–42.

Cloern, J. (2001). Our evolving conceptual model of the coastal eutrophication problem. *Marine Ecology Progress Series*, *210*, 223–253.

Cloern, J., Foster, S., & Kleckner, A. (2014). Phytoplankton primary production in the world's estuarine-coastal ecosystems. *Biogeosciences*, *11*(9), 2477–2501.

Coffey, M., Dehairs, F., Collette, O., Luther, G., Church, T., & Jickells, T. (1997). The behaviour of dissolved barium in estuaries. *Estuarine, Coastal and Shelf Science*, *45*(1), 113–121.

Collier, R., & Edmond, J. (1984). The trace element geochemistry of marine biogenic particulate matter. *Progress in Oceanography*, *13*(2), 113–199.

Coplen, T., Böhlke, J., De Bievre, P., Ding, T., Holden, N., Hopple, J., Krouse, H., Lamberty, A., Peiser, H., Revesz, K., Et al. (2002). Isotope-abundance variations of selected elements (IUPAC Technical Report). *Pure and Applied Chemistry*, *74*(10), 1987–2017.

Costanza, R. (1999). The ecological, economic, and social importance of the oceans. *Ecological Economics*, *31*(2), 199–213.

Creel, L. (2003). *Ripple effects: population and coastal regions*. Population Reference Bureau Washington, DC.

Crocker, K., & Passow, U. (1995). Differential aggregation of diatoms. *Marine Ecology Progress Series*, *117*(1), 249–257.

Cudennec, J., & Paulet, Y. (2021). Characterising inter-individual growth variability of *Patella vulgata* shell through calcein marking experiments: consequences for palaeo-environmental studies. *Environmental Archaeology*, *27*(6), 525–538.

Cudennec, J., & Paulet, Y. (2022). Variations of the stable isotope ratios of carbon and oxygen of the *Patella vulgata* (Linnæus, 1758) shells according to the vertical zonation of collect. *Geo-Marine Letters*, *42*(3), 15.

D

Dam, H., & Drapeau, D. (1995). Coagulation efficiency, organic-matter glues and the dynamics of particles during a phytoplankton bloom in a mesocosm study. *Deep Sea Research Part II: Topical Studies in Oceanography*, *42*(1), 111–123.

Daranas, A., Norte, M., & Fernández, J. (2001). Toxic marine microalgae. *Toxicon*, *39*(8), 1101–1132.

Dauphin, Y., Williams, C., & Barskov, I. (2007). Aragonitic rostra of the Turonian belemnitid Goniacamax: arguments from diagenesis. *Acta Palaeontologica Polonica*, *52*(1).

Davies, C., Coughlan, A., Hallegraeff, G., Ajani, P., Armbrecht, L., Atkins, N., Bonham, P., Brett, S., Brinkman, R., Burford, M., Et al. (2016). A database of marine phytoplankton abundance, biomass and species composition in Australian waters. *Scientific Data*, *3*(1), 1–12.

De La Rocha, C., Nowald, N., & Passow, U. (2008). Interactions between diatom aggregates, minerals, particulate organic carbon, and dissolved organic matter: Further implications for the ballast hypothesis. *Global Biogeochemical Cycles*, *22*(4).

Debelius, B., Forja, J., & Lubián, L. (2011). Toxicity of copper, nickel and zinc to *Synechococcus* populations from the Strait of Gibraltar. *Journal of Marine Systems*, *88*(1), 113–119.

Decho, A. (1990). Microbial exopolymer secretions in ocean environments: their role(s) in food webs and marine processes. *Oceanography and Marine Biology - An Annual Review*, *28*(7), 73–153.

Dehairs, F., Chesselet, R., & Jedwab, J. (1980). Discrete suspended particles of barite and the barium cycle in the open ocean. *Earth and Planetary Science Letters*, *49*(2), 528–550.

Del Amo, Y., Le Pape, O., Tréguer, P., Quéguiner, B., Ménesguen, A., & Aminot, A. (1997). Impacts of high-nitrate freshwater inputs on macrotidal ecosystems. I. Seasonal evolution of nutrient limitation for the diatom-dominated phytoplankton of the Bay of Brest (France). *Marine Ecology Progress Series*, *161*, 213–224.

Dellwig, O., Beck, M., Lemke, A., Lunau, M., Kolditz, K., Schnetger, B., & Brumsack, H. (2007). Non-conservative behaviour of molybdenum in coastal waters: Coupling geochemical, biological, and sedimentological processes. *Geochimica et Cosmochimica Acta*, *71*(11), 2745–2761.

Demarcq, H., Reygondeau, G., Alvain, S., & Vantrepotte, V. (2011). Monitoring marine phytoplankton seasonality from space. *Remote Sensing of Environment*, *117*, 211–222.

Diercks, A., & Asper, V. (1997). In situ settling speeds of marine snow aggregates below the mixed layer: Black Sea and Gulf of Mexico. *Deep Sea Research Part I: Oceanographic Research Papers*, *44*(3), 385–398.

Doré, J., Chaillou, G., Poitevin, P., Lazure, P., Poirier, A., Chauvaud, L., Archambault, P., & Thébault, J. (2020). Assessment of Ba/Ca in *Arctica islandica* shells as a proxy for phytoplankton dynamics in the Northwestern Atlantic Ocean. *Estuarine, Coastal and Shelf Science*, *237*, 106628.

Doré, J., Thébault, J., Roy, V., Dewilde, F., & Chaillou, G. (2021). Insight into shell growth dynamics of *Mactromeris polynyma* in the St. Lawrence Estuary using sclerochemistry. *Marine Chemistry*, *234*, 103987.

Doucet, F. J., Schneider, C., Bones, S., Kretchmer, A., Moss, I., Tekely, P., & Exley, C. (2001). The formation of hydroxyaluminosilicates of geochemical and biological significance. *Geochimica et Cosmochimica Acta*, *65*(15), 2461–2467.

Dreano, Y., Giovannacci, S., Dietsch-Sellami, M., Dupont, C., Gruet, Y., Hoguin, R., Ihuel, E., Leroy, A., Marchand, G., Pailler, Y., Sparfel, Y., & Tresset, A. (2007). Le patrimoine archéologique de l'ile de Béniguet (Le Conquet, Finistère). Bilan des recherches 2000-2007. *Bulletin de la Société des Sciences Naturelles de l'Ouest de la France (1983)*, *29*(3), 161–172.

Durkin, C., Van Mooy, B., Dyhrman, S., & Buesseler, K. (2016). Sinking phytoplankton associated with carbon flux in the Atlantic Ocean. *Limnology and Oceanography*, *61*(4), 1172–1187.

E

Edler, L., & Elbrächter, M. (2010). The Utermöhl method for quantitative phytoplankton analysis. *Microscopic and Molecular Methods for Quantitative Phytoplankton Analysis*, *110*, 13–20.

Edwards, M. (2004a). Phytoplankton blooms in the North Atlantic: results from the Continuous Plankton Recorder survey 2001/2002. *Harmful Algae News*, *430*(25), 1–3.

Edwards, M., Johns, D., Leterme, S., Svendsen, E., & Richardson, A. (2006a). Regional climate change and harmful algal blooms in the northeast Atlantic. *Limnology and Oceanography*, *51*(2), 820–829.

Edwards, M., Johns, D., Licandro, P., John, A., & Stevens, D. (2006b). Ecological Status Report: results from the CPR Survey 2004/2005. *SAHFOS Technical Report*, (3), 1–8.

Edwards, M., & Richardson, A. (2004b). Impact of climate change on marine pelagic phenology and trophic mismatch. *Nature*, *430*(7002), 881–884.

Eerkens, J., Byrd, B., Spero, H., & Fritschi, A. (2013). Stable isotope reconstructions of shellfish harvesting seasonality in an estuarine environment: implications for Late Holocene San Francisco Bay settlement patterns. *Journal of Archaeological Science*, *40*(4), 2014–2024.

Engel, A. (2000). The role of transparent exopolymer particles (TEP) in the increase in apparent particle stickiness (α) during the decline of a diatom bloom. *Journal of Plankton Research*, *22*(3), 485–497.

Eppley, R., Coatsworth, J., & Solórzano, L. (1969). Studies of nitrate reductase in marine phytoplankton. *Limnology and Oceanography*, *14*(2), 194–205.

F

Falkowski, P., Katz, M., Knoll, A., Quigg, A., Raven, J. A., Schofield, O., & Taylor, F. (2004). The evolution of modern eukaryotic phytoplankton. *Science*, *305*(5682), 354–360.

Falkowski, P., & Raven, J. (2013). *Aquatic photosynthesis*. Princeton University Press.

Field, C., Behrenfeld, M., Randerson, J., & Falkowski, P. (1998). Primary production of the biosphere: integrating terrestrial and oceanic components. *Science*, *281*(5374), 237–240.

Fisher, N., Guillard, R., & Bankston, D. (1991). The accumulation of barium by marine phytoplankton grown in culture. *Journal of Marine Research*, *49*(2), 339–354.

Fisher, N., & Wente, M. (1993). The release of trace elements by dying marine phytoplankton. *Deep Sea Research Part I: Oceanographic Research Papers*, *40*(4), 671–694.

Freitas, P., Clarke, L., Kennedy, H., & Richardson, C. (2009). Ion microprobe assessment of the heterogeneity of Mg/Ca, Sr/Ca and Mn/Ca ratios in *Pecten maximus* and *Mytilus edulis* (Bivalvia) shell calcite precipitated at constant temperature. *Biogeosciences Discussions*, *6*(1), 1209–1227.

Fröhlich, L., Siebert, V., Huang, Q., Thébault, J., Jochum, K., & Schöne, B. (2022a). Deciphering the potential of Ba/Ca, Mo/Ca and Li/Ca profiles in the bivalve shell *Pecten maximus* as proxies for the reconstruction of phytoplankton dynamics. *Ecological Indicators*, *141*, 109121.

Fröhlich, L., Siebert, V., Walliser, E., Thébault, J., Jochum, K., Chauvaud, L., & Schöne, B. (2022b). Ba/Ca profiles in shells of *Pecten maximus* - A proxy for specific primary producers rather than bulk phytoplankton. *Chemical Geology*, *593*, 120743.

G

Ganeshram, R., François, R., Commeau, J., & Brown-Leger, S. (2003). An experimental investigation of barite formation in seawater. *Geochimica et Cosmochimica Acta*, *67*(14), 2599–2605.

Garvey, M., Moriceau, B., & Passow, U. (2007). Applicability of the FDA assay to determine the viability of marine phytoplankton under different environmental conditions. *Marine Ecology Progress Series*, *352*, 17–26.

Gillikin, D., Dehairs, F., Lorrain, A., Steenmans, D., Baeyens, W., & André, L. (2006). Barium uptake into the shells of the common mussel (*Mytilus edulis*) and the potential for estuarine paleochemistry reconstruction. *Geochimica et Cosmochimica Acta*, *70*(2), 395–407.

Gillikin, D., Lorrain, A., Paulet, Y., André, L., & Dehairs, F. (2008). Synchronous barium peaks in high-resolution profiles of calcite and aragonite marine bivalve shells. *Geo-Marine Letters*, *28*(5), 351–358.

Gillikin, D., Wanamaker, A., & Andrus, C. (2019). Chemical sclerochronology. *Chemical Geology*, *526*, 1–6.

Giroldo, D., Vieira, A., & Paulsen, B. (2005). Extracellular polysaccharides produced by a tropical cryptophyte as a carbon source for natural bacterial populations. *European Journal of Phycology*, *40*(3), 241–249.

Gregg, W., Casey, N., & McClain, C. (2005). Recent trends in global ocean chlorophyll. *Geophysical Research Letters*, *32*(3).

Gregg, W., & Rousseaux, C. (2019). Global ocean primary production trends in the modern ocean color satellite record (1998-2015). *Environmental Research Letters*, *14*(12), 124011.

Grossart, H., Berman, T., Simon, M., & Pohlmann, K. (1998). Occurrence and microbial dynamics of macroscopic organic aggregates (lake snow) in Lake Kinneret, Israel, in fall. *Aquatic Microbial Ecology*, *14*(1), 59–67.

Grossman, E., & Ku, T. (1986). Oxygen and carbon isotope fractionation in biogenic aragonite: temperature effects. *Chemical Geology: Isotope Geoscience Section*, *59*, 59–74.

Gutierrez, T., Biller, D., Shimmield, T., & Green, D. (2012). Metal binding properties of the EPS produced by *Halomonas* sp. TG39 and its potential in enhancing trace element bioavailability to eukaryotic phytoplankton. *Biometals*, *25*(6), 1185–1194.

Güven, K., Akyüz, K., & Yurdun, T. (1995). Selectivity of heavy metal binding by algal polysaccharides. *Toxicological & Environmental Chemistry*, *47*(1-2), 65–70.

H

Hallegraeff, G. (1993). A review of harmful algal blooms and their apparent global increase. *Phycologia*, *32*(2), 79–99.

Hallegraeff, G. (2010). Ocean climate change, phytoplankton community responses, and harmful algal blooms: a formidable predictive challenge. *Journal of Phycology*, *46*(2), 220–235.

Hallegraeff, G., & Jeffrey, S. (1984). Tropical phytoplankton species and pigments of continental shelf waters of north and north-west Australia. *Marine Ecology Progress Series*, *20*(1), 59–74.

Hays, G., Richardson, A., & Robinson, C. (2005). Climate change and marine plankton. *Trends in Ecology & Evolution*, *20*(6), 337–344.

Hedegaard, C., Bardeau, J., & Chateigner, D. (2006). Molluscan shell pigments: an in situ resonance Raman study. *Journal of Molluscan Studies*, *72*(2), 157–162.

Helz, G., Miller, C., Charnock, J., Mosselmans, J., Pattrick, R., Garner, C., & Vaughan, D. (1996). Mechanism of molybdenum removal from the sea and its concentration in black shales: EXAFS evidence. *Geochimica et Cosmochimica Acta*, *60*(19), 3631–3642.

Henson, S., Beaulieu, C., & Lampitt, R. (2016). Observing climate change trends in ocean biogeochemistry: when and where. *Global Change Biology*, *22*(4), 1561–1571.

Henson, S., Sarmiento, J., Dunne, J., Bopp, L., Lima, I., Doney, S., John, J., & Beaulieu, C. (2010). Detection of anthropogenic climate change in satellite records of ocean chlorophyll and productivity. *Biogeosciences*, *7*, 621–640.

Hillebrand, H., Dürselen, C., Kirschtel, D., Pollingher, U., & Zohary, T. (1999). Biovolume calculation for pelagic and benthic microalgae. *Journal of Phycology*, *35*(2), 403–424.

Hinder, S., Hays, G., Edwards, M., Roberts, E., Walne, A., & Gravenor, M. (2012). Changes in marine dinoflagellate and diatom abundance under climate change. *Nature Climate Change*, *2*(4), 271.

Hirose, K. (2011). Chemical modeling of marine trace metals: effects of ocean acidification to marine ecosystem, In *2011 Seventh International Conference on Natural Computation*.

Ho, T., Quigg, A., Finkel, Z., Milligan, A., Wyman, K., Falkowski, P., & Morel, F. (2003). The elemental composition of some marine phytoplankton. *Journal of Phycology*, *39*(6), 1145–1159.

Höche, N., Walliser, E., & Schöne, B. (2022). Microstructural mapping of *Arctica islandica* shells reveals environmental and physiological controls on biomineral size. *Frontiers in Earth Science*, *9*, 1350.

Houghton, E. (1996). Intergovernmental Panel on Climate Change, and Groupe d'experts intergouvernemental sur l'évolution du climat Working group 2. Cambridge University Press.

Huang, Q., Wu, H., & Schöne, B. (2023). A novel trophic archive: Practical considerations of compound-specific amino acid δ15N analysis of carbonate-bound organic matter in bivalve shells (*Arctica islandica*). *Chemical Geology*, *615*, 121220.

Hudson, J., Shinn, E. A., Halley, R., & Lidz, B. (1976). Sclerochronology: a tool for interpreting past environments. *Geology*, *4*(6), 361–364.

I

Iglesias-Rodriguez, M., Halloran, P., Rickaby, R., Hall, I., Colmenero-Hidalgo, E., Gittins, J., Green, D., Tyrrell, T., Gibbs, S., Von Dassow, P., Rehm, E., Armbrust, E., & Boessenkool, K. (2008). Phytoplankton calcification in a high-CO_2 world. *Science*, *320*(5874), 336–340.

J

Jackson, G. (1995). Comparing observed changes in particle size spectra with those predicted using coagulation theory. *Deep Sea Research Part II: Topical Studies in Oceanography*, *42*(1), 159–184.

Jackson, G., & Burd, A. (2015). Simulating aggregate dynamics in ocean biogeochemical models. *Progress in Oceanography*, *133*, 55–65.

Jackson, J., Kirby, M., Berger, W., Bjorndal, K., Botsford, L., Bourque, B., Bradbury, R., Cooke, R., Erlandson, J., Estes, J., Et al. (2001). Historical overfishing and the recent collapse of coastal ecosystems. *Science*, *293*(5530), 629–637.

Jambeck, J., Geyer, R., Wilcox, C., Siegler, T., Perryman, M., Andrady, A., Narayan, R., & Law, K. (2015). Plastic waste inputs from land into the ocean. *Science*, *347*(6223), 768–771.

Jennings, B., & Parslow, K. (1988). Particle size measurement: the equivalent spherical diameter. *Proceedings of the Royal Society of London. A. Mathematical and Physical Sciences*, *419*(1856), 137–149.

Jochum, K., Garbe-Schönberg, D., Veter, M., Stoll, B., Weis, U., Weber, M., Lugli, F., Jentzen, A., Schiebel, R., Wassenburg, J., Jacob, D., & Haug, G. (2019). Nano-powdered calcium carbon-

ate reference materials: Significant progress for microanalysis? *Geostandards and Geoanalytical Research*, *43*(4), 595–609.

Jochum, K., Stoll, B., Herwig, K., & Willbold, M. (2007). Validation of LA-ICP-MS trace element analysis of geological glasses using a new solid-state 193 nm Nd: YAG laser and matrix-matched calibration. *Journal of Analytical Atomic Spectrometry*, *22*(2), 112–121.

Jochum, K., Weis, U., Stoll, B., Kuzmin, D., Yang, Q., Raczek, I., Jacob, D., Stracke, A., Birbaum, K., Frick, D., Günther, D., & Enzweiler, J. (2011). Determination of reference values for NIST SRM 610-617 glasses following ISO guidelines. *Geostandards and Geoanalytical Research*, *35*(4), 397–429.

Ju, Z., Viljoen, C., Hutchinson, P., Reinicke, J., Horgen, F., Howard, L., & Lee, C. (2016). Effects of diets on the growth performance and shell pigmentation of Pacific abalone. *Aquaculture Research*, *47*(12), 4004–4014.

K

Killingley, J. (1981). Seasonality of mollusk collecting determined from O-18 profiles of midden shells. *American Antiquity*, *46*(1), 152–158.

Kiørboe, T., & Jackson, G. (2001). Marine snow, organic solute plumes, and optimal chemosensory behavior of bacteria. *Limnology and Oceanography*, *46*(6), 1309–1318.

Klein, R., Lohmann, K., & Thayer, C. (1996). Bivalve skeletons record sea-surface temperature and $\delta^{18}O$ via Mg/Ca and $^{18}O/^{16}O$ ratios. *Geology*, *24*(5), 415–418.

Kloareg, B., & Quatrano, R. (1988). Structure of the cell walls of marine algae and ecophysiological functions of the matrix polysaccharides. *Oceanography and Marine Biology: an Annual Review*, *26*, 259–315.

Kubanek, J., Hicks, M., Naar, J., & Villareal, T. (2005). Does the red tide dinoflagellate *Karenia brevis* use allelopathy to outcompete other phytoplankton? *Limnology and Oceanography*, *50*(3), 883–895.

Kühn, S., & Raven, J. (2008). Photosynthetic oscillation in individual cells of the marine diatom *Coscinodiscus wailesii* (Bacillariophyceae) revealed by microsensor measurements. *Photosynthesis Research*, *95*, 37–44.

L

Laing, I. (2002). Effect of salinity on growth and survival of king scallop spat (*Pecten maximus*). *Aquaculture*, *205*(1-2), 171–181.

Laing, I. (2004). Filtration of king scallops (*Pecten maximus*). *Aquaculture*, *240*(1), 369–384.

Lal Shah, S. (2010). Hematological changes in *Tinca tinca* after exposure to lethal and sublethal doses of Mercury, Cadmium and Lead. *Iranian Journal of Fisheries Sciences*, *9*(3), 434–443.

Lampitt, R., Wishner, K., Turley, C., & Angel, M. (1993). Marine snow studies in the Northeast Atlantic Ocean: distribution, composition and role as a food source for migrating plankton. *Marine Biology*, *116*, 689–702.

Land, L. (1967). Diagenesis of skeletal carbonates. *Journal of Sedimentary Research*, *37*(3), 914–930.

Langer, G., Nehrke, G., Thoms, S., & Stoll, H. (2009). Barium partitioning in coccoliths of *Emiliania huxleyi*. *Geochimica et Cosmochimica Acta*, *73*(10), 2899–2906.

Laurenceau-Cornec, E., Bressac, M., Young, C., Henderson, A., Strzepek, R., Moriceau, B., Cavan, E., Halfter, S., Toullec, J., Planchon, F., & Boyd, P. (2019). The SNOWMAN: a new experimental device to improve our understanding of the Biological Carbon Pump through quantitative studies of aggregation kinetics and export time lag. *IMBeR Future Oceans2 Open Science Conference, Brest, France*.

Laurenceau-Cornec, E., Henderson, A., Young, C., Bressac, R., M. abd Strzepek, Bach, L., Moriceau, B., Toullec, J., & Boyd, P. (2020a). The SNOWMAN: a new experimental device to study quantitatively the link between phytoplankton community structure, the dynamics of marine snow formation, and export time lag. *ASLO Ocean Sciences Meeting - Session OB13B - San Diego, USA*.

Laurenceau-Cornec, E., Le Moigne, F., Gallinari, M., Moriceau, B., Toullec, J., Iversen, M., Engel, A., & De La Rocha, C. (2020b). New guidelines for the application of Stokes' models to the sinking velocity of marine aggregates. *Limnology and Oceanography*, *65*(6), 1264–1285.

Laurenceau-Cornec, E., Trull, T., Davies, D., Bray, S., Doran, J., Planchon, F., Carlotti, F., Jouandet, M., Cavagna, A., Waite, A., & Blain, S. (2015). The relative importance of phytoplankton aggregates and zooplankton fecal pellets to carbon export: insights from free-drifting sediment trap deployments in naturally iron-fertilised waters near the Kerguelen Plateau. *Biogeosciences*, *12*(4), 1007–1027.

Lawrence, M., & Kamber, B. (2006). The behaviour of the rare earth elements during estuarine mixing—revisited. *Marine Chemistry*, *100*(1-2), 147–161.

Lazareth, C., Vander Putten, E., André, L., & Dehairs, F. (2003). High-resolution trace element profiles in shells of the mangrove bivalve *Isognomon ephippium*: a record of environmental spatio-temporal variations? *Estuarine, Coastal and Shelf Science*, *57*(5-6), 1103–1114.

Lee, C., Hedges, J., Wakeham, S., & Zhu, N. (1992). Effectiveness of various treatments in retarding microbial activity in sediment trap material and their effects on the collection of swimmers. *Limnology and Oceanography*, *37*(1), 117–130.

Legrand, C., Rengefors, K., Fistarol, G., & Graneli, E. (2003). Allelopathy in phytoplankton-biochemical, ecological and evolutionary aspects. *Phycologia*, *42*(4), 406–419.

Leighton, D. (1979). A growth profile for the rock scallop *Hinnites multirugosus* held at several depths off La Jolla, California. *Marine Biology*, *51*, 229–232.

Lelong, A., Bucciarelli, E., Hégaret, H., & Soudant, P. (2013). Iron and copper limitations differently affect growth rates and photosynthetic and physiological parameters of the marine diatom *Pseudo-nitzschia delicatissima*. *Limnology and Oceanography*, *58*(2), 613–623.

Lewitus, A., Horner, R., Caron, D., Garcia-Mendoza, E., Hickey, B., Hunter, M., Huppert, D., Kudela, R., Langlois, G., Largier, J., Lessard, E., RaLonde, R., Rensel, J., Srutton, P., Trainer, V., & Tweddle, J. (2012). Harmful algal blooms along the North American west coast region: History, trends, causes, and impacts. *Harmful Algae*, *19*, 133–159.

Leynaert, A., Longphuirt, S., Claquin, P., Chauvaud, L., & Ragueneau, O. (2009). No limit? The multiphasic uptake of silicic acid by benthic diatoms. *Limnology and Oceanography*, *54*(2), 571–576.

Ling, S., & Alldredge, A. (2003). Does the marine copepod *Calanus pacificus* consume transparent exopolymer particles (TEP)? *Journal of plankton research*, *25*(5), 507–515.

Lobus, N., Kulikovskiy, M., & Maltsev, Y. (2021). Multi-element composition of diatom *Chaetoceros* spp. from natural phytoplankton assemblages of the Russian Arctic Seas. *Biology*, *10*(10), 1009.

Logan, B., Passow, U., Alldredge, A., Grossart, H., & Simont, M. (1995). Rapid formation and sedimentation of large aggregates is predictable from coagulation rates (half-lives) of transparent exopolymer particles (TEP). *Deep Sea Research Part II: Topical Studies in Oceanography*, *42*(1), 203–214.

Long, M., Moriceau, B., Gallinari, M., Lambert, C., Huvet, A., Raffray, J., & Soudant, P. (2015). Interactions between microplastics and phytoplankton aggregates: impact on their respective fates. *Marine Chemistry*, *175*, 39–46.

Longerich, H., Jackson, S., & Günther, D. (1996). Inter-laboratory note. Laser ablation inductively coupled plasma mass spectrometric transient signal data acquisition and analyte concentration calculation. *Journal of Analytical Atomic Spectrometry*, *11*, 899–904.

Lorenzen, C. (1966). A method for the continuous measurement of in vivo chlorophyll concentration. *Deep Sea Research*, *13*(2), 223–227.

Lorenzen, C. (1967). Vertical distribution of chlorophyll and phaeo-pigments : Baja California. *Deep Sea Research and Oceanographic Abstracts*, *14*(6), 735–745.

Lorrain, A., Gillikin, D., Paulet, Y., Chauvaud, L., Le Mercier, A., Navez, J., & André, L. (2005). Strong kinetic effects on Sr/Ca ratios in the calcitic bivalve *Pecten maximus*. *Geology*, *33*(12), 965–968.

Lorrain, A., Paulet, Y., Chauvaud, L., Dunbar, R., Mucciarone, D., & Fontugne, M. (2004). $\delta^{13}C$ variation in scallop shells: Increasing metabolic carbon contribution with body size? *Geochimica et Cosmochimica Acta*, *68*(17), 3509–3519.

Lorrain, A., Paulet, Y., Chauvaud, L., Savoye, N., Nézan, E., & Guérin, L. (2000). Growth anomalies in *Pecten maximus* from coastal waters (Bay of Brest, France): relationship with diatom blooms. *Journal of the Marine Biological Association of the United Kingdom*, *80*(4), 667–673.

Lundsør, E., Lømsland, E., Johnsen, T., Engesmo, A., King, A., Staalstrøm, A., Norli, M., Magnusson, J., Sørensen, K., Edvardsen, B., Et al. (2022). Marine phytoplankton community data and corresponding environmental properties from eastern Norway, 1896-2020. *Scientific Data*, *9*(1), 767.

Lyons, T., Reinhard, C., & Planavsky, N. (2014). The rise of oxygen in Earth's early ocean and atmosphere. *Nature*, *506*(7488), 307–315.

M

MacDonald, B. (1986). Production and resource partitioning in the giant scallop *Placopecten magellanicus* grown on the bottom and in suspended culture. *Marine Ecology Progress Series*, *34*, 79–86.

MacDonald, B., & Bajdik, C. (1992). Orientation and distribution of individual *Placopecten magellanicus* (Gmelin) in two natural populations with differing production. *Canadian Journal of Fisheries and Aquatic Sciences*, *49*(10), 2086–2092.

Magnesen, T., & Redmond, K. (2012). Potential predation rates by the sea stars *Asterias rubens* and *Marthasterias glacialis*, on juvenile scallops, *Pecten maximus*, ready for sea ranching. *Aquaculture International*, *20*(1), 189–199.

Majithiya, D., Yadav, A., & Ram, A. (2018). Behaviour of trace metals in the anoxic environment of Veraval harbour, India. *Marine Pollution Bulletin*, *129*(2), 645–654.

Maldonado, M., Allen, A., Chong, J., Lin, K., Leus, D., Karpenko, N., & Harris, S. (2006). Copper-dependent iron transport in coastal and oceanic diatoms. *Limnology and Oceanography*, *51*(4), 1729–1743.

Marali, S., Schöne, B., Mertz-Kraus, R., Griffin, S., Wanamaker Jr, A., Butler, P., Holland, H., & Jochum, K. (2017). Reproducibility of trace element time-series (Na/Ca, Mg/Ca, Mn/Ca, Sr/Ca, and Ba/Ca) within and between specimens of the bivalve *Arctica islandica* - A LA-ICP-MS line scan study. *Palaeogeography, Palaeoclimatology, Palaeoecology*, *484*, 109–128.

Mari, X., & Rassoulzadegan, F. (2004). Role of TEP in the microbial food web structure. I. Grazing behavior of a bacterivorous pelagic ciliate. *Marine Ecology Progress Series*, *279*, 13–22.

Mari, X., & Robert, M. (2008). Metal induced variations of TEP sticking properties in the southwestern lagoon of New Caledonia. *Marine Chemistry*, *110*(1-2), 98–108.

Markulin, K., Peharda, M., Mertz-Kraus, R., Schöne, B., Uvanović, H., Kovač, Ž., & Janeković, I. (2019). Trace and minor element records in aragonitic bivalve shells as environmental proxies. *Chemical Geology*, *507*, 120–133.

Martin, J., Hanke, A., & LeGresley, M. (2009). Long term phytoplankton monitoring, including harmful algal blooms, in the Bay of Fundy, eastern Canada. *Journal of Sea Research*, *61*(1-2), 76–83.

Martin, S. (2014). *An introduction to ocean remote sensing*. Cambridge University Press.

Masuzawa, T., Suzuki, T., Seki, K., Kosugi, T., Hibi, Y., Yamamoto, M., Takada, J., Matsushita, R., & Yanada, M. (1999). Multielement compositions of marine phytoplankton samples from coastal areas of japan by instrumental neutron activation analysis. *Biological Trace Element Research*, *71*, 331–342.

McClain, C. (2009). A Decade of Satellite Ocean Color Observations. *Annual Review of Marine Science*, *1*(1), 19–42.

McConnaughey, T., & Gillikin, D. (2008). Carbon isotopes in mollusk shell carbonates. *Geo-Marine Letters*, *28*, 287–299.

McDonnell, A., Boyd, P., & Buesseler, K. (2015). Effects of sinking velocities and microbial respiration rates on the attenuation of particulate carbon fluxes through the mesopelagic zone. *Global Biogeochemical Cycles*, *29*(2), 175–193.

McQuatters-Gollop, A., Reid, P., Edwards, M., Burkill, P., Castellani, C., Batten, S., Gieskes, W., Beare, D., Bidigare, R., Head, E., Johnson, R., Kahru, M., Koslow, J., & Pena, A. (2011). Is there a decline in marine phytoplankyon? *Nature*, *472*, E6–E7.

Menden-Deuer, S., & Lessard, E. (2000). Carbon to volume relationships for dinoflagellates, diatoms, and other protist plankton. *Limnology and Oceanography*, *45*(3), 569–579.

Mendoza, Y., Freites, L., Lodeiros, C., López, J., & Himmelman, J. (2003). Evaluation of biological and economical aspects of the culture of the scallop *Lyropecten (Nodipecten) nodosus* in suspended and bottom culture. *Aquaculture*, *221*(1-4), 207–219.

Metian, M., Bustamante, P., Cosson, R., Hédouin, L., & Warnau, M. (2008a). Investigation of Ag in the king scallop *Pecten maximus* using field and laboratory approaches. *Journal of Experimental Marine Biology and Ecology*, *367*(1), 53–60.

Metian, M., Warnau, M., Cosson, R., Oberhänsli, F., & Bustamante, P. (2008b). Bioaccumulation and detoxification processes of Hg in the king scallop *Pecten maximus*: Field and laboratory investigations. *Aquatic Toxicology*, *90*(3), 204–213.

Metian, M., Warnau, M., Hédouin, L., & Bustamante, P. (2009). Bioaccumulation of essential metals (Co, Mn and Zn) in the king scallop *Pecten maximus*: seawater, food and sediment exposures. *Marine Biology*, *156*(10), 2063–2075.

Michaels, A. (1991). Acantharian abundance and symbiont productivity at the VERTEX seasonal station. *Journal of Plankton Research*, *13*(2), 399–418.

Moore, R., Webb, M., Tokarczyk, R., & Wever, R. (1996). Bromoperoxidase and iodoperoxidase enzymes and production of halogenated methanes in marine diatom cultures. *Journal of Geophysical Research: Oceans*, *101*(C9), 20899–20908.

Moore, S., Trainer, V., Mantua, N., Parker, M., Laws, E., Backer, L., & Fleming, L. (2008). Impacts of climate variability and future climate change on harmful algal blooms and human health. *Environmental Health*, *7*((Supp 2):S4), 1–12.

Mopper, K., Zhou, J., Ramana, U., K.S.and Passow, Dam, H., & D.T., D. (1995). The role of surface-active carbohydrates in the flocculation of a diatom bloom in a mesocosm. *Deep Sea Research Part II: Topical Studies in Oceanography*, *42*(1), 47–73.

Morford, J., & Emerson, S. (1999). The geochemistry of redox sensitive trace metals in sediments. *Geochimica et Cosmochimica Acta*, *63*(11-12), 1735–1750.

Mori, C., Beck, M., Striebel, M., Merder, J., Schnetger, B., Dittmar, T., Pahnke, K., & Brumsack, H. (2021). Biogeochemical cycling of molybdenum and thallium during a phytoplankton summer bloom: A mesocosm study. *Marine Chemistry*, *229*, 103910.

Moriceau, B., Garvey, M., Ragueneau, O., & Passow, U. (2007). Evidence for reduced biogenic silica dissolution rates in diatom aggregates. *Marine Ecology Progress Series*, *333*, 129–142.

Moriceau, B., Laruelle, G., Passow, U., Van Cappellen, P., & Ragueneau, O. (2014). Biogenic silica dissolution in diatom aggregates: insights from reactive transport modelling. *Marine Ecology Progress Series*, *517*, 35–49.

Morris, A. (1975). Dissolved molybdenum and vanadium in the northeast Atlantic ocean. *Deep Sea Research and Oceanographic Abstracts*, *22*(1), 49–54.

Myklestad, S. (1995). Release of extracellular products by phytoplankton with special emphasis on polysaccharides. *Science of the Total Environment*, *165*(1-3), 155–164.

N

Nicholas, D., & Nason, A. (1955). Role of molybdenum as a constituent of nitrate reductase from soybean leaves. *Plant Physiology*, *30*(2), 135.

Nozaki, Y., Yang, H., & Yamada, M. (1987). Scavenging of thorium in the ocean. *Journal of Geophysical Research: Oceans*, *92*(C1), 772–778.

O

Och, L., & Shields-Zhou, G. (2012). The Neoproterozoic oxygenation event: environmental perturbations and biogeochemical cycling. *Earth-Science Reviews*, *110*(1-4), 26–57.

P

Paasche, E. (1980). Silicon content of five marine plankton diatom species measured with a rapid filter method. *Limnology and Oceanography*, *25*(3), 474–480.

Paasche, E. (2001). A review of the coccolithophorid *Emiliania huxleyi* (Prymnesiophyceae), with particular reference to growth, coccolith formation, and calcification-photosynthesis interactions. *Phycologia*, *40*(6), 503–529.

Pailler, Y., Stéphan, P., Gandois, H., Nicolas, C., Sparfel, Y., Tresset, A., Donnart, K., Dréano, Y., Fichaut, B., Suanez, S., Dupont, C., Audouard, L., Marcoux, N., Mougne, C., Salanova, L., Sellami, F., & Dietsch-Sellami, M. (2014). Landscape evolution and human settlement in the Iroise Sea (Brittany, France) during the Neolithic and Bronze Age, In *Proceedings of the Prehistoric Society*. Cambridge University Press.

Pailler, Y., Stéphan, P., Gandois, H., Nicolas, C., Sparfel, Y., Tresset, A., Donnart, K., Fichaut, B., Suanez, S., & Dupont, C. (2011). Évolution des paysages et occupation humaine en mer d'Iroise (Finistère, Bretagne) du Néolithique à l'Âge du Bronze. *Norois*, *220*, 39–68.

Palmer, R. (1980). Behavioral and rhythmic aspects of filtration in the bay scallop, Argopecten irradians concentricus (Say), and the oyster, *Crassostrea virginica* (Gmelin). *Journal of Experimental Marine Biology and Ecology*, *45*(2), 273–295.

Pan, Y., Subba, R., Mann, K., Brown, R., & Pocklington, R. (1996). Effects of silicate limitation on production of domoic acid, a neurotoxin, by the diatom *Pseudo-nitzschia* multiseries. I. Batch culture studies. *Marine Ecolology Progress Series*, *131*, 225–233.

Passow, U. (2002). Transparent exopolymer particles (TEP) in aquatic environments. *Progress in Oceanography*, *55*(3), 287–33.

Passow, U., & Alldredge, A. (1994). Distribution, size and bacterial colonization of transparent exopolymer particles (TEP) in the ocean. *Marine Ecology Progress Series*, *113*(1-2), 185–198.

Passow, U., & Alldredge, A. (1999). Do transparent exopolymer particles (TEP) inhibit grazing by the euphausiid *Euphausia pacifica*? *Journal of Plankton Research*, *21*(11), 2203–2217.

Passow, U., & De La Rocha, C. (2006). Accumulation of mineral ballast on organic aggregates. *Global Biogeochemical Cycles*, *20*(1), GB1013.

Pauly, D., & Christensen, V. (1995). Primary production required to sustain global fisheries. *Nature*, *374*(6519), 255–257.

Peharda, M., Schöne, B., Black, B., & Corrège, T. (2021). Reading the diaries of life – Current advances in sclerochronological research. *Palaeogeography, Palaeoclimatology, Palaeoecology*, *570*, 110373.

Picheral, M., Catalano, C., Brousseau, D., Claustre, H., Coppola, L., Leymarie, E., Coindat, J., Dias, F., Fevre, S., Guidi, L., Et al. (2021). The Underwater Vision Profiler 6: an imaging sensor of particle size spectra and plankton, for autonomous and cabled platforms. *Limnology and Oceanography: Methods*, *20*(2), 120–129.

Pinay, G., Gascuel, C., Ménesguen, A., Souchon, Y., Le Moal, M., Levain, A., Etrillard, C., Moata, F., Pannard, A., & Souchu, P. (2018). *L'eutrophisation*. éditions Quae.

Ploug, H. (2001). Small-scale oxygen fluxes and remineralization in sinking aggregates. *Limnology and Oceanography*, *46*(7), 1624–1631.

Ploug, H., Iversen, M., & Fischer, G. (2008). Ballast, sinking velocity, and apparent diffusivity within marine snow and zooplankton fecal pellets: Implications for substrate turnover by attached bacteria. *Limnology and Oceanography*, *53*(5), 1878–1886.

Ploug, H., Kühl, M., Buchholz-Cleven, B., & Jørgensen, B. (1997). Anoxic aggregates-an ephemeral phenomenon in the pelagic environment? *Aquatic Microbial Ecology*, *13*(3), 285–294.

Poitevin, P., Roy, V., Galbraith, P., & Chaillou, G. (2022). Insights into coastal phytoplankton variations from 1979 to 2018 derived from Ba/Ca records in scallop shells (*Chlamys islandica*) from a fishing ground in the northern Gulf of St. Lawrence. *Marine Environmental Research*, *181*, 105734.

Poitevin, P., Thébault, J., Siebert, V., Donnet, S., Archambault, P., Doré, J., Chauvaud, L., & Lazure, P. (2019). Growth response of *Arctica islandica* to North Atlantic oceanographic conditions since 1850. *Frontiers in Marine Science*, *6*, 483.

R

Ragueneau, O., De Blas Varela, E., Tréguer, P., Quéguiner, B., & Del Amo, Y. (1994). Phytoplankton dynamics in relation to the biogeochemical cycle of silicon in a coastal ecosystem of western Europe. *Marine Ecology Progress Series*, *106*(1-2), 157–172.

Ragueneau, O., & Tréguer, P. (1994). Determination of biogenic silica in coastal waters: applicability and limits of the alkaline digestion method. *Marine Chemistry*, *45*(1-2), 43–51.

Rainbow, P. (2007). Trace metal bioaccumulation: models, metabolic availability and toxicity. *Environment International*, *33*(4), 576–582.

Redfield, A. (1958). The biological control of chemical factors in the environment. *American Scientist*, *46*(3), 230A–221.

Rhee, G. (1974). Phosphate uptake under nitrate limitation by *Scenedesmus* sp. and its ecological implication. *Journal of Phycology*, *10*(4), 470–475.

Rice, K., Walker Jr, E., Wu, M., Gillette, C., & Blough, E. (2014). Environmental mercury and its toxic effects. *Journal of Preventive Medicine and Public Health*, *47*(2), 74.

Richard, M. (2009). Analyse de la composition élémentaire de *Pecten maximus* par HR-ICP-MS Element 2: développements méthodologiques et interprétations écologiques.) (Doctoral dissertation). Université de Bretagne Occidentale, France.

Richardson, L., & LeDrew, E. (2006). *Remote sensing of aquatic coastal ecosystem processes*. Springer.

Richon, C., & Tagliabue, A. (2019). Insights into the major processes driving the global distribution of copper in the ocean from a global model. *Global Biogeochemical Cycles*, *33*(12), 1594–1610.

Riley, J., & Roth, I. (1971). The distribution of trace elements in some species of phytoplankton grown in culture. *Journal of the Marine Biological Association of the United Kingdom*, *51*(1), 63–72.

Rombouts, I., Simon, N., Aubert, A., Cariou, T., Feunteun, E., Guérin, L., Hoebeke, M., McQuatters-Gollop, A., Rigaut-Jalabert, F., & Artigas, L. F. (2019). Changes in marine phytoplankton diversity: Assessment under the Marine Strategy Framework Directive. *Ecological Indicators*, *102*, 265–277.

Rousseaux, C., & Gregg, W. (2015). Recent decadal trends in global phytoplankton composition. *Global Biogeochemical Cycles*, *29*(10), 1674–1688.

Rykaczewski, R., & Dunne, J. (2011). A measured look at ocean chlorophyll trends. *Nature*, *472*, E5–E6.

S

Saout, C., Quéré, C., Donval, A., Paulet, Y., & Samain, J. (1999). An experimental study of the combined effects of temperature and photoperiod on reproductive physiology of *Pecten maximus* from the Bay of Brest (France). *Aquaculture*, *172*(3-4), 301–314.

Sarthou, G., Timmermans, K., Blain, S., & Tréguer, P. (2005). Growth physiology and fate of diatoms in the ocean: a review. *Journal of Sea Research*, *53*(1-2), 25–42.

Savoye, N. (2001). Origine et transfert de matière organique particulaire dans les écosystèmes littoraux macrotidaux) (Doctoral dissertation). Université de Bretagne Occidentale, France.

Schlekat, C., Decho, A., & Chandler, G. (1998). Sorption of cadmium to bacterial extracellular polymeric sediment coatings under estuarine conditions. *Environmental Toxicology and Chemistry*, *17*(9), 1867–1874.

Schlekat, C., Decho, A., & Chandler, G. (2000). Bioavailability of particle-associated silver, cadmium, and zinc to the estuarine amphipod *Leptocheirus plumulosus* through dietary ingestion. *Limnology and Oceanography*, *45*(1), 11–21.

Schöne, B. (2013). *Arctica islandica* (Bivalvia): a unique paleoenvironmental archive of the northern North Atlantic Ocean. *Global and Planetary Change*, *111*, 199–225.

Schöne, B., Castro, A., Fiebig, J., Houk, S., Oschmann, W., & Kröncke, I. (2004). Sea surface water temperatures over the period 1884-1983 reconstructed from oxygen isotope ratios of a bivalve mollusk shell (*Arctica islandica*, southern North Sea). *Palaeogeography, Palaeoclimatology, Palaeoecology*, *212*(3-4), 215–232.

Schöne, B., Fiebig, J., Pfeiffer, M., Gless, R., Hickson, J., Johnson, A., Dreyer, W., & Oschmann, W. (2005). Climate records from a bivalved Methuselah (*Arctica islandica*, Mollusca; Iceland). *Palaeogeography, Palaeoclimatology, Palaeoecology*, *228*(1-2), 130–148.

Schöne, B., Huang, X., Zettler, M., Zhao, L., Mertz-Kraus, R., Jochum, K., & Walliser, E. (2021). Mn/Ca in shells of *Arctica islandica* (Baltic Sea)-A potential proxy for ocean hypoxia? *Estuarine, Coastal and Shelf Science*, *251*, 107257.

Schöne, B., Marali, S., Jantschke, A., Mertz-Kraus, R., Butler, P., & Fröhlich, L. (2023). Can element chemical impurities in aragonitic shells of marine bivalves serve as proxies for environmental variability? *Chemical Geology*, *616*, 121215.

Schöne, B., Tanabe, K., Dettman, D., & Sato, S. (2003). Environmental controls on shell growth rates and δ^{18}O of the shallow-marine bivalve mollusk *Phacosoma japonicum* in Japan. *Marine Biology*, *142*, 473–485.

Selck, H., Decho, A., & Forbes, V. (1999). Effects of chronic metal exposure and sediment organic matter on digestive absorption efficiency of cadmium by the deposit-feeding polychaete *Capitella* species I. *Environmental Toxicology and Chemistry*, *18*(6), 1289–1297.

Shumway, S. (1987). Food resources related to habitat in the scallop *Placopecten magellanicus* (Gmelin, 1791): a qualitative study. *Journal Shellfish Research*, *6*, 89–95.

Shumway, S., Cucci, T., Lesser, M., Bourne, N., & Bunting, B. (1997). Particle clearance and selection in three species of juvenile scallops. *Aquaculture International*, *5*(1), 89–99.

Shuval, H. (2003). Estimating the global burden of thalassogenic diseases: human infectious diseases caused by wastewater pollution of the marine environment. *Journal of Water and Health*, *1*(2), 53–64.

Siebert, V., Moriceau, B., Fröhlich, L., Schöne, B., Amice, E., Beker, B., Bihannic, K., Bihannic, I., Devesa, J., Gallinari, M., Germain, Y., Grossteffan, E., Jochum, K., Lebec, T., Le Goff, M., Leynaert, A., Liorzou, C., Marec, C., Picheral, M., … Thébault, J. (2023). HIPPO environmental monitoring: Impact of phytoplankton dynamics on water column chemistry and the sclerochronology of the king scallop (*Pecten maximus*) as a biogenic archive for past primary production reconstructions. *SEANOE, 10.17882/92043*.

Siegel, D., & Franz, B. (2010). Oceanography: Century of phytoplankton change. *Nature*, *466*(7306), 569.

Slabbekoorn, H., Bouton, N., van Opzeeland, I., Coers, A., ten Cate, C., & Popper, A. (2010). A noisy spring: the impact of globally rising underwater sound levels on fish. *Trends in Ecology & Evolution*, *25*(7), 419–427.

Smayda, T. (1965). A quantitative analysis of the phytoplankton of the Gulf of Panama II. On the relationship between C14 assimilation and the diatom standing crop. *Inter-American Tropical Tuna Commission Bulletin*, *9*(7), 465–531.

Smayda, T. (1998). Patterns of variability characterizing marine phytoplankton, with examples from Narragansett Bay. *ICES Journal of Marine Science*, *55*(4), 562–573.

Smetacek, V. (1985). Role of sinking in diatom life-history cycles: ecological, evolutionary and geological significance. *Marine Biology*, *84*(3), 239–251.

Smrzka, D., Zwicker, J., Bach, W., Feng, D., Himmler, T., Chen, D., & Peckmann, J. (2019). The behavior of trace elements in seawater, sedimentary pore water, and their incorporation into carbonate minerals: a review. *Facies*, *65*(41), 1–47.

Spilling, K., Olli, K., Lehtoranta, J., Kremp, A., Tedesco, L., Tamelander, T., Klais, R., Peltonen, H., & Tamminen, T. (2018). Shifting diatom—dinoflagellate dominance during spring bloom in the Baltic Sea and its potential effects on biogeochemical cycling. *Frontiers in Marine Science*, *5*, 327.

Stecher, H., & Kogut, M. (1999). Rapid barium removal in the Delaware estuary. *Geochimica et Cosmochimica Acta*, *63*(7-8), 1003–1012.

Stecher, H., Krantz, D., Lord, C., Luther, G., & Bock, K. (1996). Profiles of strontium and barium in *Mercenaria mercenaria* and *Spisula solidissima* shells. *Geochimica et Cosmochimica Acta*, *60*(18), 3445–3456.

Stemmann, L., Picheral, M., Guidi, L., Lombard, F., Prejger, F., Claustre, H., & Gorsky, G. (2012). Assessing the spatial and temporal distributions of zooplankton and marine particles using the Underwater Vision Profiler. *Sensors for Ecology*, 119.

Stéphan, P., Pailler, Y., Tresset, A., & Gandois, H. (2011). Changements paléogéographiques de l'archipel de Molène (Finistère, Bretagne, France): implications sur les peuplements humains du Néolithique à l'Age du Bronze, In *Ancient Maritime Communities and the Relationship between People and Environment along the European Atlantic Coasts/Anciens peuplements littoraux et relations Homme/Milieu sur les cotes de l'Europe atlantique*. Archaeopress.

Sternberg, E., Tang, D., Ho, T., Jeandel, C., & Morel, F. (2005). Barium uptake and adsorption in diatoms. *Geochimica et Cosmochimica Acta*, *69*(11), 2745–2752.

Strand, Ø., Solberg, P., Andersen, K., & Magnesen, T. (1993). Salinity tolerance of juvenile scallops (*Pecten maximus* L.) at low temperature. *Aquaculture*, *115*(1-2), 169–179.

Strohmeier, T., Strand, Ø., & Cranford, P. (2009). Clearance rates of the great scallop (*Pecten maximus*) and blue mussel (*Mytilus edulis*) at low natural seston concentrations. *Marine Biology*, *156*(9), 1781–1795.

Subba Rao, D., Pan, Y., & Mukhida, K. (1998). Production of Domoic Acid by *Pseudo-nitzschia* multiseries Hasle, Affected by Lithium. *Marine Ecology*, *19*(1), 31–36.

Sun, J., & Liu, D. (2003). Geometric models for calculating cell biovolume and surface area for phytoplankton. *Journal of Plankton Research*, *25*(11), 1331–1346.

Sunda, W. (1975). The relationship between cupric ion activity and the toxicity of copper to phytoplankton (Doctoral dissertation). Massachusetts Institute of Technology.

Sunda, W. (1989). Trace metal interactions with marine phytoplankton. *Biological Oceanography*, *6*(5-6), 411–442.

Suratno, S., Puspitasari, R., Purbonegoro, T., & Mansur, D. (2015). Copper and cadmium toxicity to marine phytoplankton, *Chaetoceros gracilis* and *Isochrysis* sp. *Indonesian Journal of Chemistry*, *15*(2), 172–178.

T

Tabouret, H., Pomerleau, S., Jolivet, A., Pécheyran, C., Riso, R., Thébault, J., Chauvaud, L., & Amouroux, D. (2012). Specific pathways for the incorporation of dissolved barium and molybdenum into the bivalve shell: An isotopic tracer approach in the juvenile Great Scallop (*Pecten maximus*). *Marine Environmental Research*, *78*, 15–25.

Tachihana, S., Nagao, N., Katayama, T., Hirahara, M., Yusoff, F., Banerjee, S., Shariff, M., Kurosawa, N., Toda, T., & Furuya, K. (2020). High productivity of eicosapentaenoic acid and fucoxanthin by a marine diatom *Chaetoceros gracilis* in a semi-continuous culture. *Frontiers in Bioengineering and Biotechnology*, *8*, 602721.

Tardy, Y., Krempp, G., & Trauth, N. (1972). Le lithium dans les minéraux argileux des sédiments et des sols. *Geochimica et Cosmochimica Acta*, *36*(4), 397–412.

Tercier-Waeber, M., Stoll, S., & Slaveykova, V. (2012). Trace metal behavior in surface waters: emphasis on dynamic speciation, sorption processes and bioavailability. *Archives des Sciences*, *65*, 119–142.

Thébault, J., & Chauvaud, L. (2013). Li/Ca enrichments in great scallop shells (*Pecten maximus*) and their relationship with phytoplankton blooms. *Palaeogeography, Palaeoclimatology, Palaeoecology*, *373*, 108–122.

Thébault, J., Chauvaud, L., Clavier, J., Fichez, R., & Morize, E. (2006). Evidence of a 2-day periodicity of striae formation in the tropical scallop *Comptopallium radula* using calcein marking. *Marine Biology*, *149*, 257–267.

Thébault, J., Chauvaud, L., L'Helguen, S., Clavier, J., Barats, A., Jacquet, S., Pécheyran, C., & Amouroux, D. (2009). Barium and molybdenum records in bivalve shells: Geochemical proxies for phytoplankton dynamics in coastal environments? *Limnology and Oceanography*, *54*(3), 1002–1014.

Thébault, J., Jolivet, A., Waeles, M., Tabouret, H., Sabarot, S., Pécheyran, C., Leynaert, A., Jochum, K., Schöne, B., Fröhlich, L., Siebert, V., Amice, E., & Chauvaud, L. (2022). Scallop shells as geochemical archives of phytoplankton-related ecological processes in a temperate coastal ecosystem. *Limnology and Oceanography*, *67*(1), 187–202.

Toullec, J., Moriceau, B., Vincent, D., Guidi, L., Lafond, A., & Babin, M. (2021). Processes controlling aggregate formation and distribution during the Arctic phytoplankton spring bloom in Baffin Bay. *Elementa: Science of the Anthropocene*, *9*(1), 00001.

Toullec, J., Vincent, D., Frohn, L., Miner, P., Le Goff, M., Devesa, J., & Moriceau, B. (2019). Copepod grazing influences diatom aggregation and particle dynamics. *Frontiers in Marine Science*, *6*, 751.

Trombetta, T., Vidussi, F., Mas, S., Parin, D., Simier, M., & Mostajir, B. (2019). Water temperature drives phytoplankton blooms in coastal waters. *PloS One*, *14*(4), e0214933.

Turner, J. (2015). Zooplankton fecal pellets, marine snow, phytodetritus and the ocean's biological pump. *Progress in Oceanography*, *130*, 205–248.

Turner, J., & Tester, P. (1997). Toxic marine phytoplankton, zooplankton grazers, and pelagic food webs. *Limnology and Oceanography*, *42*(5part2), 1203–1213.

U

Uitz, J., Claustre, H., Gentili, B., & Stramski, D. (2010). Phytoplankton class-specific primary production in the world's oceans: Seasonal and interannual variability from satellite observations. *Global Biogeochemical Cycles*, *24*(3), GB3016.

V

Vander Putten, E., Dehairs, F., Keppens, E., & Baeyens, W. (2000). High resolution distribution of trace elements in the calcite shell layer of modern *Mytilus edulis*: environmental and biological controls. *Geochimica et Cosmochimica Acta*, *64*(6), 997–1011.

Vitousek, P., Mooney, H., Lubchenco, J., & Melillo, J. (1997). Human domination of Earth's ecosystems. *Science*, *277*(5325), 494–499.

W

Waeles, M., Dulaquais, G., Jolivet, A., Thébault, J., & Riso, R. (2013). Systematic non-conservative behavior of molybdenum in a macrotidal estuarine system (Aulne-Bay of Brest, France). *Estuarine, Coastal and Shelf Science*, *131*, 310–318.

Wang, P., Huang, Q., Chen, C., You, L., Liu, R., Luo, Z., Zhao, M., & Fu, X. (2019). The chemical structure and biological activities of a novel polysaccharide obtained from Fructus Mori and its zinc derivative. *Journal of Functional Foods*, *54*, 64–73.

Wang, W., Fisher, N., & Luoma, S. (1995). Assimilation of trace elements ingested by the mussel *Mytilus edulis*: effects of algal food abundance. *Marine Ecology Progress Series*, *129*, 165–176.

Wasmund, N., Kownacka, J., Göbel, J., Jaanus, A., Johansen, M., Jurgensone, I., Lehtinen, S., & Powilleit, M. (2017). The diatom/dinoflagellate index as an indicator of ecosystem changes in the Baltic Sea. Principle and handling instruction. *Frontiers in Marine Science*, *4*, 22.

West, C., Burchell, M., & Andrus, C. (2018). Molluscs and paleoenvironmental reconstruction in island and coastal settings: variability, seasonality, and sampling. *Zooarchaeology in Practice: Case Studies in Methodology and Interpretation in Archaeofaunal Analysis*, 191–208.

Westberry, T., Behrenfeld, M., Siegel, D., & Boss, E. (2008). Carbon-based primary productivity modeling with vertically resolved photoacclimation. *Global Biogeochemical Cycles*, *22*(2).

Whitfield, M. (2001). Interactions between phytoplankton and trace metals in the ocean. *Advances in Marine Biology*, *41*, 3–128.

Widdows, J., Moore, M., Lowe, D., & Salkeld, P. (1979). Some effects of a dinoflagellate bloom (*Gyrodinium aureolum*) on the mussel, *Mytilus edulis*. *Journal of the Marine Biological Association of the United Kingdom*, *59*(2), 522–524.

Williams, C., MacDonald, J., Bammler, T., Paulsen, M., Simpson, C., & Gallagher, E. (2016). From the cover: cadmium exposure differentially alters odorant-driven behaviors and expression of olfactory receptors in juvenile coho salmon (*Oncorhynchus kisutch*). *Toxicological Sciences*, *154*(2), 267–277.

Winder, M., & Sommer, U. (2012). Phytoplankton response to a changing climate. *Hydrobiologia*, *698*, 5–16.

Witbaard, R. (1996). Growth variations in *Arctica islandica* L.(Mollusca): a reflection of hydrography-related food supply. *ICES Journal of Marine Science*, *53*(6), 981–987.

Worm, B., Barbier, E., Beaumont, N., Duffy, J., Folke, C., Halpern, B., Jackson, J., Lotze, H., Micheli, F., Palumbi, S., Sala, E., Selkoe, K., Stachowicz, J., & Watson, R. (2006). Impacts of biodiversity loss on ocean ecosystem services. *Science*, *314*(5800), 787–790.

Wu, Y., Campbell, D., Irwin, A., Suggett, D., & Finkel, Z. (2014). Ocean acidification enhances the growth rate of larger diatoms. *Limnology and Oceanography*, *59*(3), 1027–1034.

Y

Yamaguchi, M., & Itakura, S. (1999). Nutrition and growth kinetics in nitrogen-or phosphorus-limited cultures of the noxious red tide dinoflagellate *Gymnodinium mikimotoi*. *Fisheries science*, *65*(3), 367–373.

Yamamoto, T., Oh, S., & Kataoka, Y. (2004). Growth and uptake kinetics for nitrate, ammonium and phosphate by the toxic dinoflagellate *Gymnodinium catenatum* isolated from Hiroshima Bay, Japan. *Fisheries Science*, *70*(1), 108–115.

Young, J. (1994). Function of coccoliths. *Coccolithophores (Ed. by A. Winter & W.G. Siesser)*, 63–83.

Z

Zhao, L., Schöne, B., & Mertz-Kraus, R. (2017). Controls on strontium and barium incorporation into freshwater bivalve shells (*Corbicula fluminea*). *Palaeogeography, Palaeoclimatology, Palaeoecology*, *465*, 386–394.

Zhou, J., Mopper, K., & Passow, U. (1998). The role of surface-active carbohydrates in the formation of transparent exopolymer particles by bubble adsorption of seawater. *Limnology and Oceanography*, *43*(8), 1860–1871.

Zingone, A., Dubroca, L., Iudicone, D., Margiotta, F., Corato, F., Ribera d'Alcalà, M., Saggiomo, V., & Sarno, D. (2010). Coastal phytoplankton do not rest in winter. *Estuaries and Coasts*, *33*, 342–361.

COLLEGE SCIENCES DOCTORAL DE LA MER BRETAGNE ET DU LITTORAL

Université de Bretagne Occidentale

Titre : *Pecten maximus*, archive multi-proxy haute-résolution de la production primaire en rade de Brest

Mots clés : Pecten maximus, Sclérochronologie, Éléments traces, Phytoplancton, Agrégats

Résumé : Les producteurs primaires sont à la base des chaînes alimentaires, et bien que le phytoplancton représente une faible biomasse, il est responsable de la moitié de la production d'oxygène de la biosphère. Environ un tiers de cette production se produit dans les écosystèmes côtiers, où les dynamiques phytoplanctoniques jouent un rôle crucial dans les cycles biogéochimiques. Des changements qualitatifs et quantitatifs dans ces dynamiques ont été observées dans certains écosystèmes côtiers, qui font l'objet de suivis environnementaux depuis plusieurs décennies. Cependant, ces reconstructions ne permettent pas de remonter assez loin dans le temps afin d'observer de tendances à long terme. Ce mémoire de thèse traite de l'utilisation de la coquille Saint-Jacques, *Pecten maximus*, pour prolonger les séries temporelles existantes. Depuis plusieurs années, cette espèce est connue pour enregistrer dans sa coquille les dynamiques phytoplanctoniques de la colonne d'eau. Ces enregistrements se présentent sous forme de traceurs chimiques (éléments traces) que le bivalve incorpore dans sa coquille en réponse aux quantités de phytoplanctons de son environnement. Plusieurs expérimentations ont été menées pour mieux comprendre l'impact du phytoplancton sur la biodisponibilité des éléments que la coquille Saint-Jacques incorpore. Des spécimens récents, récoltés *in-situ,* ont également été utilisés pour calibrer ces proxies et les appliquer à des coquilles anciennes provenant de fouilles archéologiques. L'étude de ces coquilles permet alors de comparer les environnements anciens avec les environnements actuels et ainsi de quantifier l'impact des activités humaines sur les dynamiques des producteurs primaires dans les écosystèmes côtiers.

Title : Bivalve shell-based, high-resolution multi-proxy reconstruction of marine primary production – *Pecten maximus*, Bay of Brest

Keywords : Pecten maximus, Sclerochronology, Trace elements, Phytoplankton, Aggregates

Abstract : Primary producers are the basis of marine food webs, and although phytoplankton represents a small biomass, it accounts for nearly half of the biosphere's oxygen production. Roughly one-third of this production occurs in coastal ecosystems, where phytoplankton dynamics play a crucial role in the biogeochemical cycles of carbon and associated elements. Qualitative and quantitative changes in the dynamics of phytoplankton have been observed in some coastal ecosystems, which have been subject to environmental monitoring for several decades. However, these reconstructions do not extend far enough back in time to observe long-term trends in phytoplankton temporal variations. This PhD manuscript focuses on the use of the scallop, *Pecten maximus*, to extend existing time series. For several years, this species is known to incorporate chemical tracers (trace elements) within its shell in response to the variations in phytoplankton assemblages in the water column, thereby recording micro-algae dynamics. Several experiments have been conducted during this project to better understand the impact of phytoplankton on the availability of these elements that will be incorporated in the scallop shell. Then, recent specimens have been used to calibrate these proxies which have been applied to old shells collected during several archaeological excavations. The study of these archaeological shells has enabled a comparison between an ancient environment and a recent one. Thus, it became possible to quantify the impact of human activities on primary producers dynamics in coastal ecosystems.